ANALYSIS AND FIELD VERIFICATION OF THE EFFECTS OF THERMAL GRADIENT ON CONCRETE PAVEMENT RESPONSE

By

BOUZID CHOUBANE

A DISSERTATION PRESENTED TO THE GRADUATE SCHOOL
OF THE UNIVERSITY OF FLORIDA IN
PARTIAL FULFILLMENT OF THE REQUIREMENTS
FOR THE DEGREE OF DOCTOR OF PHILOSOPHY

UNIVERSITY OF FLORIDA

1993

To those who sacrificed their lives to end
the colonial occupation of Algeria.

ACKNOWLEDGMENTS

This work would not have materialized without the teaching, the valuable guidance, and the expert advice I received from my advisor, Dr. Mang Tia. One meets a man of such character and intellectual abilities all too infrequently in life. Special appreciation is expressed to Dr. Byron E. Ruth for his valuable comments, suggestions and sense of humor. I am also grateful to Drs. David Bloomquist, Ramesh Shrestha and David Wilson for serving on my supervisory committee.

I would like to express my appreciation to the Materials Office of the Florida Department of Transportation for providing the testing facilities and personnel that have made this study possible. In particular, I am grateful to Dr. Jamshid Armaghani and Mr. Tobjorn Larsen for their cooperation and technical assistance.

I would like to thank the faculty, staff and students of the Civil Engineering Department who made my studies here so enjoyable with special thanks to Messrs. Danny Richardson, Billy Studstill and Mrs. Irene Scarso for giving so generously of their time.

Most importantly, my gratitude is owed to my family, especially my parents, Yamina Amirat and Mohamed Choubane, whose support, advice, guidance and prayers throughout my life have made this achievement possible. My debt to both of them can never be repaid in full.

I would like to acknowledge the Algerian Ministry for Higher Education for giving me the opportunity to further my education.

TABLE OF CONTENTS

LIST OF TABLES

LIST OF FIGURES

Abstract of Dissertation Presented to the Graduate School
of the University of Florida in Partial Fulfillment of the
Requirements for the Degree of Doctor of Philosophy

ANALYSIS AND FIELD VERIFICATION OF THE EFFECTS OF THERMAL GRADIENT ON CONCRETE PAVEMENT RESPONSE

By

Bouzid Choubane

August 1993

Chairperson: Mang Tia
Cochairperson: Byron E. Ruth
Major Department: Civil Engineering

This research was conducted to develop a better understanding of the behavior of concrete pavements under thermal effects. The correlation between the daily temperature fluctuations and the induced responses as measured in the field was investigated. A six-slab concrete pavement was used for this purpose.

During the first phase of the study, temperatures throughout the concrete slabs and the resulting vertical slab displacements were measured over an extended time period. An analysis was then performed to develop an effective method for determining realistic thermal-load induced stresses in concrete pavements.

Next, a field investigation was carried out (1) to verify the analytical results obtained during the first phase and (2) to check the validity and reliability of the FEACONS IV (Finite Element Analysis of CONcrete System, version 4) program, a mechanistic model used in the

analytical part of the study. During this field investigation, load induced strains and deflections were recorded at numerous locations on the test slab at various time periods, using the Falling Weight Deflectometer (FWD) as a loading device. The resulting deflections were used to estimate the pavement parameters needed to model the test slab. The dynamic and the static moduli of elasticity were determined by the laboratory tests.

The field investigations confirmed the importance and the need to account for the thermal gradient in the design and analysis of concrete pavements. The temperature data indicated that the temperature distributions were mostly nonlinear and can be represented fairly well by a quadratic equation. In addition, theoretical analysis of the induced stresses suggests the consideration of the total temperature distribution throughout the concrete slab depth rather than the temperature differential between the extreme slab fibers. A relationship between the continuous concrete slab profile variations and the daily fluctuations in thermal gradient was also established. Finally, the measured strains, as compared to the computed ones, demonstrate the reliability of FEACONS IV program in realistically analyzing the behavior of a concrete pavement.

CHAPTER 1
INTRODUCTION

Despite the long history of concrete pavement and the numerous improvements in its design and construction, there are still cases of premature failure of concrete pavements. Examples of such failures include the eastern portion of the concrete pavement of I-10 and I-75 in Sarasota and Manatee Counties.

In view of this problem, there is a need for better understanding of the mechanisms that govern the behavior of concrete pavement structures in order to improve their designs. Moreover, the concrete pavement is a highly complex structure from the stress analysis standpoint. It is supported by soil whose physical properties vary greatly from one location to another. In addition to traffic loads, it is also constantly subjected to internal stresses due to variations in temperature and/or moisture. Because of that complexity, many approaches that have been made involve limiting assumptions and, thus, neglect certain factors that could be of importance in reality. One of such factors is the slab warping due to temperature and/or moisture variations. The induced stresses can be of appreciable magnitude and may cause cracks that are detrimental if the load transfer across these cracks is lost.

Conventionally, critical stresses in concrete pavement resulting from the combined effects of pavement warping and superimposed traffic loads have been made based on the assumption of full concrete slab support by the subgrade. However, as a result of warping, this assumption is seriously in error. The fact that conventional design charts and tables,

such as those developed by the PCA, are based on this convenient concept is mainly due to the difficulty in determining the temperature variations in concrete slabs and the complexity of the analysis that takes into account thermal warping effects. Therefore, the critical conditions have not been properly evaluated.

A better understanding of the warping phenomenon may help in the understanding of some of the existing problems in concrete pavement behavior and provide better guidelines for design that would allow for the possibility that warping may result in the pavement being only partially supported when it receives traffic loads. Consequently, this research study is carried out to investigate the correlation existing between the daily temperature fluctuations and the induced responses in concrete pavements as measured in the field. These temperature variations throughout the concrete slab depth have usually been assumed, when considered, to be linear for simplicity of stress computations even though its nonlinearity has long been recognized. But concerns have been expressed in Florida that the nonlinear temperature gradient in a concrete pavement may affect its performance and would reduce its design life. The validity of such an assumption is addressed and evaluated as well.

In addition, these in situ measurements and procedures are used to investigate the validity and reliability of a rigid pavement design guide developed in a previous study [1], as well as to determine the accurate input values in the assumed mechanistic model.

In summary, the main objectives of this study are as follows:

1. To develop an experimental set-up and data acquisition system for measurement of load-induced strains in concrete slabs for verification of the analytical results generated by the FEACONS IV program.

2. To conduct a laboratory testing program to determine the dynamic elastic modulus of concrete pavement.
3. To analyze the non-linear temperature gradient effect on maximum induced stresses in concrete pavements.
4. To perform a parametric analysis of structural response of concrete pavements under critical thermal-loading conditions incorporating the effects of non-linear temperature gradient.
5. To perform field tests to measure and verify the curling of concrete slabs due to a thermal gradient.

The ultimate purpose of this research study is to investigate the effects of the pavement design variables, as measured in the field, on the performance and behavior of the pavements so that it can lead to an improved design procedure for concrete pavements.

CHAPTER 2
LITERATURE REVIEW

2.1 Introduction

The first rigid pavement in the United States was introduced in 1891 when a strip 10 feet wide and 220 feet long was built in the city of Bellefontaine, Ohio. In 1909 the first sections of rural road were constructed using portland cement concrete in Los Angeles County, California, and Wayne County, Michigan [2]. Since that time, there has been an increasing use of concrete for paving with periodical changes in design. For example, at least 20% of the major highways in England, Wales and South Africa are required to be constructed from concrete for economic reasons [3]. Hutchinson reported in 1985 that, among the more recently constructed pavements, 52.6% of the interstate and 15.3% of the primary arterial pavements in North America are made of concrete [3].

In Florida, Bill Gartner, Deputy State Highway Engineer, speaking in defense of the State Department of Transportation's decision of using concrete over asphalt for portions of I-75, stated the following supporting reasons before the Legislative Council's committee on Roads and Highways [4]:

1) Concrete pavements performed relatively well in Florida according to a list of 40 concrete paving projects that had exceeded their design service lives and were still in good condition.
2) Concrete pavement maintenance costs could be substantially less than that of asphalt pavements.

3) Concrete pavements would provide continuity of pavement surface type in areas with numerous concrete bridges for overpasses and interchanges.

4) The interruption of traffic for maintenance and repair could be minimized.

5) Generally, asphalt pavements tend to lose their skid resistance at a higher rate than concrete pavements. Consequently, it would be safer to drive on a concrete pavement than on an asphalt pavement of the same age.

2.2 Concepts of Rigid Pavements

A rigid pavement consists of a relatively thin slab built over a subgrade or base course. The subgrade is the prepared and compacted soil forming the foundation of the pavement system. The need of a uniform subgrade support has long been recognized because the service life of a pavement is considerably affected by the stability and the strength of the supporting soil foundation. As a result, soil classifications have been established to identify a subgrade soil as possessing physical properties similar to those of known behavior and is, subsequently, expected to furnish the same degree of stability under the same conditions of moisture and climate.

There are also a number of tests to estimate the strength of the supporting soil. The most widely used one for rigid pavement is the plate loading test to determine the modulus of subgrade reaction.

The base course or subbase is defined as the layer between the subgrade and the pavement and it may or may not be needed. It is used for different reasons that include control of pumping, control of frost action, drainage, control of shrinkage and swelling of the subgrade, and

structural improvement [5]. It may consist of one or more properly compacted layers of granular or stabilized material. Highway departments have adopted standard specifications related to composition, plasticity index and compaction.

Nevertheless, the major part of the structural capacity is derived from the slab itself because of its high modulus of elasticity and its rigidity. The fact that the load is usually carried in bending has often been referred to as beam action [5].

There are four basic types of concrete pavement: (1) plain, (2) simply reinforced, (3) continuously reinforced, and (4) prestressed.

Plain concrete pavements are usually jointed at 15 to 20 feet spacing and, by definition, do not contain steel for crack control or load transfer except at the longitudinal joints where tie bars are used to prevent the joint from opening and to permit it to act as a hinge joint [5]. However, it is common practice to use load transfer devices across the joints by either inserting dowels or providing skewed non-dowelled joints.

Simply-reinforced concrete pavements have a wire mesh steel between joints to control cracking due to thermally induced expansion and contraction. The function of steel reinforcement is mainly to hold the interlocking faces of the crack in tight contact to maintain load transfer across the crack and thus preserve the original load-carrying capacity of the slab. Moreover, as soon as the concrete cracks, the tensile stress is transferred to the steel reinforcement. Consequently, a sufficient steel area is needed to resist the forces tending to pull the crack faces apart. This required area of steel is given by the following expression derived by equating the maximum frictional force developed in the slab to the tensile resistance of the steel:

$$A_s = FLW/2f_s \quad (2.1)$$

where

A_s = required area of steel per foot of width or length

F = coefficient of subgrade friction

L = distance between free joints

W = weight of slab

f_s = allowable tensile stress in steel.

Continuously reinforced concrete pavements contain relatively high percentage of steel reinforcement to carry the load in the cracked sections. They are usually placed without joints except for construction and some expansion joints and therefore, the pavement is allowed to crack in a random pattern. These cracks are held together by continuous steel reinforcement. The purpose of the concrete is to carry the wheel load while the steel is to keep cracks tightly together so that there is effective load transfer across the cracks.

Prestressed concrete pavements are placed with adequate steel to provide a prestress on the concrete and, thus, increase its tensile load-carrying capacity. Its thickness may be less than other rigid pavement types for equal load support. They are more complex to design than the conventional pavements because of certain conditions that are not covered by elastic theory. This type of pavement is not widely used in North America because of its high cost [6].

According to Stock, the plain concrete is the most widely used type because of its simplicity and, therefore, its low cost [3].

2.3 Function of Pavement Joints

Early concrete pavements were built without longitudinal or transverse joints. As a result, longitudinal cracks were developed leading to

serious distress (spalling, faulting, and separation). In addition, transverse cracks occurred at variable spacing shortly after construction. Consequently, expansion, contraction, and longitudinal joints spaced at suitable intervals were introduced in an attempt to control the inevitable cracks and minimize the distress of rigid pavements.

Moreover, the introduction of expansion and contraction joints led to concern over the generated weakness of the pavement at these joints. Load transfer devices, generally in the form of dowels, were therefore adopted.

2.3.1 Types of Joints

Joints for rigid pavements can be divided into the following four basic groups: (1) contraction joints, (2) expansion joints, (3) construction joints and (4) hinge or warping joints. Figure 2.1 shows the different joint types.

2.3.1.1 Contraction joints. Contraction joints are transverse joints used to relieve tensile stresses resulting from contraction and warping of the concrete. For a conventional dummy-groove joint, as shown in Figure 2.1-a, a groove is cut or formed at the pavement surface to make certain that cracking will occur at this location. The joint groove may be formed by sawing or by placing a small metal bar having the size of the required joint in the uncured concrete and then remove the bar as soon as feasible [7]. Load transfer at this joint is made by grain interlock of the cracked lower portion of the slab. However, in some cases dowel bars are placed across the joint.

2.3.1.2 Expansion joints. Expansion joints are constructed with a clean break throughout the depth of the slab to allow expansion to take place (Figure 2.1-c). In this case, the joint has no aggregate interlock and load transfer devices are therefore required.

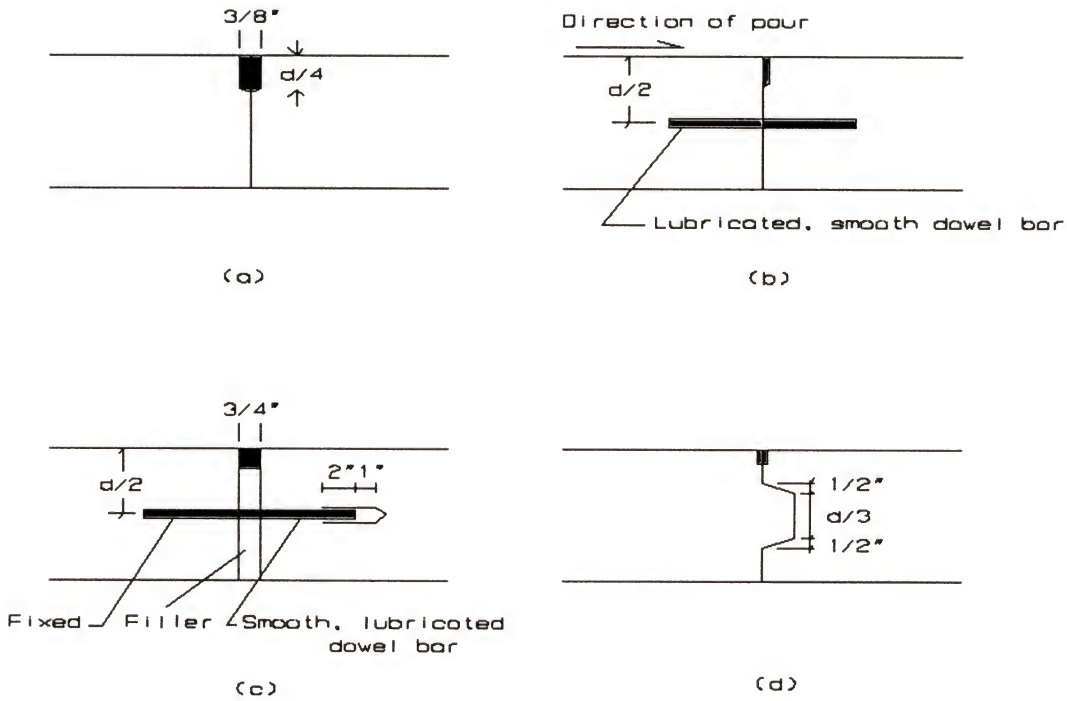

Figure 2.1 Typical Joints: (a) Dummy Groove Contraction, (b) Butt Contraction, (c) Expansion and (d) Keyed Hinge or Warping [5]

Some countries have discontinued the use of the expansion joints for highways because of their high susceptibility to pumping action and inadequacy of load transfer [5]. Furthermore, high expansion stresses are primarily a function of the source and type of coarse aggregate [7]. Subsequently, distress due to blowups can be minimized by a careful selection of coarse aggregate which relieves the use of expansion joints on most construction.

2.3.1.3 Construction joints. Construction joints are used at the transition from old to new construction, such as at the end of a day's pour. The butt type, as illustrated in Figure 2.1-b, is most commonly used in highway work and contain dowel bars for transferring the load across the joint [5].

2.3.1.4 Hinge or warping joints. Hinge and/or warping joints are employed to control cracking along the longitudinal joint of a pavement. The type of joint used depends mainly on the method of pouring the concrete slabs. If one lane at a time is constructed, keyed joints are usually used (see Figure 2.1-d). The dummy-groove type, however, is the most adequate type of longitudinal warping joint to use in the case of a two-lane construction. Tie bars are also placed at interval of about 3 feet to assure that grain interlock is maintained [7].

2.4 Distress Mechanisms in Concrete Pavements

The failure of a pavement before the end of its designed life generally results from loss of its structural strength. In the analysis of rigid pavements, the stress-inducing parameters could be widely categorized in the following classes: (1) restrained temperature and moisture deformation, (2) externally applied loads, (3) volume changes of the supporting material, and (4) continuity of the subgrade support [5].

According to Yoder, the distress of rigid pavements can be caused by (1) the deterioration or deficiency of the pavement itself that could be due to freezing and thawing, use of nondurable materials, scaling resulting from use of salts for ice removal etc., and (2) the structural inadequacy of the pavement-base-subgrade structure that leads to pavement pumping and blowing, corner breaks, faulted or depressed joints etc. [5]. However, distress may be due to a combination of different causes.

Major types of pavement distress are listed in Table 2.1, which displays also the severity, description, and mechanism of each distress.

2.5 Temperature and Moisture Induced Stresses in a Pavement Slab

Volume changes, in the form of contraction, expansion or warping of the slab, result from temperature and/or moisture changes and are of greatest consequence in concrete pavement. The induced stresses can be of appreciable magnitude and may cause cracks that are detrimental if the load transfer across these cracks is lost.

2.5.1 Contraction Stresses

Concrete changes in volume with a change in temperature and/or moisture. Thus a concrete slab, if it is free to move, contracts with a drop in temperature. However, such movement of the slab is often resisted by friction between the bottom of the slab and the subgrade. Consequently, tensile stresses are developed with their peak magnitude at the center of the slab. These stresses increase with the increase of slab length.

If the generated tensile stress in the concrete exceeds the allowable value, the slab may be expected to crack transversely. Then if it is desired to prevent the occurrence of a contraction crack, the slab may be limited to a certain length.

Table 2.1 Jointed Concrete Pavement Distress [43]

Type of Distress	Description	Mechanism
1. Blow-up	A localized upward movement of the slab edges (buckling) or shattering in the vicinity of the joint	Joint lockup caused by infiltration of incompressible materials into the joint space resulting in excessive bending stresses
2. Corner Break	A crack intersecting the joints at a distance less than 6 ft on either side measured from the corner of the slab	Load repetition combined with loss of support, poor load transfer across joint and excessive upward curling
3. Depression	Surface areas having elevations lower that those of the surrounding pavement	Settlement or consolidation of the foundation soil due to poor soil compaction
4. Joint Faulting	Difference of elevation across a joint	Lack of load transfer, differential settlement or uneven support between adjacent slabs associated with pumping
5. Longitudinal Cracks	Cracks generally parallel to the pavement centerline	Improper longitudinal joints construction, or loss of foundation support and excessive curling
6. Popout	A small piece of concrete breaking loose from the pavement surface	Freeze-thaw action, unsound aggregates
7. Pumping	Ejection of material by water through joints or cracks	Free water in the supporting layer ejected due to slab deflection under moving loads
8. Scaling	Breakdown of the slab wearing surface	Concrete surface disintegration caused by deicing salts, traffic, improper construction, freeze-thaw cycles, and steel reinforcement too close to the surface
9. Spalling	Breakdown of the slab at joints or cracks	Excessive stresses at the joint or crack, disintegration of the concrete, poorly designed or constructed load transfer device
10. Transverse Cracks	Cracks at right angles to the pavement centerline	Combination of heavy load repetition, excessive curling, and drying shrinkage

2.5.2 Expansion Stresses

If a concrete slab is subjected to a uniform increase in temperature, the slab will expand. A long length slab may buckle or blow up if this expansion is resisted. This could be prevented by installing transverse expansion joint.

However, frictional force at slab-subgrade interface resists a major part of this expansion, and that the compressive stresses generated by this restraint are generally quite small as compared with the compressive strength of concrete.

2.5.3 Temperature Induced Warping Stresses

2.5.3.1 Introduction. When a concrete pavement is subjected to a temperature differential between the top and bottom surfaces, it tends to curl. During the day the temperature at the slab surface is greater than that at the bottom. Consequently, the slab curls downward at the edges with the resulting effect, due to the slab weight restraint, of placing the top fibers of the slab in compression and those in the bottom in tension. Conversely, at night the coolest temperature is at slab surface and, therefore, the curling is upward with the top of the slab being in tension and the bottom in compression.

A major consequence of the phenomenon is the possibility of the pavement being only partially supported when it receives traffic loads. Thus, curling is of importance in the design of concrete pavements because (1) the resulting flexural stresses may be of considerable magnitude and in some cases could exceed those due to externally applied loads, and (2) the warping or curling may cause a partial loss of subgrade support.

2.5.3.2 Historical overview of slab warping analyses. Various investigators have made extensive study of the temperature curling phenomenon and its generated stresses. Pavement curling was first significantly

measured at the Bates Experimental Road near Bates, Illinois, in the early 1920s where it was discovered that temperature differences between pavement surfaces results in considerable curling of slab [8]. A maximum vertical movement of 0.25 inches at corners of slabs was recorded.

Goldbeck, in 1919, developed an equation for approximating the stresses in concrete pavement slabs in the case of an unsupported slab corner that may result from temperature and moisture differentials [9]. This equation, better known as the "corner formula", is as follows:

$$\sigma = 3P/h^2 \tag{2.2}$$

where

σ = maximum tensile stress in a diagonal direction on the top of slab near a rectangular corner;

P = load applied at a point at the corner; and

h = thickness of the concrete slab.

Older, in analyzing the strain measurement taken on the Bates Test Road, verified this formula [8]. However, according to Kelley, the corner formula gives much higher stresses than the actual stresses in pavement slabs even under extreme conditions of warping [10].

The concepts used in deriving this formula served as a basis for many of the formulas developed later on. In 1926, Westergaard published the earliest analytical work on pavement stresses due to uniform temperature gradients [11]. His analysis covered cases of (1) the slab of infinite length and width, (2) the slab of finite width and infinite length and (3) the slab of finite length and width. However the important magnitude of these stresses was not generally recognized until the Arlington Road tests.

Later, Bradbury used Westergaard's concepts to develop the following general equations for computation of temperature warping stresses [12]:

Edge stress: $$\sigma = C_x E\alpha\Delta T/2 \quad (2.3)$$

Interior stresses: $$\sigma_x = (E\alpha\Delta T/2)[(C_x + \mu C_y)/(1 - \mu^2)] \quad (2.4)$$

$$\sigma_y = (E\alpha\Delta T/2)[(C_y + \mu C_x)/(1 - \mu^2)] \quad (2.5)$$

where

E = modulus of elasticity of concrete;

α = thermal coefficient of expansion of concrete;

ΔT = temperature difference between top and bottom of slab;

μ = Poisson's ratio of concrete; and

C_x, C_y = warping stress coefficients.

The coefficients C_x and C_y are function of the free length and width depending on the direction in which the curling stress is required. The values of these warping stress coefficients are given by the normograph in Figure 2.2. The maximum warping stresses computed using these equations can be as high as 375 psi for a 9-in slab. Bradbury also developed the following approximate expression for corner warping stress:

$$\sigma = [(E\alpha\Delta T)/3(1 - \mu)]\cdot\sqrt{a/\ell} \quad (2.6)$$

in which

ℓ = the radius of relative stiffness $= \sqrt[4]{\dfrac{Eh^2}{12(1-\mu^2)k}}$

a = radius of area of load contact.

During the 1930's, extensive experimental studies were carried by the Bureau of Public Roads in Arlington, Virginia, to investigate the different factors, including the slab temperature and moisture conditions, that affect the design of concrete pavements and, therefore, evaluate the

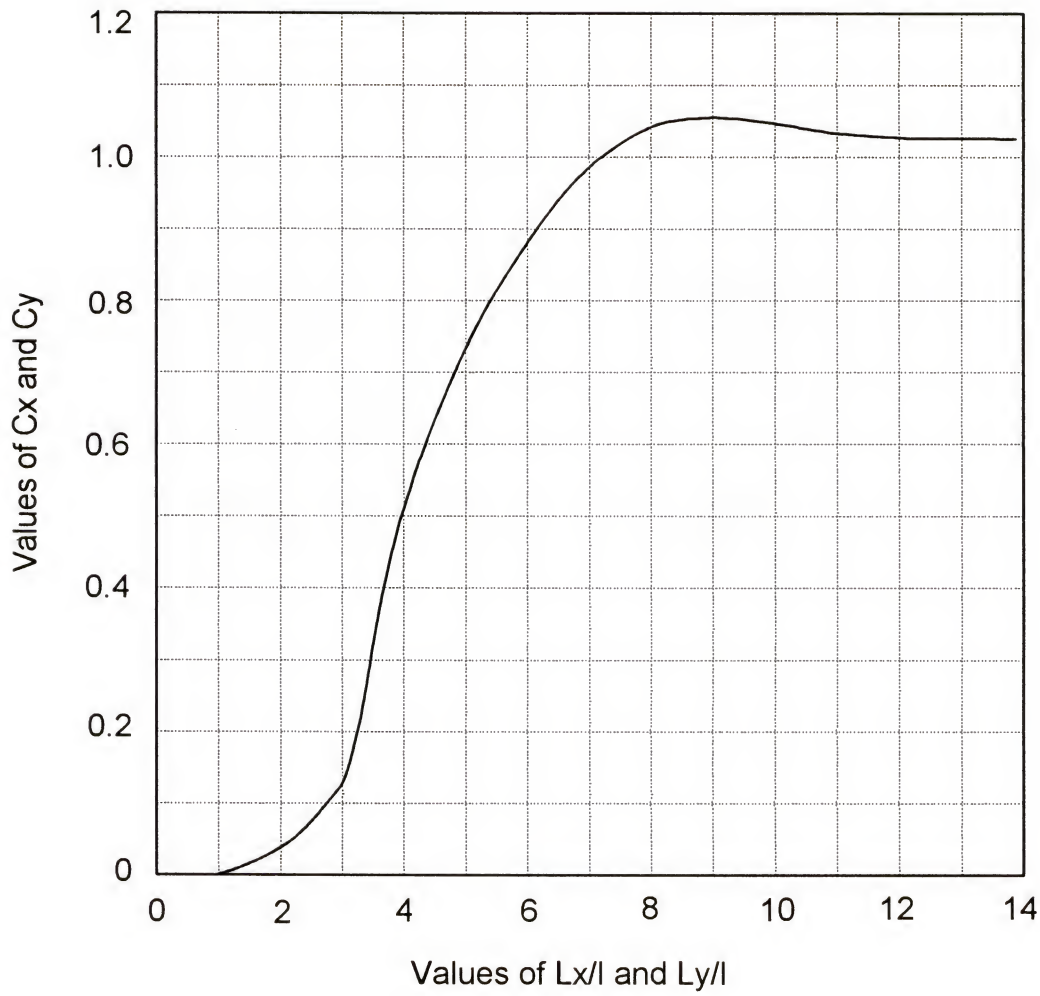

Figure 2.2 Bradbury's Warping Stress Coefficients [12]

existing pavement stress theories at that time [13]. The various curled shapes of 10x20 foot slabs were measured with a clinometer and thermocouples were used to obtain the temperature measurements throughout the slab depths. The resulting experimental data are probably some of the first reliable data on curling of rigid slabs. The values of maximum temperature differentials observed during these tests are summarized in Table 2.2. It can be seen from that table that (1) the maximum temperature differential increases with the increase of slab depth, (2) the maximum positive temperature differential occurs during daytime and is greater in summer than in winter and (3) the minimum negative temperature differential occurs at night. From these measurements, Bradbury suggested, for design purposes, the use of a maximum positive temperature differential of 3°F per inch of slab thickness and a maximum negative differential of 1°F per inch of slab thickness [12]. The investigators, Teller and Sutherlands, concluded also that the uniform temperature gradient results in the most critical stress condition due to curling even though the curved gradient is the more usual temperature distribution. It was also found that when the corner is warped downward and therefore has full support with the subgrade, the observed stresses matched well with those computed using the Westergaard equation, while when the case is reversed at night time, the measured stresses were much higher than those given by Westergaard corner formula. Consequently, using these measured stress data, a purely empirical expression for computing stresses at corner was developed [13]. It has a same general form as the Westergaard corner formula but takes into account the reduction of subgrade support due to warping and is as follow:

$$\sigma = (3P/h^2)\left[1 - \left[\frac{a\sqrt{2}}{\ell}\right]^{1.2}\right. \tag{2.7}$$

Table 2.2 Values of Maximum Temperature Differential, in °F, Observed in Arlington Road Tests [10]

	6-inch slab				9-inch slab	
	April to August		September to February		April to August	
	Day	Night	Day	Night	Day	Night
Maximum	+24.3	-6.5	+15.6	-6.7	+31.0	-9.2
Minimum	+18.7	-4.5	+ 8.2	-1.3	+22.3	-5.7
Average	+21.2	-5.8	+11.8	-4.1	+26.9	-7.5

In 1940 Thomlinson modified Westergaard's approach by assuming a simple harmonic temperature variation at the slab top surface [14]. Using the heat flow laws, he reached the conclusion that a curved temperature gradient existed throughout the slab depth. However, the magnitude of the stresses computed were less than those of Westergaard corroborating Teller and Sutherlands findings.

The analyses of Westergaard and Thomlinson for computation of warping stresses were both based on full subgrade support.

Another experimental study designed to determine the effect of climatic changes on the load-carrying capacity of a concrete slab was conducted at the University of Minnesota in 1941 [15]. A 16.5x17 foot slab of 7 inch thickness was built and instrumented for that purpose. Slab movements due to temperature and moisture changes were recorded. Cyclic daily temperature variations were observed. A temperature differential of less than 2°F per inch was obtained ninety-six percent of the time in the study slab. The moisture content in the slab reached its peak in March and its low point in August. This type of study provided valuable data for design of pavements for the local conditions.

In 1951, Pickett made significant changes to Westergaard equations by developing semi-empirical formulas for the case of a corner load that consider the effect on the loading stress of curling at the corner [16]. He considered two conditions:

1. Protected corners: at least 20% of the load is transferred from one slab corner to the other. The tensile stress is given by:

$$f_t = \frac{3.36\ P_i}{h^2}\left(1 - \frac{\sqrt{a/\ell}}{0.925 + 0.22\ (a/\ell)}\right) \qquad (2.8)$$

2. Unprotected corners: one corner must carry over 80% of the load.

For this case, the tensile stress is given by:

$$f_t = \frac{4.2\ P_i}{h^2}\left(1 - \frac{\sqrt{a/\ell}}{0.925 + 0.22\ (a/\ell)}\right) \qquad (2.9)$$

where:

ℓ = the radius of relative stiffness = $\sqrt[4]{\frac{Eh^2}{12(1-\mu^2)k}}$.

h = slab thickness

P_i = the load P increased by the impact factor.

In 1959 Harr and Leonards developed an analytical procedure to determine stresses and deflections in concrete pavements due to temperature and moisture differentials and the extent of the subgrade support [17]. It is essentially an extended and computerized version of the Westergaard analysis. The analytical model adopted considers the bending of circular slabs of uniform thickness resting on homogeneous foundations whose reaction against the slab is proportional to the deflection. Numerical solutions were obtained for deflections and radial stresses for several combinations of parameters, i.e., elastic modulus, slab radius, slab thickness, modulus of subgrade reaction, temperature differential, linear coefficient of thermal expansion and Poisson's ratio, were considered and the results were presented in a nomograph form. This analysis was for curled-up conditions. Later, Wiseman, jointly with Harr and Leonards, completed the analysis and developed a theory for the curled-down slab [18]. Experimental tests were then conducted to validate this analysis. A 12x25 foot and 8" thick slab, constructed and instrumented on a soil-cement subbase at Purdue University, was subjected to temperature gradients under controlled conditions and deflections were recorded. These measured deflections were reported to correlate well with those computed.

At the AASHTO Road Test, built near Ottawa, Illinois, in the 1950s, relative changes in slab surface elevation as well as the corresponding temperatures at different depths of pavement slabs and at different times of the day were measured [19]. These measurements were also taken at different seasons. From the obtained data, a relationship between slab curling and temperature differential was established.

Huang and Wang developed in the early 1970s a finite-element computer program for analysis of concrete pavement slabs that took into account the upward curling due to a negative temperature differential, assuming linear temperature gradient [20]. Two recently developed programs, WESLIQUID [21] and JSLAB [22], also include the capability of computing curling stresses related to temperature differential.

In 1989, Ioannides and Salsilli-Murua presented, on the basis of the finite element program ILLI-SLAB results, an analytical solution to the problem of a slab-on-grade under combined effect of temperature and wheel loading [23]. In their closed-form solution, the maximum combined tensile stress in the slab under edge loading is determined by applying a multiplication factor, which is function of the temperature differential, to the Westergaard equation.

However, the curling computed using the finite element programs has not been correlated with field measurements of slab curling.

2.5.4 Moisture Induced Warping Stresses

A difference in moisture content between the top and bottom of a concrete pavement slab causes it to curl in the same manner as does a temperature differential. When the top of slab is dryer than the bottom the edges curl upward and when the moisture differential is reversed the edges of the slab curl downward. However, very little information is available about the evaluation of stresses due to moisture.

According to Kelley [10], the warping of a slab due to moisture differential is a seasonal change that takes place slowly over a considerable period of time. The observations made during the Arlington Road tests indicated that during the hot summer days when temperature and moisture differentials are both at maximum, the curling caused by one is in the opposite direction to that caused by the other [13]. Consequently, the stresses due to moisture reduce rather than increase the thermal stresses.

2.6 Methods for Analytical Analysis of Rigid Pavements

Several theories of rigid pavement design have been developed over the years. They basically all derive from the theory of elasticity because a rigid pavement can be modeled as a structural element or a plate resting on an elastic foundation.

Timoshenko distinguishes three types of plate bending: (1) thin plates with small deflections, (2) thin plates with large deflections, and (3) thick plates [24]. Since the deflections of pavement slabs are small as compared with their thickness, they can be classified in the first category. In this case, LaGrange, in 1811, obtained the following differential equation that describes the deflections w of a slab surface subjected to a uniform load, q, applied perpendicular to its surface:

$$D\left(\frac{\partial^4 w}{\partial x^4} + 2\frac{\partial^4 w}{\partial x^2 \partial y^2} + \frac{\partial^4 w}{\partial y^4}\right) = q - kw \qquad (2.10)$$

Where K is the modulus of subgrade reaction and D is the flexural rigidity of the slab given by:

$$D = Eh^3/12(1 - \mu^2) \qquad (2.11)$$

The main existing theories of rigid pavement analysis include: (1) continuously supported slabs, (2) layered systems, and (3) finite element method. This section will discuss and describe these theories and the

various load-stress equations developed for use in concrete pavement design.

2.6.1 Continuously Supported Slabs Method

Westergaard's work was the first serious attempt to find a theoretical solution for rigid pavement design [25] by deriving a complete solution of equation (2.10). In 1926 he developed solutions for critical stresses and deflections under a single load for three cases of loading, namely (1) interior, (2) edge, and (3) corner, using the classical bending theory of a medium-thick plate to represent the slab, and the subgrade was assumed to act as a series of uniformly distributed spring supporting the slab or as a so-called Winkler foundation. Thus, the vertical pressure of the base on the slab is a constant, k (modulus of subgrade reaction), times the deflection.

The equations for stresses for the three loading cases as developed by Westergaard are as follows:

$$\sigma_i = 0.31625 \frac{P}{h^2} \left[4 \log_{10} \left(\frac{\ell}{b} \right) + 1.0693 \right] \tag{2.12}$$

$$\sigma_e = 0.57185 \frac{P}{h^2} \left[4 \log_{10} \left(\frac{\ell}{b} \right) + 0.3593 \right] \tag{2.13}$$

$$\sigma_c = \frac{3P}{h^2} \left[1 - \left(\frac{a\sqrt{2}}{\ell} \right)^{0.6} \right] \tag{2.14}$$

where

P = point load, in pounds;

σ_i = maximum tensile stress in pounds per square inch at the bottom of the slab directly under the load, when the load is applied

at a point in the interior of the slab at a considerable distance from the edges;

σ_e = maximum tensile stress in pounds per square inch at the bottom of the slab directly under the load at the edge, and in a direction parallel to the edge;

σ_c = maximum tensile stress in pounds per square inch at the top of the slab, in a direction parallel to the disector of the corner angle, due to a load applied at the corner;

h = thickness of the concrete slab in inches;

μ = Poisson's ratio for concrete (taken as 0.15 in these equations);

E = modulus of elasticity of the concrete in pounds per square inch;

k = subgrade modulus in pounds per cubic inch;

a = radius of area of load contact in inches (the area is circular in the case of corner and interior loads and semicircular for edge loads);

b = radius of equivalent distribution of pressure at the bottom of the slab = $\sqrt{1.2a^2 + h^2} - 0.675h$; *and*

ℓ = the radius of relative stiffness = $\sqrt[4]{\frac{Eh^2}{12(1-\mu^2)k}}$.

Hogg [26] and Hall [27] considered the subgrade as a semi-infinite elastic medium and used the elastic properties of subgrade to develop a mathematical model for determining the maximum stress and deflection under a single load at the interior position of a semi-finite concrete slab.

In 1951 the work of Westergaard and of Hogg was extended by Pickett and Ray [28] with their work at Kansas State College to consider the

effect of any loading configuration. The solutions were in the form of influence charts.

In 1969 Pickett and Niu developed a solution to the problem of a cracked pavement subjected to a single load that takes into account the effect of a discontinuity on the deflection and moments in the pavement slab [29].

Ionnides et al. derived new equations for both stress and displacement based on the comparison of Westergaard's solutions to results obtained using the ILLI-SLAB finite element program [30]. This investigation of the validity of the Westergaard equations through these comparisons led the authors to establish new equations for corner loading case and to assert the validity of Westergaard solution for interior loading when the smallest slab dimension is at least three to four times the radius of relative stiffness.

According to Majidzadeh, the continuously supported slab analysis has certain shortcomings that include (1) the limited application to a two-layer pavement, (2) non-applicability to slabs with finite dimensions, (3) the effects of voids or partial subgrade support can be not analyzed, and (4) uniformity of thickness, subgrade support, and material properties must be met [31].

2.6.2 Layered Systems Method

Some investigators consider the pavement behavior as better approximated by a three-layered system than as a slab on a foundation. The layer theory assumes that the modulus of elasticity, Poisson's ratio and the thickness of each layer are variables.

The stresses due to loading in an elastic multiple-layered system such as a slab or slab-and-base resting on a uniform subgrade were first analyzed by Burmister even though he did not provide a numerical solution

of the deflection or stress [32]. These stresses have been evaluated later on by other researchers but these equations have been mainly used in the flexible pavement analysis.

The complete analysis of systems of any number of layers subjected to different loading conditions was not possible until the age of computer. In 1963 Chevron Research Company Developed the first computer program for analysis of five-layer elastic systems subjected to a single load. Since then a certain number of programs having the same capability have been developed such as ELSYMS and VESYS.

This method of analysis is valid only in the case of interior loading. In addition, some of the features of concrete pavement such as cracks, reinforcement, voids under the slab, curling and warping can not be analyzed.

2.6.3 Finite Element Method

The theories previously described are limited in their assumptions on realistic pavement behavior. They involve mainly single-load application on uniform homogeneous isotropic slabs of uniform thickness supported by uniform foundation. In those theories, in-plane forces and applied couples or moments can not be handled.

In order to analyze concrete pavement slabs that are not limited by many of these above limitations, finite element techniques were developed to formulate the problem. The finite element method allows considerable freedom in plan configuration loading, flexural stiffness and boundaries conditions. It has been used by a number of investigators for analyzing rigid pavement slabs on an elastic foundation. The concrete slab is modeled by an assemblage of rectangular elements joined at discrete finite numbers of nodal points. The subgrade is considered to behave either as an elastic foundation or as a Winkler foundation. In a Winkler foundation,

the subgrade is represented by springs having a constant modulus of reaction K_s. This means that the deflection at any point of the foundation surface depends only on the forces at that point. In an elastic continuum foundation the subgrade is treated as an idealized elastic half-space which implies that the deflection at any given point depends not only on the forces at that point but also on the forces or deflections at other points. This difference in the behavior of the two types of foundation is illustrated in Figure 2.3.

2.7 Existing Computer Models for Concrete Pavement Slab Analysis

Various finite-element models have been developed for analysis of the concrete pavement system like slab models, plain strain models, prismatic models, three-dimensional models, etc. However, the most accurate ones would be the three-dimensional models where the actual geometrical configuration of the whole system can be taken into account, but the amount of discretization and the computer cost required for the solution make them impractical. Consequently, the concrete pavement slabs are often modeled as medium-thick plates supported by an idealized subgrade while the aggregate interlock, keyway and dowel bars at joints are modeled as linear and rotational springs. This chapter describes a few of the existing computer models for concrete pavement analysis as well as the respective assumptions and modeling techniques used in their development.

2.7.1 ILLI-SLAB

In ILLI-SLAB, a computer program developed at the University of Illinois, a concrete slab is modeled as an assemblage of rectangular plate bending elements with three degrees of freedom per node, namely (1) a vertical displacement in the z direction, (2) a rotation about the x-axis and (3) a rotation about the y-axis [33]. The slab is also modeled to incor-

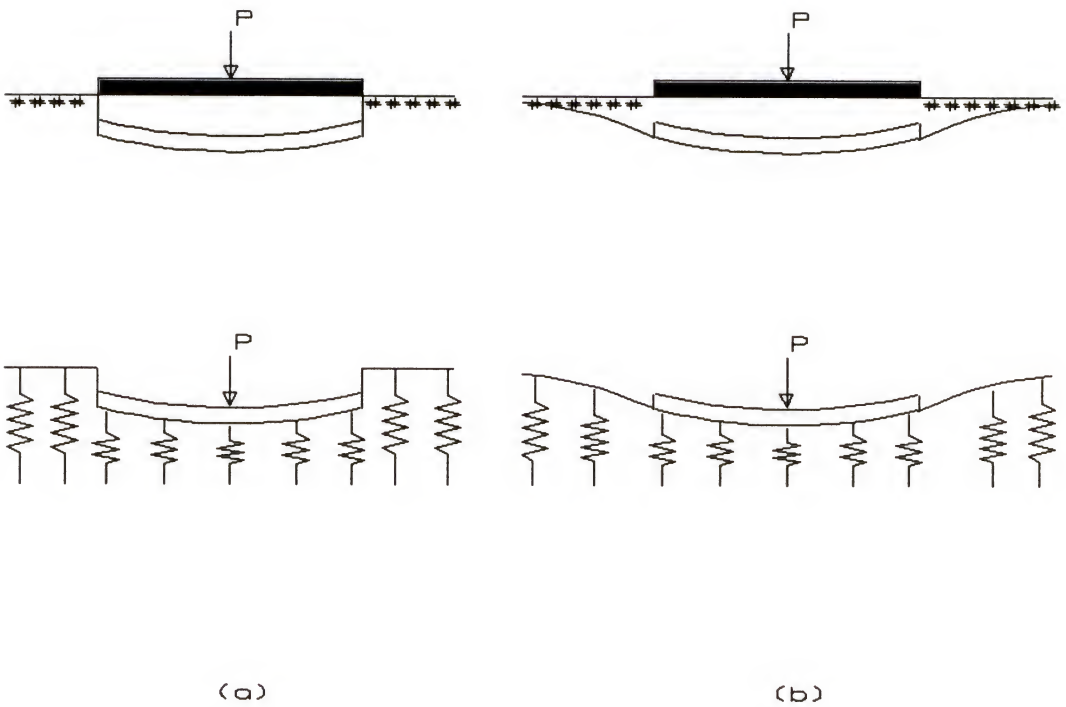

Figure 2.3 Relative Behavior of the Two Subgrade Models, (a) Winkler Foundation, (b) Elastic Continuum Foundation [7]

porate one or two layers, a subbase or/and an overlay for example, with the option of bond between layers.

The subgrade is considered as a Winkler foundation modeled by a series of vertical springs evenly supporting the slab. The spring elements have one degree of freedom per node, the vertical displacement. The corresponding force is determined by multiplying the deformation of the element by the spring constant. This spring constant represents the modulus of subgrade reaction.

Dowels are modeled as bar elements having two degrees of freedom per node, a vertical displacement and a rotation around a horizontal transverse axis, thus allowing the bar to transfer both a vertical shear force and a moment. Moreover, the aggregate interlock and keyway joints are modeled as vertical spring elements with one degree of freedom per node.

This program is capable of modeling a jointed concrete pavement of up to six slabs or continuously reinforced concrete pavements, incorporating the shoulders. However, the program does not consider the loss of subgrade support due to curling or voids.

2.7.2 JSLAB

The JSLAB program was developed by the Portland Cement Association using a similar model as ILLI-SLAB [22]. The main difference is that the effects of temperature differential are considered by a resulting moment along the edge that is a function of temperature gradient, the elastic modulus and the coefficient of thermal expansion of concrete. A linear temperature gradient is assumed.

2.7.3 WESLIQUID and WESLAYER

Both of these finite element models, developed by the U.S. Army Engineer Waterways Experiment Station, are also based on the classical theory of thin plates with small deformations where the slab is considered

as an assemblage of rectangular plate bending elements having three degrees of freedom per node [21]. The basic difference between these two models resides in their respective modeling of the sublayers. While the sublayers are considered as an elastic layered solid in the WESLAYER model, they are assumed as a Winkler foundation in the WESLIQUID model. Consequently, in the WESLIQUID model, the forces due to the reaction at the sublayers are simply added to the forces of the plate bending elements at any given node. The resulting deflections at the subgrade surface are computed using the Boussinesq's solution. In the WESLAYER model, the deflections at any given point depend not only on the forces at the node but also on the forces and deflections at other nodes. The Burmister's equations are used to compute the deflections in this case. The sublayers stiffness matrix is obtained by inverting the flexibility matrix.

The two models consider both shear and moment transfer across the joints and have three options for analyzing shear transfer and one for moment transfer.

Both models consider also the linear temperature gradient effects on the concrete slab as well as full or partial contact between slab and sublayer.

2.7.4 FEACONS

A computer program named FEACONS (Finite Element Analysis of CONcrete Slabs) was developed at the University of Florida to analyze the response of a concrete pavement system subjected to a combination of concentrated and distributed loads [1,34]. This program considers the following factors in the analysis, namely (1) weight of the concrete slabs, (2) voids beneath the concrete slabs, (3) effects of joints and edges and (4) effects of temperature differentials between the top and bottom surfaces of the slabs.

A jointed concrete pavement is modeled as a three-slab system while a slab is considered as an assemblage of rectangular elements with three degrees of freedom per node as developed by Melosh [35] and Zienkiewicz and Cheung [36]. The program has also the option of considering a stiff subbase as a separate layer but in full contact and unbonded to the concrete slabs. In such a case, the subbase is modeled similarly to the concrete slab as a thin plate.

The subgrade is assumed as a Winkler foundation modeled by a series of vertical springs at the nodes and the subgrade voids are modeled as initial gaps between the slab and the springs at the specified nodes. Load transfer across the joints are modeled by linear and rotational springs connecting the slabs at the nodes of the elements along the joints. Frictional effects at the edges are modeled by linear springs at the nodes along the edges.

2.8 Instrumentation of Rigid Pavements

2.8.1 Introduction

The purpose of field instrumentation of pavements is to collect data on the performance of the pavements under actual traffic and environmental conditions. These data can be used to verify existing design procedures or theoretical calculations and to correlate them with actual performance of pavements. Furthermore, with these measured data, the components of the rigid pavement such as slab (edge, corner, center and joint), reinforcement (dowels and tie bars), base, and subbase could be studied and analyzed. Among the instruments used to measure the pavement responses such as deflections and deformations, strains, stresses, and pore pressures, are: strain gages, linear variable differential transducers (LVDT), pressure cells, accelerometers and velocity gages. The sensors are

selected to provide sufficient measurement range for the expected responses. A few of these instruments will be reviewed in this chapter.

A sensor is the first element of a typical electromechanical measuring chain. It usually converts a physical or mechanical parameter to a voltage. However, the voltage level is, generally, so low that a direct signal processing is impossible. In such a case, the voltage is conditioned using a signal conditioner system to produce a higher level signal. This conditioning consists of amplifying the sensor electrical output and establishing the zero reference measuring point within the system. The signal conditioner is the second element of the chain. The amplified output is, then, transmitted to a display or recording unit, the last component of the measuring chain.

2.8.2 Strain Gages

Strain gages are the most widely used devices to measure strains in pavement concrete slab with very high resolution. They consist of thin metallic foil attached to a thin insulating backing called a carrier matrix. They are suitable for measuring both static and dynamic strains. The electrical resistance of the gage varies linearly with strain and ranges from 30 to 6000 ohms, with 120 ohms and 350 ohms being the most commonly used values for experimental stress analysis. Higher resistance gages are typically used in transducer applications. The strain in the pavement is determined by measuring the change in the electrical resistance of the gage.

The gage length is an important factor in determining the gage performance. The recommended gage length of strain gages for concrete slabs is usually two to four times the maximum aggregate size. This gage length is recommended to make sure that the measured strain is representative of that of the concrete including aggregate and mortar.

The strain gages are mounted on the top of the concrete slab using an epoxy. The concrete surface has to be smooth and dust-free to have good bonding in order to assure that the strains are fully transmitted from the surface to the grids and to measure the resulting resistance changes. These mounted gages are usually considered as short-term instrumentation due to the abrasive action of weather and traffic. For more protection, the gage could be installed in a groove one-quarter inch deep.

In order to provide means of measuring both the compressive and tensile strains in a concrete slab, a research team from Iowa State University used two strain gages at each desired location, at the top and at the bottom of the slab [37]. The two sensors were equidistant from the slab neutral axis to get equal and opposite compressive and tensile strain values. The sensors were positioned in such a way as to verify the strains occurring at the edge, middle, and corner of the slab and to compare them to the strain values used in the design equation. The sensors were placed longitudinally at mid-slab locations in equal transverse spacing increments. The gage was attached to a bar to reach a specific location in the concrete as the concrete was placed. At the edges, the sensors were placed six inches away from the shoulder to reduce the influence of the shoulder material. The gages used, identified as a PML-60 model, are 60 mm long and 1 mm wide and are imbedded in an epoxy capsule of 125 mm by 15 mm by 5 mm covered with grit. Thirty concrete strain gages were installed; three of them did not work and one gave intermittent response during a field testing.

The welded strain gage is mostly used on steel such as reinforcement, dowels and tie bars in rigid pavements. It is a precision foil sensor bonded to a metal carrier for spot welding to structures and components. Bonded gages could also be used. An advantage of this type of

gage over the bonded one is the pre-attached lead wires of 10 inches long and, therefore, is less time consuming in its installation. It is also well-suited to high-temperature testing. The weldable strain gage, model LWK-06-W250B-350, used in the Iowa State University project measures 6.35 mm long by 3.18 mm wide, and has a nominal resistance of 350 ohms, a strain range of ±5,000 micro-strain and a temperature range of -195 to +260 degrees centigrade.

To measure reinforcement strains, the Iowa State University investigators attached the selected strain gages to the bottom of the dowels in order to give the gages maximum physical protection during installation [37]. The sensors were placed on selected bars under the wheel paths, near the centerline joint, the transverse mid-slab and near the edges of the pavement section in each lane. This was done to provide measurements of the maximum strain on the bars due to loading the surface. Of fifty weldable gages placed, one provided no circuit and another showed signs of damage and inconsistent results during a field test.

Because of their relative low cost and lightness, a large number of strain gages could be used to investigate the behavior of a structure. However, appropriate signal conditioning and readout equipment are needed.

One of the major sources of error is due to installation effects. A satisfactory operation of strain gages is dependent on a good installation, waterproofing, and mechanical protection.

2.8.3 Deflection Gages

Deflection gages record deflections and deformations in a pavement structure. Two types of sensors have been used successfully to record the deflections of the pavements: a linear variable differential transducer (LVDT) and a strain gage [38].

LVDT is an electromechanical device that transforms a deflection to a proportional voltage output. Its sensitivity to a displacement depends on the maximum displacement that it can measure and the amplification applied to the gage signal. The LVDT is attached to the top of a rod that is driven into the subgrade at a certain depth and registers the defections relative to a reference point of a particular layer in the pavement. The hole made through the pavement to accommodate the rod has to be lined so that the rod is free from the surrounding material and, therefore, would not reinforce the pavement [39]. Both permanent and transient deflections can be measured.

The strain gage system for deflection measurement consists of four strips of high tension steel on which strain gages are mounted. The metal strips are fixed at one end and connected on the other end so that they deflect as cantilevers.

The deflection measurement is, generally, relative to a reference depth in the pavement foundation. The mid-slab and the sides of the transverse joint are the positions with critical deflection.

Measurement of horizontal movements provides data on the openings at cracks and joints and can be used to evaluate their effects on load transfer.

To measure pavement deflection, the Iowa State University team used a Displacement Transducer DC-DT series 240-000 with a working range of ±0.500 volts, by Trans-Tek Inc., in locally built housings in the wheel paths [37]. Thirteen gages were installed and just one showed signs of fluctuating voltage during testing.

2.8.4 Temperature Measurement

Devices like thermistors, thermocouples, or electrical resistance thermometers (RTD) have been used to measure the pavement temperature and

to determine frost and thaw penetration depths with time. The sensors are usually mounted on a reinforcing bar that is inserted vertically into the pavement layers to provide sensors at the depths needed. Temperature readings can be taken periodically or continuously at different depths of the pavement. The data are, then, displayed directly or as a voltage output, depending on the type of device used to monitor the sensors.

Thermocouples are the most frequently used. They are simply electrical junctions of two wires made of dissimilar metals [40]. They operate on the basis that, when two dissimilar metals are put in contact with each other, a voltage is induced at their junction. This voltage is function of the characteristic of the wire materials used and indicates the temperature difference between the two junctions. Figure 2.4 illustrates the typical thermocouple measurement circuit.

There are several type of thermocouples. However those fabricated from copper and constant wires or type T have the lowest limits of error and greatest sensitivity in the temperature range -60 to +140°F [41]. They provide about 22 microvolt/°F of output at 32°F.

A characteristics comparison of the three types of temperature sensors most commonly used in field, namely thermocouple, thermistor and the electrical resistance thermometer (RTD), is shown in Table 2.3.

A grid sensor, model WTG-50C, by Micro Measurements, Inc. was used in Iowa to measure the concrete, air and base material temperature [37]. The gage, composed of a strain grid mounted on a thin nickel foil, has a temperature range of -195 to +260 degrees centigrade and a nominal resistance of 50.0 ± 0.15 ohms at 23.9 degrees centigrade and, is not sensitive to strain. The grid is 6.35 mm by 3.18 mm bonded in a resin mold of 9.53 mm by 3.18 mm. The temperature is determined by the strain in the nickel foil. The sensors were placed in such a way to have the top sensor

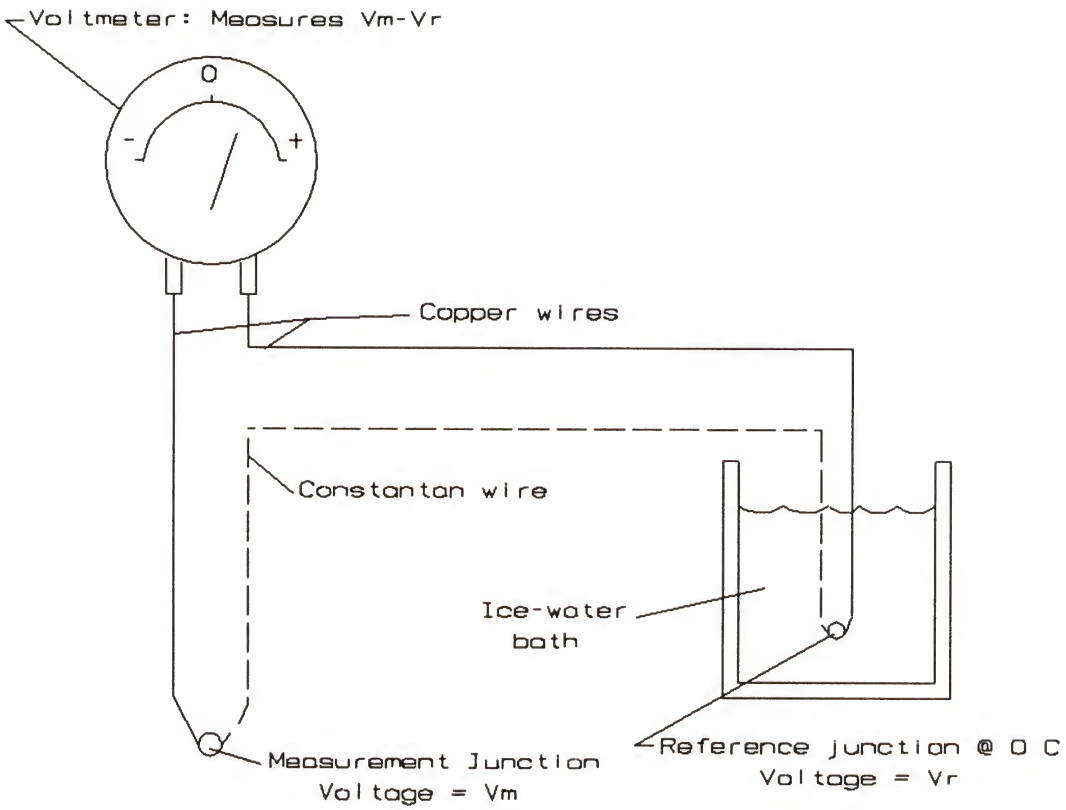

Figure 2.4 Typical Type T Thermocouple Measurement Circuit [40]

Table 2.3 A Characteristics Comparison of Thermocouple, Thermistor, and Electrical Resistance Thermometer (RTD) [41]

	RTD	THERMISTOR	THERMOCOUPLE
Accuracy*	0.01 to 0.1°F	0.1 to 1°F	1 to 10°F
Stability*	Less than 0.1% drift in 5 years	0.2°F drift/yr.	1°F drift/yr.
Sensitivity*	0.1 to 10 ohms/°F	50 to 500 ohms/°F	50 to 500 volts/°F
Range	-420 to 1600°F	-150 to 550°F	-300 to 3100°F
Output	1 to 6 V	1 to 3 V	0 to 60 mV
Power (100-ohm load)	4×10^{-2} watt	8×10^{-1} watt	2×10^{-7} watt
Features	Greatest accuracy over wide wide spans; greatest stability	Greatest sensitivity	Greatest economy; highest range

*Varies with range and point on scale.

one inch below the pavement and base surfaces, and two inches above and nine inches below the subgrade. All of the 16 gages installed responded positively during a field testing.

2.8.5 Pore Pressure Cells

The behavior of a pavement foundation depends on whether or not the foundation is saturated. Pore pressure could develop in a partially saturated pavement foundation due to dynamic vehicle loadings. Therefore, it is desirable to evaluate pore pressures in order to compute the effective stresses.

The main concern in the design of a pressure cell is the ability to place the pressure cell in the soil without significantly disturbing the existing state of stress in the soil mass [42].

A pore pressure cell designed by the US Army Engineers Waterways Experiment Station (WES) has been satisfactorily used in the field [38]. The cell has to be embedded in air-free sand. A porous stone allows the pore fluid to enter a small cavity. The changes of fluid pressure in the cavity, and, therefore, pore pressure, are measured by a small absolute pressure transducer. The stone pore size has to be small enough to prevent blockage by soil grains and large enough to let fluid flow [39].

2.8.6 Accelerometers

An accelerometer is an electronic integrator that converts the acceleration measurements to deflection. In general, the displacement of a point can be evaluated by double-integrating the acceleration signal of that point. Therefore, the pavement deflection can be measured by integrating the output signal of an accelerometer either by electrical hardware or through software after digitization [42]. However, it is used for determining peak deflections rather than for defining the shape of the de-

flection wave and it applies only to transient measurements. It is intended for general use in vehicle ride analysis.

2.8.7 Velocity Measurement

One of the devices used to measure the linear velocity of an object as it is displaced is a LVT or Linear Velocity Transducer. It is a sensor that produces an electrical output directly proportional to the time rate of change of rectilinear displacement. It is generally used for dynamic measurement such as the measurement of vibration on a pavement. Its vibration tolerance varies from 20 Hz to 2 kHz and has a temperature range of -65°F to +200°F.

2.8.8 Data Collection System

The data collection system needed in a pavement monitoring system has to provide on-site collection and efficient storing of multiple gage outputs. It is selected based on the number of channels of data and the desired sampling frequency. It could consist of a power source, signal conditioners for the sensors, and hardware and software to handle the data. This hardware could be composed of a micro-computer with a graphics monitor and associated card. A software for the data collection and analysis is also needed. The data is recorded in either analog or digital modes and could either be processed on site or at a central location.

The output of the system could be in the form of graphical display and numerical list of data for each load and at any of the individual sensors that is selected for data collection.

Organizations like the Portland Cement Association (PCA) and the Alberta Research Council have complete systems that combine data collection with on-site processing (data reduction, analysis and storage). The Alberta Research Council Mobile Data Acquisition System consists of the following components: (1) Display (video terminal, hard copy terminal and

a digital plotter), (2) Signal Conditioning (16 channels with sequential sampling, 50 sec per sensor), (3) Data Storage (5000 data point buffer, dual disk for system operation and mass data storage), and (4) Computer (PDP 11/24) [38].

In the Iowa project, the data was collected through a microcomputer controlled data acquisition system at the site and transmitted through a phone to a central site at Ames for analysis to determine the maximum and minimum strains, mean values, areas under the strain curves and the length and rate of increase and decrease of strain. This information will be used to compare the static and dynamic weights of the vehicles, the weight to strain magnitude, weight to deflection and frequencies of the strains to the expected pavement damage [37]. The data collection system used was a HP 3852A Data Acquisition and Control Unit with two extender units (3853A) [37].

CHAPTER 3
FIELD AND LABORATORY TESTING PROGRAM

3.1 Description of the Concrete Test Pavement

A six-slab concrete pavement, constructed at the Materials Office of the Florida Department of Transportation (FDOT), was used to investigate the pavement response to temperature and load in this research. Each slab is 20 ft long, 12 ft wide and 9 in thick. The adjoining slabs 1 and 2 and 4 and 5 are connected by dowels, respectively, as illustrated in Figure 3.1.

The test pavement was constructed to be representative of in-service Florida concrete pavements in August 1982. The slabs were laid on a native roadbed soil consisting mainly of granular materials classified as A-3 according to AASHTO Soil Classification. The average Limerock Bearing Ratio (LBR) of the compacted subgrade was 50 [44].

Five thermocouples were embedded in the slab concrete at different levels at the time of construction to monitor pavement temperatures. These thermocouples are positioned at 1, 2.5, 4.5, 6.5 and 8 inches below the top surface of the fourth slab center. The ambient temperature was measured by another thermocouple that was housed inside a wooden box mounted on a 5 ft pole.

3.2 In Situ Measurements of Load-Induced Pavement Response

Two major factors that influence significantly the structural behavior of a rigid pavement are (1) temperature gradient and (2) load (magnitude and position). The purpose of this in situ testing scheme was to

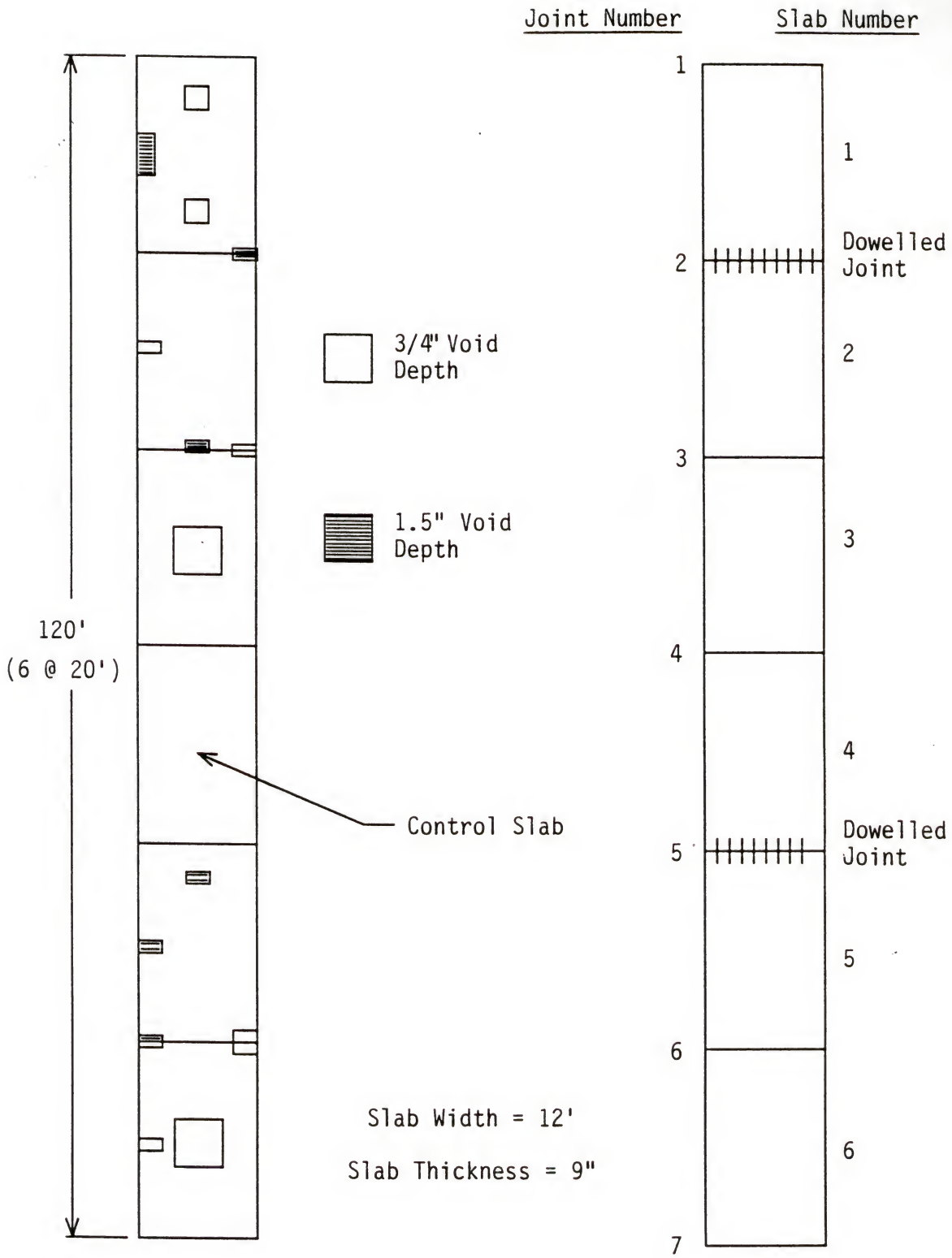

Figure 3.1 Plan of the Test Slabs [44]

characterize the load-induced response of the test slabs corresponding to various temperature differentials and load positions. For this task, the Falling Weight Deflectometer was used as a loading device because of its ability to simulate pavement response under moving wheel path.

The following sections describe the FWD testing device and the testing program and procedures for measuring the load-induced pavement response.

3.2.1 Falling Weight Deflectometer

The FWD used to evaluate the load response of the test slabs in this study is a Dynatest 8000 System made by Dynatest Inc., as shown in Figure 3.2. It can generate loads ranging between 2,000 and 24,000 lb by varying the drop heights and drop weights. It is trailer mounted and towed by a van. It consists of a loading system and a set of velocity transducers for measuring peak surface deflections. The testing operation is controlled by a data processing and computer system housed inside the tow van.

The FWD test consists of delivering an impulse load to a pavement surface by dropping a known mass from a predetermined height onto a set of rubber buffers or springs connected to an 11.8-inch loading plate. The pulse duration is usually between 25 to 30 milliseconds. Figure 3.3 shows an idealized model of the FWD system.

The force applied to the pavement can be determined by equating the initial potential energy of the system to the stored strain energy of the springs when the mass is at rest. Therefore:

$$F = (2Mghk)^{1/2} \qquad (3.1)$$

Figure 3.2 Dynatest 8000 System

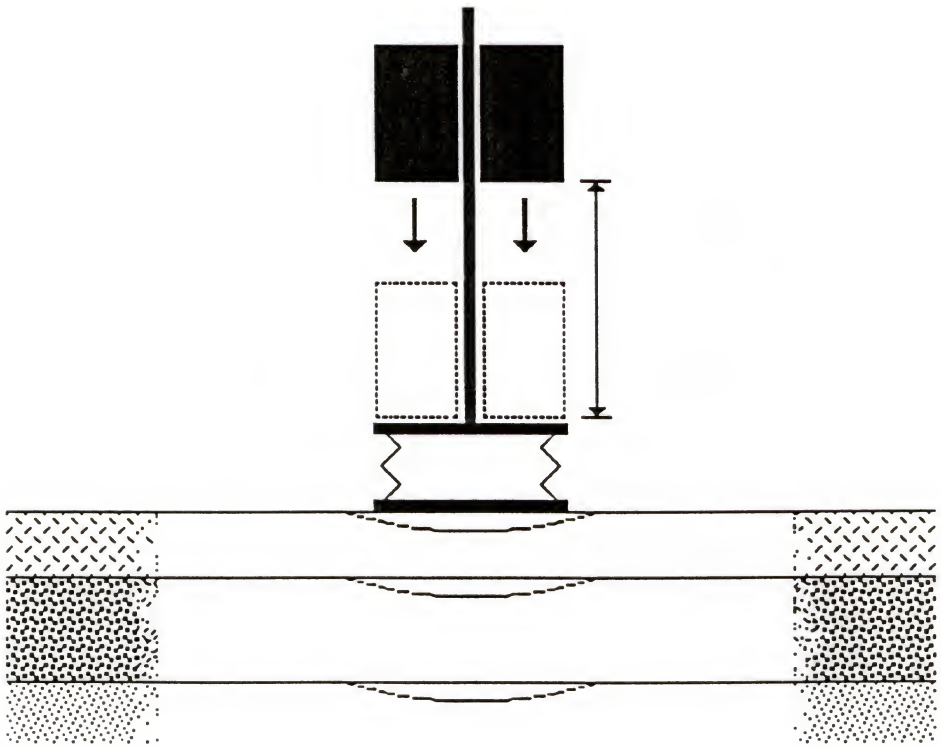

Figure 3.3 Idealized Model of the FWD System

where

M = falling mass,

g = acceleration due to gravity,

h = drop height, and

k = spring constant.

A load cell, attached to the loading plate, is used to measure the peak force. The maximum load-induced deflections are usually measured by velocity transducers (geophones). One geophone is located in a hole at the center of the loading plate, while the others are normally housed in brackets secured on a bar that can be lowered with the loading plate.

The signals from all the sensors are transmitted to a microprocessor-based control and recording system. The data are then stored automatically on a magnetic tape through a HP-85 computer.

3.2.2 Instrumentation of Concrete Pavement Slabs for Strain Measurement

3.2.2.1 Instrumentation. The instrumentation used in measuring slab strains consists of a strain gage Conditioner/Amplifier system and a Digital Oscilloscope.

The main function of the strain gage conditioner and amplifier system is to generate conditioned high-level signals from strain gage inputs for display or recording on an external equipment (a Digital Oscilloscope, in this study).

The system can be composed of (1) one or more 2-channel strain gage conditioners (2) one or more power supplies (each power supply will handle up to 10 channels).

Because of the low order of magnitude of resistance changes to be dealt with, the strain gages are connected to an electric circuit within the system. This circuit, called a bridge, allows the change in strain

gage to be measured with precision. When only one strain gage is used, the circuit is called a quarter bridge.

The circuit was adjusted in such a way to get zero voltage under no-load conditions. The voltage reading under load conditions was used to compute the strain. The measured voltage when the load was applied is proportional to the change of resistance ΔR in the strain gage. Hence, using the definition of gage factor, the equivalent strain was obtained:

$$\epsilon = \Delta R/KR \tag{3.2}$$

where K is a gage factor.

Since we were dealing with low values of voltage, amplifiers within the conditioner system were used to get a larger output signal.

Figure 3.4 illustrates the strain gage conditioner and amplifier system, model 2100 by Measurements Group, Inc., used in this study for generating conditioned high-level signals from strain gage inputs.

The type of oscilloscope used in this study was a computer-transformed digital oscilloscope which consists of a portable IBM PC compatible computer, a R1005 Digital Oscilloscope board which plugs into the computer, and the accompanying data scope software. The R1005 board and the software by Rapid Systems, Inc., transform an IBM PC into a digital oscilloscope.

The main function of the oscilloscope is to receive signals from the conditioner system and display the information on the screen. The data displayed can be recorded and saved on a regular 5 1/4" floppy disk to be analyzed and displayed at a later time.

The y-axis of the display represents the number of volts selected per division and x-axis corresponds to the time period per division which is determined by the sampling rate selected. A rate of 2 ms/division was chosen. Each division represents 20 data values. Therefore, the sampling

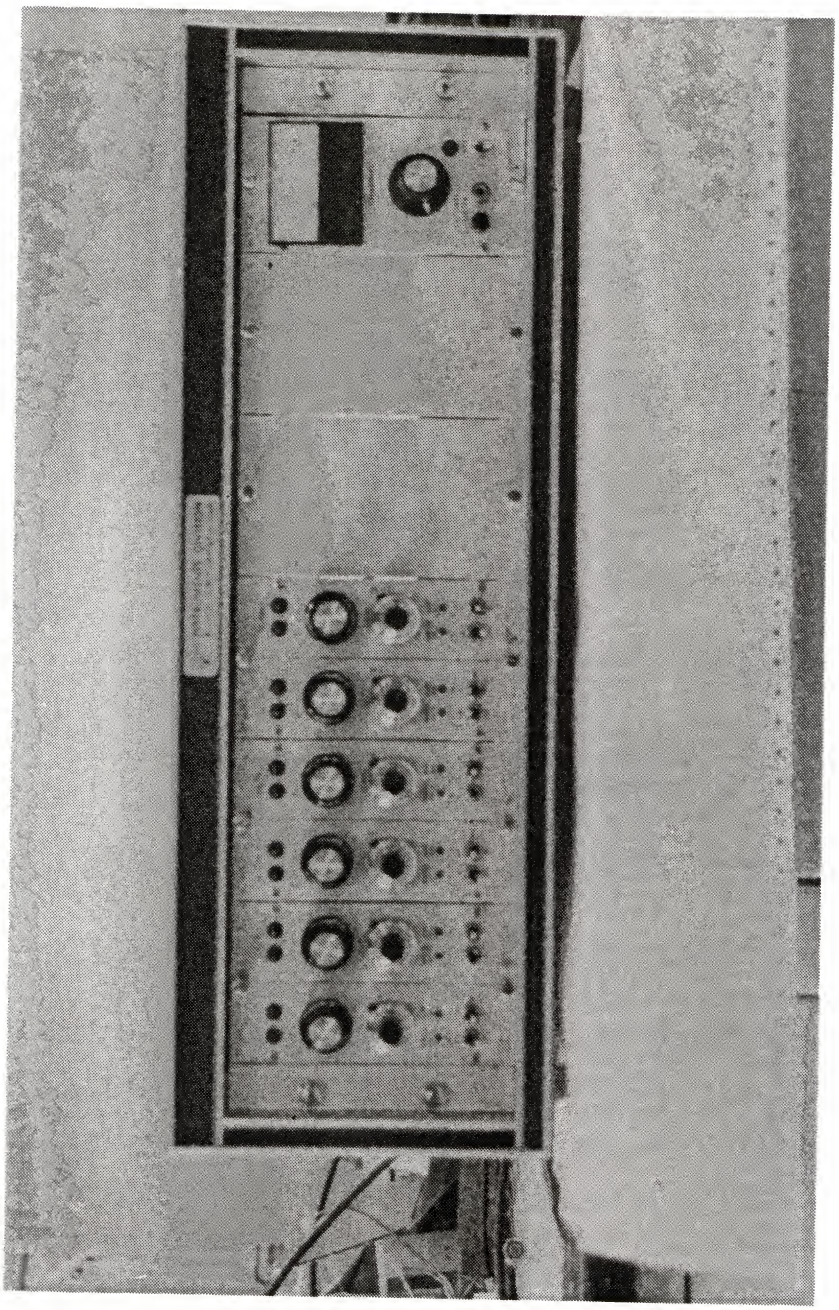

Figure 3.4 Strain Gage Conditioner/Amplifier System, Model 2100

frequency is 0.1 ms/point. Since the duration of the FWD load is usually in the range of 25 to 30 ms, 250 to 300 data points could be recorded for each wave produced by the FWD load. To make sure that all the signals produced would be recorded, 32500 data points were recorded per test. Hence, the duration of each process was 3.25 seconds (32500 x 0.1ms). However, once the data were displayed on the screen, only the portion of data containing the load induced wave were saved onto the floppy disk in order to conserve computer storage space on site and analysis time.

Before starting the test, the oscilloscope had to be triggered. This allowed it to start taking the data. There are three main trigger modes, namely, automatic, analog, and digital. Each mode has a normal and a stop option. When the stop option is selected, the system enters the paused mode after a single data set is acquired. Since the measured signal was very low, it was very difficult to trigger the oscilloscope by means of the signal. Thus, the mode Automatic(s) was used. Once the system is started, it will trigger automatically, read the specified number of data and then enter the pause mode. This is essentially a manual trigger. The system had to be started manually at the same time as the FWD load was dropped to collect data for each test.

3.2.2.2. Strain gage layouts. Strain gages of EA-06-20 CBW-120 type, by Micro Measurements, Inc., with a resistance of 120 ± 02 ohms were used. These gages were attached to a slab on the Test Road. Figures 3.5 through 3.7 show the different strain gage layouts used in the different testing phases of this study. During the first two field tests, two strain gages, one in longitudinal and one in transverse directions were used at each location. For the third field test, just one strain gage was used at each location.

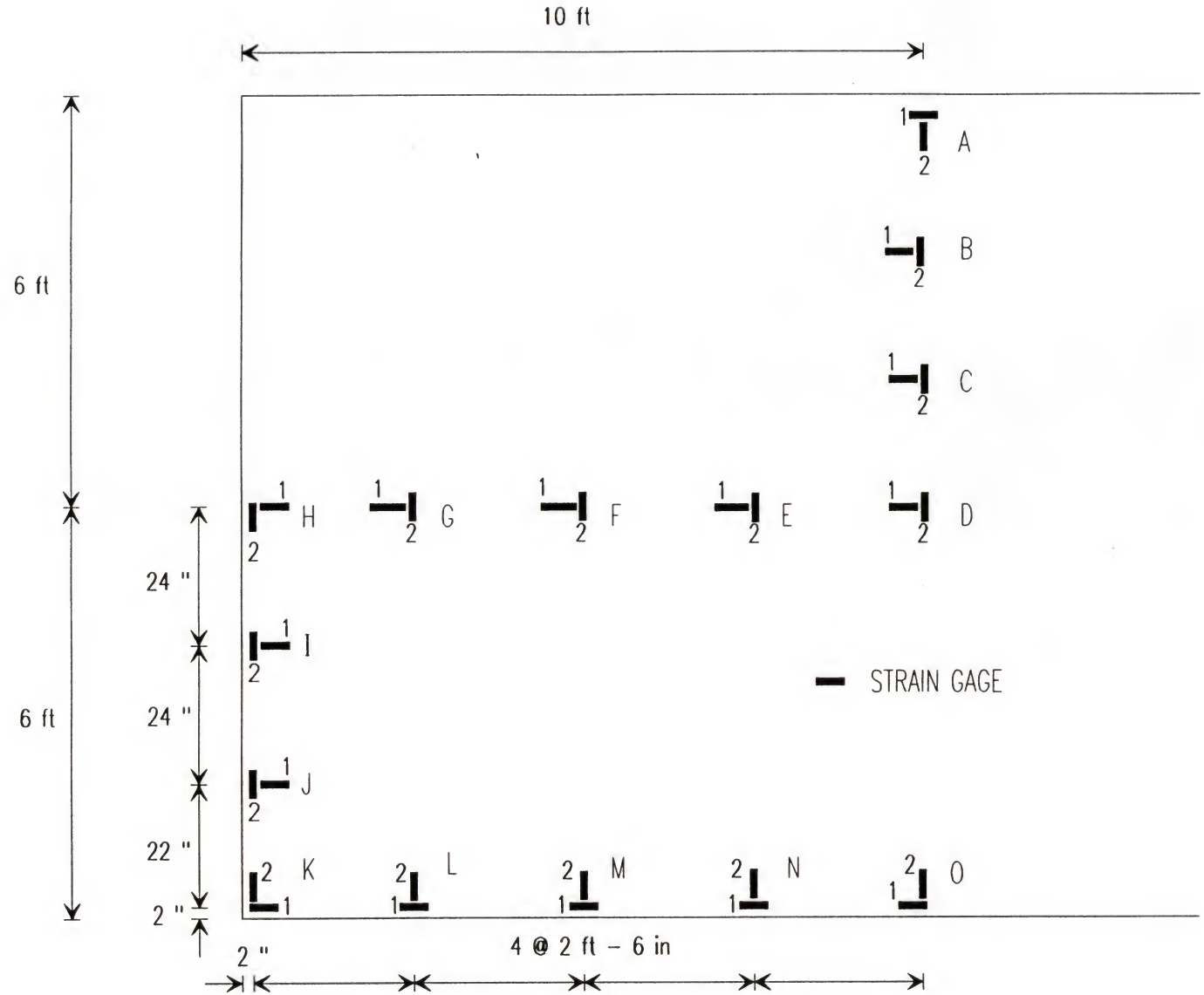

Figure 3.5 Strain Gages Layout Used in July 1988 Field Test

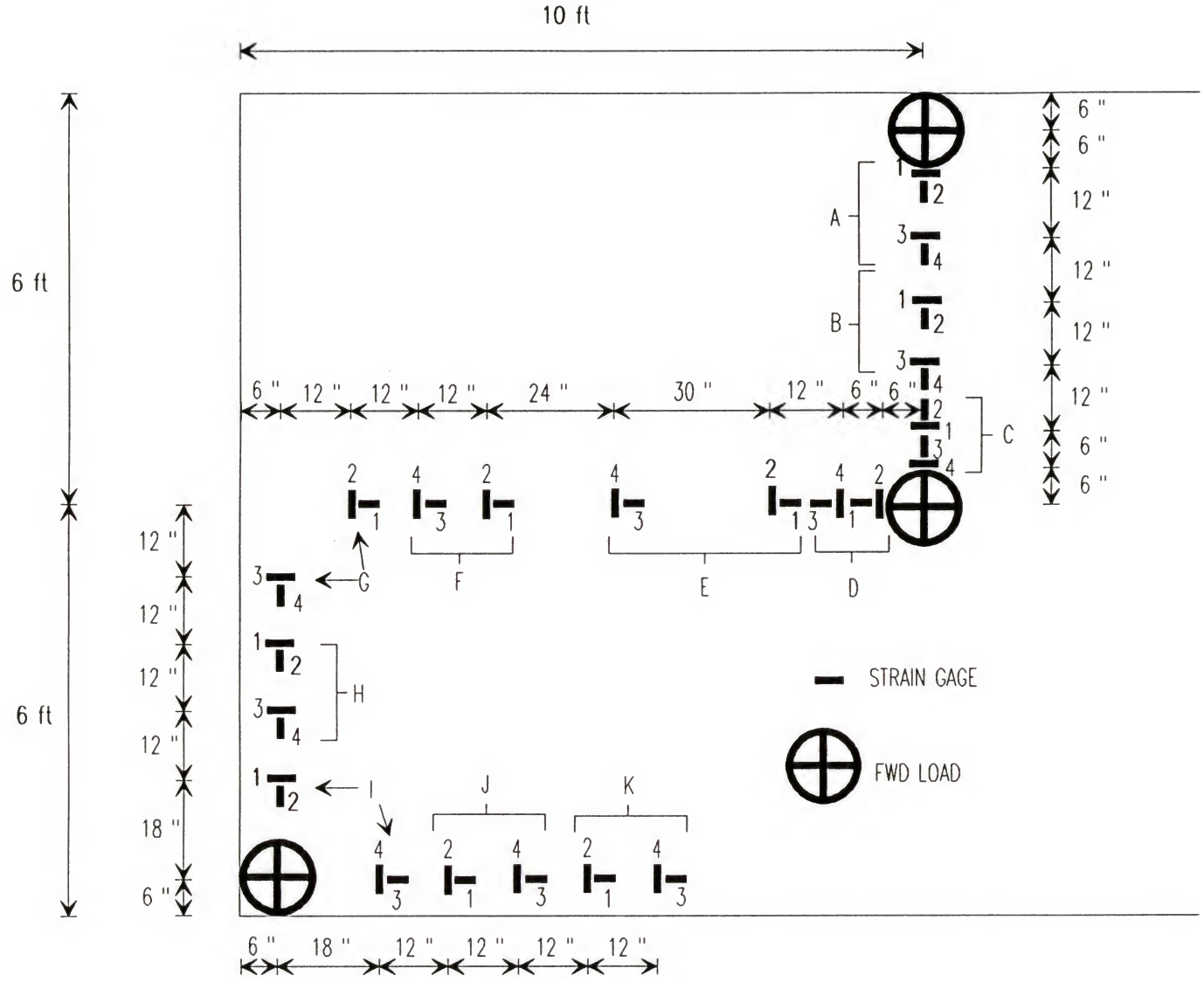

Figure 3.6 Strain Gages Layout Used in January 1989 Field Test

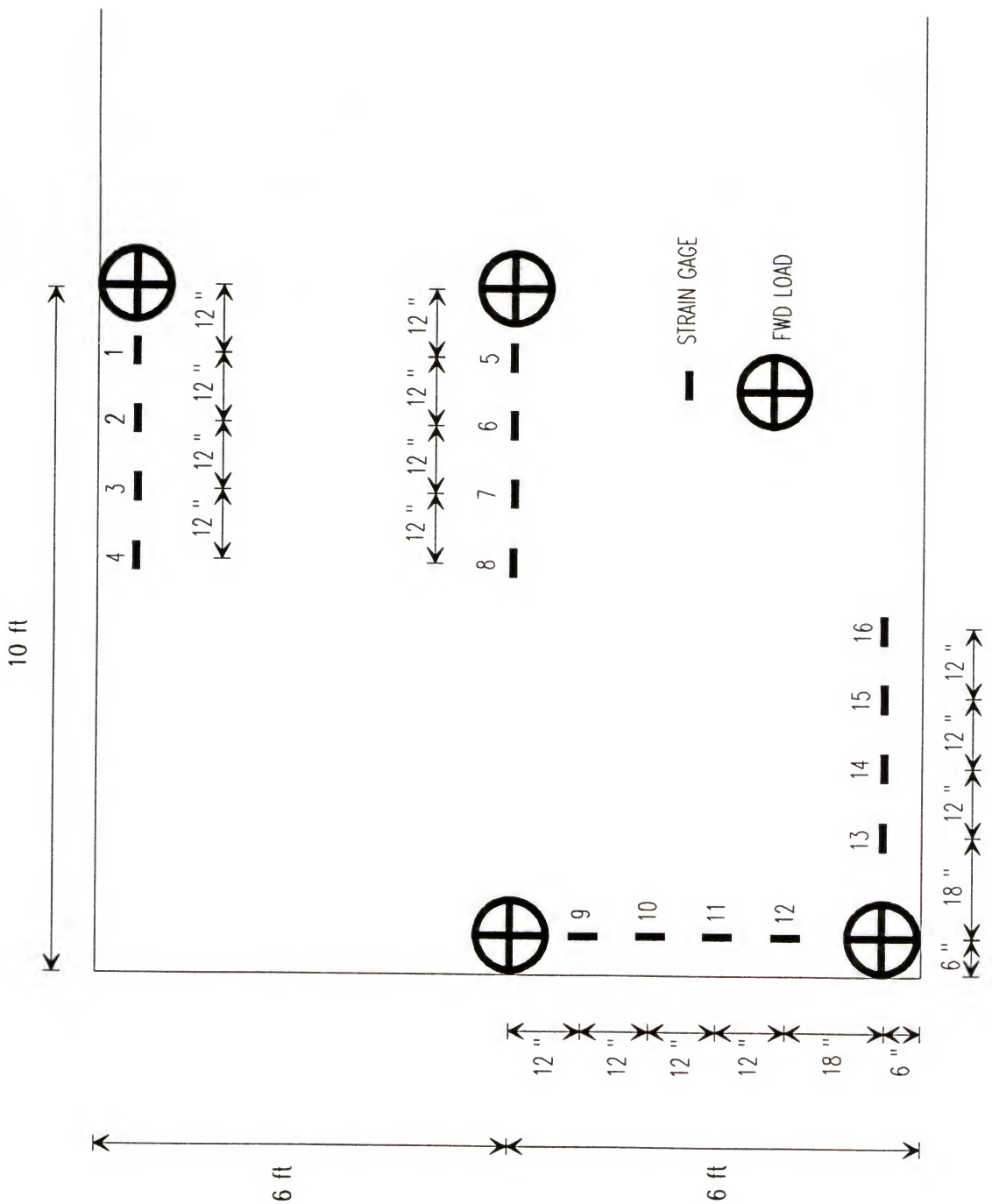

Figure 3.7 Strain Gages Layout Used in June 1989 Field Test

Before attaching the strain gages, the surface had to be prepared according to the following step-by-step procedure:

1. Grind and polish each area to be gaged to get a smoother area. (Rough area may cause malfunctioning of the gage.)
2. Clean meticulously the area using a conditioner and neutralizer liquids.
3. Apply a layer of uniform thickness of epoxy, EPY-150 KIT type, to fill any void and let it cure for a day.
4. Apply a light coat of adhesive to the gage backing and attach it to the desired area.
5. Apply a constant pressure (by placing a concrete cylinder on top of it, for instance) for a better adhesion and let it cure for another day.
6. Solder the wires to the strain gages.
7. Apply another layer of epoxy for waterproofing and insulating the gages.

3.2.2.3 Instrument set-up. The instrumentation was set up in the field following the steps below:

1. On the power supply of the strain indicator unit, turn the channel selector to "AC". Turn the power switch ON. The red pilot lamp should light and the meter should read between 9 and 11 on the scale. This is done to check the adequacy of the input current to the power supply.
2. On the power supply, turn the channel selector to "DC". The meter should read very near the line at 10 on the scale to ensure that there is no internal short in one of the conditioner modules.

3. Connect strain gages to strain indicator. In our testing program, two channels were used. Channel 1 and 2 inputs were connected to the longitudinal and transverse strain gages, respectively.
4. Set the desired excitation on each channel. This is done by turning the channel selector to channel 1 and adjust BRIDGE EXCIT using a small screw driver to read the desired bridge voltage of 5 volts on the power supply meter. Turn channel selector to channel 2 and repeat the same procedure.
5. Adjust the AMP BAL for each channel by using a small screw driver; adjust each AMP BAL until both lamps are OFF. If both lamps are lit, it is an indication of excessive noise at the input.
6. Adjust balance on each channel. On each channel, turn the EXCIT switch to ON, then turn the BALANCE control to extinguish OUTPUT lamps. This is done to initialize the voltage to zero under no load conditions.
7. Connect outputs to digital oscilloscope. Channel outputs 1 and 2 are connected respectively to the BNC connectors A and B, which are input terminals to the oscilloscope.

   The system is now ready to record data.

3.2.3 Testing Procedures

3.2.3.1 Measurement of deflections. In order to provide realistic pavement parameters (such as the concrete modulus, E_c, subgrade modulus, K_s, edge stiffness, K_e, joint shear stiffness, K_l and joint torsional stiffness, K_t) that can be used as an input into the FEACONS IV program, which was used as the analytical tool in the course of this study, three sets of deflection data caused by various FWD loads were measured and recorded during the first field test. They were the (1) deflections along the longitudinal centerline caused by FWD loads applied at the slab center at

nighttime, (2) deflections along the edge caused by FWD loads applied at the edge center at the daytime and (3) deflections along the joint on both the loaded and unloaded side caused by FWD loads applied at the joint center at daytime. Three load levels, 300 kPa, 570 kPa and 1000 kPa, were used at each loading position. The use of three load levels was to check the linearity of FWD load-deflection characteristics. Of these three levels of load, the one of 570 kPa, which corresponded to a total load of 9 kips, was used thereafter. The corresponding measured deflection basin was then interpreted and used, in conjunction with the DBCONPAS II program, to back-estimate the in situ pavement parameters needed for modeling the concrete pavement. This back-calculation was accomplished through an iterative procedure of matching the measured deflections with those computed by using an assumed set of pavement parameters.

3.2.3.2 Measurement of strains. It is known that different temperature differentials in a concrete slab will cause it to curl in different ways. A positive temperature differential in the slab will cause it to curl up in the interior, while a negative temperature differential will cause it to curl up at the edges and joints. To cover both of these two extreme curling conditions, two sets of tests were performed during the three field tests, one at midday with a positive temperature differential in the slab and the other at night corresponding to a negative temperature differential. The night tests were performed at early morning between 4 A.M. and 8 A.M., and the day tests were conducted at midday from 12 noon to 5 P.M, on July 28th 1988, on the first week of January 1989, and on the 8th of June 1989.

FWD loads were applied to the test slab at different positions. The load positions were (1) edge center, (2) slab center, (3) joint center, (4) edge center on the other side of the slab which had a void of size of

1 ft x 2.5 ft x 3/4 inch underneath the slab and (5) slab corner. Position (4) was not used in the last two field tests to reduce the number of gages and testing time. Two levels of FWD load were used at each position, i.e, 570 kPa and 1000 kPa, during the first field test and just one load level at 1000 kPa was used during the last two. The FWD load-induced strains were measured by strain gages attached on the slab at various locations. The layouts of the strain gages were presented in Section 3.2.2.2 and shown in Figure 3.5 through 3.7.

3.3 In Situ Measurements of Thermal-Induced Pavement Deflection Profile

Daily temperature variations within the concrete slab are important to rigid pavement behavior because the temperature gradient between the top and bottom of a concrete slab can vary considerably during a 24-hour cycle resulting in its warping. For instance, if the top of the slab is warmer than the bottom, the slab corners tend to curl downwards. Conversely, if the top is cooler than the bottom upward curling occurs.

A parameter generally used to study the effect of temperature gradient is temperature differential (DT), the algebraic difference between the temperatures of the top and bottom of a concrete slab.

This phase of this study was carried out to study the influence of temperature on the resulting concrete pavement response. For that purpose, a series of tests were conducted to measure the various slab profiles corresponding to different temperature differentials.

3.3.1 Monitoring of Slab and Air Temperatures

The temperature of the concrete slab at various depths and the air temperature were measured and recorded throughout the testing period. The thermocouples were connected to a Fluke programmable data logger that recorded the temperature at 15-minute interval. The slab temperature was measured at the depths of 1 inch, 2.5 inches, 4.5 inches, 6.5 inches and

8 inches from the top surface of the slab. The temperature differential in the slab at a certain time was calculated by subtracting the temperature measured at the depth of 8 inches from that measured at the depth of 1 inch. The temperature differential was also used to model the concrete pavement for calculating the thermal-load-induced stresses.

3.3.2 Slab Deflection Profile Measurement

Slab deflection profiles were measured using a mechanical device, developed by the Portland Cement Association (PCA). As shown in Figure 3.8, it consists of a 1 ft-long beam with a dial gage with two-inch travel graduated in thousandths of an inch at one end and a micrometer at the other end. A fixed pod, located in between, assures the device to rest in equilibrium on the slab surface. A level, on top mid-surface of the beam indicates the horizontal position while it is adjusted manually using the micrometer. The readings can be taken once the complete horizontal position is reached.

As shown in Figure 3.9, small square metal plates were installed, six inches apart, on the Test Slab surface at different positions. These plates provided not only reference points for use in the slab deflection profile analysis but were also means of equilibrium support for the measuring instrument.

The procedure followed in taking measurements on the reference plates was as follows.

The device was first placed in the position shown in Figure 3.8 with a dial gage resting on one plate, the pod on the next plate and the micrometer on the third plate. The instrument was leveled in this position using the micrometer and the respective readings of the dial gage and the micrometer were then recorded.

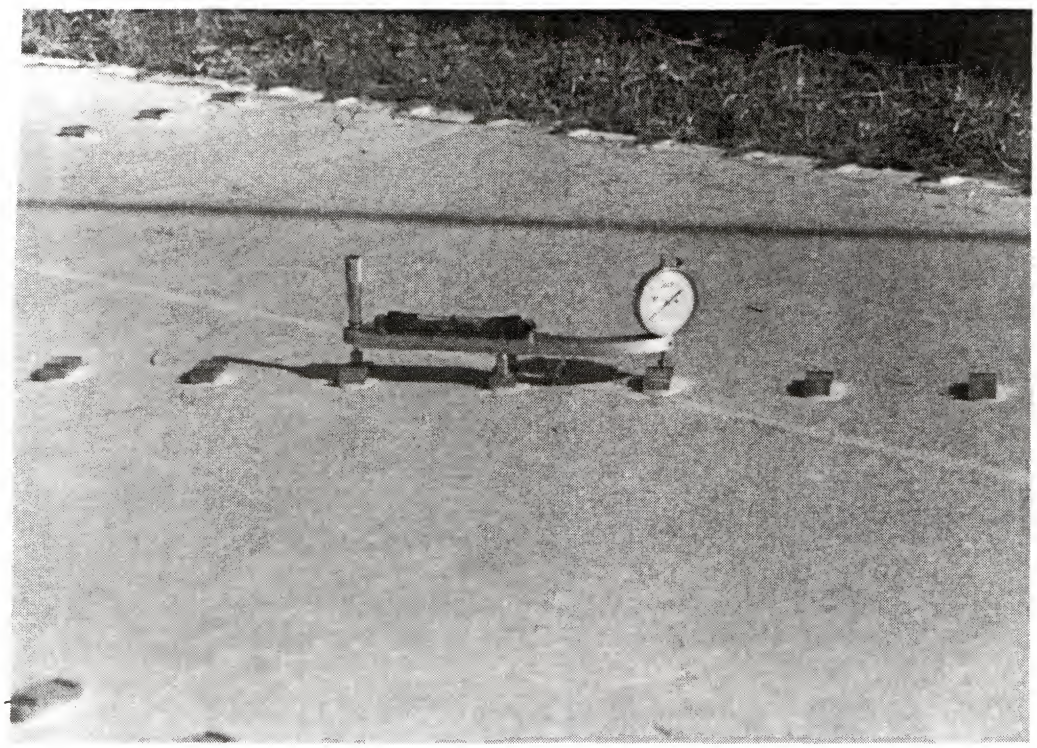

Figure 3.8 Mechanical Device Used in Mesuring Slab Deflection Profiles

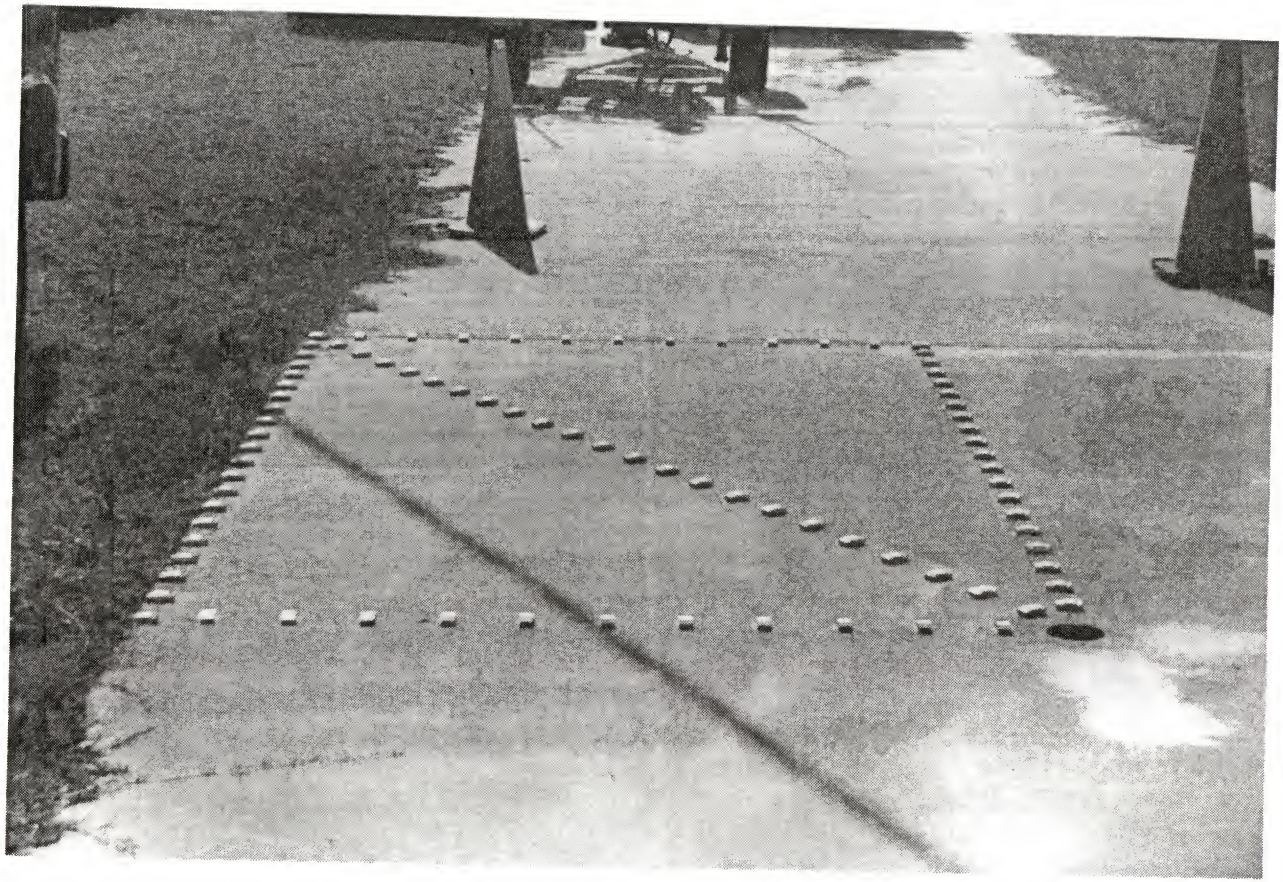

Figure 3.9 Layout of the Slab Profile Measuring Postions

The relative deflection measurement of the two locations, which are one-foot apart, is given by the algebraic difference between the dial gage and micrometer respective readings. Before starting the test, the device has to be calibrated in order to able it to produce consistent and reliable readings.

The measurements were taken along the longitudinal and transversal directions of the slab and, also, along the joint and edge. The layout of the testing positions on the Test Slab is shown in Figure 3.9. These curl readings are referenced to a metal rod, illustrated in Figure 3.10, driven into the subgrade at a depth where no significant movement will occur.

3.4 Laboratory Testing to Determine Elastic Moduli

A laboratory testing program was performed to determine the static and dynamic elastic moduli of typical pavement concretes used in Florida.

Typical Florida pavement concretes were prepared in the laboratory and used in this testing program. Four different mixes were made using four different aggregates, namely #89 Brooksville limestone, #67 Brooksville limestone, #67 Calera limestone and #67 river gravel.

In order to have a good base for data analysis, two replicate batches per mix were made. From each batch of concrete, two 6x6x30-inch beam specimens and six 6x12-inch cylindrical specimens were made. Two half-inch strain gages were attached to the bottom of each beam specimen, at mid-length in longitudinal direction. Three other gages were attached to the side of each cylinder specimen at 120° from one another.

3.4.1 Measurement of Dynamic Elastic Modulus

The concrete beam specimens were supported at their nodal positions two inches from its ends. The strain gages were connected to the signal conditioner which was hooked up to a computer-transformed oscilloscope in a same manner as previously described. The loading/vibrating device was

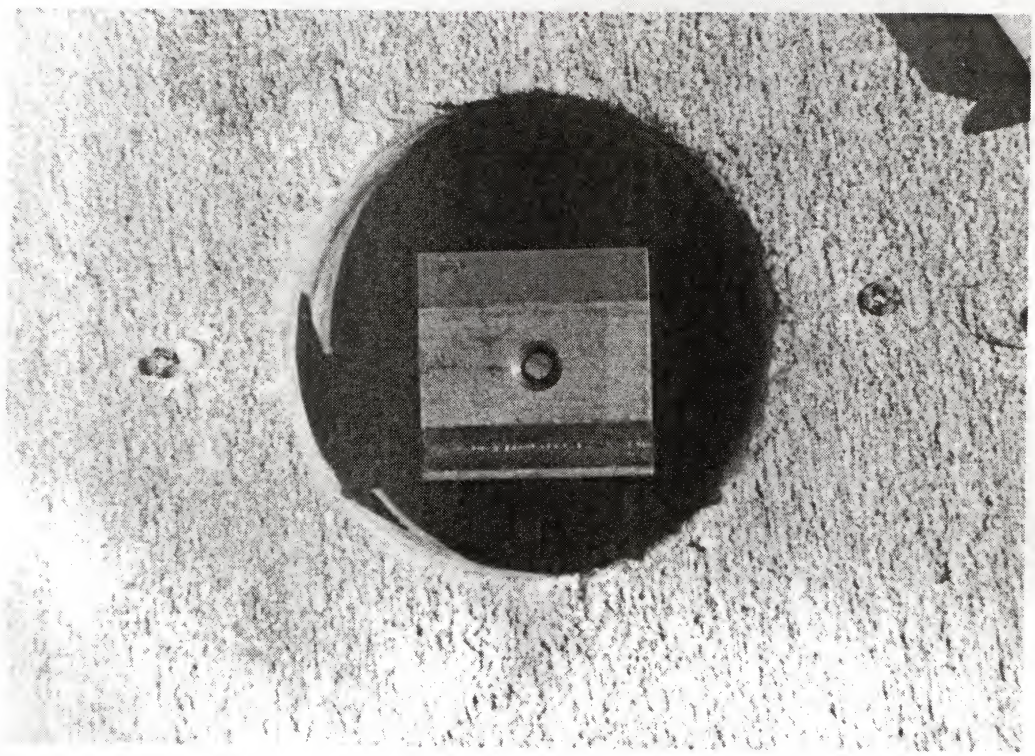

Figure 3.10 Curl Readings Metal Rod Reference Located at the Slab Center

a MTS machine. The frequencies used were 1, 3, 5 and 7 Hz. A flexural third-point loading of 1 kip was adopted for the beams and a compressive load of approximately 20 kips for the cylinders. Strain waves were recorded at 0, 300, 700, 1000, 2000, 3000, 4000, and 5000 cycles at each respective frequency. Mean peak value of these strain waves, relatively to the number of gages, was used to compute the dynamic modulus for each frequency and corresponding cycle.

3.4.2 Measurement of Static Elastic Modulus

For the determination of the elastic modulus of each concrete specimen, the strain gages were connected to and calibrated with Vishay/Ellis strain indicator. Strain readings from the strain gages were recorded at every 500 pound and 3000 pound load intervals for cylinders and beams, respectively, as the concrete specimen was loaded in the standard compressive strength test. The means of the strain readings, relatively to the number of gages, were used to plot the stress-strain diagrams to be used for determination of the modulus of elasticity. The modulus value is the secant modulus at one-half of the compressive strength, f'_c.

CHAPTER 4
TEMPERATURE VARIATIONS AND CURLING IN CONCRETE PAVEMENTS

4.1 Introduction

Daily temperature fluctuation within the concrete slab is an important factor affecting the concrete pavement behavior. The thermally-induced slab movements could influence significantly (a) the load transfer between adjacent slabs and (b) the degree of support offered by the subgrade, which affect the maximum load-induced stresses in the slab and, consequently, the durability or the life expectancy of the structure. Temperature data are, therefore, of value in computing displacements of the slab or the curling stresses due to temperature differences within the slab.

A parameter generally used to analyze the effect of temperature gradient is the temperature differential (DT), which is the algebraic difference between the temperatures of the top and bottom surfaces of a concrete slab. It is a positive value when the temperature at the top is higher than that of the bottom, and it is negative when the upper surface is cooler than the bottom of the slab.

This chapter deals with the thermal-induced vertical displacement, in the absence of loads other than gravity, measured at selected locations on the surface of the test slabs. As background information on slab curling, it also presents the results of the analysis of temperature data obtained from the concrete pavement test slabs located at the FDOT Materials Office. The data have been arranged to show the following: (1) relation between daily range in air temperature and daily range in

slab temperature; (2) typical hourly differentials in temperature between top and bottom of slab; (3) temperature gradient from top to bottom of slab.

This chapter also includes an experimental and analytical study carried out to determine and model the actual temperature distribution within typical concrete pavement slabs in order to evaluate its different components.

4.2 Temperature Data Analysis

4.2.1 Observed Air and Concrete Slab Temperatures

It is well known that the air temperature and solar radiation have a direct influence on the performance of a concrete pavement. Figures 4.1 through 4.3 show typical daily variations of air and top pavement temperatures measured at the test slabs. From these figures, it can be observed that a close relationship between daily air and pavement temperatures existed. These variations of temperature follow a pattern that could be approximated by a sine wave. The pavement temperatures were up to 30°F higher than the air temperatures. This temperature difference is higher during the mid-afternoons when there is greater slab absorption of solar heat due to a greater angle of incidence of the sun's rays, and it is lower at the times when the air temperature is near the average air temperature in a cycle as shown in Figures 4.4 through 4.6.

It can be also observed that maximum temperatures occur at mid-days between 12 P.M. to 4 P.M. and minimum temperatures occur in early mornings. If pavement and air temperatures reach their respective peak simultaneously, minimum pavement temperature would occur approximately one hour after the minimum air temperature is reached.

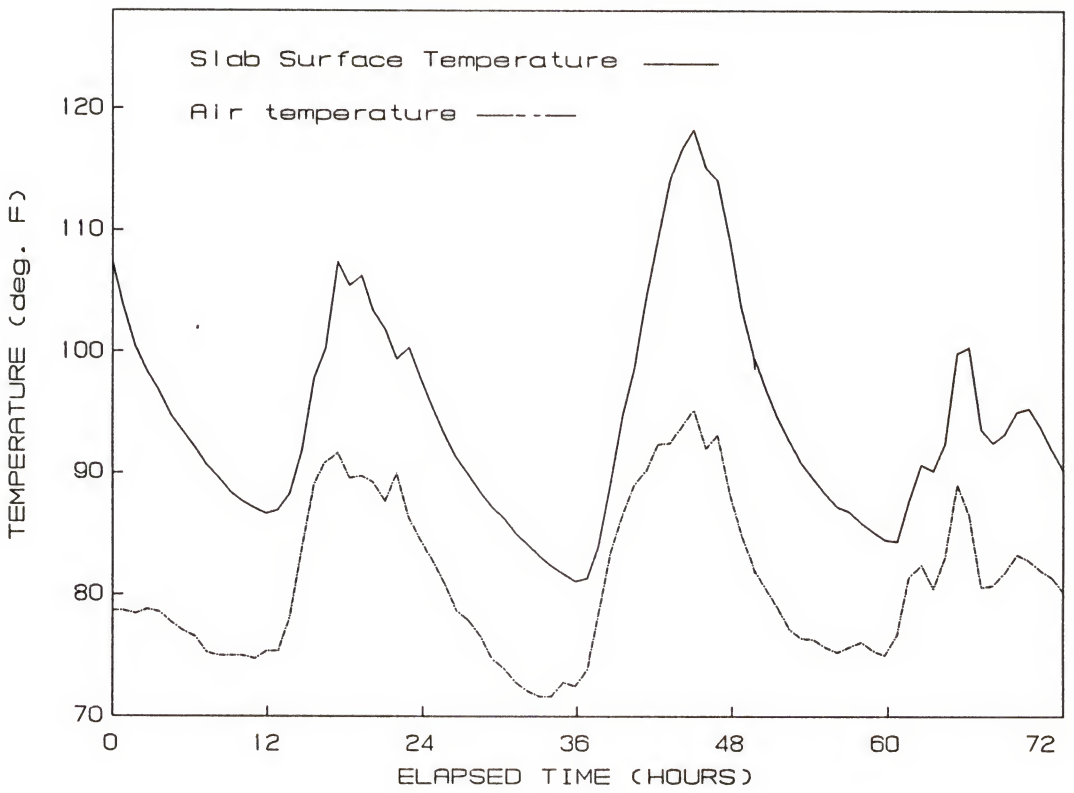

Figure 4.1 Typical Variations of Air and Slab Surface Temperatures as Recorded on the Test Slabs, Starting on 07/25 at 7:00 P.M.

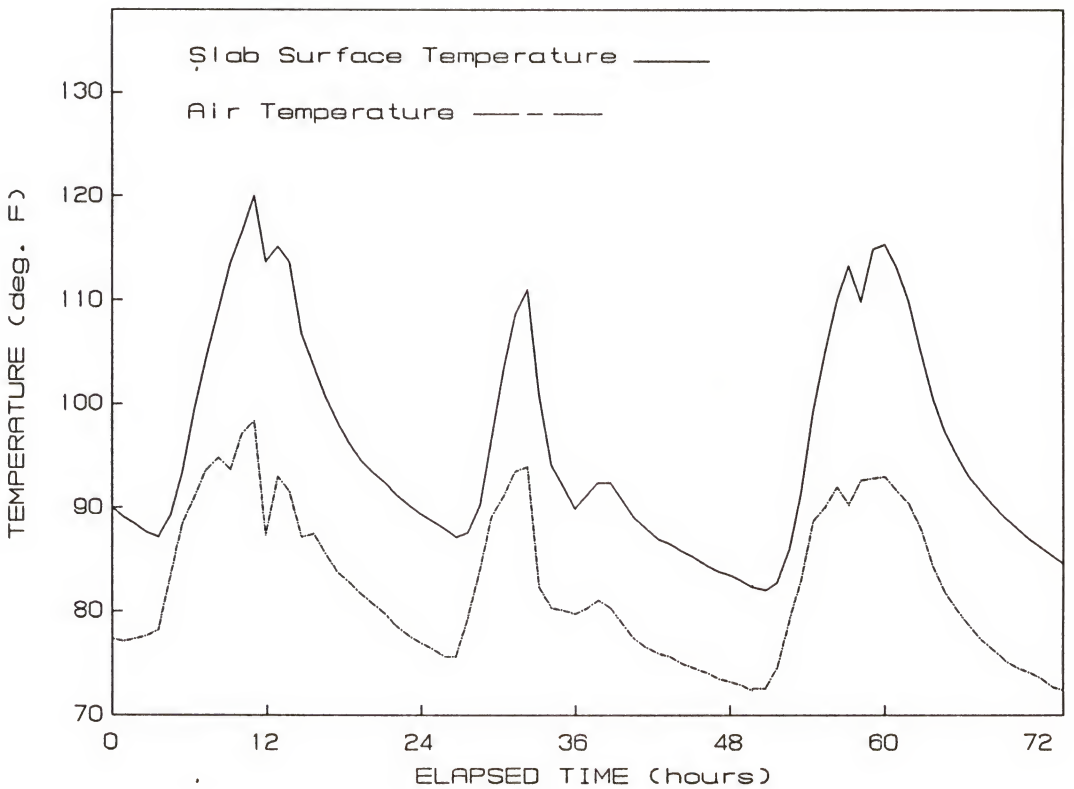

Figure 4.2 Typical Variations of Air and Slab Surface Temperatures as Recorded on the Test Slabs, Starting on 08/02 at 4:00 A.M.

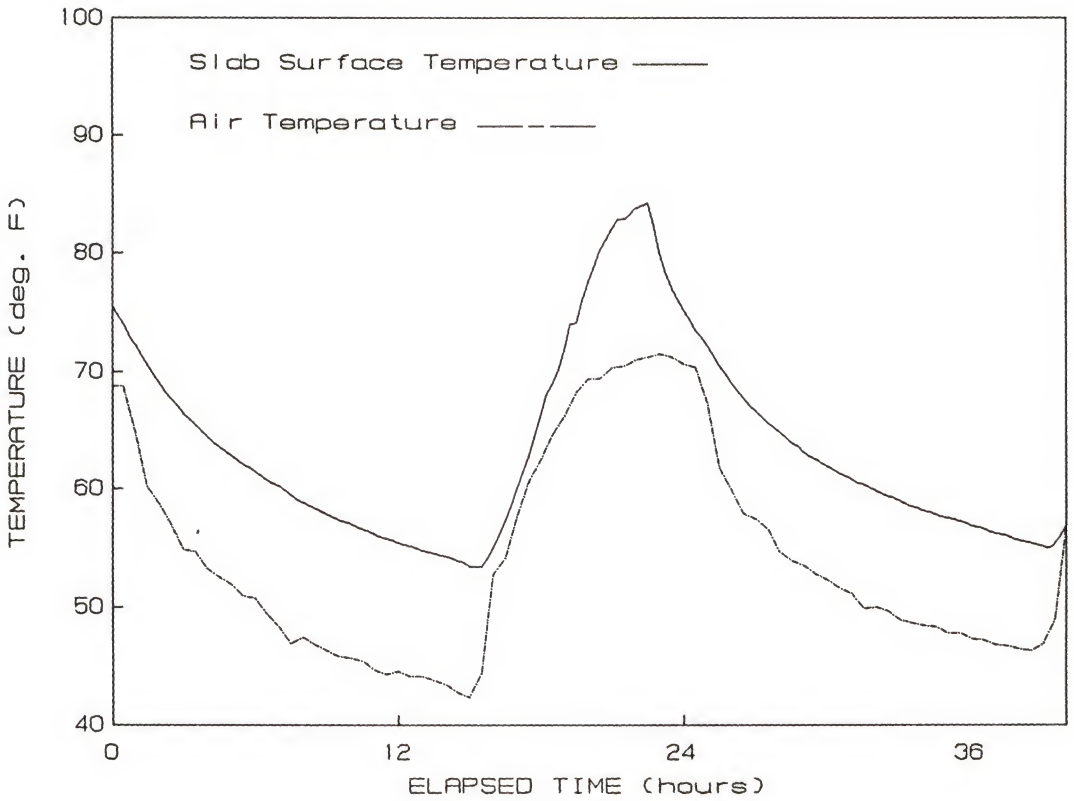

Figure 4.3 Typical Variations of Air and Slab Surface Temperatures as Recorded on the Test Slabs, Starting on 11/19 at 4:00 P.M.

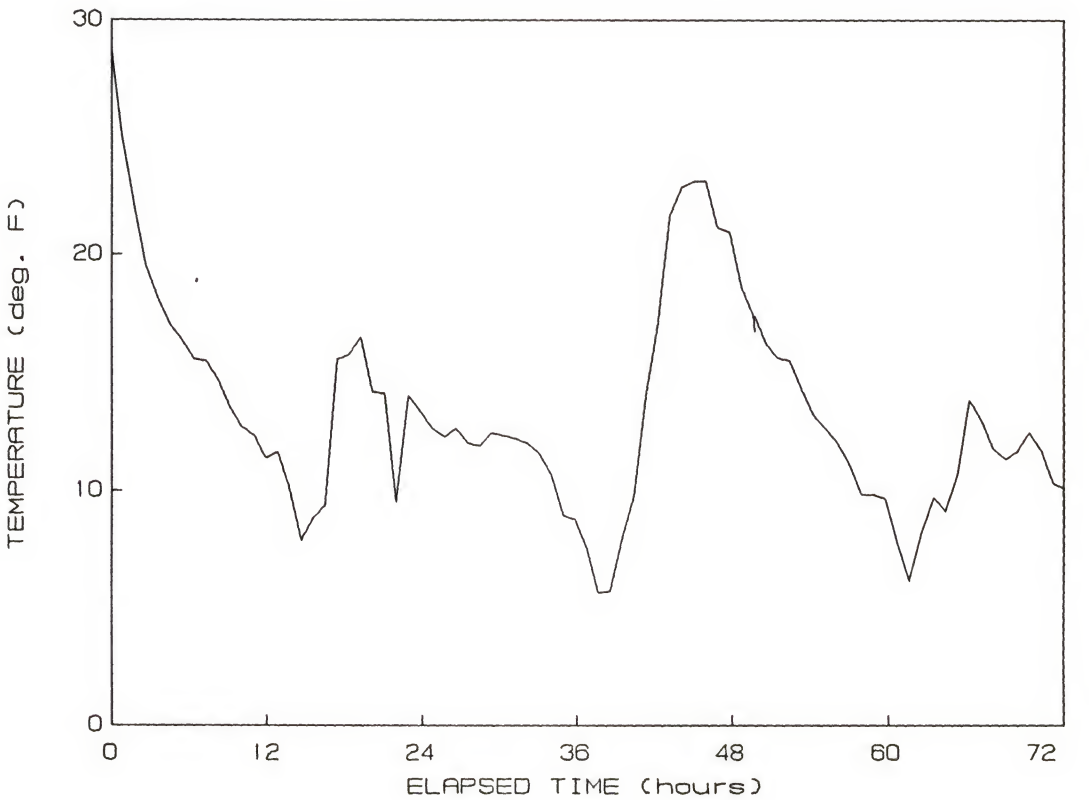

Figure 4.4 Typical Variation of Temperature Differential Between Air and Slab Surface as Recorded on the Test Slabs, Starting on 07/25 at 7:00 P.M.

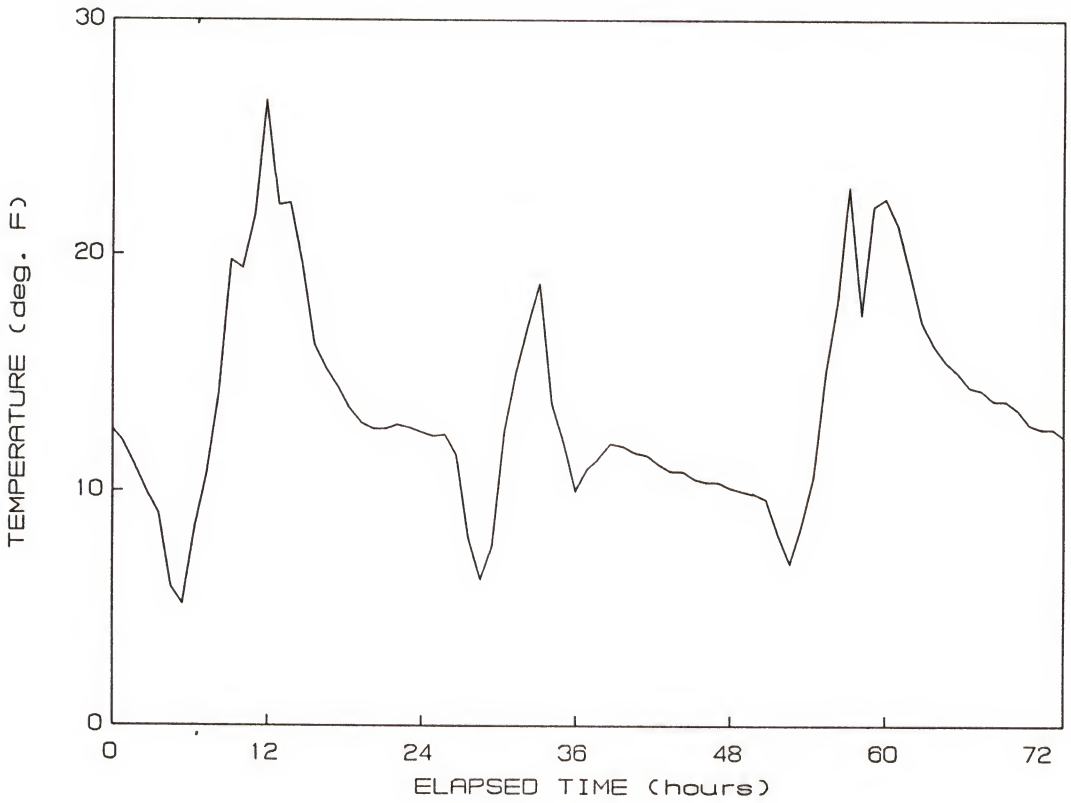

Figure 4.5 Typical Variation of Temperature Differential Between Air and Slab Surface as Recorded on the Test Slabs, Starting on 08/02 at 4:00 A.M.

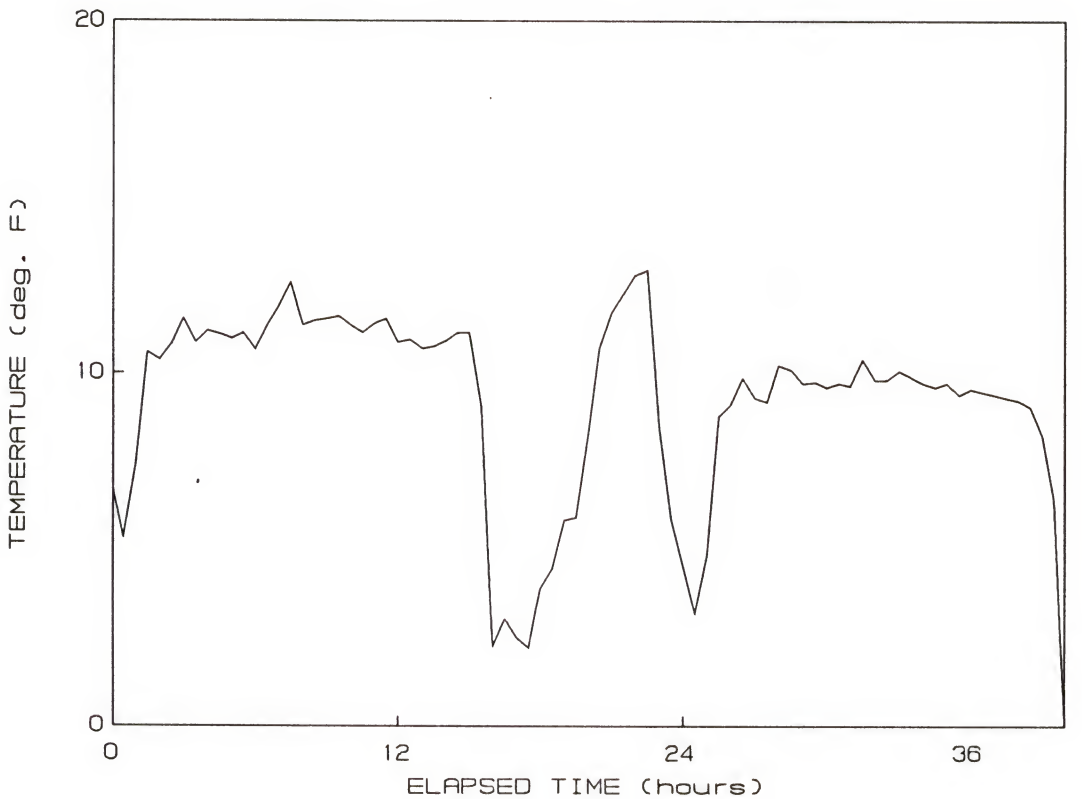

Figure 4.6 Typical Variation of Temperature Differential Between Air and Slab Surface as Recorded on the Test Slabs, Starting on 11/19 at 4:00 P.M.

4.2.2 Temperature Differential

The average temperature of a concrete slab varies daily and yearly. The daily temperature changes are of a major importance to deflection measurements since the subsequent temperature gradient can vary significantly during a 24-hour cycle, thus affecting the curling of the concrete slabs.

As stated previously, temperature differential (DT) is the parameter commonly used to analyze the effect of temperature gradient. It is the result of the slow conduction of heat in concrete, and is a function of the thermal properties of concrete and the thickness of the slab.

One of the methods for predicting temperature differentials is by using the Fourier's law governing the heat conduction in a body. If the respective quantities of heat absorbed and released by a body are assumed to be equal, the Fourier's law could be expressed in the following equation:

$$\frac{dT}{dt} = \lambda / c\rho \left(\frac{\partial^2 T}{\partial x^2} + \frac{\partial^2 T}{\partial y^2} + \frac{\partial^2 T}{\partial z^2} \right) \qquad (4.1)$$

where

T = body temperature

t = time

p = mass density

λ = thermal conductivity of the body

c = specific heat of the body

x,y = coordinates in the horizontal plane, and

z = coordinate perpendicular to the plane (x,y).

If the horizontal-plane thermal flow is neglected, the equation would become:

$$dT/dt = a\, d^2T/d^2z \qquad (4.2)$$

where a is the diffusivity coefficient.

Typical temperature differentials as recorded on the test slabs are shown in Figures 4.7 through 4.9. The difference in temperature is plotted as a plus ordinate when the top of the slab is warmer than the bottom, and as minus ordinate when the top is cooler than the bottom. From these figures, it can be noticed that the variations of temperature differentials also follow a pattern that approximates a sine wave similar to the one of air and pavement temperatures. Generally, the temperature differential is positive during the daytime and negative during the nighttime.

As recorded during the present study, the maximum positive temperature differential occurred between 1 P.M. to 4 P.M. while the negative temperature differential reached its peak at about 6 A.M. The zero temperature differential was observed at approximately 9 A.M. and 7 P.M. In addition, a maximum temperature differential of 31°F, corresponding to 3.4°F per inch of slab depth, was measured.

Such temperature differentials produce warping stresses which are of importance in the design of concrete pavements.

4.2.3 Temperature Distribution Throughout the Slab Depth

Typical variations of temperature at different slab depths are shown in Figures 4.10 through 4.12. These variations follow a sine wave pattern with a phase shift or lag at different slab depths due to the rate of solar heat absorption. The magnitude of temperature variation decreases with the slab depth. At nighttime, slab temperatures are lower at the surface than at the bottom of the slab. At day time, after a short transition, the phenomenon is reversed.

These observations are typical of the temperature attenuation and phase shift characteristics of heat conduction in a body.

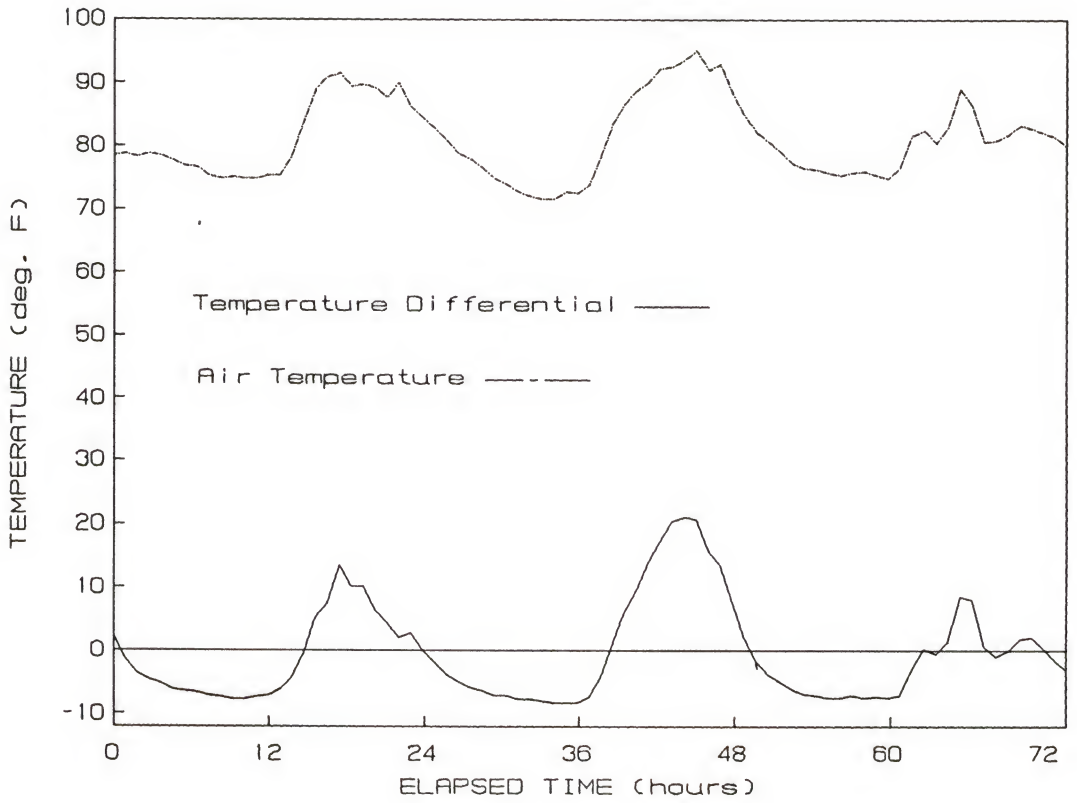

Figure 4.7 Typical Variations of Temperature Differential Between Top And Bottom of Slab and Air Temperature as Recorded on the Test Slabs, Starting on 07/25 at 7:00 P.M.

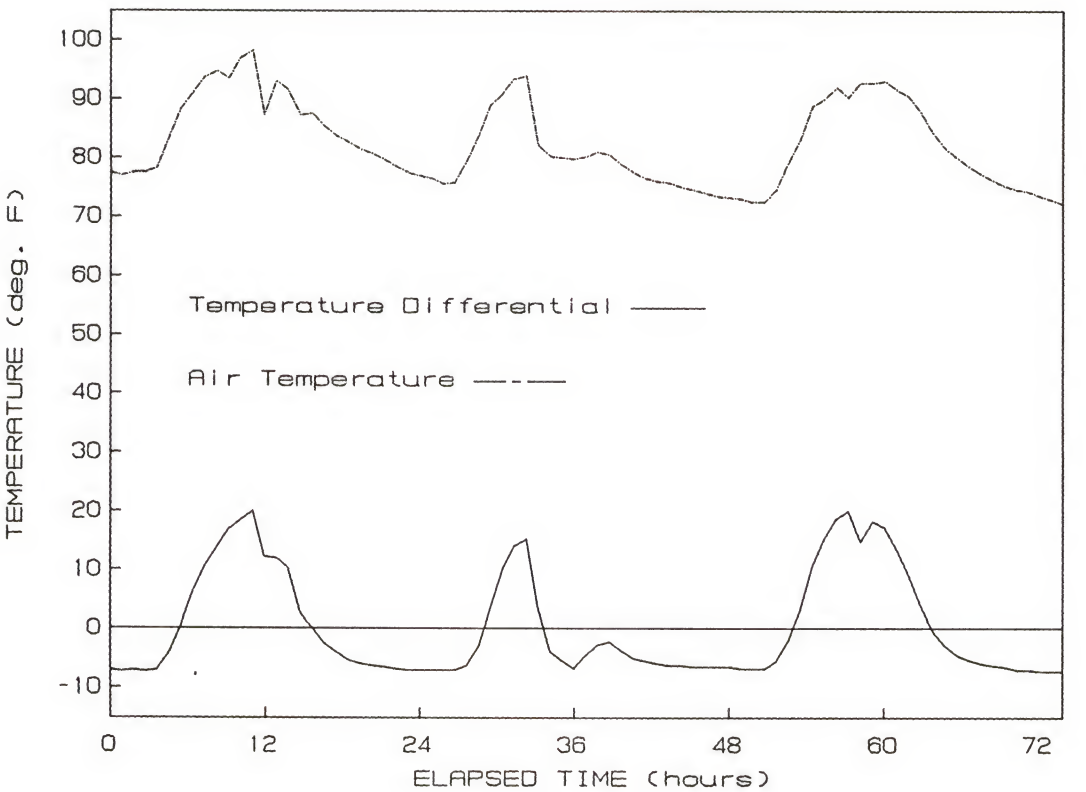

Figure 4.8 Typical Variations of Temperature Differential Between Top and Bottom of Slab and Air Temperature as Recorded on the Test Slabs, Starting on 08/02 at 4:00 A.M.

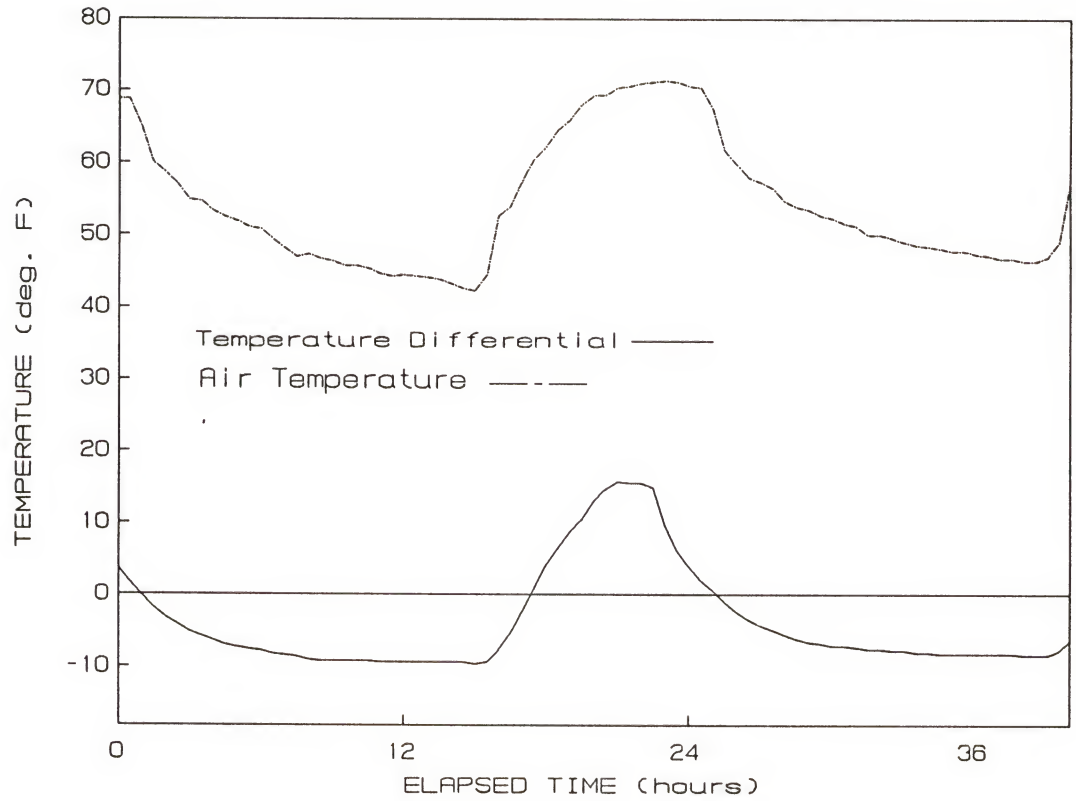

Figure 4.9 Typical Variations of Temperature Differential Between Top and Bottom of Slab and Air Temperature as Recorded on the Test Slabs, Starting on 11/19 at 4:00 P.M.

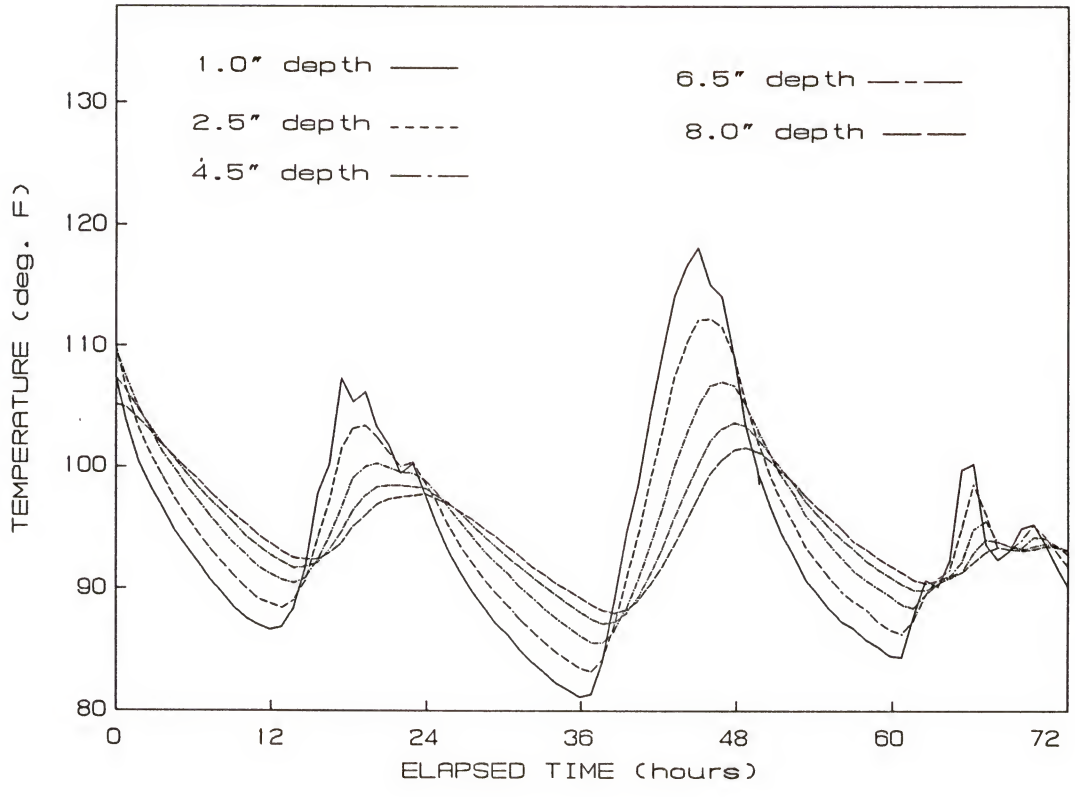

Figure 4.10 Typical Variations of Temperature at Different Slab Depths as Recorded on the Test Slabs, Starting on 07/25 at 7:00 P.M.

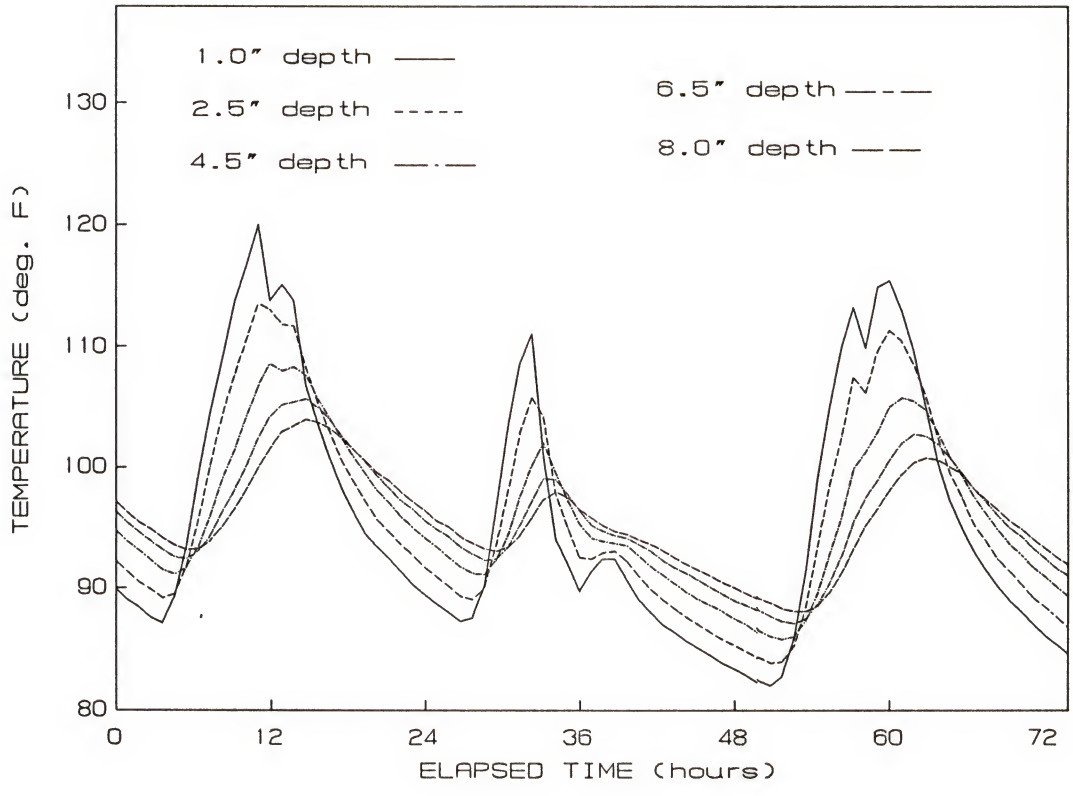

Figure 4.11 Typical Variations of Temperature at Different Slab Depths as Recorded on the Test Slabs, Starting on 08/02 at 4:00 A.M.

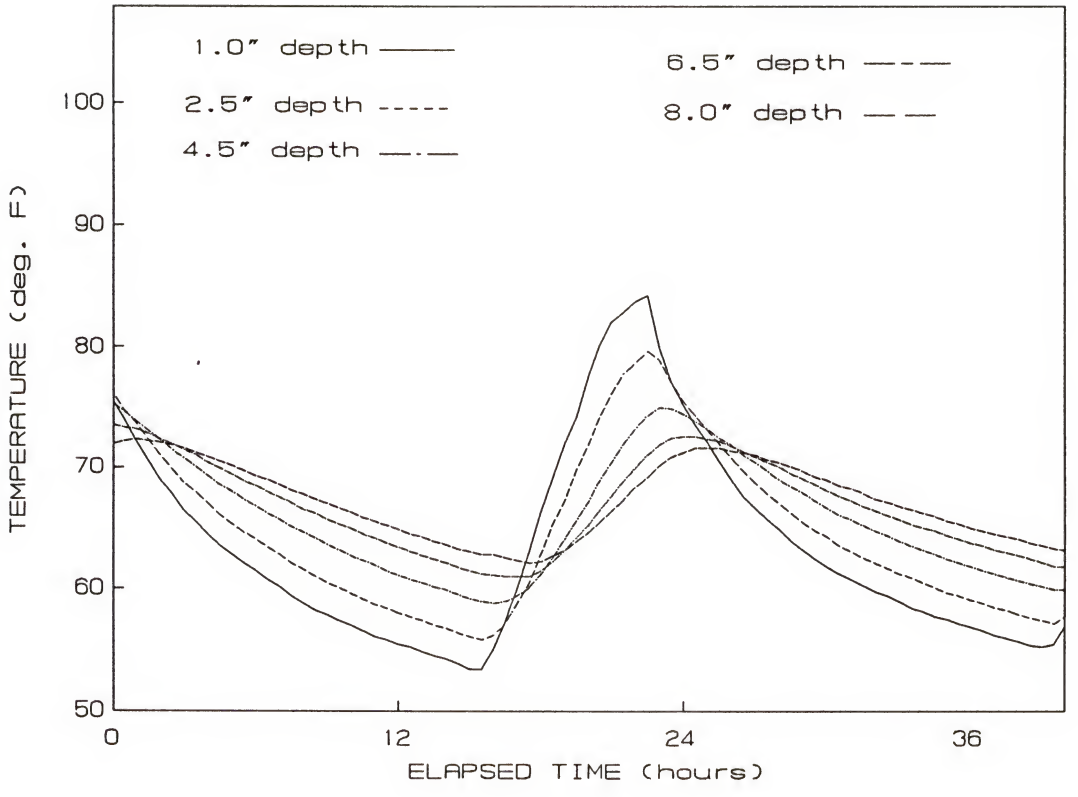

Figure 4.12 Typical Variations of Temperature at Different Slab Depths as Recorded on the Test Slabs, Starting on 11/19 at 4:00 P.M.

According to Bergstrom [45], the temperature at any given depth z below the surface varies according to the following equation:

$$T = a \cdot \exp\left(-\frac{z}{x}\sqrt{\frac{\pi}{T}}\right) \cdot \sin\left(\frac{2\pi t}{T} - \frac{z}{x}\sqrt{\frac{\pi}{T}}\right) \qquad (4.3)$$

where T = 24 hours

t = time

a = amplitude

x = diffusivity = $\lambda/\gamma c$

λ = thermal conductivity

c = specific heat

γ = weight per unit volume.

Figure 4.13 illustrates a typical daily variation in pavement temperature at different depths according to formula (4.3). It can be seen that the minimum temperature on top of the slab occurred at 6:00 A.M. when the maximum negative temperature differential was also reached. However the maximum temperature on top occurred at about 6:00 P.M.

In a recent study [46], Faraggi et al. gave another expression, similar in the general form to that of Bergstrom's, of the temperature at any depth z at a given time t, by solving the equation (4.2) based on the assumption of a sinusoidal temperature variation over a period of time. That solution is expressed as:

$$T_{zt} = T_M + t_o \cdot \exp\left(-z\sqrt{\frac{\pi}{aT}}\right) \cdot \sin\left(\frac{2\pi t}{T} - z\sqrt{\frac{\pi}{aT}}\right) \qquad (4.4)$$

where

T_{zt} = temperature at depth z at instant t

t_M = average temperature of bottom or surface, or both, over an interval of 24 hr

t_o = range of temperature variation in the pavement surface during the 24-hr interval

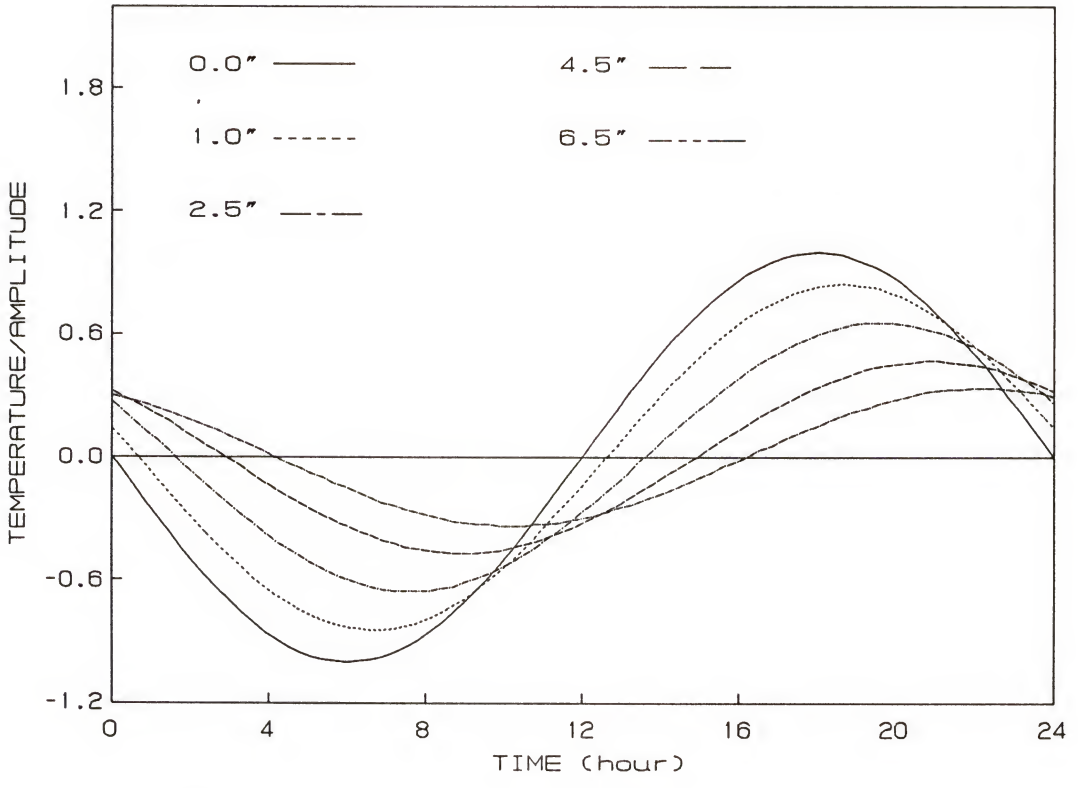

Figure 4.13 Typical Daily Temperature Variation Profile at Different Slab Depths According to Bergstrom's Model.

T = period of cyclic variation in temperature; and

a = diffusivity coefficient.

4.2.4 Temperature Gradient Analysis

Several methods for rigid pavement design and analysis that take into account the effect of the temperature fluctuation have been developed over the years. These methods are all based, for simplicity, on the assumption that this temperature variation, from top to bottom of the slab, is linear, eventhough the nonlinearity of the temperature distribution throughout the slab has long been recognized. Even with the advent of the computer age, most of the currently used finite-element computer programs that allow considerable freedom in loading configuration, flexural stiffness and boundary conditions, such as WESLIQUID [21], WESLAYER [21], JSLAB [22], ILLI-SLAB [33] and FEACONS [1,34], consider only the linear temperature gradient effects on concrete slab.

The nonlinearity of temperature distribution within the concrete pavement slab was first measured in the Arlington Road Tests in the early 1930's [13]. In 1940, Thomlinson reached the same conclusion by assuming a simple harmonic temperature variation at the slab top surface in combination with the heat flow laws [14].

Figures 4.14 through 4.25 show the typical recorded variations in temperature distribution throughout the test slab for various time of the day at different periods of the year. From these figures, the nonlinearity of the temperature distribution is apparent. According to Lang [15], the variations from the straight line relationship are relatively small and not important in the design and warping stress computations, and consequently the temperature gradient can be approximated as linear for convenience. The validity of such an assumption and the effect of a nonlinear temperature gradient on pavement performance need to be addressed

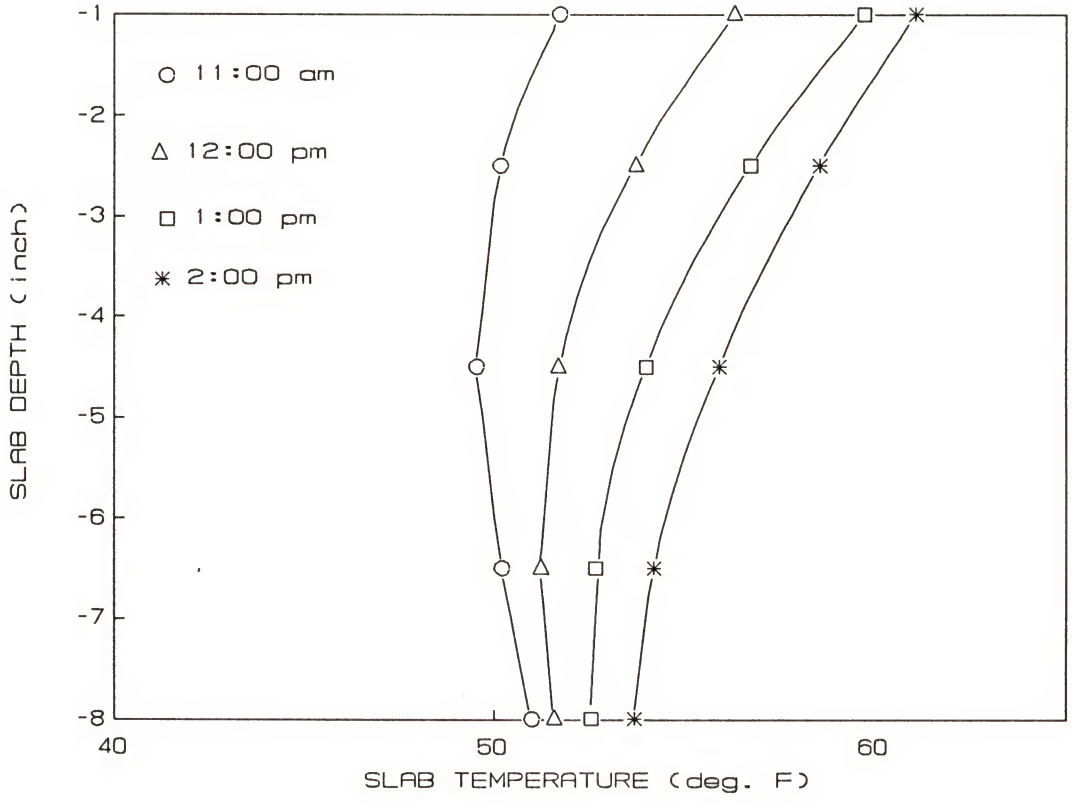

Figure 4.14 Typical Temperature Variations Througout the Test Slab Corresponding to a Positive Temperature Differential as Recorded for the Month of January

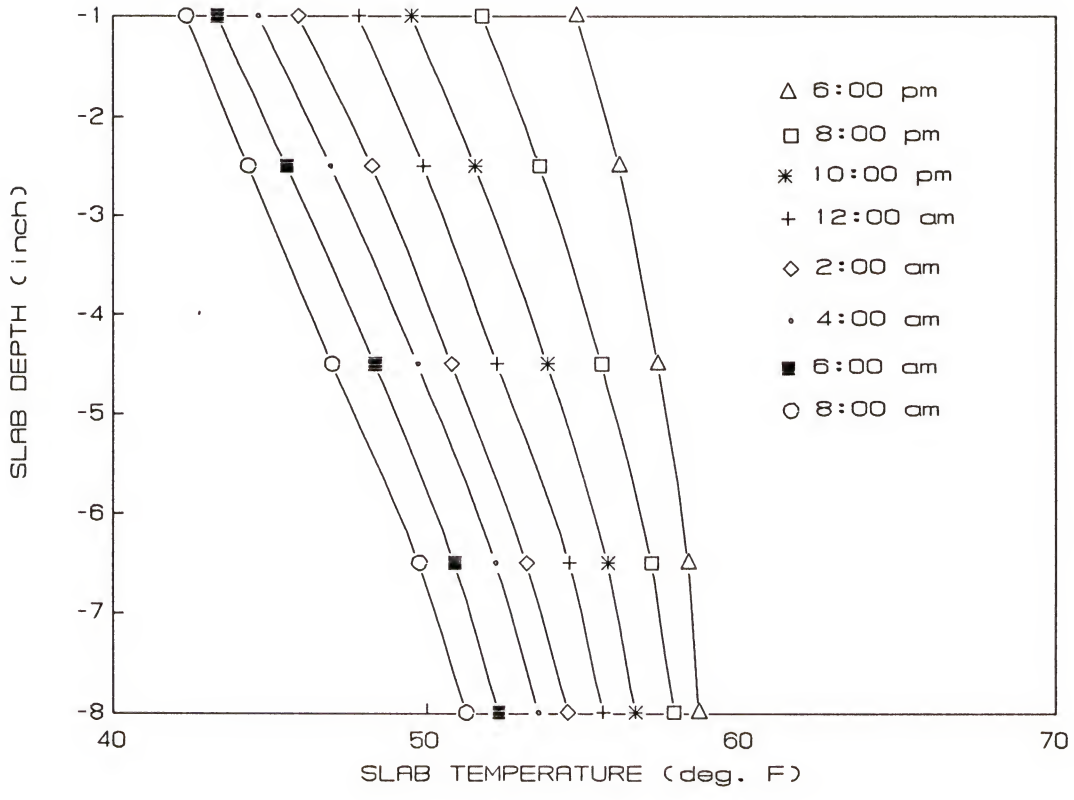

Figure 4.15 Typical Temperature Variations Througout the Test Slab Corresponding to a Negative Temperature Differential as Recorded for the Month of January

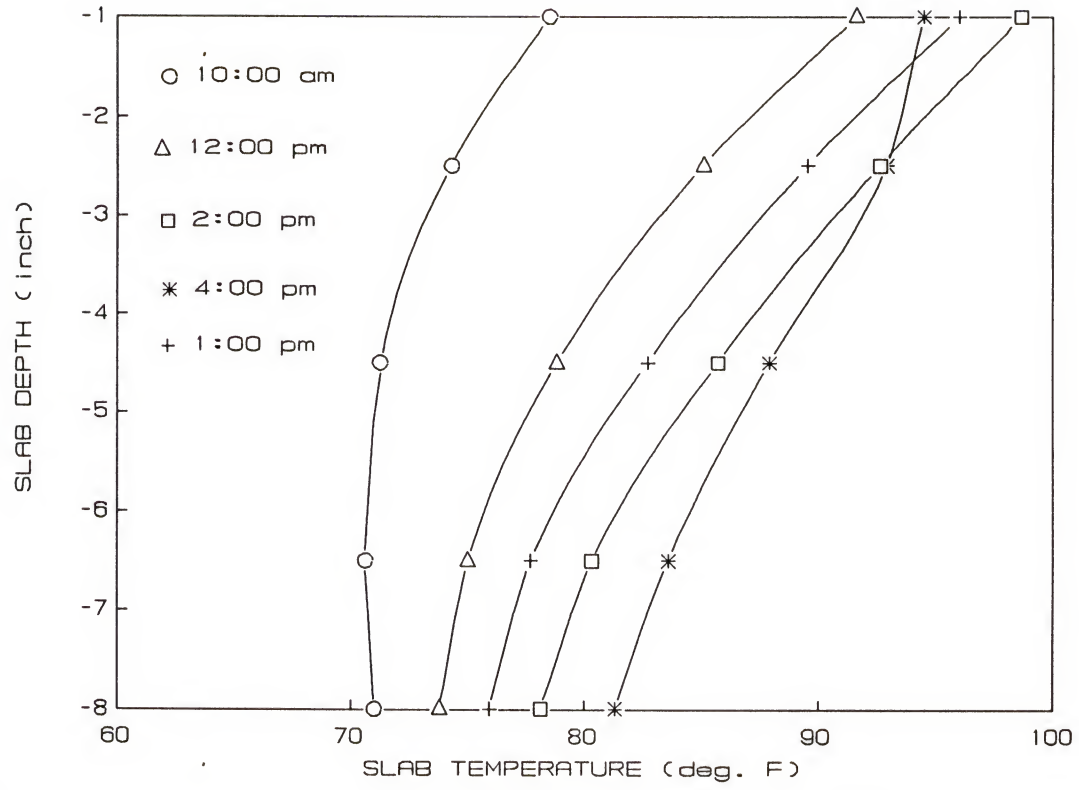

Figure 4.16 Typical Temperature Variations Througout the Test Slab Corresponding to a Positive Temperature Differential as Recorded for the Month of April

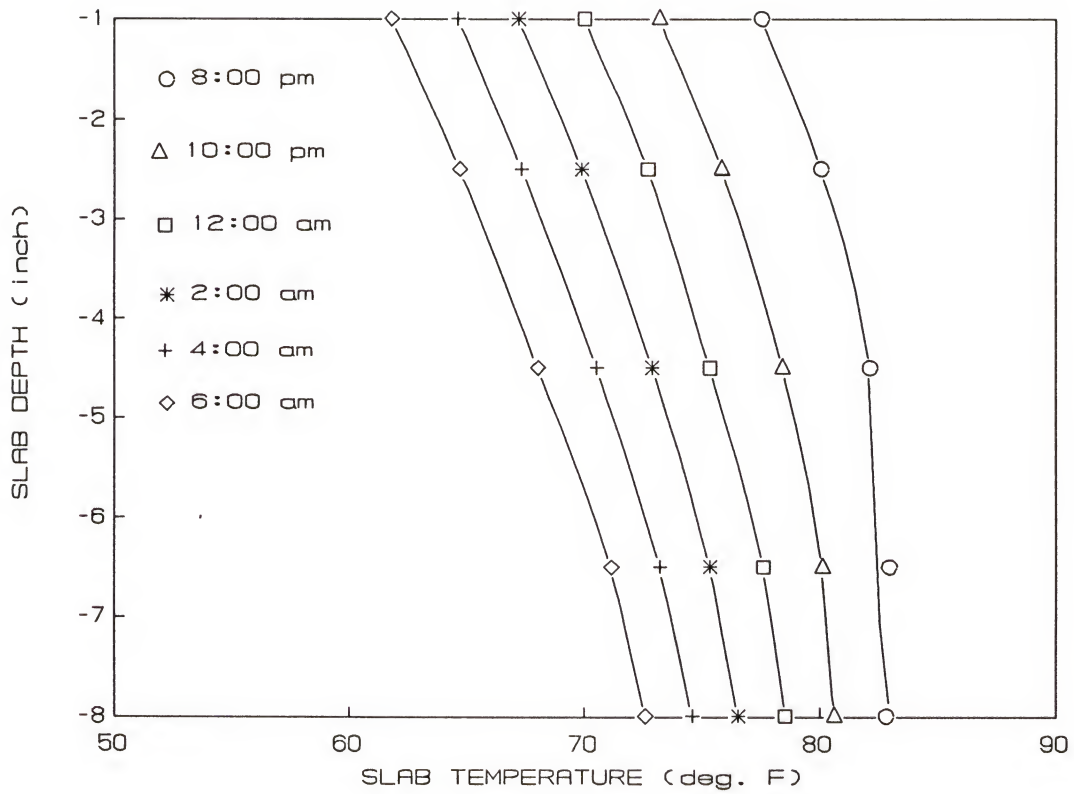

Figure 4.17 Typical Temperature Variations Througout the Test Slab Corresponding to a Negative Temperature Differential as Recorded for the Month of April

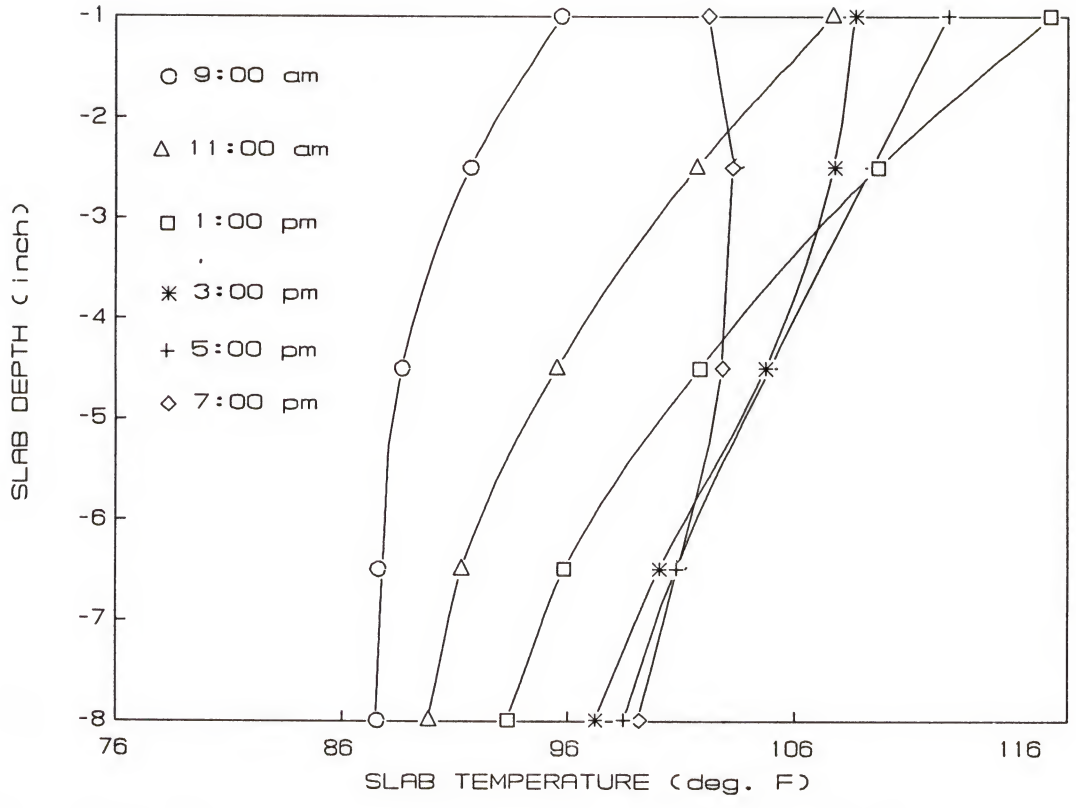

Figure 4.18 Typical Temperature Variations Througout the Test Slab Corresponding to a Positive Temperature Differential as Recorded for the Month of June

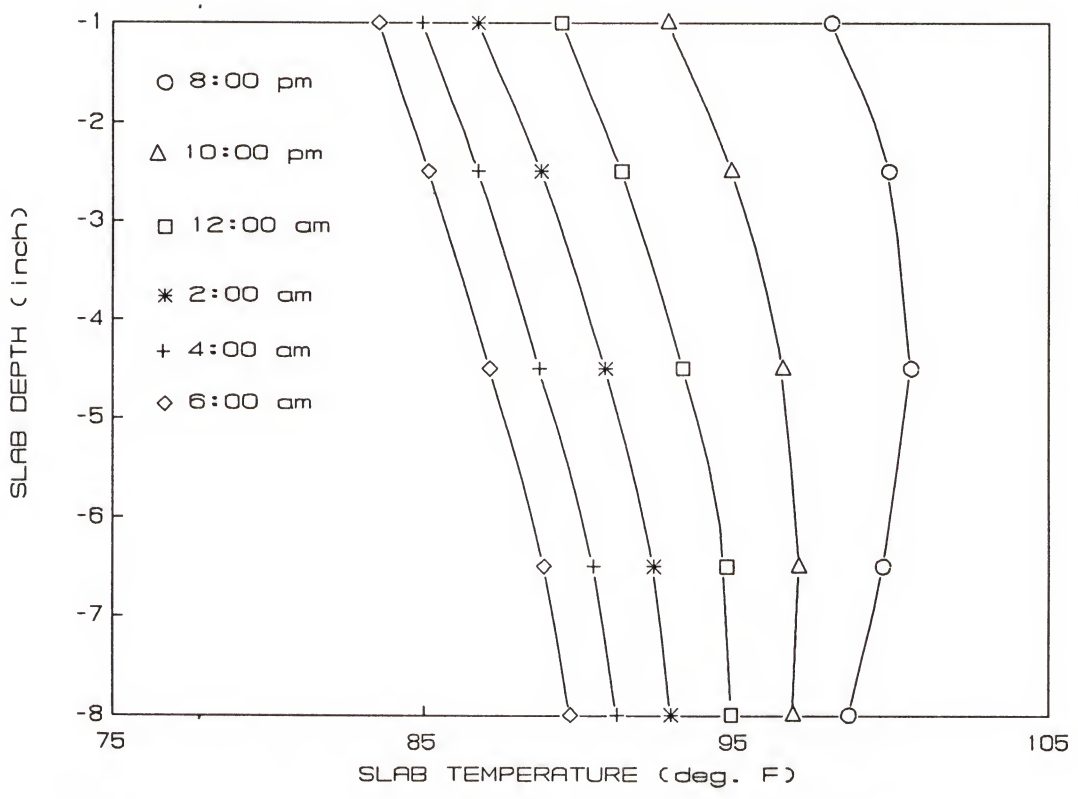

Figure 4.19 Typical Temperature Variations Througout the Test Slab Corresponding to a Negative Temperature Differential as Recorded for the Month of June

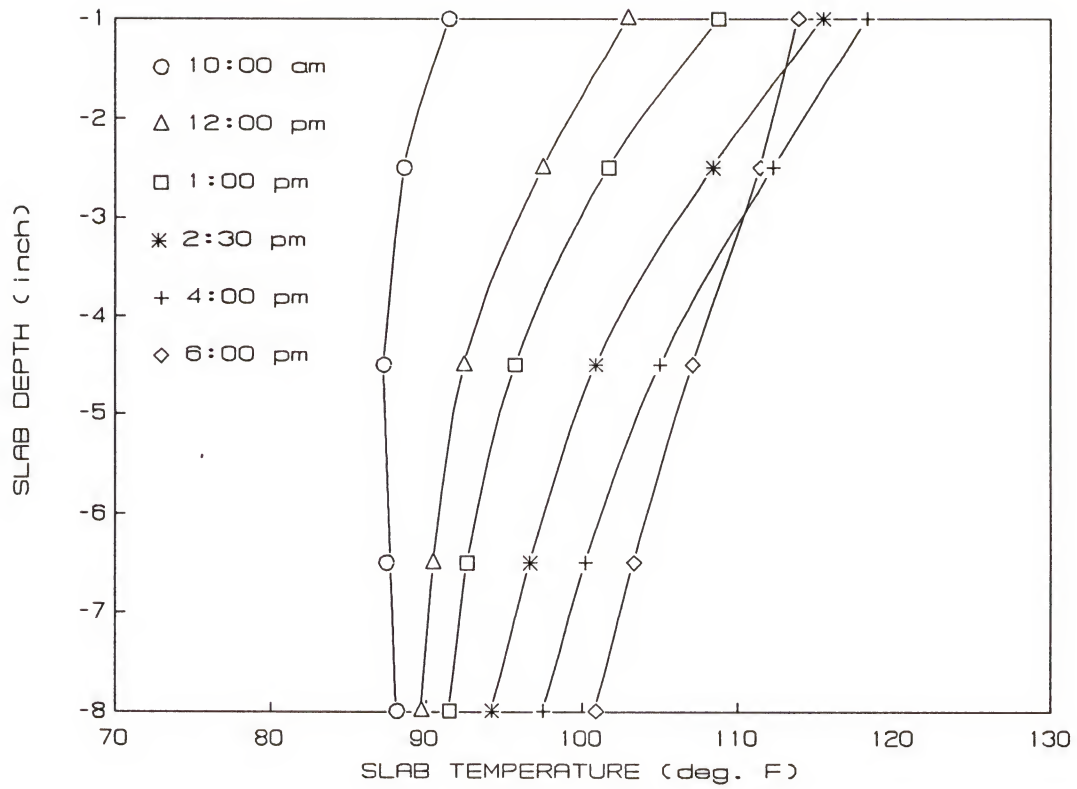

Figure 4.20 Typical Temperature Variations Througout the Test Slab Corresponding to a positive Temperature Differential as Recorded for the Month of July

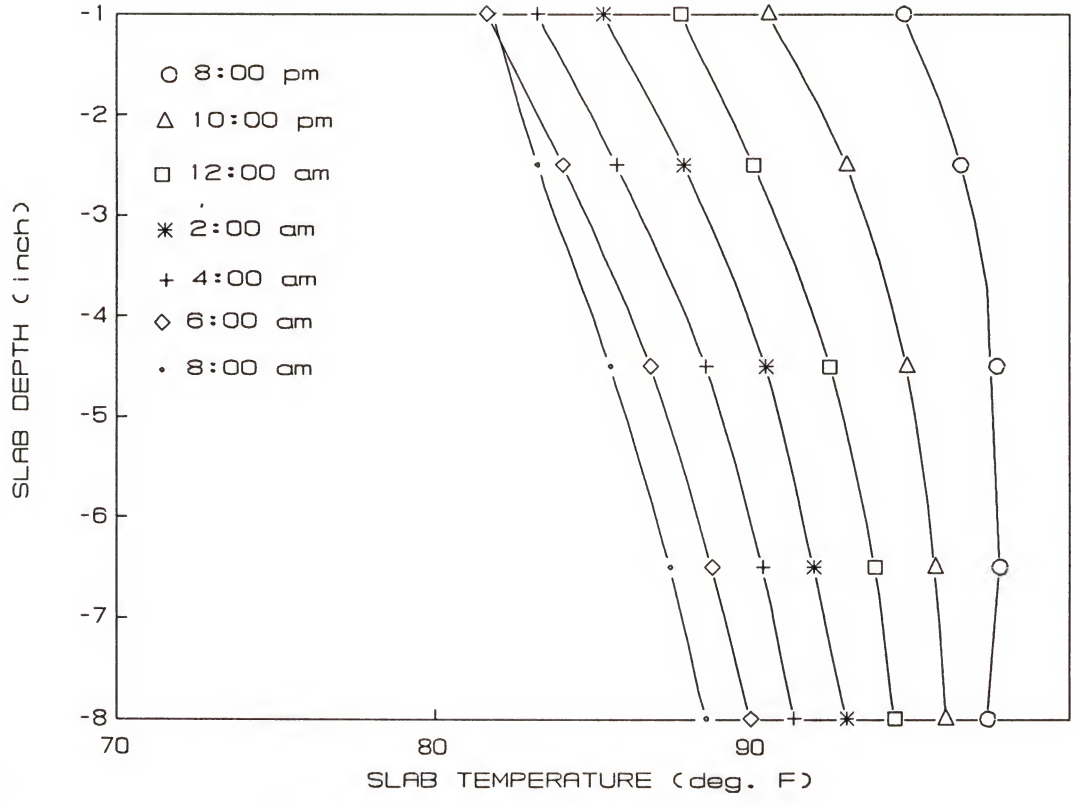

Figure 4.21 Typical Temperature Variations Througout the Test Slab Corresponding to a Negative Temperature Differential as Recorded for the Month of July

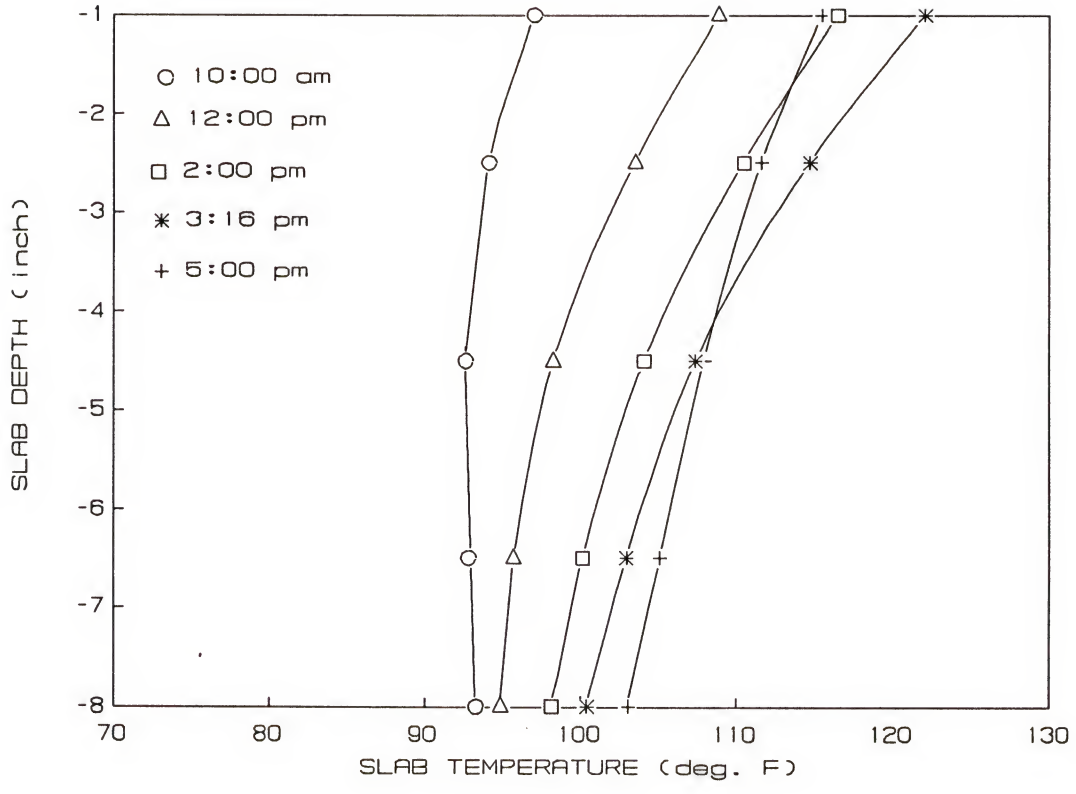

Figure 4.22 Typical Temperature Variations Througout the Test Slab Corresponding to a Positive Temperature Differential as Recorded for the Month of August

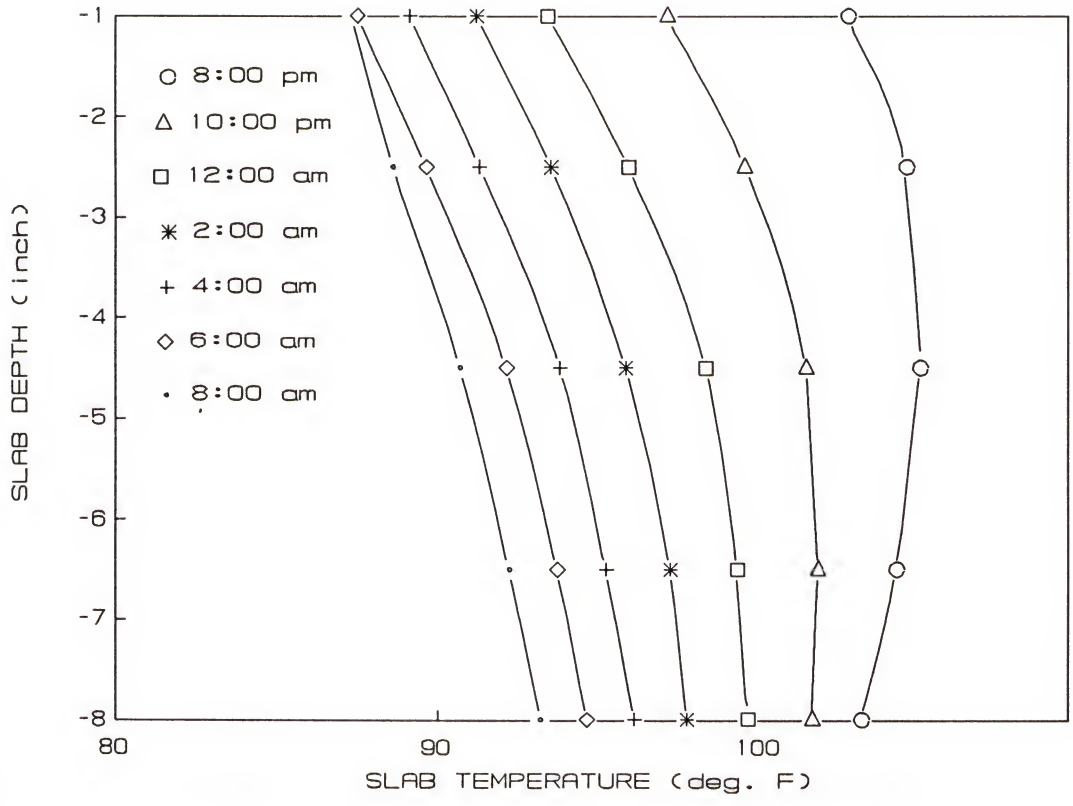

Figure 4.23 Typical Temperature Variations Througout the Test Slab Corresponding to a Negative Temperature Differential as Recorded for the Month of August

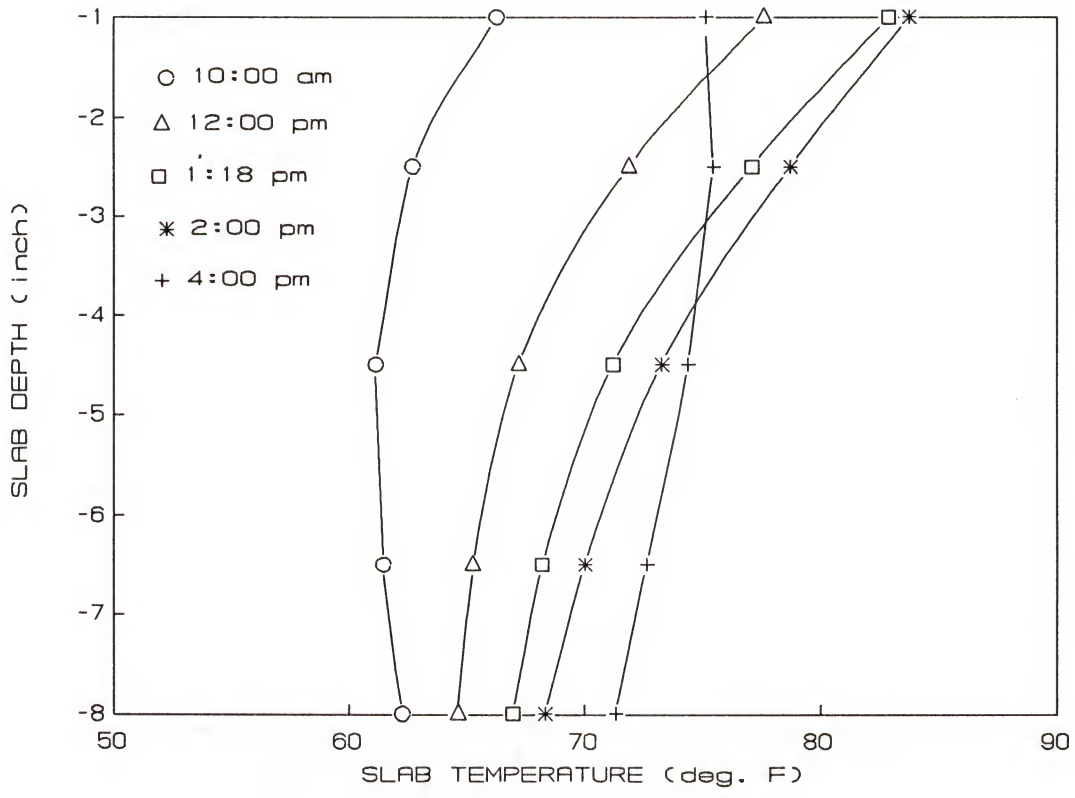

Figure 4.24 Typical Temperature Variations Througout the Test Slab Corresponding to a Positive Temperature Differential as Recorded for the Month of November

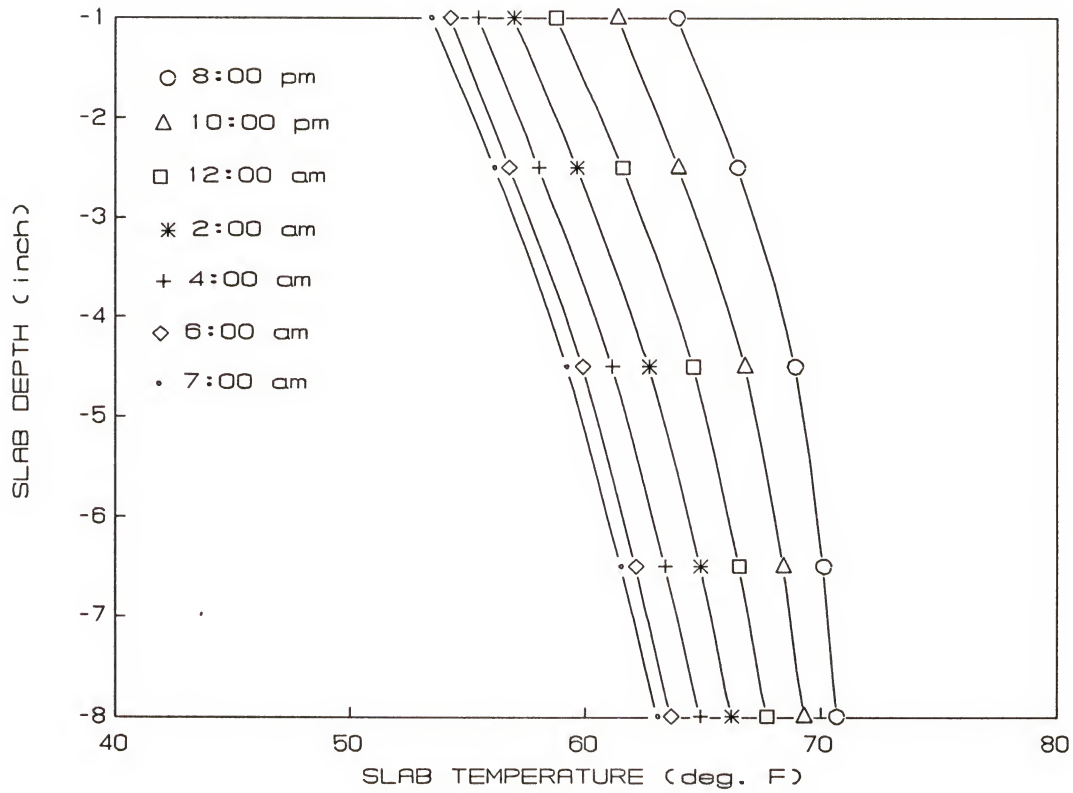

Figure 4.25 Typical Temperature Variations Througout the Test Slab Corresponding to a Negative Temperature Differential as Recorded for the Month of November

and evaluated. Subsequently, the different temperature gradient components must be characterized in order to isolate the non-linear component of it.

The following subsections deal with the analysis, evaluation and mathematical modelling of the actual temperature gradient and its different components.

4.2.4.1 Typical temperature gradient components. The temperature gradient can be typically divided into three components: (1) a component that causes axial displacement, (2) a component that causes the bending, and (3) the nonlinear component, as illustrated in Figure 4.26.

The temperature component that is related to the axial displacement, as shown in Figure 4.26(1), is taken as the average temperature throughout the slab and is determined by computing the total area under the temperature gradient curve and dividing it by the depth of the pavement slab. The curling or bending temperature component, as shown in Figure 4.26(2), is the linear variation of temperature which would produce the same moment as the moment of the area remained after subtracting the average area from the total area under the gradient curve. The nonlinear temperature, as shown in Figure 4.26(3), is determined by subtracting the two previous temperature components from the total temperature profile.

4.2.4.2 Mathematical modeling of the thermal gradient. In order to isolate and study the effect of the nonlinearity of temperature variation, a mathematical model was used. From an analysis of the temperature data, it appeared that a quadratic equation could be used to express the temperature as a function of slab depth. This is illustrated in Figures 4.27 through 4.37. The general form of the equation is:

$$t = A + By + Cy^2 \qquad (4.5)$$

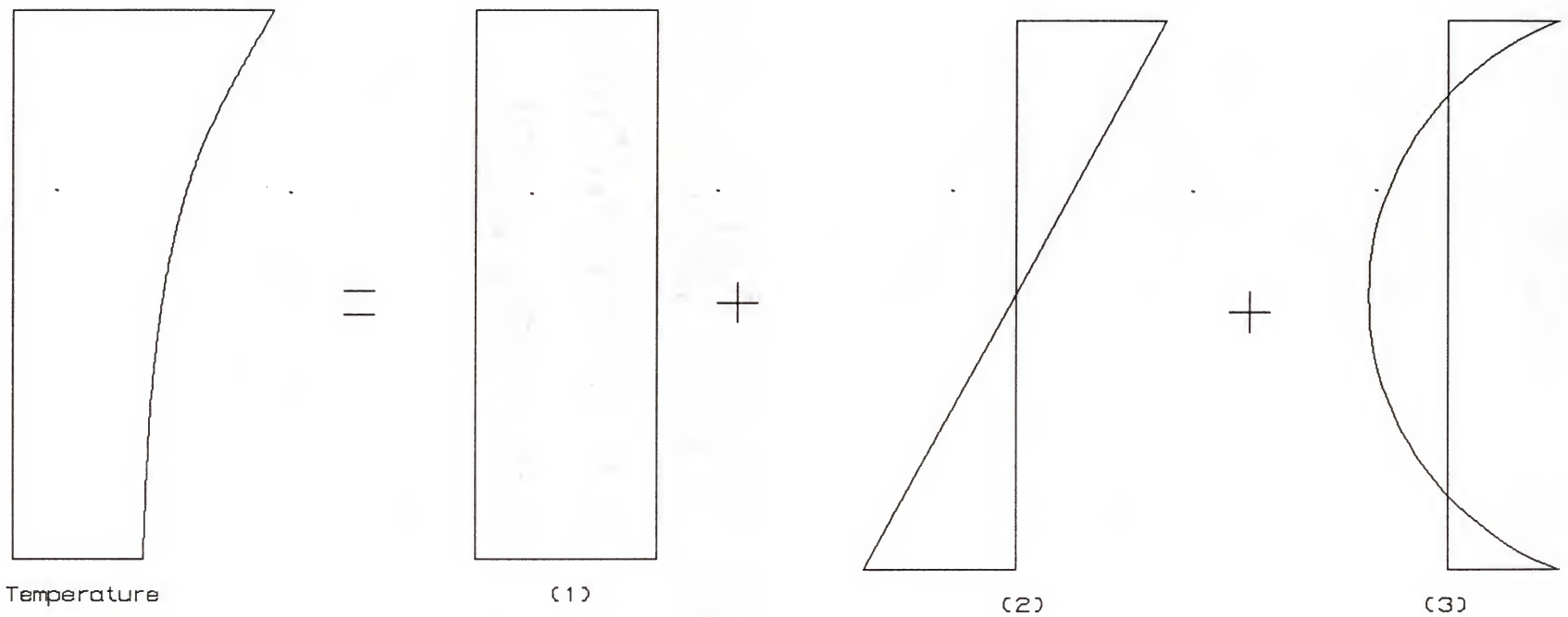

Figure 4.26 Typical Temperature Variation Profile Throughout a Slab and its Three Components, (1) Component causing Axial Displacement, (2) Component Causing Bending and (3) Non-linear Temperature Component.

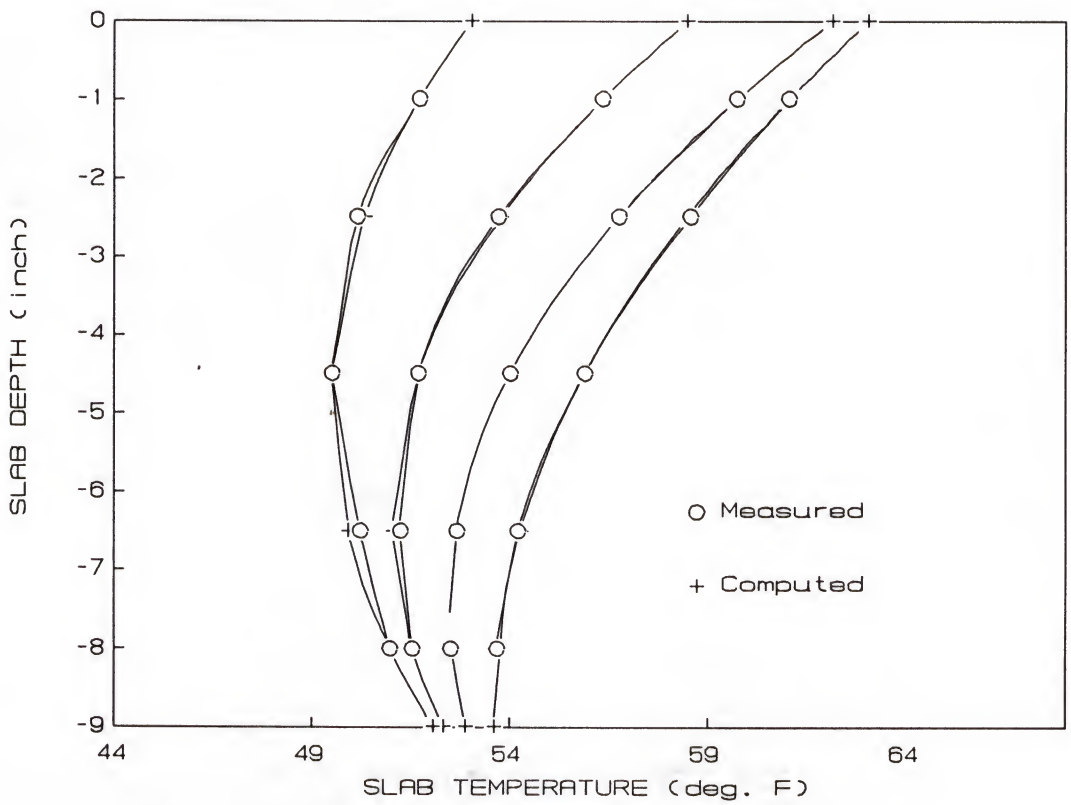

Figure 4.27 Computed vs. Measured Temperature Variations Throughout the Test Slab Corresponding to a Positive Temperature Differential as Recorded for the Month of January

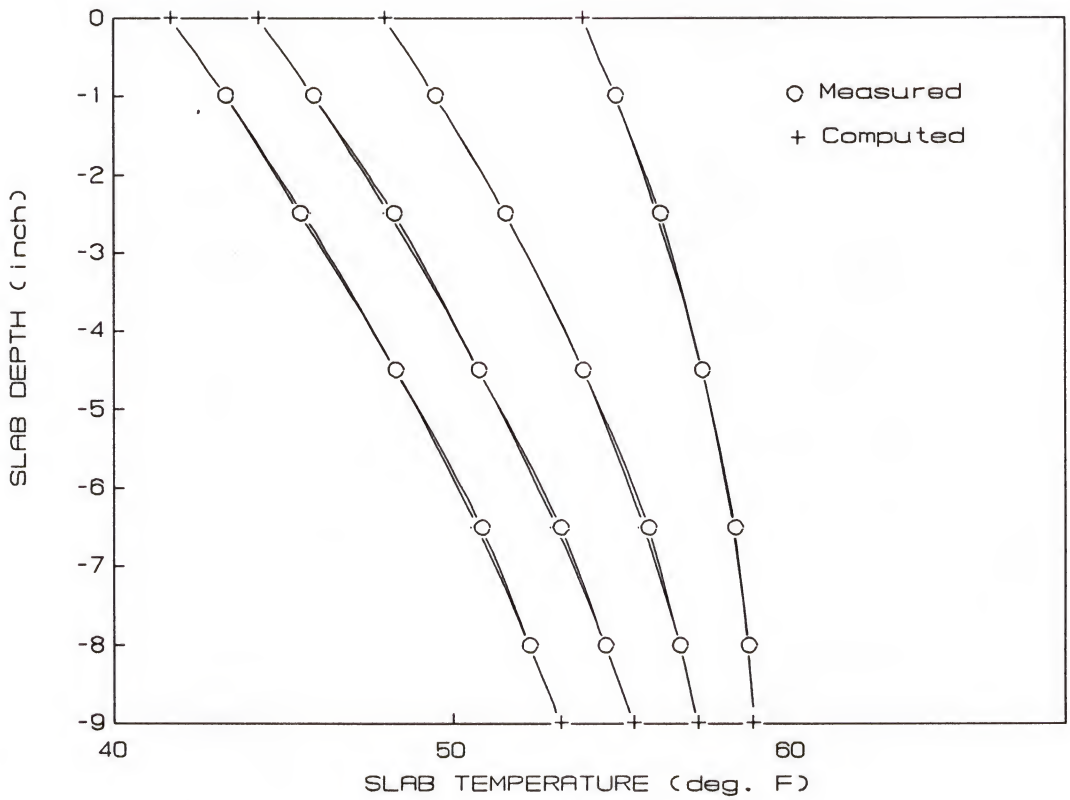

Figure 4.28 Computed vs. Measured Temperature Variations Throughout the Test Slab Corresponding to a Negative Temperature Differential as Recorded for the Month of January

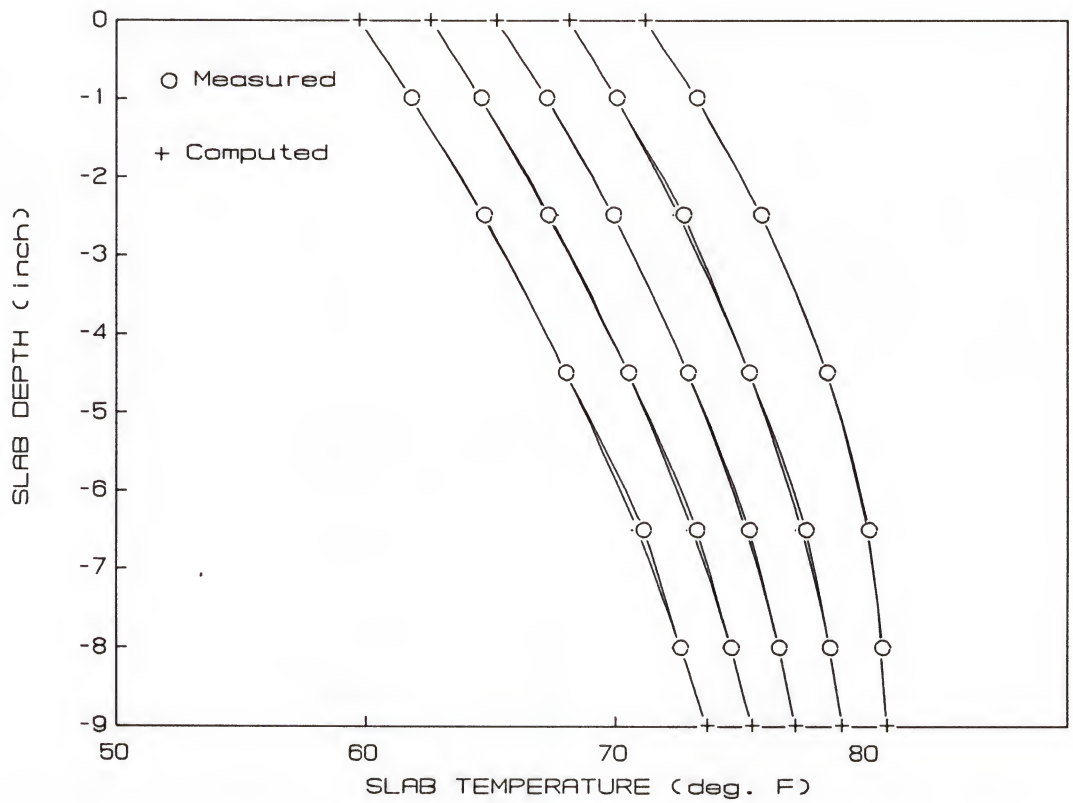

Figure 4.29 Computed vs. Measured Temperature Variations Throughout the Test Slab Corresponding to a Negative Temperature Differential as Recorded for the Month of April

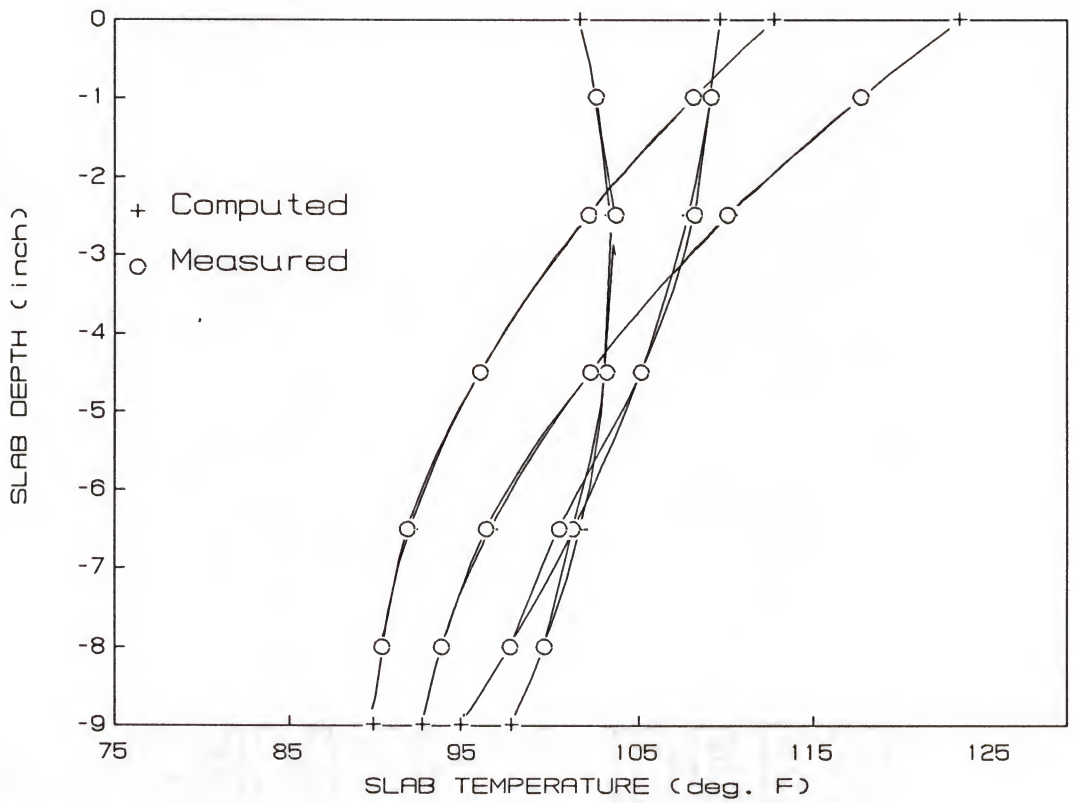

Figure 4.30 Computed vs. Measured Temperature Variations Throughout the Test Slab Corresponding to a Positive Temperature Differential as Recorded for the Month of June

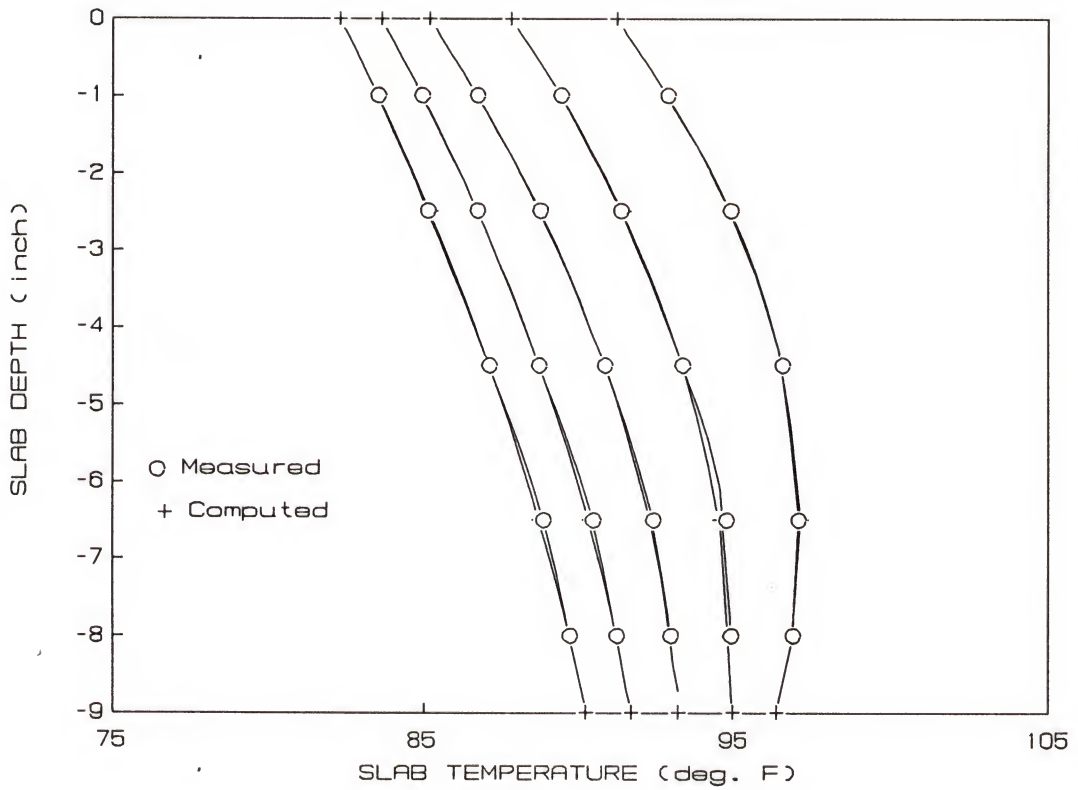

Figure 4.31 Computed vs. Measured Temperature Variations Throughout the Test Slab Corresponding to a Negative Temperature Differential as Recorded for the Month of June

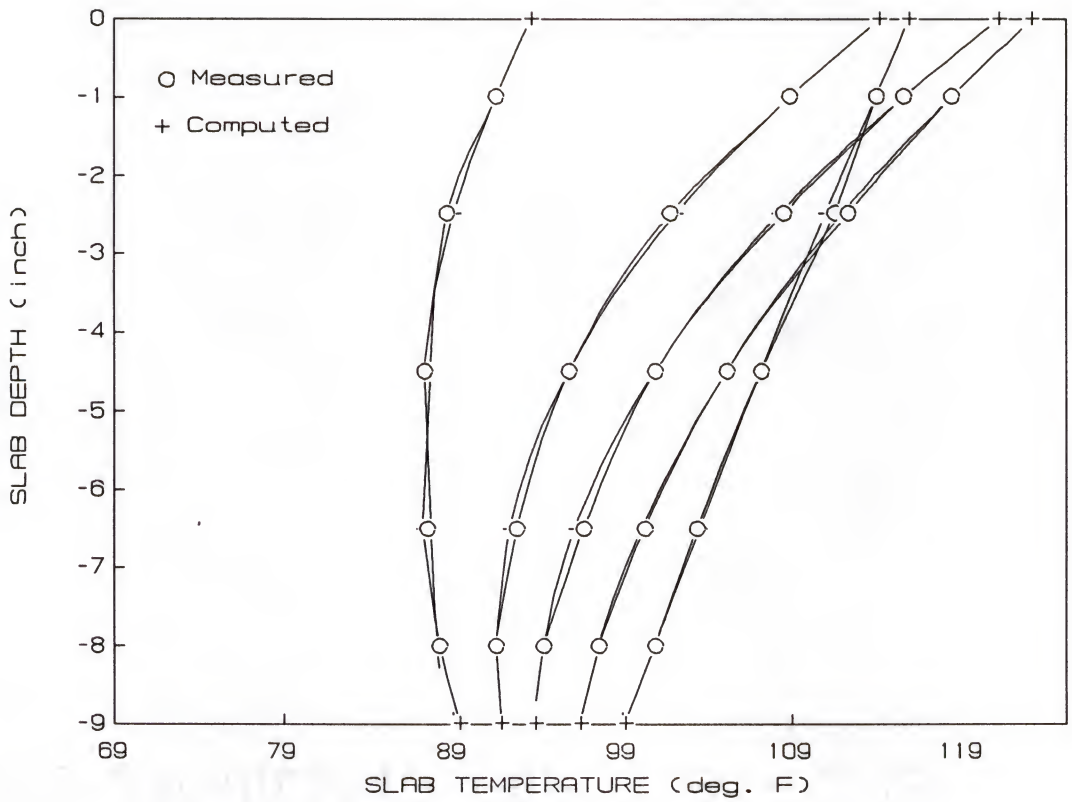

Figure 4.32 Computed vs. Measured Temperature Variations Throughout the Test Slab Corresponding to a positive Temperature Differential as Recorded for the Month of July

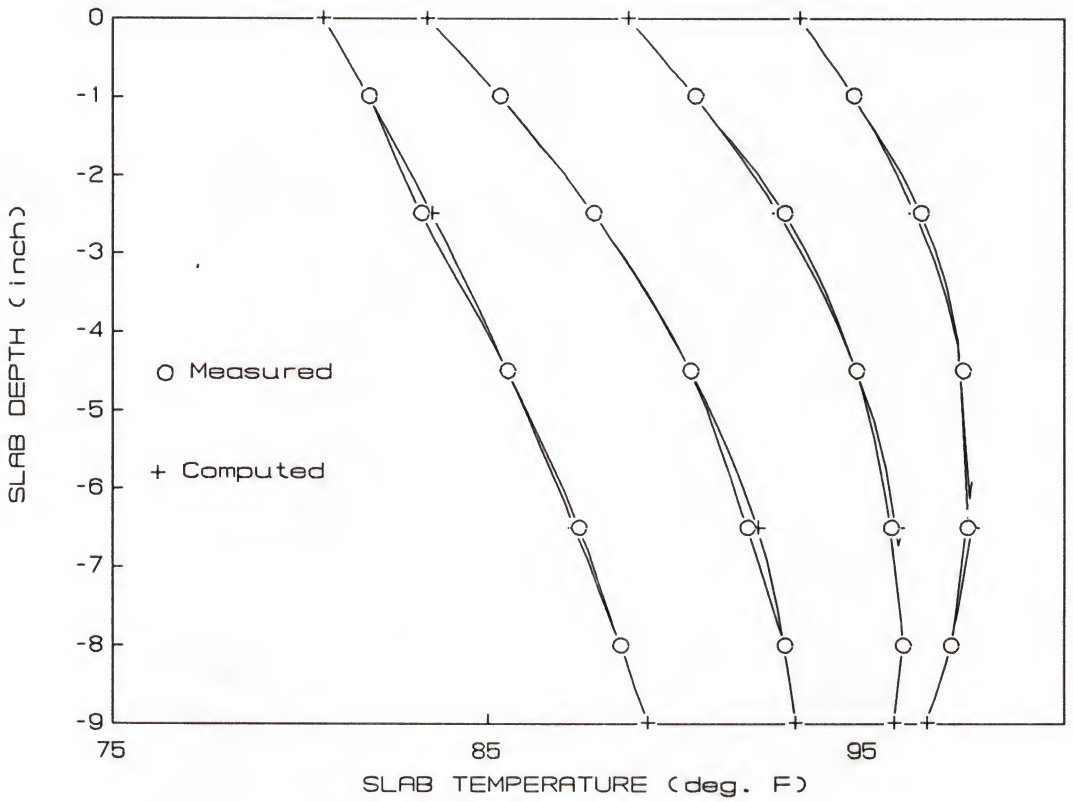

Figure 4.33 Computed vs. Measured Temperature Variations Throughout the Test Slab Corresponding to a Negative Temperature Differential as Recorded for the Month of July

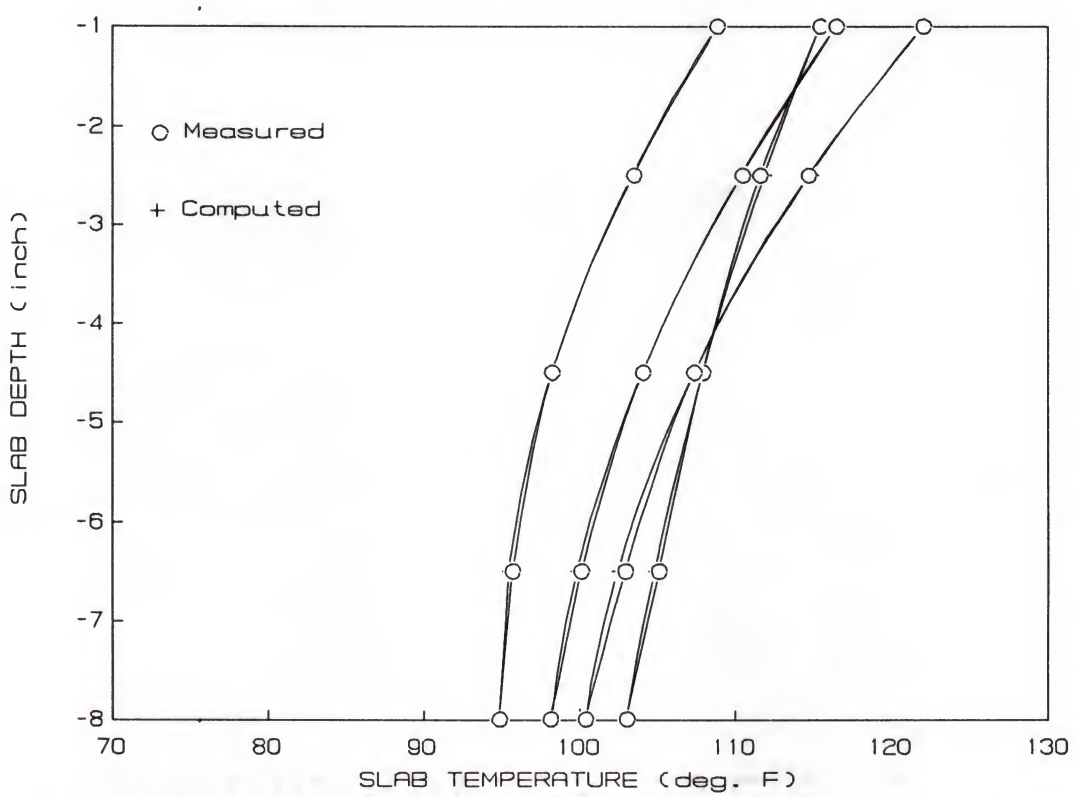

Figure 4.34 Computed vs. Measured Temperature Variations Throughout the Test Slab Corresponding to a Positive Temperature Differential as Recorded for the Month of August

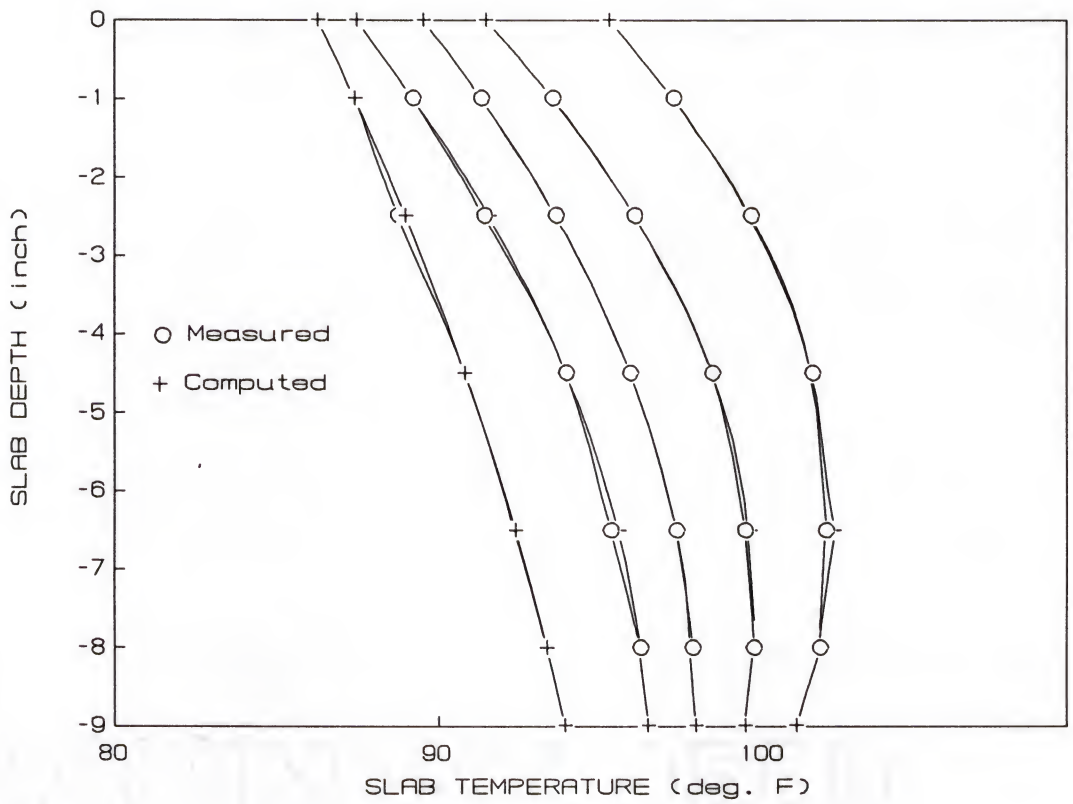

Figure 4.35 Computed vs. Measured Temperature Variations Throughout the Test Slab Corresponding to a Negative Temperature Differential as Recorded for the Month of August

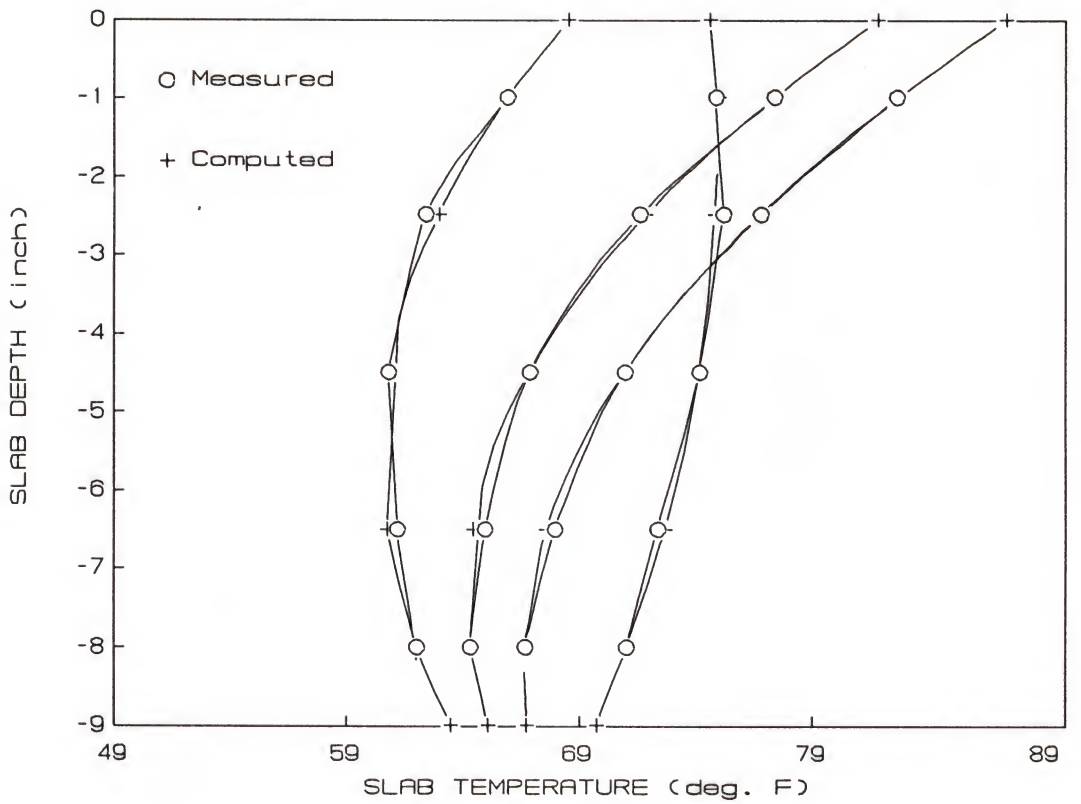

Figure 4.36 Computed vs. Measured Temperature Variations Throughout the Test Slab Corresponding to a Positive Temperature Differential as Recorded for the Month of November

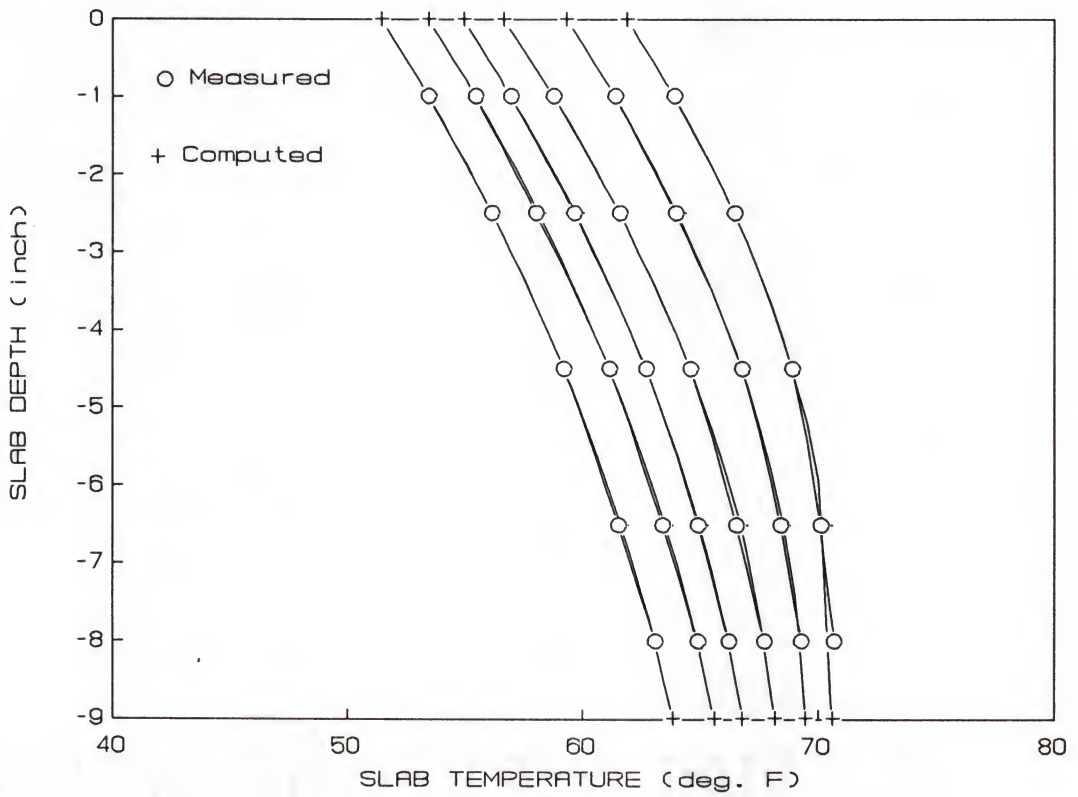

Figure 4.37 Computed vs. Measured Temperature Variations Throughout the Test Slab Corresponding to a Negative Temperature Differential as Recorded for the Month of November

where:

t = temperature in deg. F

y = slab depth, with y = 0 at top and y = d at bottom

The factors A,B, and C are determined by fitting three measured temperatures across the slab depth to the quadratic equation. If these three temperature readings were taken at the top (t_t), at the middle (t_m) and at the bottom of the slab (t_b), the factors A, B and C would be defined as follows:

$$A = t_t$$

$$B = (4t_m - 3t_t - t_b)/d$$

$$C = 2(t_t + t_b - 2t_m)/d^2$$

Table 4.1 summarizes the representative values of these coefficients A, B and C as well as the corresponding temperature differentials for a daily cycle at various time periods.

The temperature component causing axial displacement is determined by integrating the temperature across the section and dividing the integral (area under the curve) by the slab thickness as follows:

$$t_{axial} = \left(\frac{1}{d}\int_0^d t\,dy = \frac{1}{d}\int_0^d (A + By + Cy^2)\,dy\right.$$

$$= A + B(d/2) + C(d^2/3) \qquad (4.6)$$

The temperature component causing bending of the slab is determined by taking the moment of the area remained after subtracting the axial component from the total area under the curve, and then finding a linear temperature distribution which would produce the same moment.

The moment is taken with respect to the mid-depth of the slab

let $y' = (d/2) - y$ such that:

if y = 0 then $y' = d/2$

and if y = d then $y' = -(d/2)$

Table 4.1 Representative Values of the Coefficients A, B and C of the Quadratic Equation (4.5) as Computed for a Daily Cycle at Various Time Periods.

Period of the Year	Typical Daily Cycle Time	A	B	C	Temp. Diff. DT
Jan.	11:00 am	53.03836	-1.45816	0.149795	0.99
	12:00 pm	58.47224	-2.33591	0.183673	6.15
	01:00 pm	62.11836	-2.58102	0.172653	9.24
	02:00 pm	63.05142	-2.13142	0.12	9.46
	06:00 pm	53.80979	1.010408	-0.05020	- 5.03
	08:00 pm	50.41081	1.408367	-0.05918	- 7.88
	10:00 pm	47.97265	1.578979	-0.06163	- 9.22
	00:00 am	46.37285	1.477142	-0.04	-10.05
	02:00 am	44.24959	1.669387	-0.04897	-11.06
	04:00 am	42.90612	1.734897	-0.05102	-11.48
	06:00 am	41.67204	1.671632	-0.04367	-11.51
	08:00 am	40.90163	1.413877	-0.01551	- 3.37
April	10:00 am	81.88979	-3.67959	0.289795	9.64
	12:00 pm	96.68979	-5.40816	0.318367	22.88
	01:00 pm	100.9938	-5.25918	0.265306	25.84
	02:00 pm	103.2591	-4.87551	0.216326	26.36
	04:00 pm	96.38571	-1.88571	-1.2E-15	16.97
	08:00 pm	75.46938	2.189795	-0.15918	- 6.81
	10:00 pm	71.16326	2.159183	-0.12244	- 9.51
	00:00 am	68.1	1.985714	-0.08571	-10.93
	02:00 am	65.18571	2.1	-0.08571	-11.96
	04:00 am	62.58367	2.089795	-0.07346	-12.86
	06:00 am	59.73469	2.130612	-0.06530	-13.89

Table 4.1 Continued.

Period of the Year	Typical Daily Cycle Time	A	B	C	Temp. Diff. DT
June	09:00 am	98.73816	-3.31775	0.239591	10.45
	11:00 am	112.3161	-4.91938	0.263265	22.95
	01:00 pm	122.8802	-5.95183	0.281632	30.75
	03:00 pm	109.18	-0.35714	-0.14285	14.78
	05:00 pm	115.2114	-2.54857	0.057142	18.31
	07:00 pm	101.2197	1.123265	-0.17306	3.91
	08:00 pm	96.50530	1.727959	-0.18326	- 0.71
	10:00 pm	91.15979	1.796122	-0.13591	- 5.16
	00:00 am	87.80530	1.662244	-0.09755	- 7.06
	02:00 am	85.18428	1.605714	-0.08	- 7.97
	04:00 am	83.61408	1.368979	-0.05306	- 8.02
	06:00 am	82.31448	1.246734	-0.04122	- 7.88
July	08:00 pm	93.28367	1.546938	-0.13061	- 3.34
	10:00 pm	88.70204	1.924489	-0.12653	- 7.07
	00:00 am	85.86122	1.948979	-0.11020	- 8.61
	02:00 am	83.36530	2.040816	-0.10612	- 9.77
	04:00 am	81.22653	2.075510	-0.10204	-10.41
	06:00 am	79.72857	1.957142	-0.08571	-10.67
	08:00 am	80.61428	1.214285	-0.02857	- 8.61
	10:00 am	93.53673	-2.34489	0.208163	4.24
	12:00 pm	107.3326	-4.75102	0.318367	16.97
	01:00 pm	114.0122	-5.66734	0.355102	22.24
	02:30 pm	121.0408	-5.96734	0.326530	27.26
	04:00 pm	123.0183	-5.05102	0.232653	26.61
	06:00 pm	115.7877	-2.00408	0.016326	16.71
	08:00 pm	100.6693	1.846938	-0.21632	0.9

Table 4.1 Continued.

Period of the Year	Typical Daily Cycle Time	A	B	C	Temp. Diff. DT
August	09:00 am	90.99591	-0.14897	0.053061	- 2.96
	10:00 am	99.17551	-2.37959	0.204081	4.88
	12:00 pm	113.1510	-4.64489	0.293877	18
	02:00 pm	121.2836	-5.05306	0.269387	23.66
	03:16 pm	127.6326	-5.95102	0.318367	27.77
	05:00 pm	118.0204	-2.72653	0.106122	15.94
	07:00 pm	105.1408	1.346938	-0.18775	3.08
	08:00 pm	101.8367	1.526530	-0.16326	- 0.51
	10:00 pm	95.61836	2.148979	-0.16734	- 5.79
	00:00 am	91.83877	2.208163	-0.14693	- 7.97
	02:00 am	89.88979	1.920408	-0.11020	- 8.36
	04:00 am	87.81632	1.881632	-0.09795	- 9
	06:00 am	86.3	1.785714	-0.08571	- 9.13
	08:00 am	86.66326	1.173469	-0.03673	- 7.59
Nov.	08:00 pm	61.90224	2.138367	-0.13061	- 8.66
	10:00 pm	59.27816	2.189387	-0.11755	-10.18
	12:00 am	56.61142	2.257142	-0.10857	-11.52
	02:00 am	54.90693	2.133265	-0.09020	-11.89
	04:00 am	53.41183	2.090612	-0.08244	-12.14
	06:00 am	52.31469	2.009183	-0.07387	-12.1
	07:00 am	51.39204	2.085918	-0.07795	-12.46
	09:00 am	60.78142	-0.96714	0.145714	- 3.1
	10:00 am	68.82632	-2.87265	0.256326	5.09
	12:00 pm	82.05326	-4.76653	0.323265	16.71
	01:18 pm	87.53387	-4.97346	0.299591	20.49
	02:00 pm	87.79612	-4.26510	0.228979	19.84
	04:00 pm	74.87102	0.336530	-0.09755	4.87

Since $t_{total} = A + By + Cy^2$ (4.7)

and $t_{axial} = A + B(d/2) + C(d^2/3)$ (4.8)

therefore $t_{total} - t_{axial} = By + Cy^2 - B(d/2) - C(d^2/3)$ (4.9)

furthermore, with $y = (d/2) - y'$

the expression (4.9) becomes

$$t_{total} - t_{axial} = -C(d^2/12) - (B + Cd)y' + Cy'^2 \quad (4.10)$$

The moment, taken with respect to slab mid-depth, will be then as follows:

$$M = \int_{-d/2}^{d/2} (t_{total} - t_{axial})y'dy' = -(B + Cd)d^3/12 \quad (4.11)$$

For a linear temperature distribution with a maximum magnitude of $T_{curling}$, the moment caused by this temperature distribution is:

$$M = 2T_{curling}(d/4)(d/3) = T_{curling}(d^2/6) \quad (4.12)$$

By setting this moment to be equal to the moment as expressed in equation (4.11), $t_{curling}$, at any depth y, can be solved to be:

$$t_{curling} = (B + Cd)[y - (d/2)] \quad (4.13)$$

Lastly, the nonlinear temperature component is determined as follows:

$$t_{nonlinear} = t_{total} - t_{axial} - t_{curling}$$

$$= C[y^2 - dy + (d^2/6)] \quad (4.14)$$

From this expression, it is apparent that, if the coefficient C is positive, the extreme fibers of the slab would tend to expand. This condition is reversed if the coefficient C is negative. Furthermore, it can also be seen from Table 4.1 that this coefficient C, and subsequently the non-linear temperature component, is not directly correlated to the temperature differential.

In the case of the assumption of a linear temperature gradient, where the coefficient C is zero, two temperature components only remain,

i.e., (1) temperature component related to axial displacement and (2) the curling temperature component related to slab bending.

Following the same procedure as stated previously, these two components can be determined by the following equations:

$$t_{axial} = A + B(d/2) \tag{4.15}$$

$$t_{curling} = B[y - (d/2)] \tag{4.16}$$

4.2.4.3 Comparison with other models. Various models for predicting temperatures in concrete pavements have been developed by researchers such as Thomlinson [14], Barber [47], Bergstrom [45], Thompson [48] and Hsieh et al [49]. The one presented by Hsieh is a three-dimensional computer model that uses the finite-difference scheme of Beam and Warming [50]. The model is based on the coupled theories of heat-moisture conduction through a semi-finite, isotropic and homogeneous porous medium. The input required for this computer program are weather data and the material properties of the concrete and soil.

A comparison made between the computed temperature variations using this computer model and the quadratic equation (4.5) is illustrated in Figures 4.38 through 4.41. The predicted temperature variations from Hsieh's model match well with those from the quadratic equation unless there is a drastic change in temperature at the top two inches of the slab as it can be seen in Figures 4.39 and 4.41. In that case, if the temperature differential is positive, the quadratic equation gives comparatively higher temperatures at the top half of the slab and lower temperatures at the lower half. This observation is reversed in the case of a negative temperature differential.

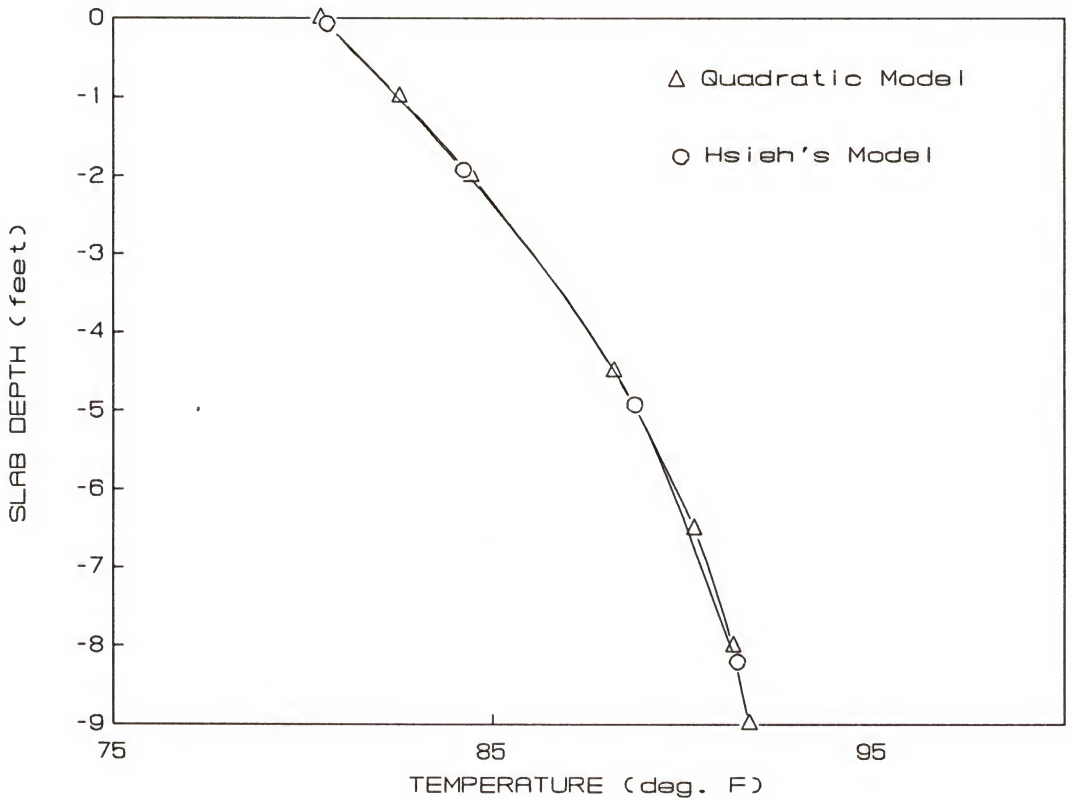

Figure 4.38 Predicted Temperature Distribution Throughout the Slab Depth Using, Respectively, the Quadratic Equation and Hsieh's Model for Full-Sun Simulation at 5:00 A.M.

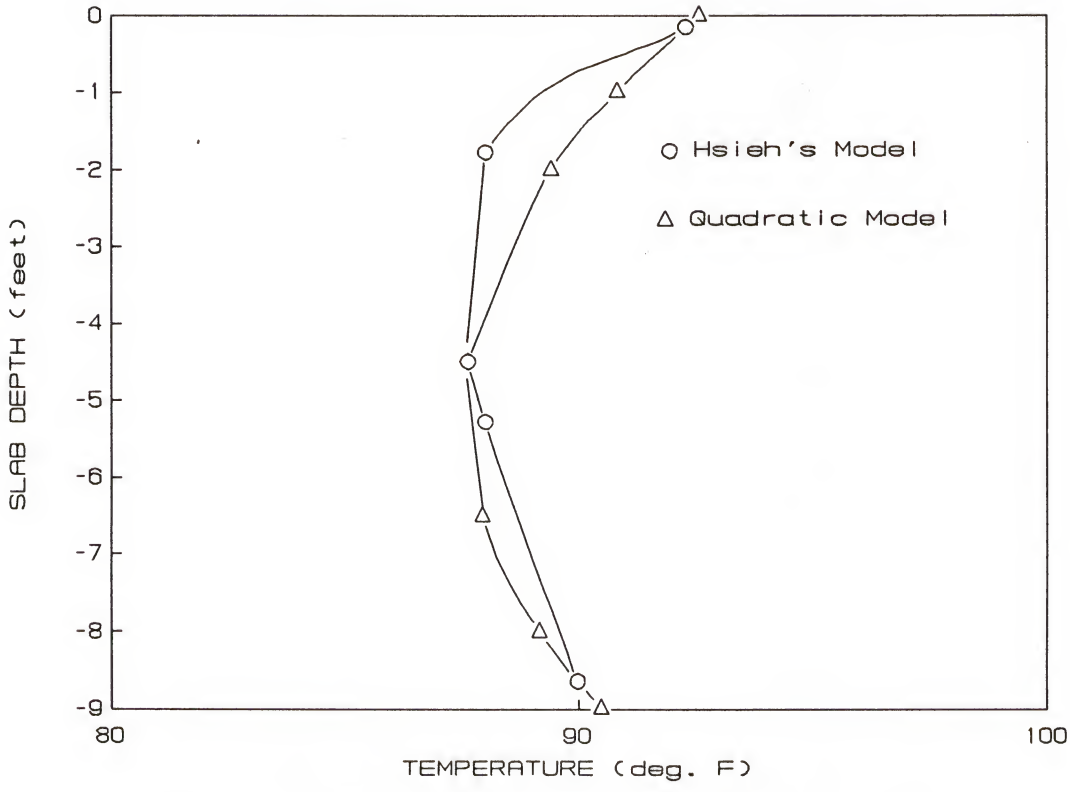

Figure 4.39 Predicted Temperature Distribution Throughout the Slab Depth Using, Respectively, the Quadratic Equation and Hsieh's Model for Full-Sun Simulation at 8:00 A.M.

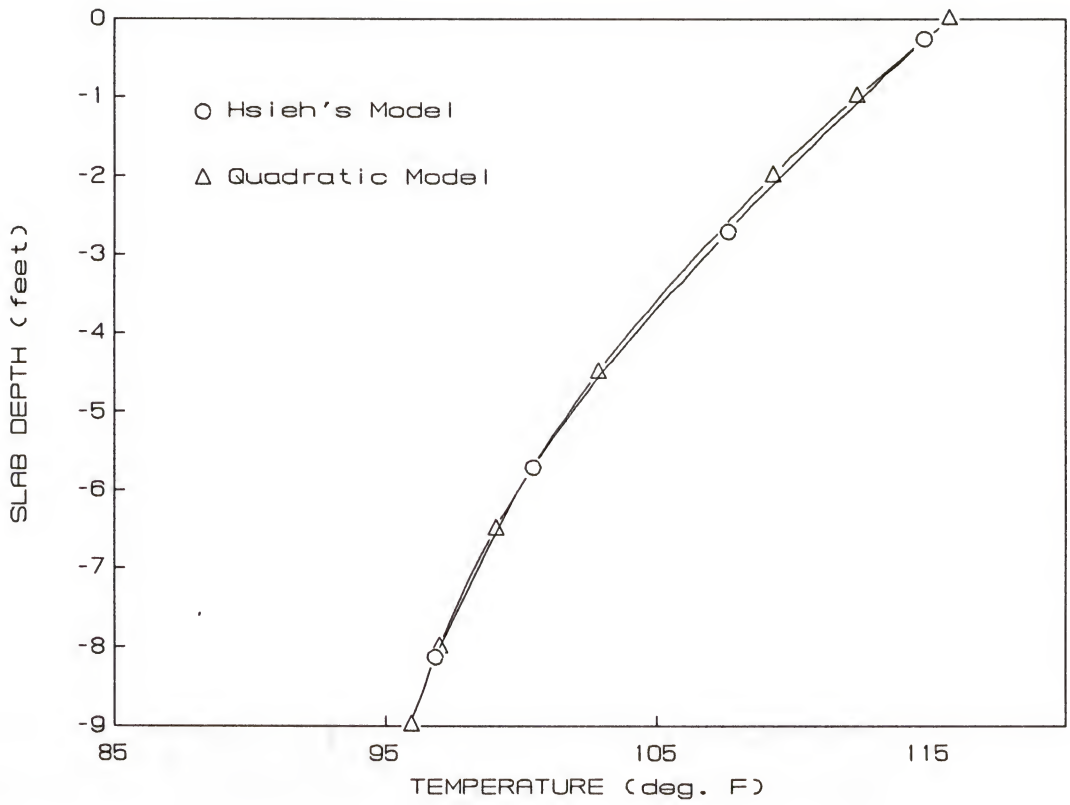

Figure 4.40 Predicted Temperature Distribution Throughout the Slab Depth Using, Respectively, the Quadratic Equation and Hsieh's Model for Full-Sun Simulation at 2:00 P.M.

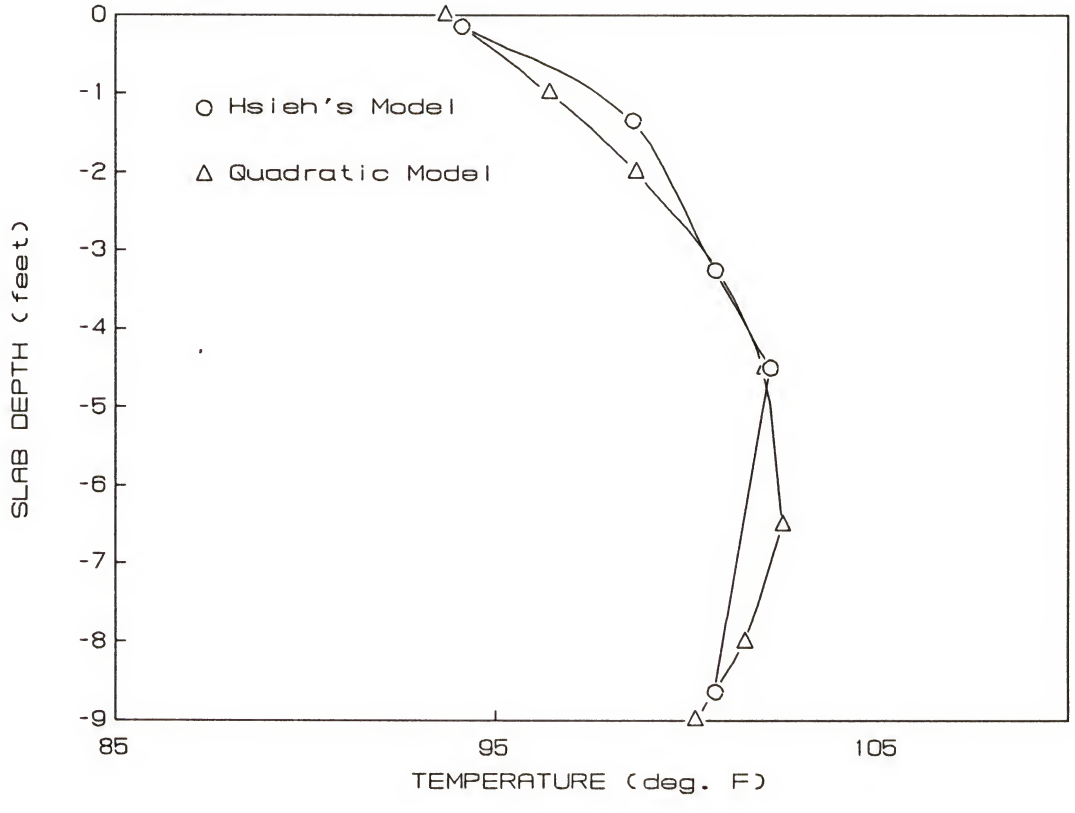

Figure 4.41 Predicted Temperature Distribution Throughout the Slab Depth Using, Respectively, the Quadratic Equation and Hsieh's Model for Full-Sun Simulation at 6:00 P.M.

4.3 In Situ Measurements of Thermal-Induced Pavement Deflection Profile

4.3.1 Introduction

It is well known that a temperature and/or moisture difference between the top and bottom of a concrete slab results in change of shape called warping or curling, which is a prominent parameter in the analysis of concrete pavements behavior. It causes the corners and edges to rise and fall, relatively to the center, thus affecting the conditions of slab support. A maximum vertical movement of 0.25 inches at corners of slabs was recorded at the Bates Experimental Station in the early 1920s [8].

Under ideal conditions, the concrete slab tends to dome up when its top surface is warmer than its bottom. With a reversal of relative temperatures, the edges and joints may lift. The conceptual presentation of these relative concrete pavement responses to temperature differentials are illustrated in Figure 4.42.

In view of this phenomenon, a field testing program was carried out to investigate the significant and the extent of the influence of the temperature on the concrete slab behavior. Internal slab temperature distributions and in situ thermal-induced vertical displacements, in the absence of loads other than gravity, at selected locations on the test slab surface were measured at various time. The equipment and testing methodology were presented in section 3.3. The intent of this task is to provide in situ measurements establishing the continuous concrete slab profile relative variations as a consequence of daily fluctuations in thermal gradient and moisture.

The following section presents the findings and the analysis of the data collected during this investigation.

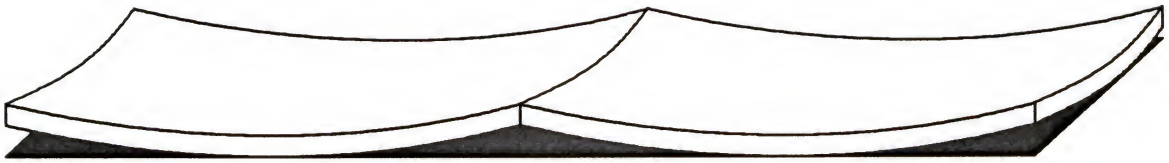

(a)

(b)

Figure 4.42 Conceptual Presentation of Concrete Slab Response to Thermal Gradient, (a) Upward Slab Curling and (b) Downward Slab Curling

4.3.2 Test Results Analysis

As stated previously, a major consequence of the temperature gradient occurring in the concrete slab during a normal day is the slab tendency to curl upwards if the concrete surface is hotter than the bottom, and downwards if the top surface is cooler than the bottom. This will cause the deflections measured near the edge and in the center of the slab, respectively, to be different.

Figures 4.43 through 4.56 illustrate the relative slab deflection profiles as measured on the test slab. It is noticeable from these figures that a change in temperature differential induces a change in the slab profile. This is more apparent when the deflection measurements corresponding to the lowest temperature differential recorded were used as reference for each field test as shown in Figures 4.53 through 4.56.

A maximum deflection variation of approximately 1/4 of an inch was measured at the center of the slab during the month of November when the temperature differential increased from 2 to 15^{o}F.

It should be noted that these measured slab profile variations are induced by temperature and moisture changes. However, since the moisture fluctuation was not monitored, its effect on these measurements, even though, apparent can not be accurately determined.

The low magnitude of the theoretical curling computed using the FEACONS IV program and summarized in Tables 4.2 to 4.5 as compared to the measured curling suggests that the model used in this program to determine the curling due to temperature gradient and slab weight was not be adequate.

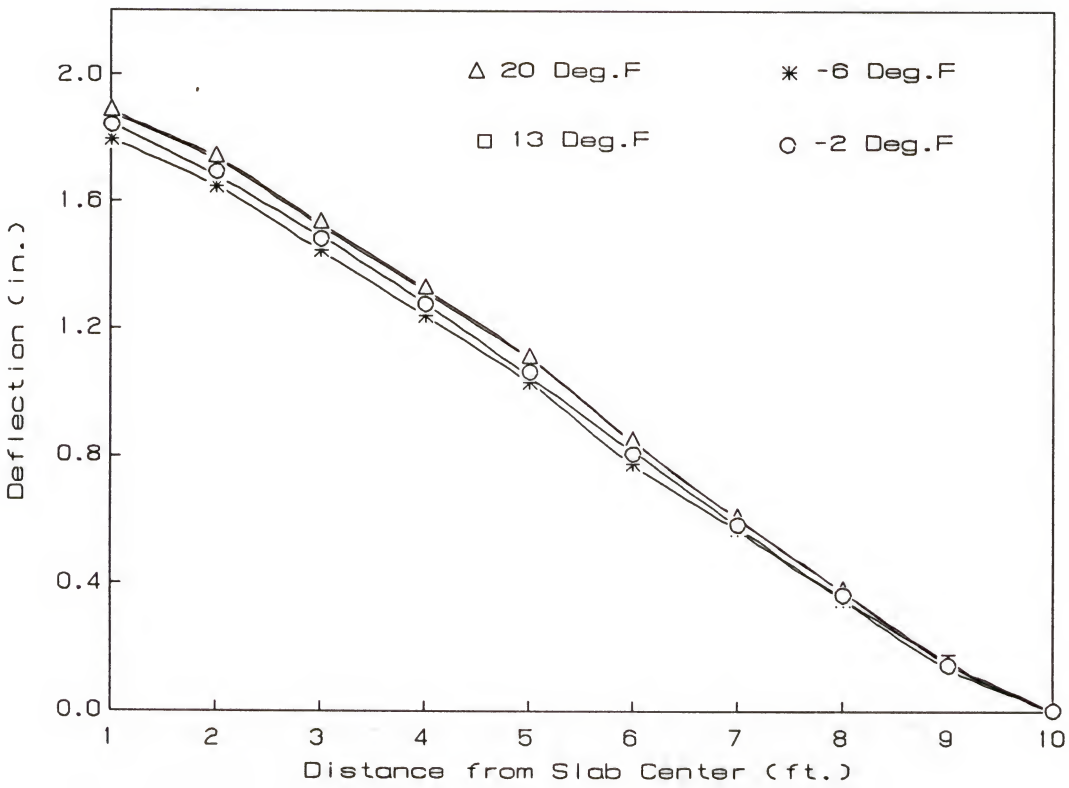

Figure 4.43 Test Slab Profile Variations Along the Slab Longitudinal Direction Referenced to the Slab Joint Center as Measured on the Month of July

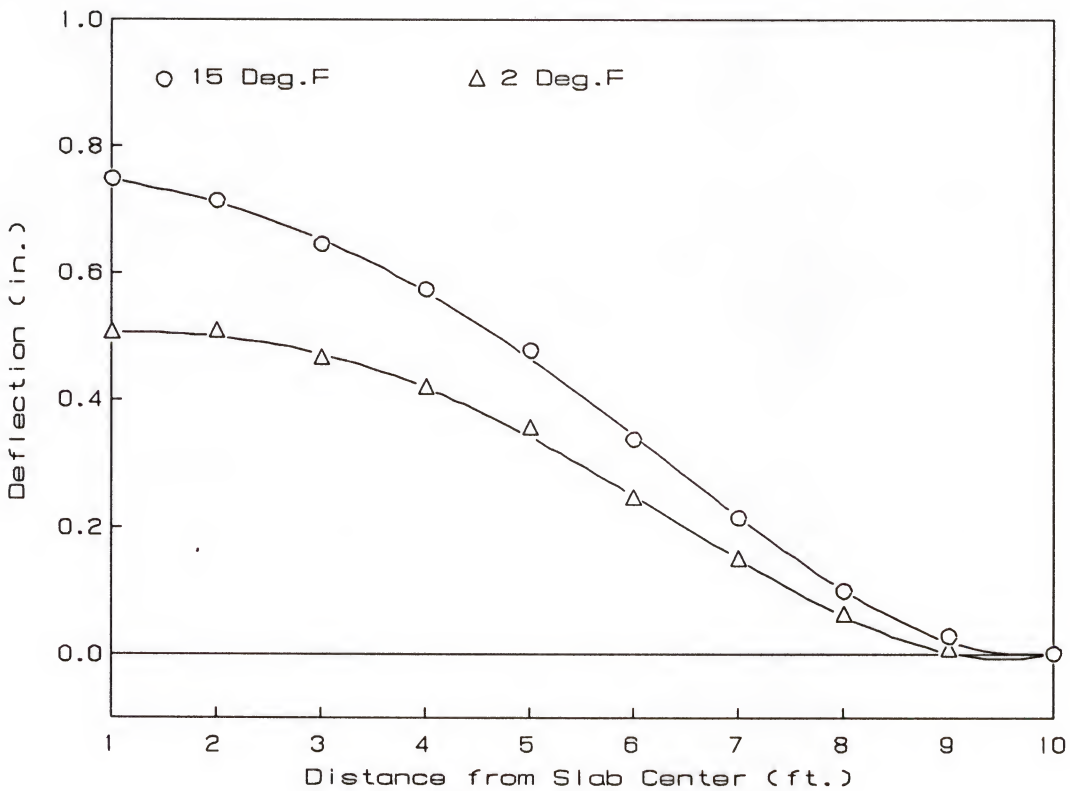

Figure 4.44 Test Slab Profile Variations Along the Slab Longitudinal Direction Referenced to the Slab Joint Center as Measured on the Month of November

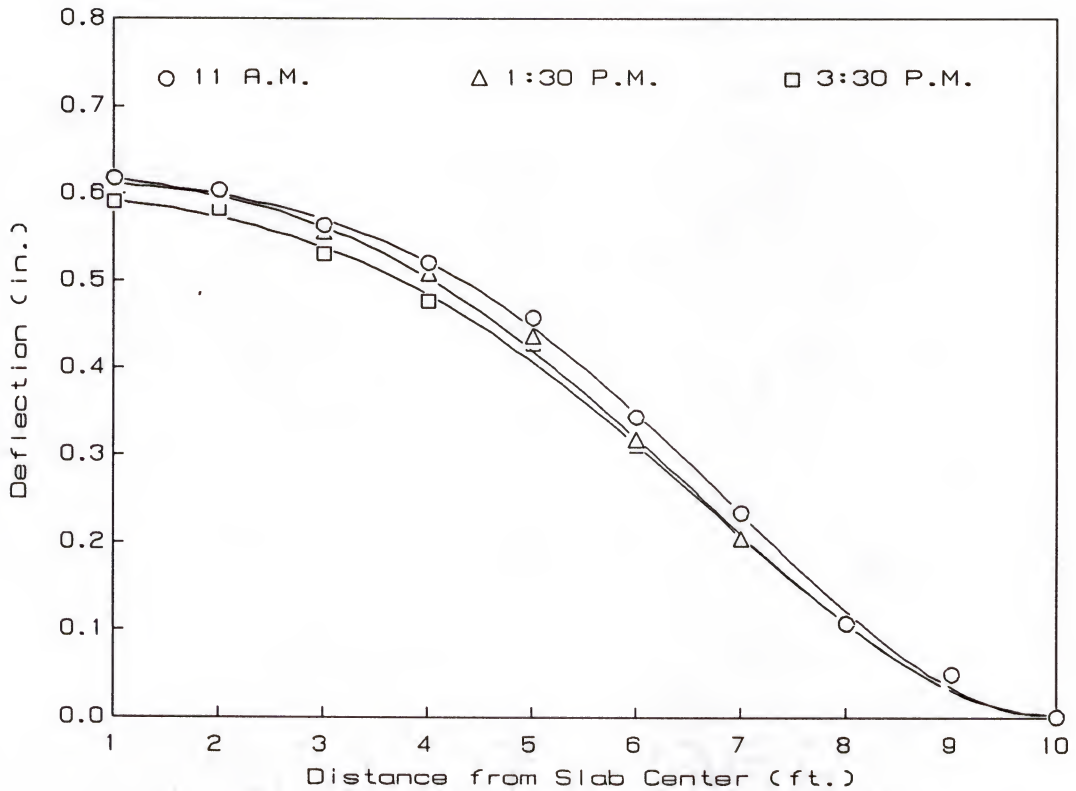

Figure 4.45 Test Slab Profile Variations Along the Slab Longitudinal Direction Referenced to the Slab Joint Center as Measured on the Month of May

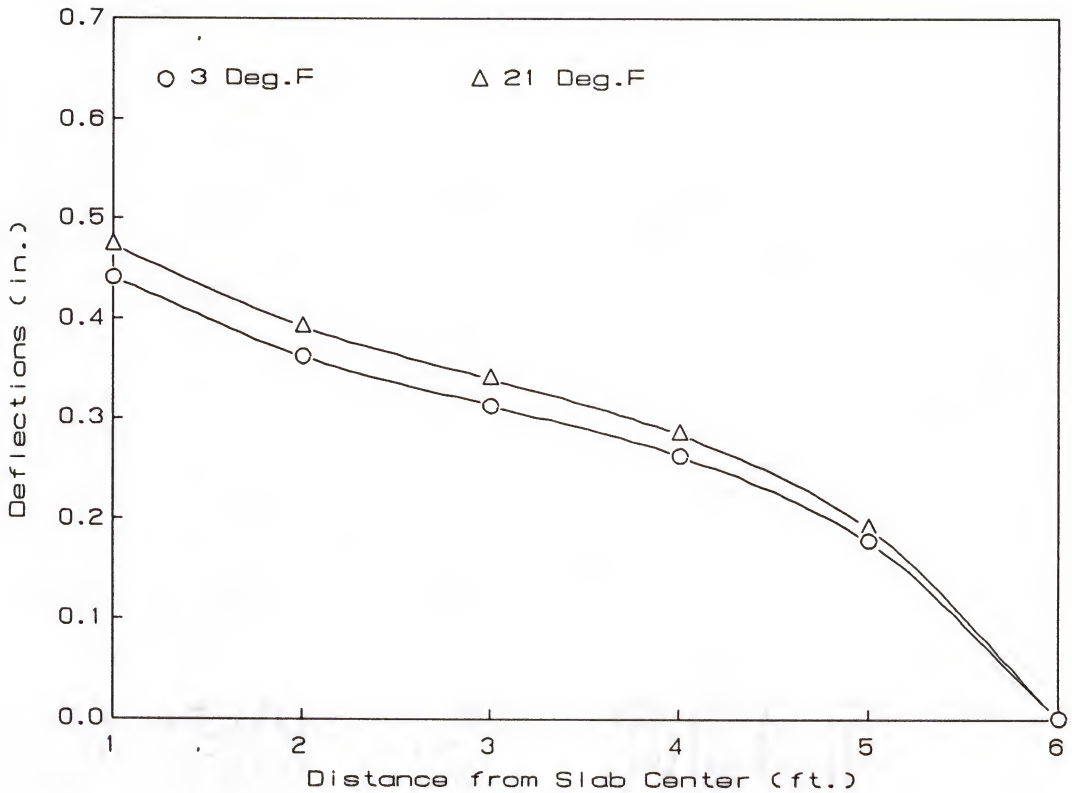

Figure 4.46 Test Slab Profile Variations Along the Slab Transversal Direction Referenced to the Slab Edge Center as Measured on the Month of July

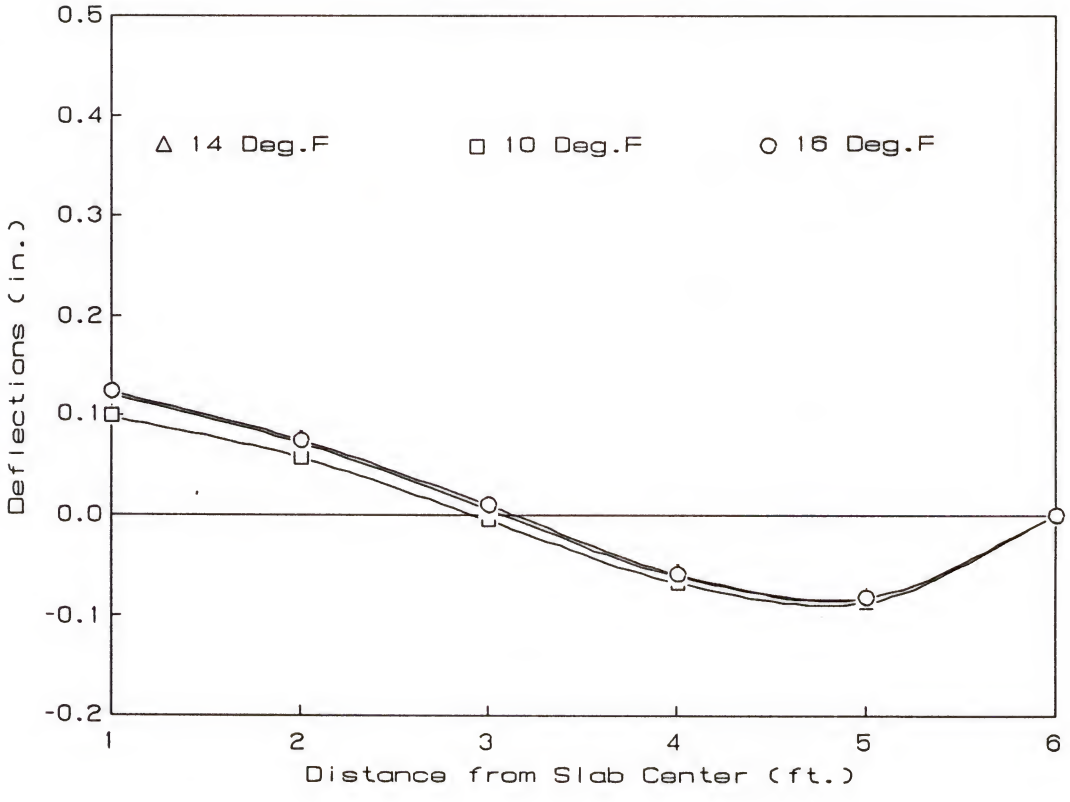

Figure 4.47 Test Slab Profile Variations Along the Slab Transversal Direction Referenced to the Slab Edge Center as Measured on the Month of September

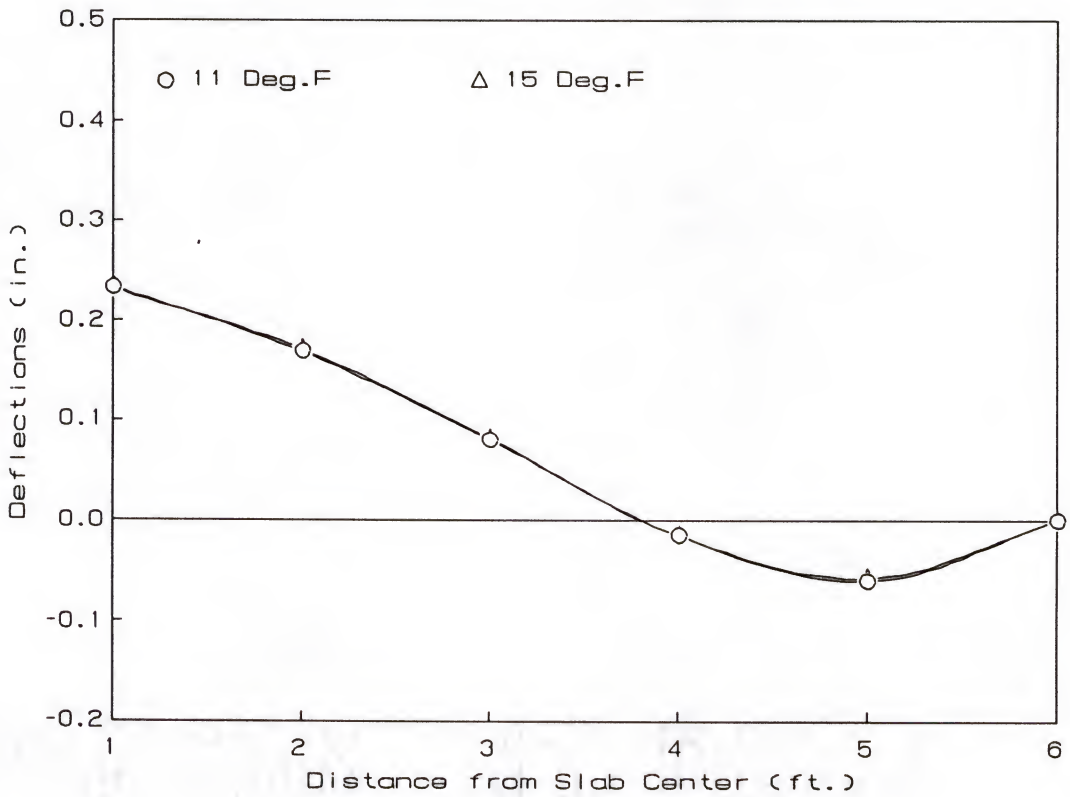

Figure 4.48 Test Slab Profile Variations Along the Slab Transversal Direction Referenced to the Slab Edge Center as Measured on the Month of November

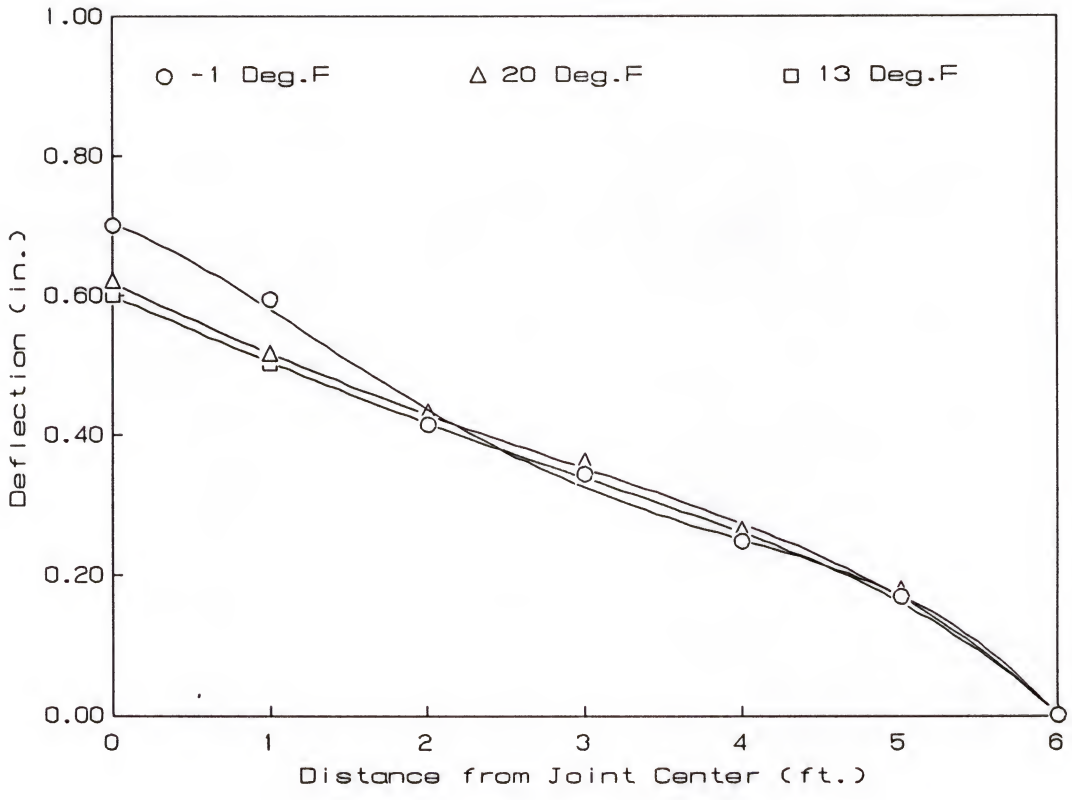

Figure 4.49 Test Slab Profile Variations Along the Slab Joint Direction Referenced to the Slab Joint Corner as Measured on the Month of July

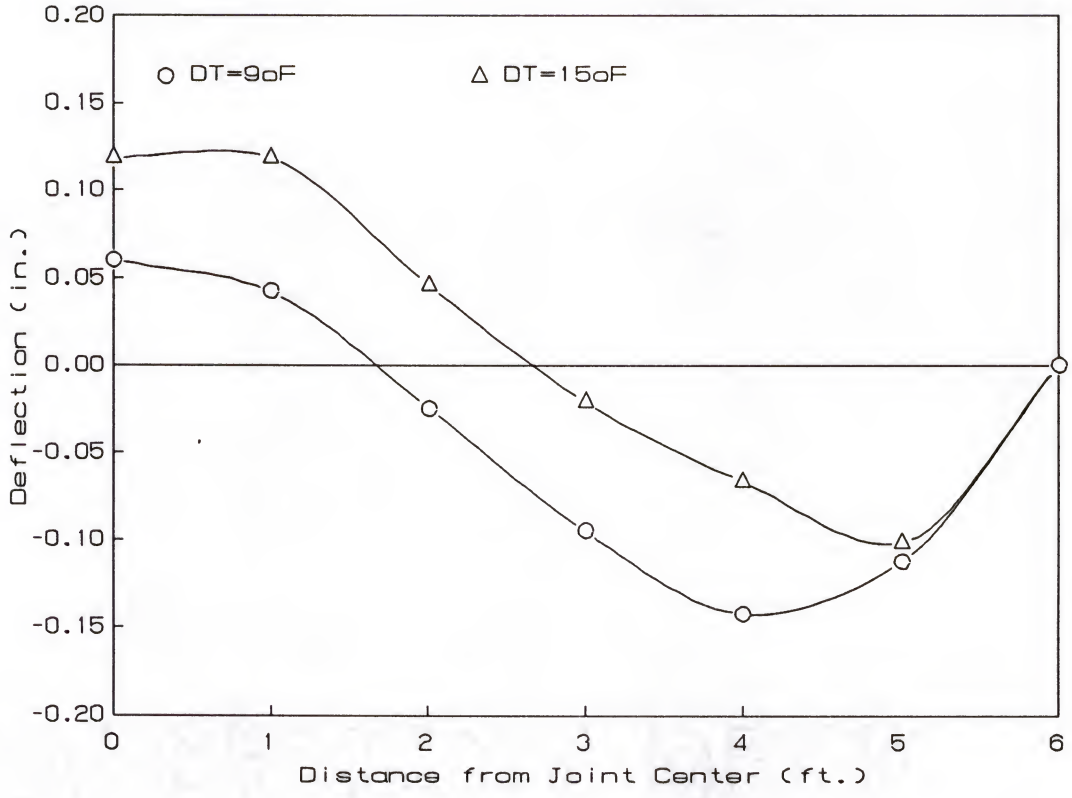

Figure 4.50 Test Slab Profile Variations Along the Slab Joint Direction Referenced to the Slab Joint Corner as Measured on the Month of November

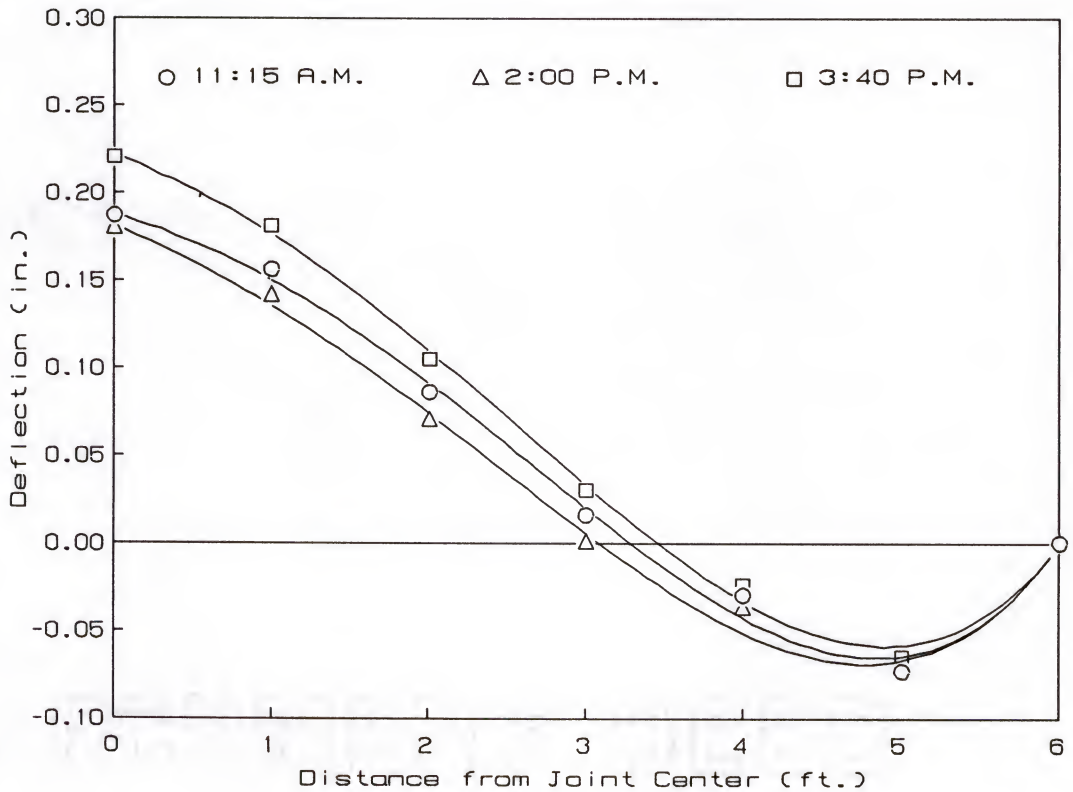

Figure 4.51 Test Slab Profile Variations Along the Slab Joint Direction Referenced to the Slab Joint Corner as Measured on the Month of May

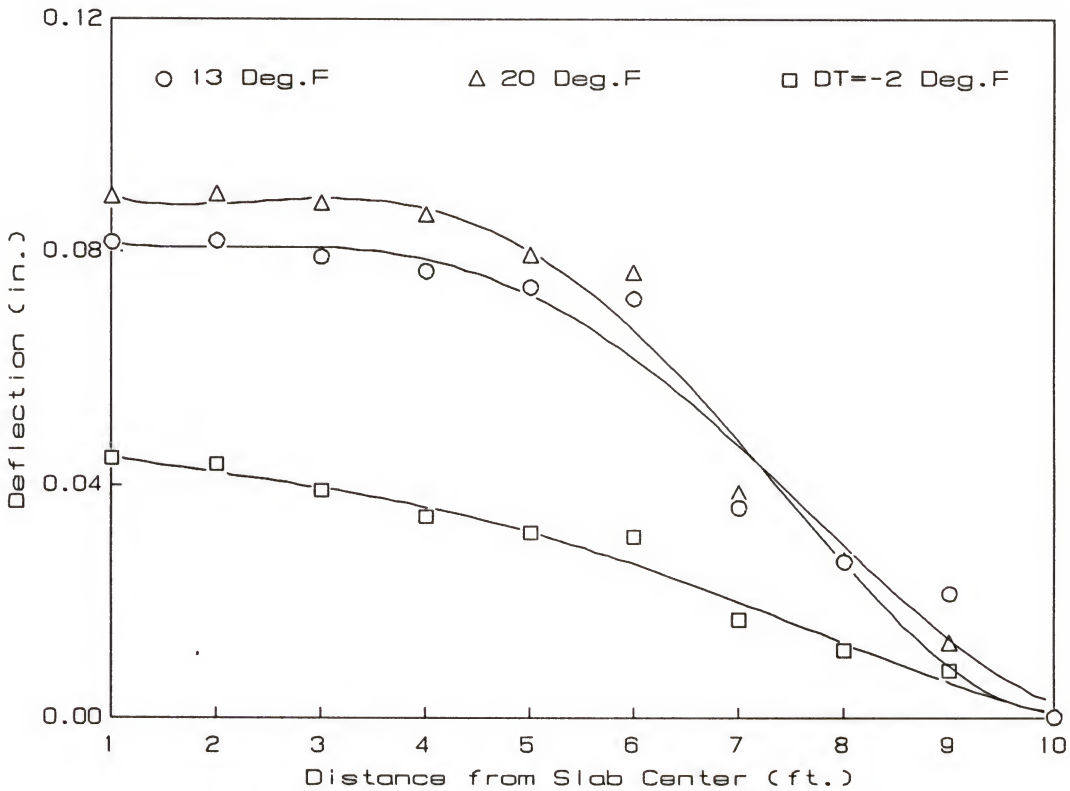

Figure 4.52 Test Slab Profile Variations Along the Slab Longitudinal Direction Using the Data Corresponding to a Temperature Differential of -6°F as a Reference as Measured on the Month of July

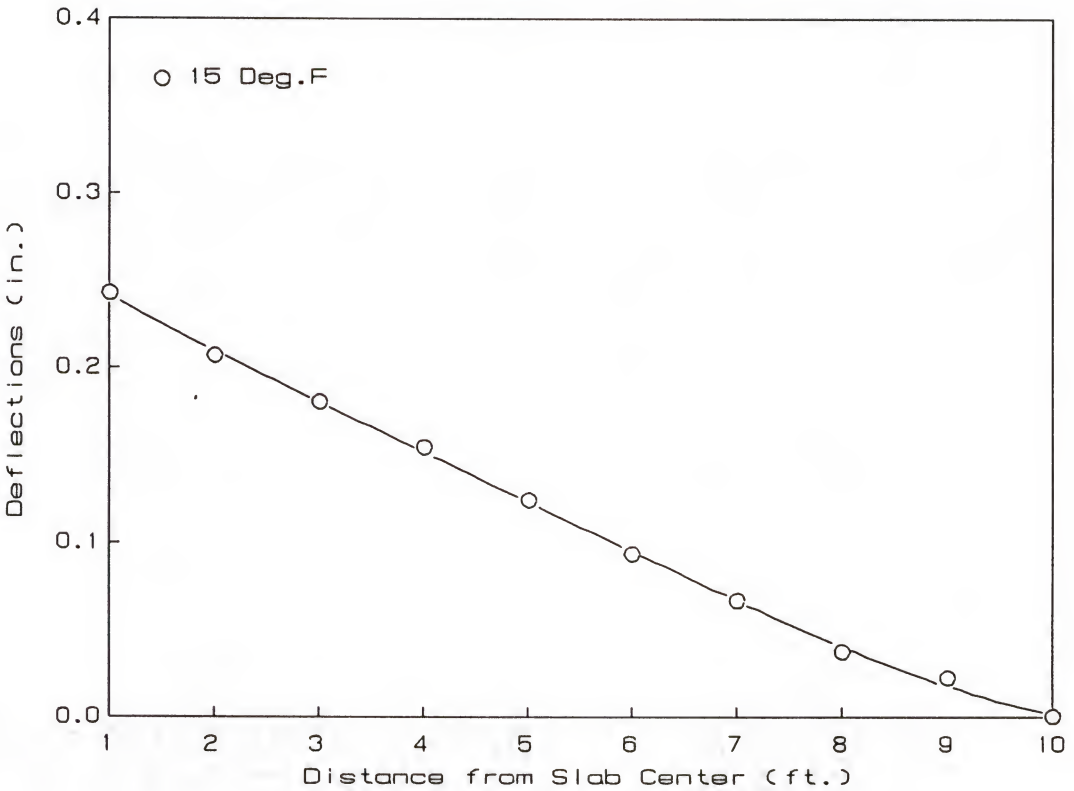

Figure 4.53 Test Slab Profile Variations Along the Slab Longitudinal Direction Using the Data Corresponding to a Temperature Differential of 2°F as a Reference as Measured on the Month of November

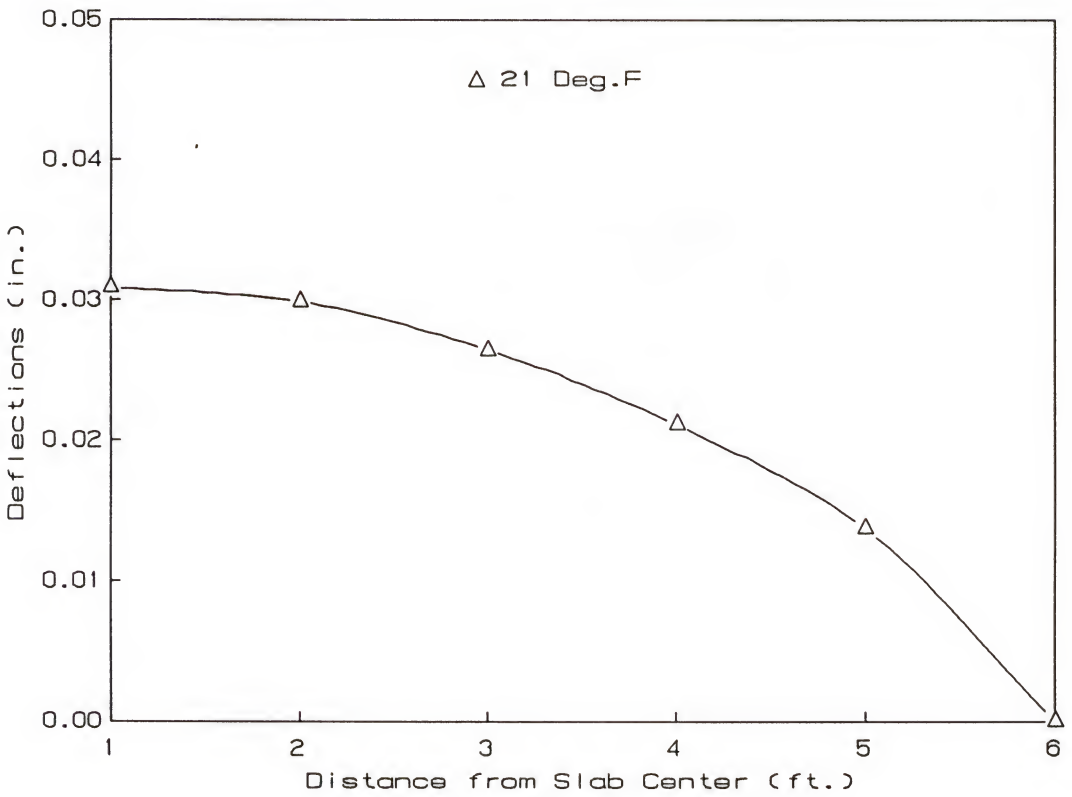

Figure 4.54 Test Slab Profile Variations Along the Slab Transversal Direction Using the Data Corresponding to a Temperature Differential of 3°F as a Reference as Measured on the Month of July

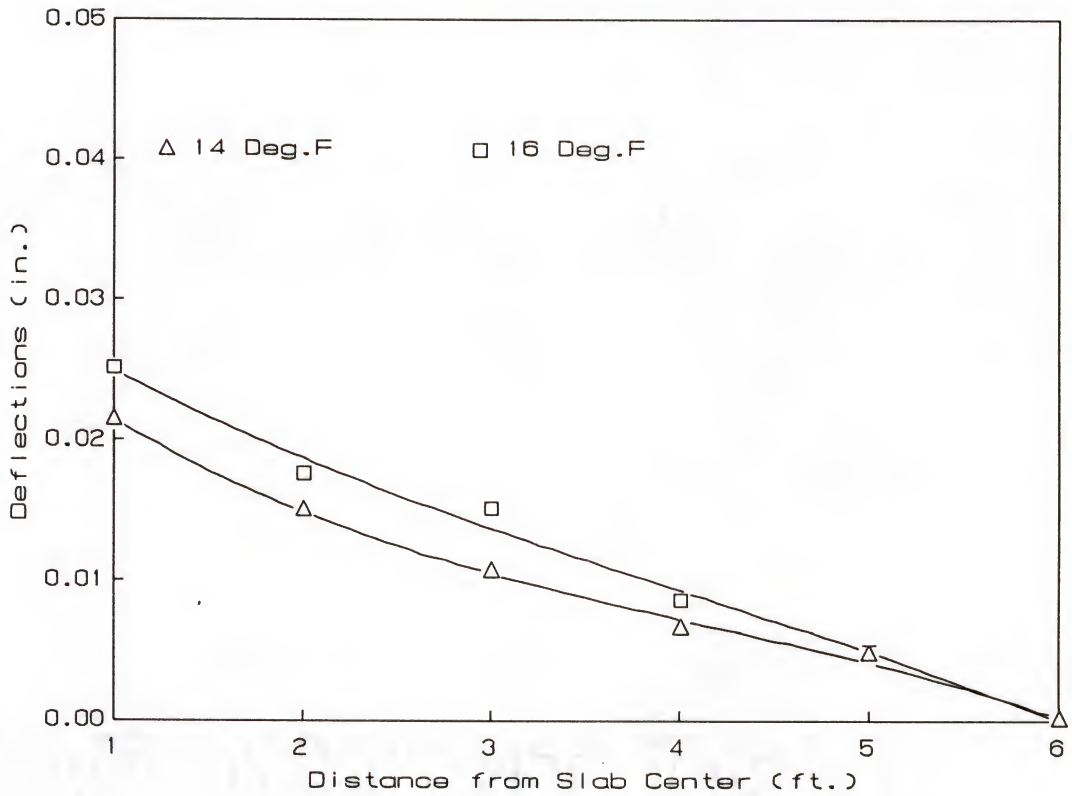

Figure 4.55 Test Slab Profile Variations Along the Slab Transversal Direction Using the Data Corresponding to a Temperature Differential of 10°F as a Reference as Measured on the Month of September

Table 4.2 Respective Analytical Deflections, in inches, Along the Slab Longitudinal Centerline as Computed Using FEACONS IV Program for Various Temperature Conditions

Distance from Slab Joint (ft)	TEMPERATURE DIFFERENTIALS						
	DT=-10°F	Dt=-6°F	DT=-2°F	DT=10°F	DT=13°F	DT=15°F	DT=21°F
0.0	-0.00306	-0.00016	0.001634	0.006179	0.007079	0.007775	0.009058
0.5	-0.00111	0.000929	0.001994	0.004371	0.004657	0.004944	0.004784
1.0	0.000577	0.001868	0.002301	0.002819	0.002567	0.002495	0.001034
2.0	0.003237	0.003315	0.002772	0.000417	-0.00071	-0.00136	-0.00503
3.5	0.005687	0.004587	0.002772	-0.00176	-0.00376	-0.00499	-0.01115
4.5	0.006548	0.004998	0.003175	-0.00252	-0.00487	-0.00634	-0.01368
5.5	0.006994	0.005181	0.003297	-0.00290	-0.00547	-0.00708	-0.01532
6.5	0.007172	0.005224	0.003346	-0.00304	-0.00573	-0.00741	-0.01629
7.5	0.007201	0.005145	0.003351	-0.00303	-0.00580	-0.00749	-0.01682
8.5	0.007171	0.005145	0.003335	-0.00297	-0.00578	-0.00746	-0.01707
9.5	0.007137	0.005101	0.003314	-0.00291	-0.00575	-0.00739	-0.01716
10	0.007129	0.005099	0.003298	-0.00289	-0.00573	-0.00736	-0.01717

Table 4.3 Respective Analytical Deflections, in inches, Along the Slab Transverse Centerline as Computed Using FEACONS IV Program for Various Temperature Conditions

Distance from Edge of Slab (ft)	TEMPERATURE DIFFERENTIALS						
	DT=-10°F	DT=-6°F	DT=-2°F	DT=10°F	DT=13°F	DT=15°F	DT=21°F
0.0	-0.00481	-0.00166	0.001106	0.008794	0.010396	0.01156	0.013525
0.5	-0.00099	-0.00036	0.001532	0.006604	0.007442	0.008125	0.008236
1.0	-0.00059	0.000774	0.001901	0.004697	0.004854	0.005111	0.003532
1.5	0.001101	0.001745	0.002237	0.003056	0.002611	0.002496	-0.00062
2.0	0.002541	0.002565	0.002481	0.001662	0.000689	0.000252	-0.00424
3.0	0.004731	0.003799	0.002878	-0.00047	-0.00229	-0.00325	-0.01006
4.0	0.006141	0.004582	0.003128	-0.00188	-0.00429	-0.00560	-0.01411
5.0	0.006923	0.005007	0.003263	-0.00268	-0.00544	-0.00697	-0.01652
5.5	0.007113	0.005106	0.003295	-0.00287	-0.00572	-0.00731	-0.01713
6.0	0.007182	0.005137	0.003305	-0.00294	-0.00582	-0.00743	-0.01734

Table 4.4 Respective Analytical Deflections, in inches, Along the Slab Edge as Computed Using FEACONS IV Program for Various Temperature Conditions

Distance from Slab Corner (ft)	TEMPERATURE DIFFERENTIALS						
	DT=-10°F	Dt=-6°F	DT=-2°F	DT=10°F	DT=13°F	DT=15°F	DT=21°F
0.0	-0.01577	-0.00681	-0.00033	0.016218	0.020617	0.023509	0.033138
0.5	-0.0138	-0.00573	0.000005	0.014528	0.018368	0.020887	0.02923
1.0	-0.01206	-0.00480	0.000296	0.013081	0.016438	0.018632	0.025842
2.0	-0.00926	-0.00335	0.000738	0.010881	0.013485	0.015172	0.020559
3.5	-0.00657	-0.00207	0.001099	0.009029	0.010960	0.012190	0.015795
4.5	-0.00559	-0.00166	0.001195	0.008496	0.010204	0.011284	0.014184
5.5	-0.00506	-0.00149	0.001218	0.008326	0.009930	0.010946	0.013412
6.5	-0.00483	-0.00147	0.001201	0.008371	0.009943	0.010956	0.013171
7.5	-0.00477	-0.00153	0.001166	0.008513	0.010090	0.011135	0.013215
8.5	-0.00479	-0.00160	0.001132	0.008664	0.010257	0.011348	0.013361
9.5	-0.00481	-0.00165	0.001109	0.008767	0.010372	0.011506	0.013486
10	-0.00482	-0.00166	0.001105	0.008791	0.010396	0.011547	0.013519

Table 4.5 Respective Analytical Deflections, in inches, Along the Slab Joint as Computed Using FEACONS IV Program for Various Temperature Conditions

Distance from Slab Corner (ft)	TEMPERATURE DIFFERENTIALS						
	DT=-10°F	DT=-6°F	DT=-2°F	DT=10°F	DT=13°F	DT=15°F	DT=21°F
0.0	-0.01577	-0.00681	-0.00033	0.016218	0.020617	0.023509	0.033138
0.5	-0.01354	-0.00558	0.000046	0.014294	0.018052	0.020534	0.028709
1.0	-0.01156	-0.00449	0.000377	0.012614	0.015805	0.017927	0.024799
1.5	-0.0098	-0.00355	0.000662	0.011172	0.013871	0.01568	0.021406
2.0	-0.00827	-0.00275	0.000902	0.009955	0.012232	0.013775	0.018503
3.0	-0.00586	-0.00151	0.001261	0.008124	0.009749	0.010887	0.014036
4.0	-0.00424	-0.00071	0.001486	0.006962	0.008160	0.009036	0.011108
5.0	-0.00331	-0.00027	0.001606	0.006329	0.007288	0.008019	0.009464
5.5	-0.00308	-0.00016	0.001634	0.006179	0.007081	0.007777	0.009066
6.0	-0.003	-0.00013	0.001643	0.006130	0.00708	0.007697	0.008932

CHAPTER 5
NON-LINEAR TEMPERATURE GRADIENT EFFECT ON STRUCTURAL RESPONSE OF RIGID PAVEMENTS

5.1 Introduction

It has long been recognized that critical stresses in concrete pavements result from the combined effects of pavement warping and superimposed traffic loads. The computation of such stresses has conventionally been made based on the assumption of a linear thermal gradient. The fact that the various methods for rigid pavement design and analysis that have been developed over the years, including the most currently used finite-element computer models such as WESLIQUID [21], WESLAYER [21], JSLAB [22], ILLI-SLAB [33] and FEACONS [1,34], are based on this convenient concept is mainly due to the difficulty in determining the temperature variations in concrete slabs and the complexity of the analysis that takes into account the non-linear thermal gradient effects. A better understanding of this nonlinearity may help in the understanding of some of the existing problems in concrete pavement behavior and provide better guidelines for design and analysis of concrete pavements.

This chapter presents the results of an experimental and analytical study to determine the effect of a non-linear temperature gradient on the behavior of a typical concrete pavement in Florida.

5.2 FEACONS IV Computer Program

An essential analytical tool, a computer program named FEACONS IV (Finite Element Analysis of CONcrete Slabs, version IV), developed at the University of Florida to analyze the response of a concrete pavement

system subjected to a combination of applied loads and temperature changes [1,34], was used during the course of this study to compute the bending stresses in the case of a linear temperature distribution throughout the concrete pavement depth.

Prior to its use, and as part of this research work, the effectiveness and suitability of this analytical model in realistically analyzing the behavior of concrete pavements was first evaluated and checked as described in chapter 7.

This section describes the basic features and the computational procedures of the FEACONS IV program.

5.2.1 Basic Features of FEACONS IV

In analyzing the response of a concrete pavement system subjected to a combination of concentrated and distributed loads the FEACONS IV computer program considers the following factors:

1. The weight of the concrete slabs.
2. The subgrade voids beneath the concrete slabs.
3. The effects of joints.
4. The looseness of the dowel bars.
5. The effects of edges.
6. The effects of temperature differentials between the top and the bottom of the slabs.
7. Nonlinear subgrade response characteristics.
8. Composite slabs made up of two different layers bonded together.
9. A stiff subbase or base layer between the concrete slabs and the subgrade.

The output of the program could consist of the following:

1. The initial deflections of concrete slabs due to their own weight and temperature effects.

2. The deflections of concrete slabs due to applied loads.
3. The moments in the concrete slabs.
4. The stresses and principal stresses at the top and the bottom of the slabs.
5. The maximum deflection, moments, stresses and principal stresses in the concrete slabs.

5.2.2 Modeling of a Concrete Pavement in FEACONS IV

5.2.2.1 Modeling of a Concrete Slab. The response characteristics of a concrete slab are influenced mainly by its two adjacent slabs, thus it is usually adequate to model a concrete pavement as a three-slab system.

In that order of idea, a jointed concrete pavement is modeled in FEACONS IV as a three-slab system while a slab is considered as an assemblage of rectangular plate bending elements with three degrees of freedom per node. These three degrees of freedom at each node consist of (1) a lateral deflection, w, (2) a rotation about the x-axis, θ_x, and (3) a rotation about the y-axis, θ_y. Therefore, the corresponding forces at each node are (1) the downward force, f_w, (2) the moment in the x direction, $f_{\theta x}$, and (3) the moment in the y direction, $f_{\theta y}$. A typical rectangular plate element and its corresponding nodal forces and displacements are shown in Figure 5.1.

The three displacements at node i can be denoted as:

$$\begin{bmatrix} w_i \\ \phi_{xi} \\ \phi_{yi} \end{bmatrix} \tag{5.1-a}$$

The twelve nodal displacement of the element can be denoted as:

$$u^e = \begin{bmatrix} u_i \\ u_j \\ u_k \\ u_l \end{bmatrix} \tag{5.1-b}$$

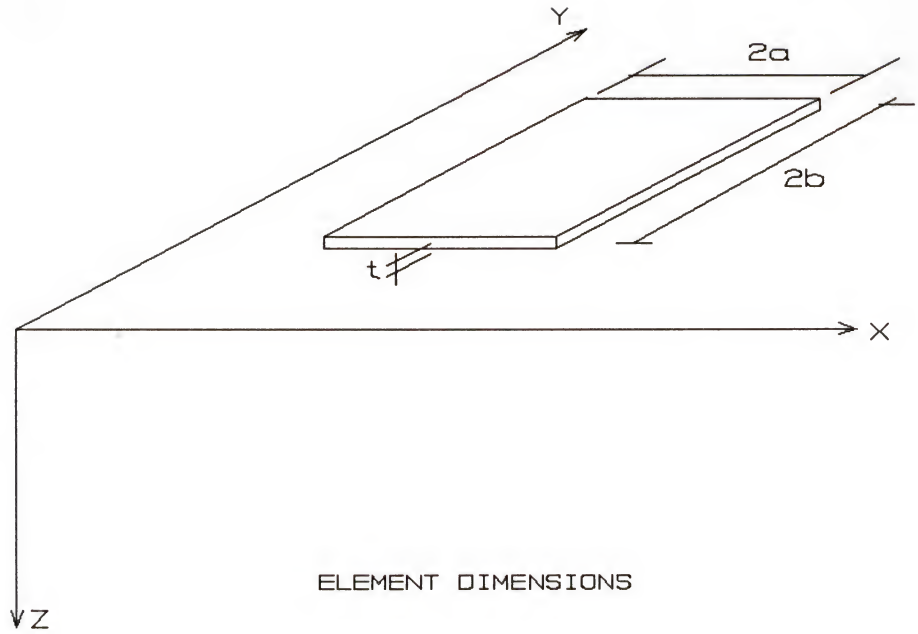

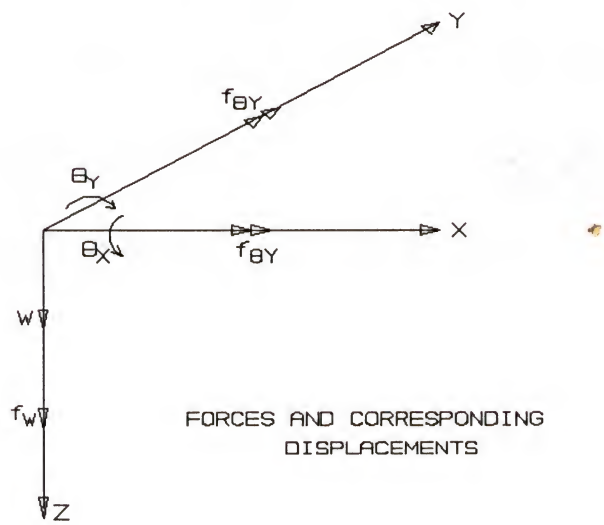

Figure 5.1 A Typical Rectangular Plate Element

The forces at node i can be denoted as:

$$f_i = \begin{bmatrix} f_w \\ f_{\theta x} \\ f_{\theta y} \end{bmatrix} \tag{5.2-a}$$

The twelve nodal forces of the element can be denoted as:

$$f^e = \begin{bmatrix} f_i \\ f_j \\ f_k \\ f_l \end{bmatrix} \tag{5.2-b}$$

The twelve nodal displacements are related to the twelve nodal forces by the element stiffness matrix, k, as follow:

$$f^e = k\ u^e \tag{5.3}$$

Explicit expressions for the element stiffness matrix, as evaluated by Zienkiewicz [36], are used in FEACONS IV program to generate the element stiffness matrices of the respective rectangular plate elements considered to model a homogeneous slab and a composite slab.

5.2.2.2 Modeling of a Stiff Subbase Layer. The program has the option of considering a stiff subbase as a separate layer but in full contact and unbonded to the concrete slabs. In such a case, the subbase is modeled similarly to the concrete slab as a thin plate. Thus, a same expression as for an isotropic material is used to generate the element stiffness matrices for this layer.

5.2.2.3 Modeling of the Subgrade. The subgrade is assumed as a Winkler foundation modeled by a series of vertical springs at the nodes while the subgrade voids are modeled as initial gaps between the slab and the springs at the specified nodes. If a gap exists, a spring stiffness of zero would be used. Either a linear or a nonlinear load-deformation relationship for the springs can be specified. In the linear case, the subgrade stiffness remains constant as long as the slab and the subgrade

are in full contact with one another. However, in the nonlinear case, a load-deformation relationship of the following form is used:

$$F = Ad + Bd^2 \tag{5.4}$$

where:

F = force/area

d = deflection

A and B = coefficients to be specified in the input.

The subgrade stiffness is thus equal to A + 2Bd, which varies with the deflection.

5.2.2.4 Modeling of Joints and Edges. Load transfers across the joints are modeled by linear and rotational springs connecting the slabs at the nodes of the elements along the joints. Frictional effects at the edges are modeled by linear springs at the nodes along the edges. Looseness of the dowel bars is modeled by a specified slip distance such that shear and moment stiffnesses become fully effective only when the slip distance is overcome.

5.2.2.5 Equivalent Nodal Loads Due to Uniform Distributed Loads. When a uniform distributed load q is applied on a rectangular plate bending element, the equivalent nodal loads can be derived to be:

$$f_D = 4\ abq \begin{bmatrix} 1/4 \\ -b/12 \\ a/12 \\ 1/4 \\ b/12 \\ a/12 \\ 1/4 \\ -b/12 \\ -a/12 \end{bmatrix} \tag{5.5}$$

The above expression is used by FEACONS IV in computing the equivalent nodal loads due to uniform distributed loads.

5.2.2.6 Equivalent Nodal Loads Due to Uniform Temperature Gradients. When the temperature varies linearly from the top to the bottom of the rectangular plate element with a temperature differential of ΔT, the equivalent nodal loads can be evaluated to be:

$$f_T = \frac{Et^2 \alpha \Delta T}{12(1-\upsilon)} \begin{bmatrix} 0 \\ a \\ -b \\ 0 \\ -a \\ -b \\ 0 \\ a \\ b \\ 0 \\ -a \\ b \end{bmatrix} \tag{5.6}$$

where:

α = Coefficient of thermal expansion

ΔT = (Temperature at top) - (Temperature at bottom)

t = Thickness of plate element

For a composite element made up of a top layer with a thickness of t_1 and an elastic modulus of E_1, bonded to a bottom layer with a thickness of t_2 and an elastic modulus E_2, the equivalent nodal loads due to the same temperature differential of ΔT can be derived to be:

$$f_T = \frac{\overline{EI}}{(1-\upsilon)} \frac{\alpha \Delta T}{t} \begin{bmatrix} 0 \\ a \\ -b \\ 0 \\ -a \\ -b \\ 0 \\ a \\ b \\ 0 \\ -a \\ b \end{bmatrix} \tag{5.7}$$

where:

t = Total thickness of the composite slab.

$$\overline{EI} = E_1 I_1 + E_2 I_2 \tag{5.8}$$

$$I_1 = t_1 3/12 + t_1 (t_2 + t_1/2 - \overline{z})^2 \tag{5.9}$$

$$I_2 = t_2 3/12 + t_2 (\overline{z} - t_2/2)^2 \tag{5.10}$$

$$\overline{z} = \{t_2 + t_1 (t_1 + t_2) / [t_1 + t_2 (E_2/E_1)]\}/2 \tag{5.11}$$

Equations 5.6 and 5.7 are used in FEACONS IV to compute the equivalent nodal loads due to uniform temperature gradients in homogeneous slabs and composite slabs, respectively.

5.2.3 FEACONS IV Computational Procedures

The computational procedures performed by FEACONS IV program are described in the following subsections.

5.2.3.1 Computation of slab deflections. An incremental procedure is used in computing the respective slab deflections due to the weight of the slabs, thermal gradients and applied loads.

The equivalent nodal force vector, F, due to the slab weight, thermal gradient or applied loads is first computed. Then the force vector is divided by the specified number of increments to obtain the incremental load vector, ΔF. The deflections, ΔU caused by the incremental force vector are computed from the stiffness equation given below:

$$K (\Delta U) = \Delta F \tag{5.12}$$

where:

K = Global stiffness matrix.

ΔU = Vector of incremental nodal deflections.

ΔF = Vector of incremental nodal forces.

The global stiffness matrix, K, is constructed from the respective stiffness matrices of the element, the joint spring elements, the edge and the subgrade springs, depending upon to the finite element mesh selected and the deflections of the slab.

After each computation of incremental deflections, the global stiffness matrix K is modified according to the new deflection positions of the slab. The new K is then used to compute the next set of incremental deflections. The computed incremental deflections are then summed up to obtain the total induced deflections.

The weight of the slabs is modeled as a uniform distributed load. The structure force vector due to the weight of the slabs is constructed from the force vectors of the plate elements due to a uniform distributed load. The structure force vector due to the effect of the thermal gradient is generated from the equivalent nodal forces on a plate element due to a uniform thermal gradient. The structure force vector due to applied loads is constructed from the concentrated nodal forces and the element force vector due to uniform distributed loads.

5.2.3.2 Computation of internal moment intensities. The internal moments per unit length at the nodes are calculated from the final nodal deflections. The nodal deflections for each element are first extracted from the final structure deflection vector and then used to compute the internal moment intensities of the element at the nodes. The internal moment intensities at the nodes of each element are computed according to the following equation:

$$M = \begin{bmatrix} M_i \\ M_j \\ M_k \\ M_l \end{bmatrix} = Su^e \tag{5.13}$$

where:

$$M_i = \begin{bmatrix} M_x \\ M_y \\ M_{xy} \end{bmatrix}_i \text{, moment intensities at node } i.$$

u^e = element nodal displacements.

S = stress matrix

For homogeneous slabs, the computed moment intensities at each node are then adjusted for the curvatures due to thermal gradients according to the following expression:

$$\begin{bmatrix} M_x \\ M_y \\ M_{xy} \end{bmatrix}_{\text{adjusted}} = \begin{bmatrix} M_x \\ M_y \\ M_{xy} \end{bmatrix}_{\text{initial}} + \frac{Et^2 \alpha \Delta T}{12(1-\upsilon)} \begin{bmatrix} 1 \\ 1 \\ 0 \end{bmatrix} \tag{5.14}$$

For composite slabs, the computed moment intensities are adjusted as:

$$\begin{bmatrix} M_x \\ M_y \\ M_{xy} \end{bmatrix}_{\text{adjusted}} = \begin{bmatrix} M_x \\ M_y \\ M_{xy} \end{bmatrix}_{\text{initial}} + \frac{\overline{EI}\, \alpha \Delta t}{t(1-\upsilon)} \begin{bmatrix} 1 \\ 1 \\ 0 \end{bmatrix} \tag{5.15}$$

where all the variables are as defined earlier.

The moment intensities at each node are the two bending moment intensities M_x and M_y, and the twisting moment intensity M_{xy}. M_x is the

bending moment intensity due to σ_x, flexural stress in the x direction. M_y is due to σ_y, flexural stress in the y direction. M_{xy} is due to τ_{xy}, shearing stress in the xy direction.

Two elements that are incident at the same node may have different moment intensities for that node. This is because that only continuity of nodal displacements is required and that the moment intensities are dependent on the individual geometry of an element and thus are unique for an individual element.

In order to obtain more representative values of moment intensities at a node, the program calculates the average values of the moment intensities as computed from the adjoining elements, and uses them for computation of stresses.

5.2.3.3 Computation of stresses. Flexural and shearing stresses are calculated from the moment intensities by using classical thin plate theory. The stresses at the top of the slab are computed by the following equations:

For Homogeneous Slabs

$$\sigma_x = -6M_x/t^2 \tag{5.16}$$

$$\sigma_y = -6M_y/t^2 \tag{5.17}$$

$$\tau_{xy} = 6M_{xy}/t^2 \tag{5.18}$$

For Composite Slabs

$$\sigma_x = -(t-\bar{z})\, M_x E_1 / \overline{EI} \tag{5.19}$$

$$\sigma_y = -(t-\bar{z})\, M_y E_1 / \overline{EI} \tag{5.20}$$

$$\tau_{xy} = (t-\bar{z})\, M_{xy} E_1 / \overline{EI} \tag{5.21}$$

The stresses at the bottom of the slab are computed by the following equations:

For Homogeneous Slabs

$$\sigma_x = 6\, M_x/t^2 \tag{5.22}$$

$$\sigma_y = 6\ M_y/t^2 \tag{5.23}$$

$$\tau_{xy} = -6\ M_{xy}/t^2 \tag{5.24}$$

For Composite Slabs

$$\sigma_x = \overline{z}\, M_x E_2 / \overline{EI} \tag{5.25}$$

$$\sigma_y = \overline{z}\, M_y E_2 / \overline{EI} \tag{5.26}$$

$$\tau_{xy} = -\overline{z}\, M_{xy} E_2 / \overline{EI} \tag{5.27}$$

In the above equations (5.16 through 5.27), all the variables are as defined earlier.

The program computes the principal stresses from the flexural and shear stresses using the classical Mohr Circle theory. The program can also obtain the maximum deflections, moments, stresses and principal stresses for specified regions of interests.

5.3 Thermal Stress Analysis

5.3.1 Comparison Study of Linear Thermal Gradient Induced Stresses

As reviewed in Chapter 2, several empirical or semi-empirical methods of determining thermal warping stresses have been proposed as early as 1926 when Westergaard presented his well known mathematical analysis on the subject.

Using Westergaard's concepts, Royall D. Bradbury developed equations for the computation of the temperature-induced warping stresses at different positions of concrete pavement slabs [12].

In this section, the thermal stresses caused by the respective temperature differentials between top and bottom of the concrete slab as recorded from the test slabs were computed by means of FEACONS IV program and also by means of the Bradbury's equations for comparison purpose.

5.3.1.1 Warping stresses according to Bradbury's equations. The general Bradbury's expressions for computing warping stresses due to temperature differential are as follows:

Edge stress: $\sigma = C_x E\alpha\Delta T/2$ (5.28)

Interior stresses: $\sigma_x = (E\alpha\Delta T/2)[(C_x + \mu C_y)/(1 - \mu^2)]$ (5.29)

$\sigma_y = (E\alpha\Delta T/2)[(C_y + \mu C_x)/(1 - \mu^2)]$ (5.30)

where

E = modulus of elasticity of concrete;

α = thermal coefficient of expansion of concrete;

ΔT = temperature difference between top and bottom of slab;

μ = Poisson's ratio of concrete; and

C_x, C_y = warping stress coefficients.

The coefficients C_x and C_y are functions of the free length and width depending on the direction in which the curling stress is required. The values of these warping stress coefficients are given by the normograph in Figure 2.3.

Consequently, for a slab 20 ft long, 12 ft wide and 9 in thick, with an assumed coefficient of thermal expansion of $6x10^{-6}/°F$, a modulus of elasticity of 4500 psi and a Poisson's ratio of 0.2 for concrete, and a subgrade stiffness of 300 pci, the coefficients C_x and C_y are determined to be equal to 1.064 and 0.609, respectively. Then, the equations (5.28) through (5.30) would only be functions of the temperature differentials as follow:

Edge stress: $\sigma = 14.364\Delta T$ (5.31)

Interior stresses: $\sigma_x = 16.675\Delta T$ (5.32)

$\sigma_y = 11.556\Delta T$ (5.33)

From the equations above, it can be observed that the maximum warping stresses computed according to Bradbury's formulas occur at the interior of the slab and run in the longitudinal direction. Using the temperature data recorded during the course of this study, typical values

of thermal stresses are computed for a daily cycle according to Bradbury's equations and summarized in Table 5.1, along with the corresponding computed stresses from the FEACONS program.

5.3.1.2 Comparative results. The maximum warping stresses computed using Bradbury's equations are 513 psi and 232 psi for the conditions of maximum positive and negative temperature differentials, respectively, as recorded for the months of June at 1:00 P.M. and April at 6:00 A.M., while the corresponding maximum thermal stresses computed using FEACONS IV are respectively 418 psi for the daytime and 216 psi for the nighttime conditions.

It can be noticed from Table 5.1 that the computed stress values are relatively close to one another for the nighttime conditions, i.e, approximately 11% difference between the higher and the lower values, while Bradbury's equation gave relatively higher stresses for the daytime conditions. It is believed that the differences are due to the fact that the FEACONS IV program can take into account the possible loss of contact between the slab and the subgrade while Bradbury's method does not.

5.3.2 Non-Linear Thermal Gradient Induced Stress

To determine the stresses caused by the non-linear temperature component as expressed in Equation (4.14), it is assumed that a plane cross-section in the concrete slab remains plane throughout the thermal changes. The constraint to keep the cross-section plane would cause thermal stresses to be induced. These induced stresses can be determined by multiplying the negative of the non-linear temperature component by the coefficient of thermal expansion and the modulus of elasticity of concrete, as follows:

$$\sigma = - E_c \alpha t_{nonlinear} = - E_c \alpha C[y^2 - dy + (d^2/6)] \qquad (5.34)$$

Table 5.1 Representative Values of Maximum Warping Stresses as Computed for a Daily Cycle Using Bradbury's Equations and FEACONS IV, Respectively.

Period of the Year	Typical Daily Cycle Time	Temperature Differential	Stresses (psi)	
			Bradbury	FEACONS IV
January	11:00 am	0.99	17	16
	12:00 pm	6.15	103	102
	01:00 pm	9.24	154	147
	02:00 pm	9.46	158	151
	06:00 pm	- 5.03	84	84
	08:00 pm	- 7.88	191	128
	10:00 pm	- 9.22	154	149
	00:00 am	-10.05	168	181
	12:00 pm	-11.06	183	176
	00:00 am	-11.48	191	181
	06:00 am	-11.51	182	181
	08:00 am	-3.37	56	56
April	10:00 am	9.64	191	154
	12:00 pm	22.88	382	309
	01:00 pm	25.84	191	352
	02:00 pm	26.36	440	359
	04:00 pm	16.97	283	250
	02:00 pm	-6.81	114	112
	12:00 pm	-9.51	159	153
	00:00 am	-10.93	182	176
	00:00 am	-11.96	193	181
	04:00 am	-12.86	214	200
	06:00 am	-13.89	232	216

Table 5.1 -- continued

Period of the Year	Typical Daily Cycle Time	Temperature Differential	Stresses (psi)	
			Bradbury	FEACONS IV
June	09:00 am	10.45	174	164
	11:00 am	22.95	383	300
	01:00 pm	30.75	513	116
	03:00 pm	14.78	246	228
	05:00 pm	18.31	305	263
	07:00 pm	3.91	65	56
	08:00 pm	- 0.71	12	70
	00:00 pm	- 5.16	56	86
	00:00 am	- 7.06	118	116
	02:00 am	- 7.97	133	170
	00:00 am	-8.07	144	130
	06:00 am	- 7.86	131	128
July	09:00 am	-3.34	56	56
	10:00 pm	-7.07	178	116
	00:00 am	-8.61	144	139
	02:00 am	-9.77	163	167
	04:00 am	-10.41	174	167
	06:00 am	-10.67	178	170
	09:00 am	-8.61	144	139
	10:00 am	4.24	71	70
	12:00 pm	16.97	283	263
	01:00 pm	22.24	371	300
	02:30 pm	27.26	455	371
	04:00 pm	-8.61	444	362
	06:00 pm	16.71	279	249
	08:00 pm	0.9	15	15

Table 5.1 -- continued

Period of the Year	Typical Daily Cycle Time	Temperature Differential	Stresses (psi)	
			Bradbury	FEACONS IV
August	04:00 am	-2.96	49	50
	10:00 am	4.88	81	84
	02:00 pm	18	395	258
	02:00 pm	23.66	395	322
	03:16 pm	27.77	463	378
	05:00 pm	15.94	266	241
	04:00 am	3.08	51	51
	08:00 pm	-0.51	9	9
	10:00 pm	-5.79	97	96
	00:00 am	-7.97	133	129
	08:00 am	-8.36	139	145
	04:00 am	-9	150	145
	08:00 am	-9.13	152	194
	08:00 am	-7.59	127	129
November	08:00 pm	23.66	144	190
	10:00 pm	-12.14	170	194
	00:00 am	-11.52	198	181
	00:00 am	-11.89	198	187
	07:00 am	-12.14	202	187
	08:00 am	-12.1	202	145
	07:00 am	-12.46	266	194
	09:00 am	-3.1	52	52
	10:00 am	5.09	85	84
	10:00 pm	16.71	279	249
	01:18 pm	20.49	342	295
	02:00 pm	19.84	331	287
	04:00 pm	4.87	81	80

This stress is a function of (1) the coefficient C, (2) the coefficient of thermal expansion α and (3) the concrete modulus of elasticity E_c.

Since the non-linear temperature component does not affect the bending of the concrete slab, its effects on the total stresses in the concrete slab would be independent of the effects of the other factors. The total stress distribution can be obtained by adding algebraically the bending stress due to a linear temperature gradient as computed by the FEACONS IV program to the corresponding stress due to the non-linear component of the temperature distribution as given by the Equation 5.34.

The temperature data recorded on the test slabs were used to determine the thermal stresses in the concrete slabs by taking the effects of the non-linear temperature component into account. The concrete was assumed to have a constant coefficient of thermal expansion of $6 \times 10^{-6}/°F$ and a modulus of elasticity of 4500 ksi. The stress due to the non-linear temperature component in a 9-inch thick slab is given by the following expression:

$$\sigma = - 27C(y^2 - 9y + 13.5) \qquad (5.35)$$

From this expression, it can be seen that, if the coefficient C is positive, the extreme fibers of the slab tend to expand and cause internal compressive stresses at these positions while tensile stresses would result at slab mid-depth. This condition is reversed if the coefficient C is negative. This observation is valid for any slab thickness.

From the analysis of the temperature data recorded on the test slabs at different depths, representative values of the coefficient C as well as those of the other coefficients A and B of the assumed temperature distribution model were computed for different conditions in section 4.2.4 and summarized in Table 4.1. As stated previously, it can be observed from that table that the coefficient C, and therefore magnitude of the stresses

as given by equation (5.35), is not directly correlated to the temperature differentials between the top and bottom of the slab but is affected by the temperature distribution throughout the slab thickness.

Since the concrete is much weaker in tension than in compression, the only values of the coefficient C of interest in this analysis are the negative ones. In this case, the tensile stresses caused by the non-linear temperature component are additive to those resulting from either a positive or negative temperature differential. Consequently, since a positive and a negative temperature differentials cause tensile stress respectively at the bottom and at the top of the slab, the relative critical warping conditions would result from a combination of either a maximum positive or negative temperature differential and a maximum negative C value that would induce maximum tensile stress at the bottom or at the top of the concrete slab, respectively.

5.3.3 Non-Linear Temperature Distribution Effects on Warping Stresses

Representative values of stresses due to the non-linear temperature component, bending stresses due to the linear temperature component, and the total stresses as determined in a daily cycle for various time periods according to Florida conditions are shown in Table 5.2. As a convention, the tensile stresses are computed as positive values while the compressive stresses are negative.

It can be observed from Table 5.2 that the maximum compressive stresses due to the non-linear temperature component generally occurred between noon to 1 P.M., while the warping tensile stress at the extreme fibers of the slab reached its peak between 8 to 10 P.M. A maximum tensile stress of 79 psi was computed for the month of July at 8 P.M.

Since concrete is much weaker in tension than in compression, the tensile stresses are much more critical and of more concern than the

Table 5.2 Representative Computed Total Stresses at the Extreme Slab Fibers Caused by the Non-Linear Temperature Distribution in a Daily Cycle

Period of the Year	Typical Daily Cycle Time	STRESSES (psi)				
		Non-Linear	Bending		Total	
		Top & Bottom	Top	Bottom	Top	Bottom
January	11:00 am	-55	-16	16	-71	-39
	12:00 pm	-97	-102	102	-169	35
	01:00 pm	-63	-147	147	-210	84
	02:00 pm	-44	-151	154	-195	107
	06:00 pm	18	84	-84	102	-66
	08:00 pm	22	128	-176	150	-106
	10:00 pm	22	149	-149	171	-127
	00:00 am	18	161	-181	176	-146
	02:00 am	18	176	-176	194	-158
	04:00 am	19	181	-181	200	-162
	06:00 am	16	181	-181	197	-165
	08:00 am	6	56	-56	62	-54
April	10:00 am	-106	-154	154	-260	48
	12:00 pm	-116	-309	359	-425	193
	01:00 pm	-97	-352	352	-448	250
	02:00 pm	-79	-359	359	-438	250
	06:00 pm	0	-250	250	-260	250
	08:00 pm	58	112	-112	170	-54
	10:00 pm	45	153	-153	198	-108
	00:00 am	31	174	-174	205	-143
	02:00 am	31	188	-188	219	-157
	04:00 am	27	200	-200	227	-173
	06:00 am	24	216	-216	240	-192

Table 5.2 -- continued.

Period of the Year	Typical Daily Cycle Time	STRESSES (psi)				
		Non-Linear	Bending		Total	
		Top & Bottom	Top	Bottom	Top	Bottom
June	09:00 am	-87	-164	164	-251	77
	11:00 am	-96	-310	310	-406	214
	01:00 pm	-103	-418	318	-521	315
	03:00 pm	50	-228	228	-176	280
	05:00 pm	-21	-263	263	-284	242
	07:00 pm	63	-64	64	-1	128
	08:00 pm	67	12	-12	79	55
	10:00 pm	50	86	-86	196	-36
	00:00 am	36	116	-176	152	-80
	02:00 am	29	128	-128	158	-100
	04:00 am	48	139	-139	149	-111
	06:00 am	15	128	-128	149	-118
July	08:00 pm	48	56	-56	104	-8
	10:00 pm	48	116	-116	162	-70
	00:00 am	40	139	-139	179	-99
	02:00 am	48	157	-167	196	-118
	04:00 am	37	167	-167	201	-130
	06:00 am	31	170	-170	201	-139
	08:00 am	10	139	-139	149	-129
	10:00 am	-76	-70	70	-146	-8
	10:00 pm	-116	-250	250	-366	134
	01:00 pm	-129	-300	300	-430	171
	02:30 pm	-119	-371	371	-490	252
	05:00 pm	-85	-362	362	-447	277
	06:00 pm	-6	-249	249	-255	243
	08:00 pm	79	-15	15	64	94

Table 5.2 -- continued.

Period of the Year	Typical Daily Cycle Time	STRESSES (psi)				
		Non-Linear	Bending		Total	
		Top & Bottom	Top	Bottom	Top	Bottom
August	09:00 am	-74	50	-96	30	-69
	10:00 am	-74	-81	81	-155	7
	12:00 pm	-107	-258	258	-365	151
	02:00 pm	-98	-322	322	-420	224
	03:16 pm	-116	-378	378	-494	262
	05:00 pm	-39	-241	241	-280	202
	02:00 pm	68	-51	81	17	119
	08:00 pm	60	9	-9	69	51
	12:00 pm	61	96	-96	157	-35
	00:00 am	54	129	-129	183	-75
	00:00 am	40	135	-135	175	-95
	04:00 am	40	145	-140	181	-109
	06:00 am	31	147	-147	175	-116
	08:00 am	13	123	-129	136	-110
November	08:00 pm	40	140	-140	188	-92
	12:00 pm	13	163	-163	206	-120
	10:00 am	40	191	-181	221	-161
	00:00 am	33	187	-187	220	-154
	04:00 am	40	191	-194	221	-161
	06:00 am	28	140	-190	217	-163
	04:00 am	28	194	-194	222	-166
	09:00 am	-53	52	-52	-1	-109
	10:00 am	-53	-81	81	-177	-9
	12:00 pm	-118	-249	249	-367	131
	01:18 pm	-109	-295	295	-404	186
	02:00 pm	83	-287	287	-370	204
	04:00 pm	36	-80	80	-44	116

compressive stresses. Table 5.2 shows that the non-linear temperature component tends to increase the total maximum tensile stress in the slab at nighttime when the temperature differentials are negative, while it tends to reduce the maximum tensile stress during daytime when positive temperature differentials occur. A maximum stress, due to the consideration of a non-linear temperature distribution, of 240 psi was computed for the condition of 6 A.M. during the month of April, while the computed stress without the consideration of the non-linear temperature effects was 216 psi. This amounts to an increase of approximately 11% in tensile stress. Conversely, a maximum computed bending stress of 418 psi was obtained for the month of June at 1 P.M., while the corresponding computed total stress with the consideration of the non-linear temperature effects was 315 psi. It represents a 25% reduction in computed tensile stress. A maximum percent increase in computed tensile stress of 661% was obtained in August, when the consideration of the effects of non-linear temperature distribution increased the slab tensile stress from 9 to 69 psi.

5.4 Non-Linear temperature Gradient Effect on Structural Response of Concrete Pavements Under Critical Conditions

The first part of this chapter consisted of analyzing the effect of the non-linear temperature distribution on the warping stresses only. However, in concrete pavement analysis and design, it is essential to consider the simultaneous effect of load and temperature variation. Knowledge on how concrete pavements behave under critical thermal and loading conditions in a case of non-linear temperature distribution throughout the slab depth is lacking at present. Thus, an analysis of the effect of the temperature gradient nonlinearity on the structural response of a typical Florida concrete pavements under critical thermal-loading conditions was performed.

5.4.1 Method of Analysis

A previous research study [1] showed that the critical load positions are at the edge and corner of the slab for the conditions of positive and negative temperature differentials, respectively. Therefore, these two load positions were used in this analysis.

FEACONS IV program, in conjunction with equation (5.35), was used to compute the maximum thermal-loading stresses according to Florida conditions for the respective assumptions of linear and non-linear temperature distributions. A reference applied load of a 22-kip single-axle load (two 11-kip at 6 feet apart), which represents the approximate maximum allowable load in Florida, was used. The maximum positive and negative temperature differentials in a daily cycle as recorded at various time of the year were considered.

A typical pavement system with the following dimensions and properties was used:

1. Slab of 20 ft length, 12 ft width and 9 in thickness.
2. Concrete modulus of 4500 ksi.
3. Subgrade modulus of 300 pci.

5.4.2 Analysis of Results

Stresses induced by the above conditions are illustrated in Figure 5.2 through 5.13. The tensile stresses are plotted as positive while the negative values represent compressive stresses.

Figures 5.2 to 5.7 correspond to the conditions of corner loading and maximum negative temperature differential in a daily cycle and Figures 5.8 to 5.13 illustrate the case of edge loading and maximum positive temperature differential.

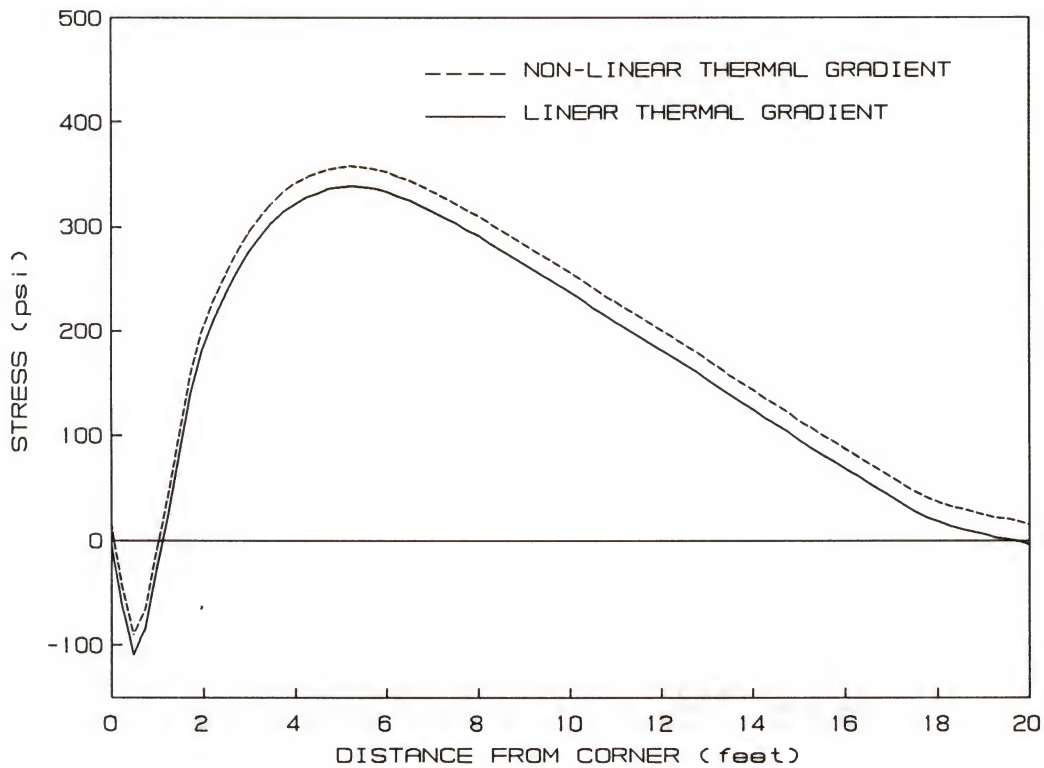

Figure 5.2 Maximum Flexural Stress Along the Slab Edge Caused by a 22-Kip Single Axle Load Applied at the Slab Corner and a Maximum Negative Temperature Differential of 11.51°F as Recorded for a Typical Daily Cycle Corresponding to the Month of January at 6:00 A.M.

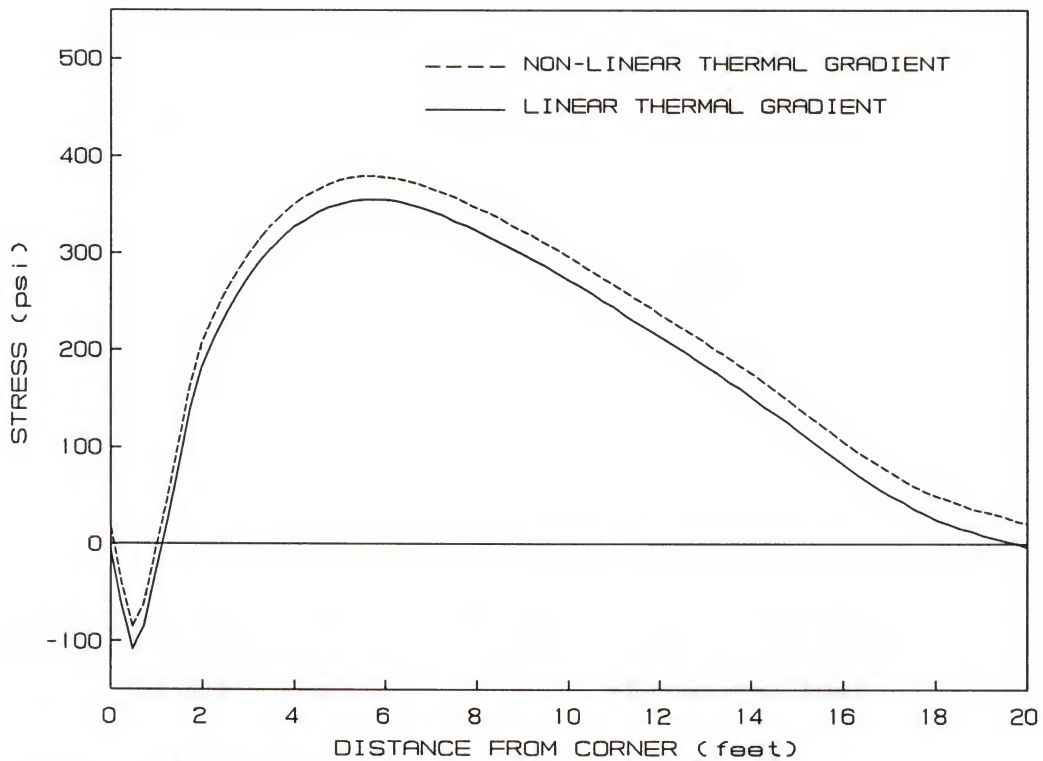

Figure 5.3 Maximum Flexural Stress Along the Slab Edge Caused by a 22-Kip Single Axle Load Applied at the Slab Corner and a Maximum Negative Temperature Differential of 13.89°F as Recorded for a Typical Daily Cycle Corresponding to the Month of April at 6:00 A.M.

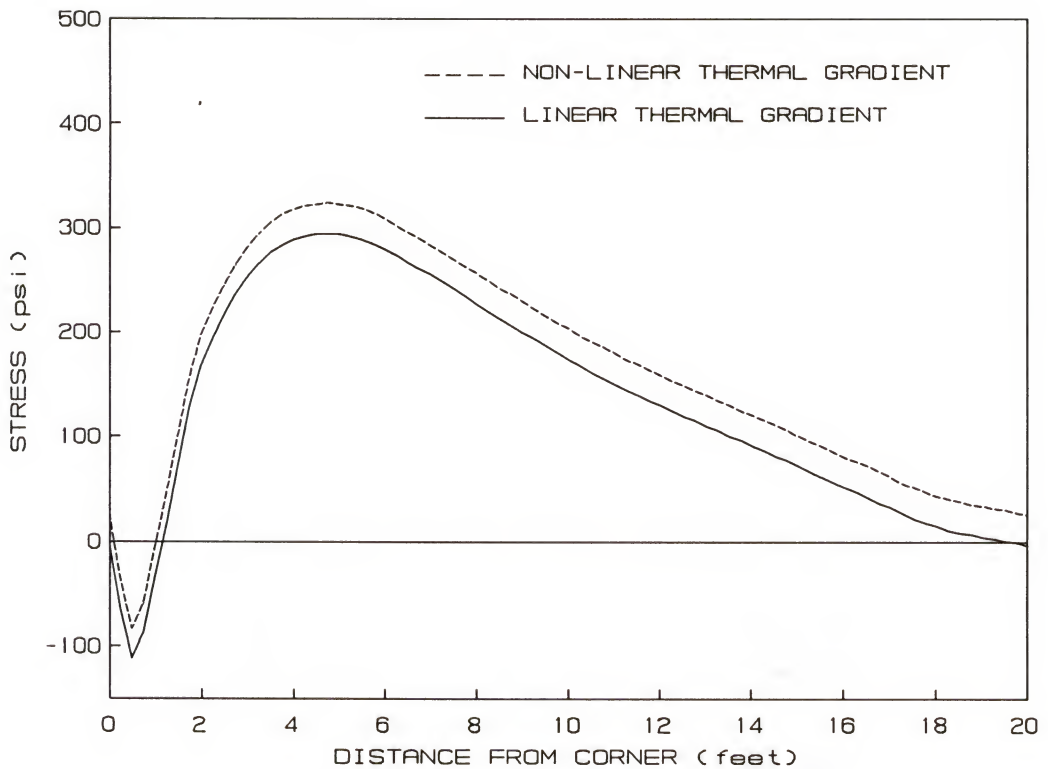

Figure 5.4 Maximum Flexural Stress Along the Slab Edge Caused by a 22-Kip Single Axle Load Applied at the Slab Corner and a Maximum Negative Temperature Differential of 8.02°F as Recorded for a Typical Daily Cycle Corresponding to the Month of June at 4:00 A.M.

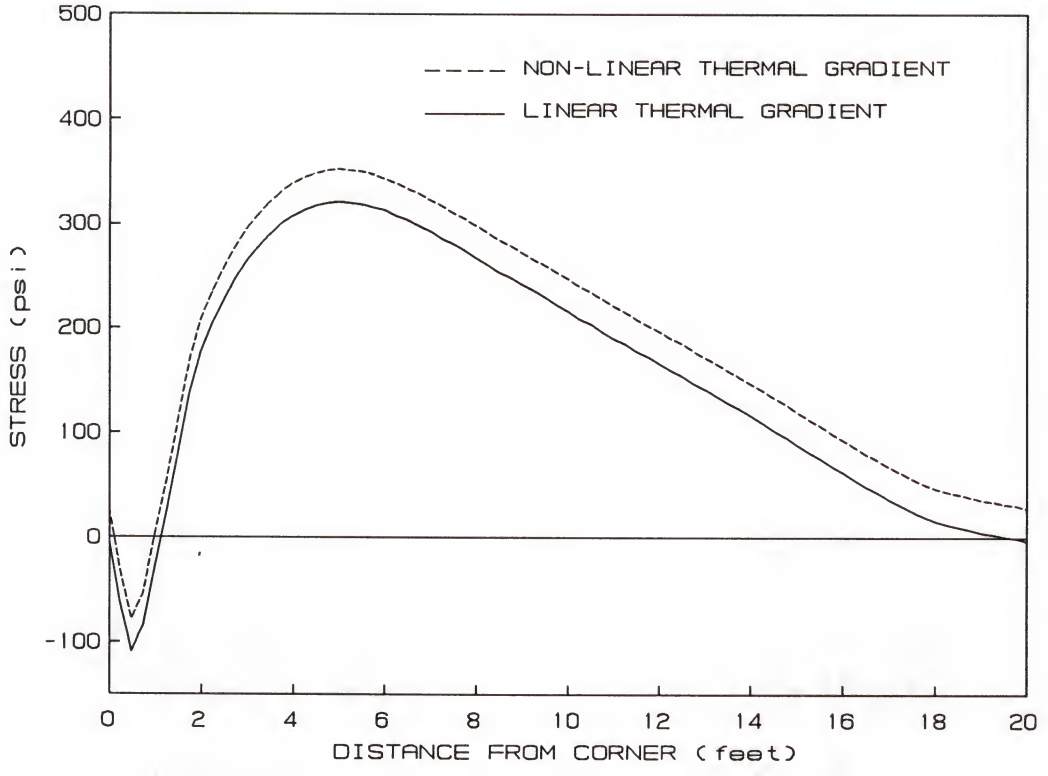

Figure 5.5 Maximum Flexural Stress Along the Slab Edge Caused by a 22-Kip Single Axle Load Applied at the Slab Corner and a Maximum Negative Temperature Differential of 10.67°F as Recorded for a Typical Daily Cycle Corresponding to the Month of July at 6:00 A.M.

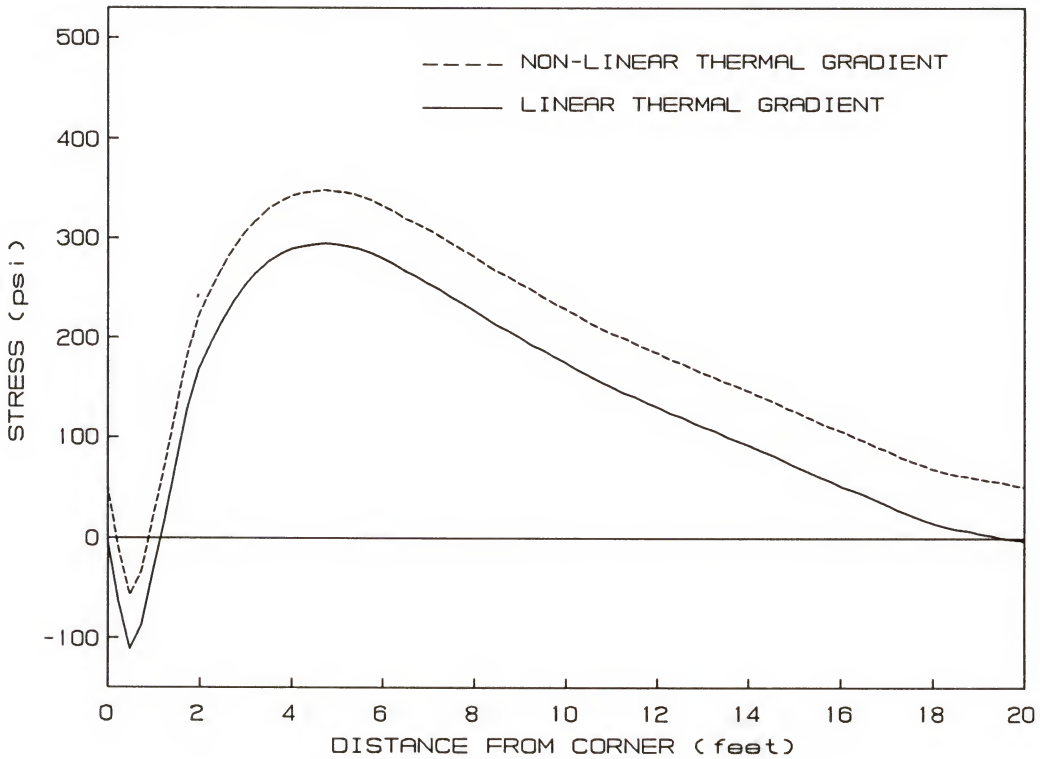

Figure 5.6 Maximum Flexural Stress Along the Slab Edge Caused by a 22-Kip Single Axle Load Applied at the Slab Corner and a Maximum Negative Temperature Differential of 9.13°F as Recorded for a Typical Daily Cycle Corresponding to the Month of August at 6:00 A.M.

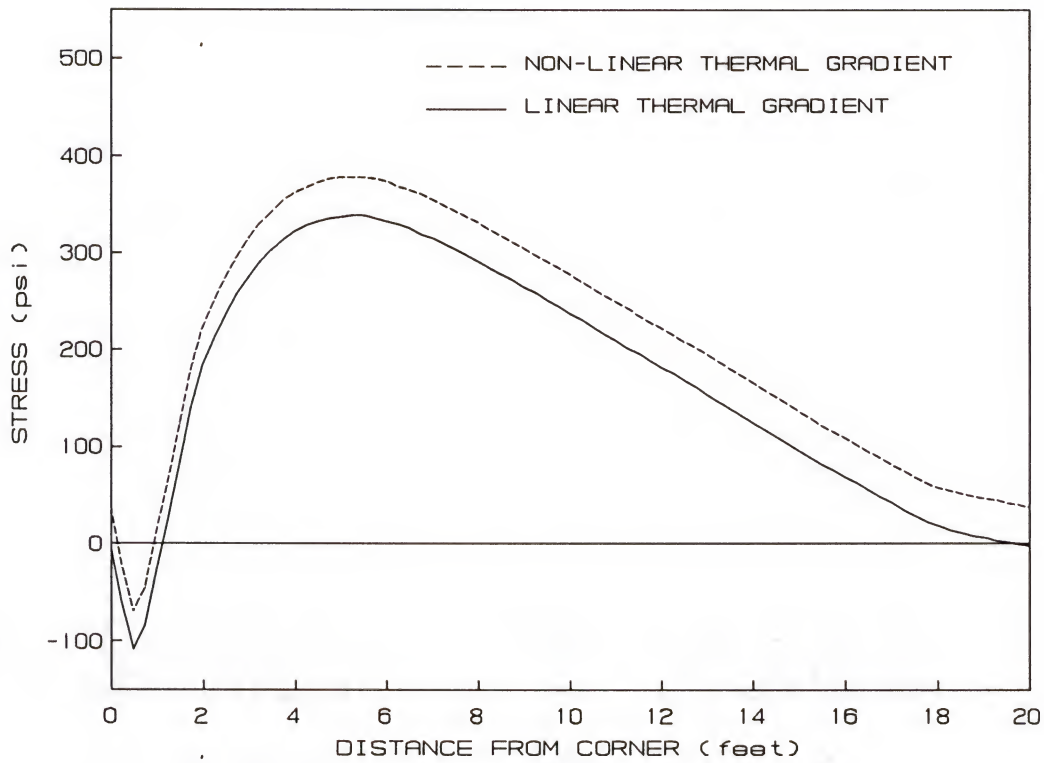

Figure 5.7 Maximum Flexural Stress Along the Slab Edge Caused by a 22-Kip Single Axle Load Applied at the Slab Corner and a Maximum Negative Temperature Differential of 12.46°F as Recorded for a Typical Daily Cycle Corresponding to the Month of November at 7:00 A.M.

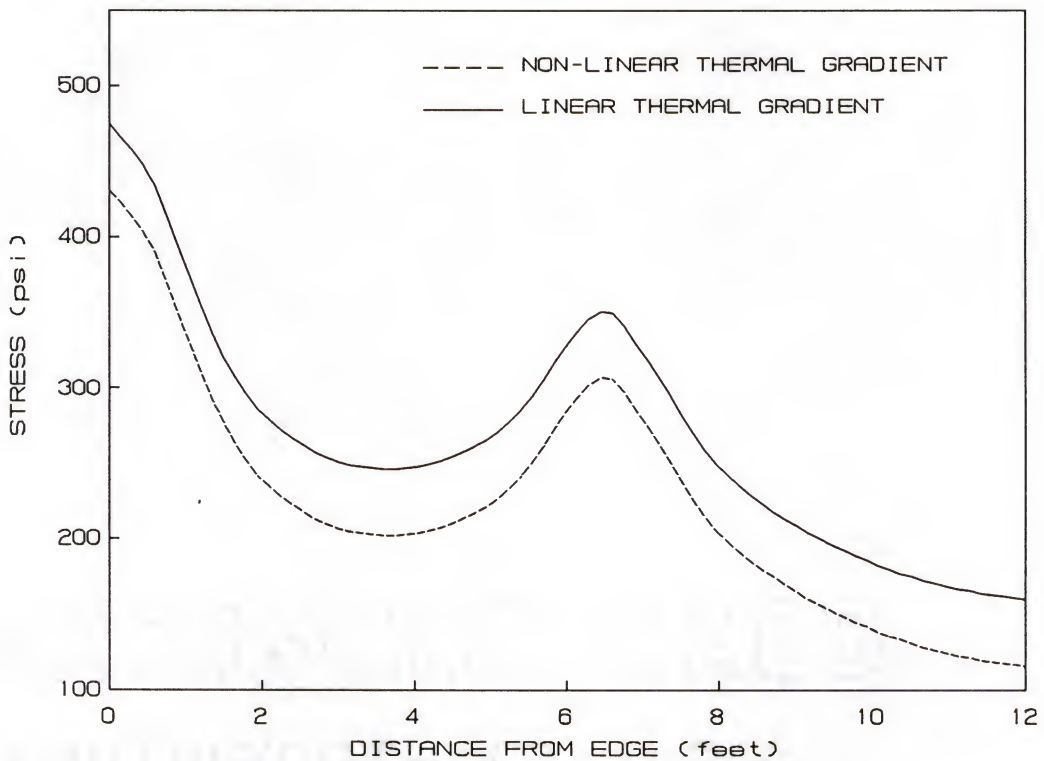

Figure 5.8 Maximum Flexural Stress Along the Transverse Centerline Caused by a 22-Kip Single Axle Load Applied at the Slab Edge and a Maximum Positive Temperature Differential of 9.46°F as Recorded for a Typical Daily Cycle Corresponding to the Month of January at 2:00 P.M.

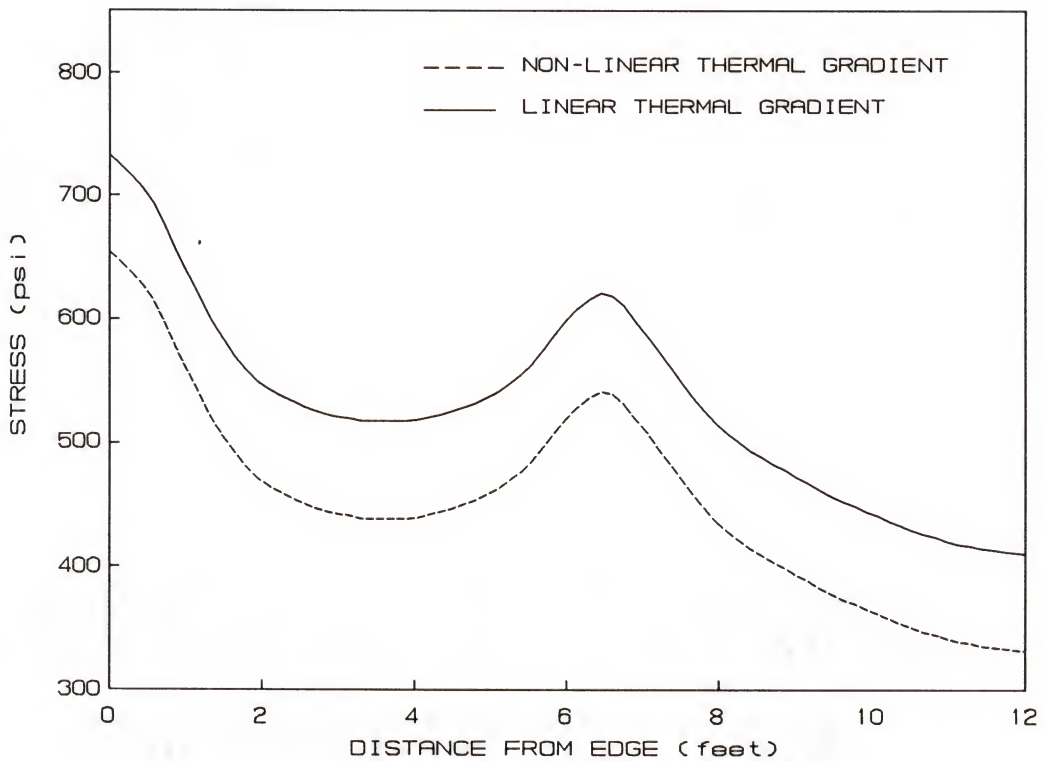

Figure 5.9 Maximum Flexural Stress Along the Transverse Centerline Caused by a 22-Kip Single Axle Load Applied at the Slab Edge and a Maximum Positive Temperature Differential of 26.36°F as Recorded for a Typical Daily Cycle Corresponding to the Month of April at 2:00 P.M.

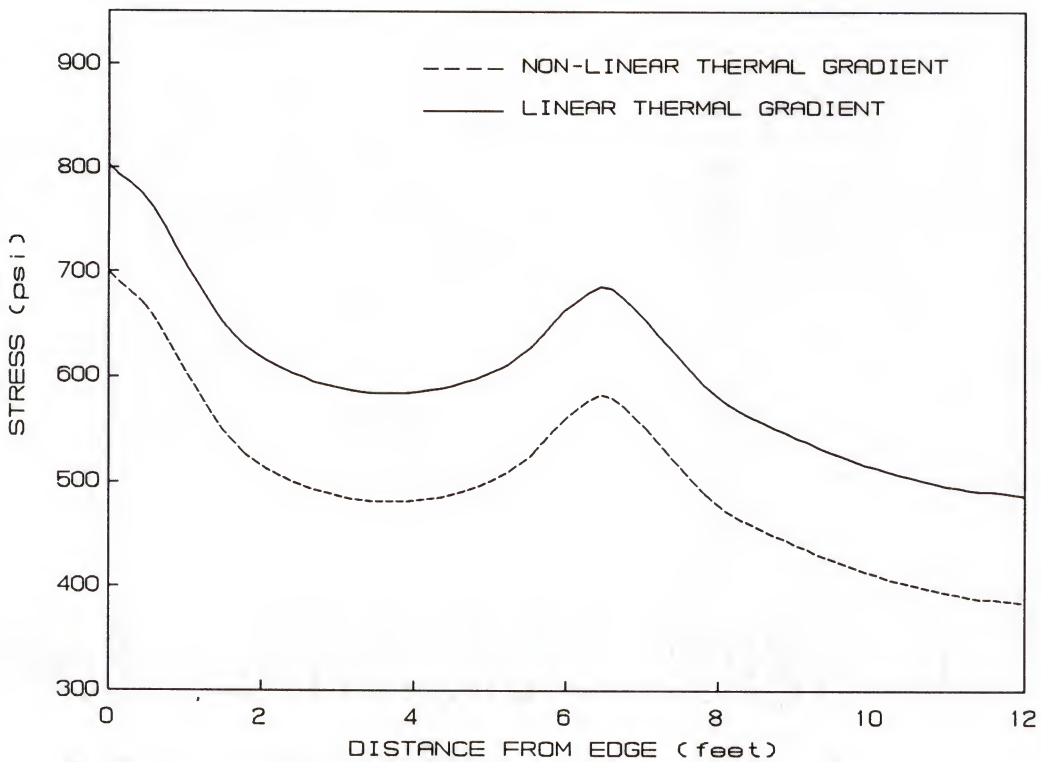

Figure 5.10 Maximum Flexural Stress Along the Transverse Centerline Caused by a 22-Kip Single Axle Load Applied at the Slab Edge and a Maximum Positive Temperature Differential of 30.75°F as Recorded for a Typical Daily Cycle Corresponding to the Month of June at 1:00 P.M.

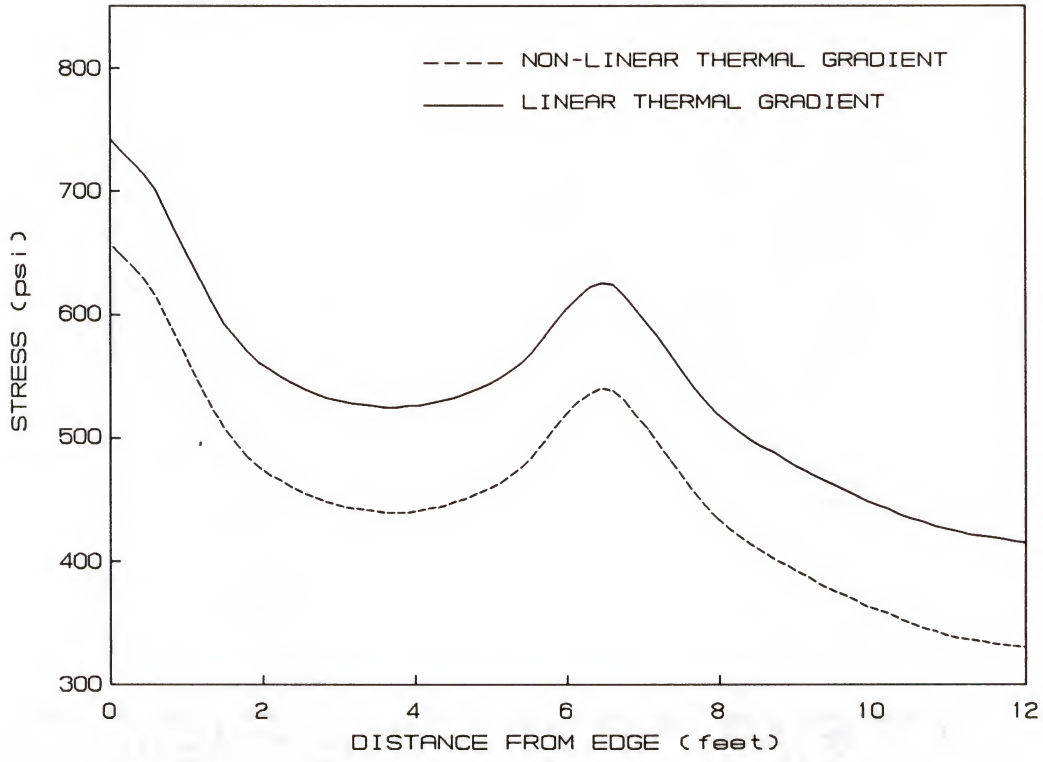

Figure 5.11 Maximum Flexural Stress Along the Transverse Centerline Caused by a 22-Kip Single Axle Load Applied at the Slab Edge and a Maximum Positive Temperature Differential of 27.26°F as Recorded for a Typical Daily Cycle Corresponding to the Month of July at 2:30 P.M.

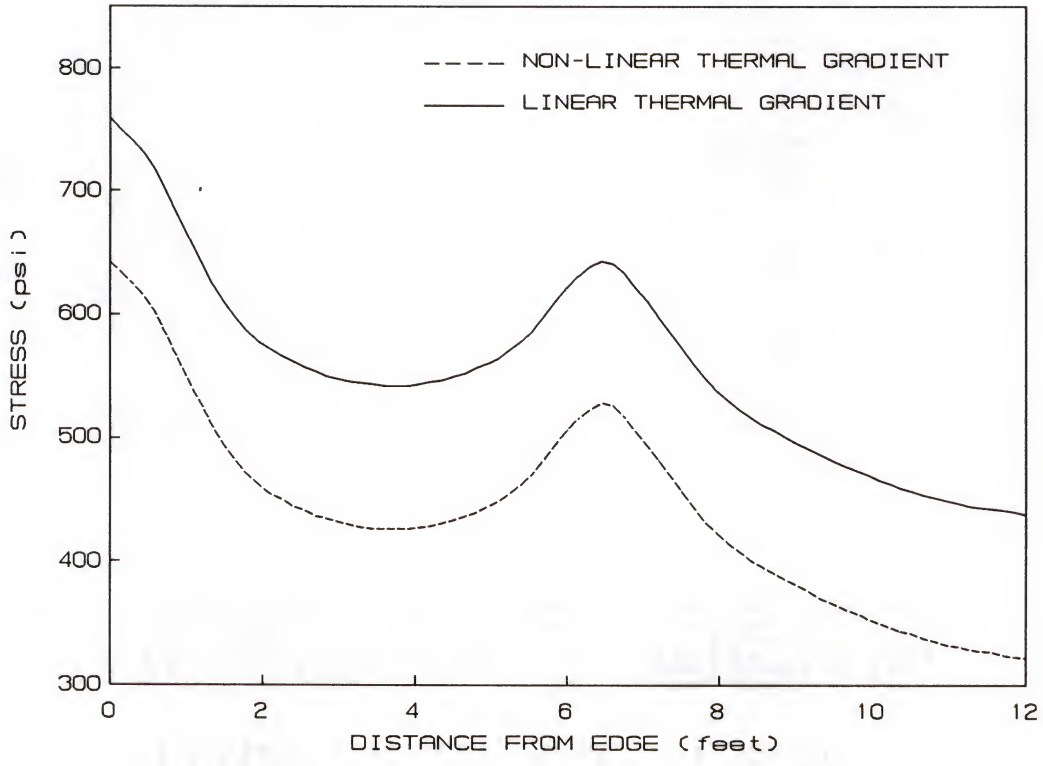

Figure 5.12 Maximum Flexural Stress Along the Transverse Centerline Caused by a 22-Kip Single Axle Load Applied at the Slab Edge and a Maximum Positive Temperature Differential of 27.77°F as Recorded for a Typical Daily Cycle Corresponding to the Month of August at 3:16 P.M.

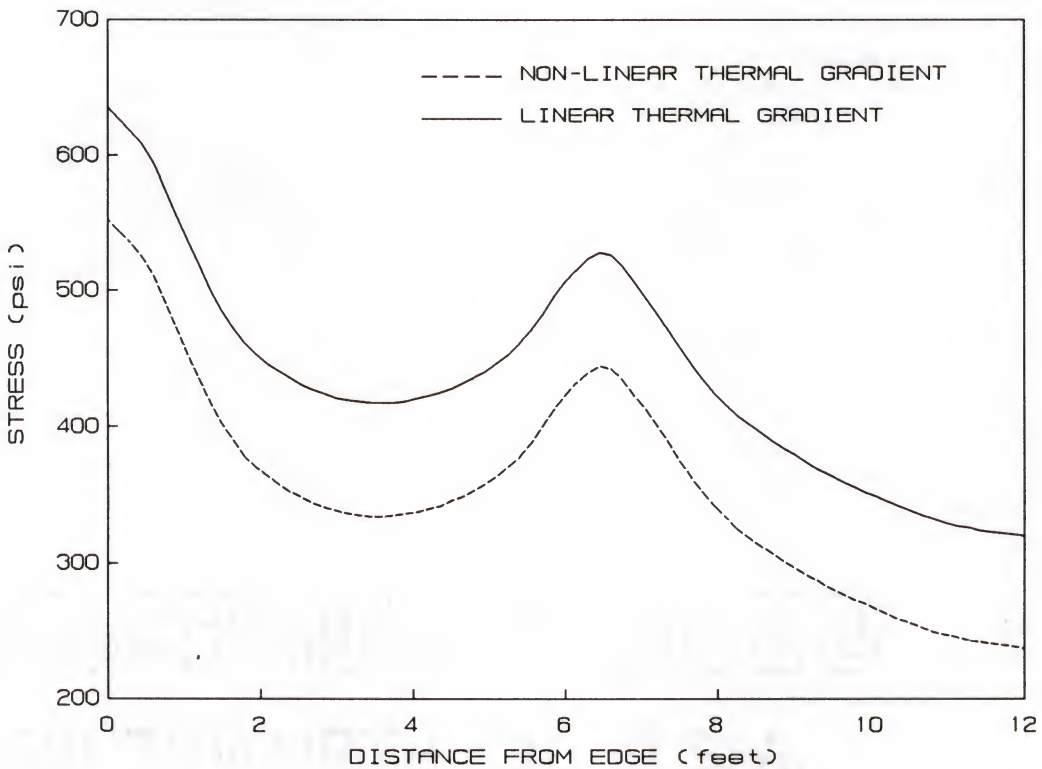

Figure 5.13 Maximum Flexural Stress Along the Transverse Centerline Caused by a 22-Kip Single Axle Load Applied at the Slab Edge and a Maximum Positive Temperature Differential of 20.49°F as Recorded for a Typical Daily Cycle Corresponding to the Month of November at 1:18 P.M.

It can be noticed from these figures that the assumption of a linear temperature differential overestimates the stresses for daytime conditions while it underestimates them for the nighttime conditions.

For the daytime condition, the assumption of a non-linear temperature distribution decreased the maximum stresses by 11 to 15%. For the case analyzed, the maximum difference was recorded for the month of August at 3:16 P.M. when the maximum flexural stress was reduced from 759 to 643 psi. Furthermore, this nonlinearity increased the maximum stress for the nighttime condition by 6 to 19%. The maximum increase was recorded for the month of August at 00:00 A.M. when the maximum flexural stress was increased from 294 to 348 psi.

5.5 Conclusion

The main finding in this study is that when the temperature distribution is assumed to be linear, the maximum computed tensile stresses in the concrete slab tend to be higher for the daytime condition, and lower for the nighttime condition, as compared to the computed stresses with the consideration of the effects of the non-linear temperature distribution. The magnitude of these computed tensile stresses are, however, more critical for the assumption of a linear temperature gradient according to Florida conditions.

This analysis dealt only with the effects of temperature variations. If the additive moisture variation effects at nighttime were included, the resulting non-linear stresses would possibly have been much higher, thus the consideration of a non-linear temperature distribution might govern in the critical stress analysis.

A more rigorous analysis would be the one that effectively takes into account both temperature and moisture variation effects, specifically for the nighttime conditions.

CHAPTER 6
LABORATORY TESTING PROGRAM TO DETERMINE THE DYNAMIC MODULUS OF ELASTICITY

6.1 Introduction

One of the important physical properties of concrete which affect the maximum thermal-load induced stresses in a pavement slab is the elastic modulus of concrete. As shown in a previous study [1], the maximum computed thermal-load induced stress increases as the elastic modulus of the concrete increases. The static elastic modulus of concrete is relatively easier to measure than the dynamic elastic modulus, and thus the static modulus is usually used in the computation of the maximum stresses. However, since traffic loads are usually applied dynamically to the pavement slabs, it should be more appropriate to use the dynamic modulus in the analysis. Data on the dynamic elastic moduli of Florida pavement concrete and the relationship between the dynamic and static moduli are lacking at present.

A laboratory testing program was performed to determine the static and dynamic elastic modulus of typical pavement concretes used in Florida. This chapter describes the laboratory set-up, procedures and results from this laboratory testing program.

6.2 LABORATORY TESTING PROGRAM

6.2.1 Concrete Mixes Used

Typical Florida pavement concretes were prepared in the laboratory and used in the testing program. Four different mixes, all with a water-cement ratio of 0.53, were made using four different aggregates, namely

#89 Brooksville limestone, #67 Brooksville limestone, #67 Calera limestone and #67 river gravel. The physical properties of the coarse aggregates are summarized in Table 6.1.

The fine aggregate used for all mixtures was a fine sand from Goldhead, Florida. The physical properties of this sand are as follows:

Bulk specific gravity (SSD)	2.65
Absorption (%)	0.12
Fineness modulus	2.12

The cement used is type III portland cement manufactured by General Portland, Inc., Tampa, Florida. The physical and chemical properties of the cement used are displayed in Tables 6.2 and 6.3, respectively.

An admixture, WRDA-79, was used, when necessary, to adjust the slump of the fresh concrete to a target slump of 3 inches. The admixture meets all the requirements of ASTM C494 Type A Type D, and is classified as a water-reducer and retarder. An air entraining admixture, DAREX AEA, was also used.

Table 6.4 presents the concrete mixes evaluated in this laboratory study. Two replicate batches per mix were made in order to have a good base for analysis. For each batch of concrete, two 6" x 6" x 30" beam specimens and six 6" x 12" cylindrical specimens were made. The mix proportions are summarized in Table 6.5.

6.2.2 Properties of Fresh Concrete

The concrete batches used in this laboratory testing program were mixed in a rotary-type mixer. A total of 8 batches (3.2 cubic feet each) of concrete were prepared. The aggregates and cement were added and mixed for 3 minutes with approximately 80% of the required mixing water. After

Table 6.1 Physical Properties of Coarse Aggregates

Property	Coarse Aggregates			
	Brooksville #67	Brooksville #67	Calera #67	River Gravel #67
Bulk Specific Gravity Gravity (SSD)	2.40	2.41	2.6	2.76
Absorption (%)	6.30	5.13	0.885	0.38
Unit Weight (lb/ft)	85.60	82.80	102.0	102.0

Table 6.2 Physical Properties of Type III Cement

Fineness by Blaine air permeability test, cm/g	6410
Setting Time (Gilmore)	
Initial, hrs:mins	2:05
Final, hrs:mins	3:55
Compressive Strength	
1 Day, psi	3960
3 Days, psi	5290
7 Days, psi	6450
Air Entrainment, %	6.30

Table 6.3 Chemical Properties of Type III Cement

Silicon Dioxide (SiO_2), %	20.1
Aluminum Oxide (Al_2O_3), %	5.0
Ferric Oxide (Fe_2O_3), $	3.0
Magnesium Oxide (MgO), %	1.0
Sulfur Trioxide (SO_3), %	4.2
Loss on Ignition, %	1.9
Insoluble Residue, %	0.21
Alkalis (%Na_2O + 0.658K_2O), %	0.33
Tricalcium Silicate, %	58.0
Dicalcium Silicate %	14.0
Tricalcium Aluminate, %	8.4
Tetracalcium Alumino-Ferrite, %	9.0

Table 6.4 Concrete Mixes Evaluated

Aggregate Type		Brooksville Limestone	Calera Limestone	River Gravel
Max. Agg. Size	#67	X	X	X
	#89	X		

3 minutes, the mixer was shut off and the concrete allowed to rest for 2 minutes. Thereafter, the remaining water was added to the mixture and mixing was continued for 2 more minutes. A slump test was performed according to the ASTM method C143 to determine if the target slump of 3 inches has been reached. If the slump was too low, a water-reducing admixture was added and mixed for two more minutes. Another slump test was run. The process was repeated until the target slump was reached.

For each batch of concrete, the following tests were run on the fresh concrete:

1. Slump test according to ASTM C143.
2. Air content test according to ASTM C173.

The air content of freshly mixed concrete by the volumetric method was used in accordance with the ASTM standard method C173. The results of these tests are shown in Table 6.6.

All of these specimens were cured under a plastic cover for about 24 hours before being removed from the molds and subjected to moist curing conditions.

6.2.3 Tests on Hardened Concrete

6.2.3.1 Curing of concrete specimens. Specimens were cured in a moist room for 35 days after they were removed form the molds. The moist room conforms to the ASTM requirements of the greater than 98% relative humidity and 73 ±3°F temperature. The specimens were then removed from the moist room and allowed to cure in room environment before testing.

6.2.3.2 Tests on hardened concrete. Flexural strength tests were performed in accordance with the ASTM Standard Test Method C78 using simple beam with third point loading. The modulus of rupture is computed as follows:

Table 6.5 Proportioning of Mix Ingredients

Aggregate	Brooksville #67	Brooksville #89	Calera	River Gravel
Cement (lb/cy)	602.30	628.49	567.22	567.22
Coarse Agg. (lb/cy)	1428.32	1180.40	1894.75	1894.75
Sand (lb/cy)	1160.42	1344.40	984.62	1099.59
Water (lb/cy)	319.22	333.10	300.63	300.63
Air-Entraining Admixture (ml)	10	10	12	18
Water-redu. Admixture (ml)	--	46	--	25

Table 6.6 Properties of Fresh Concrete

Aggregate Type	Batch #	Slump (in)	Air Content (%)
Brooksville #89	1 2	3 5	5 7
Brooksville #67	1 2	5 4.5	3.5 6.0
Calera #67	1 2	2.75 2.75	6.0 6.1
River Gravel	1 2	2 3.5	3.3 6.5

$$f_r = PL/bd^2$$

where: P = maximum applied load

L = span length

b = average width of specimen

d = average depth of specimen

Compressive strength tests were performed in accordance with ASTM standard test method C39-83b for cylindrical concrete specimens.

The tests on hardened concrete were run after the dynamic testing on specimens and the results are summarized in Table 6.7.

6.2.3 Measurement of Dynamic and Static Elastic Modulus

The measurement of the dynamic modulus of elasticity requires the following: (1) a method of supporting the specimen so that it will vibrate freely, (2) a loading device that is part of the vibrating system, (3) instrumentation to condition and amplify the load-induced signal, and (4) equipment to collect the data.

Two half-inch strain gages were attached to the bottom of each beam specimen, at mid-length in longitudinal direction. Three gages were attached to the side of each cylinder specimen at 120°F form one another.

The concrete beam specimens were supported at its nodal position 2 inches from its ends. The strain gages were connected to the signal conditioner which was hooked up to a computer-transformed oscilloscope. The loading/vibrating device was a MTS machine. The frequencies used were 1, 3, 5 and 7 Hz. A flexural third-point loading of 1 kip was adopted for the beams and a compressive load of approximately 20 kips for the cylinders. Strain waves were recorded at 0, 300, 700, 1000, 2000, 3000, 4000 and 5000 cycles at each respective frequency. Mean peak value of these strain waves, relative to the number of gages, was used to compute the

Table 6.7 Flexural and Compressive Strength Test Results

Aggregate Type	Batch #	Beam #	Flexural Strength (psi)	Cylinder #	Compressive Strength (psi)
Brooksville #89	1	1	544	1	6048
		2	--	2	6320
	2	1	557	1	5931
		2	--	2	5988
Brooksville #67	1	1	479	1	55114
		2	492	2	5404
	2	1	572	1	5602
		2	494	2	5142
Calera #67	1	1	689	1	6593
		2	720	2	6437
	2	1	667	1	6479
		2	778	2	6755
River Gravel	1	1	562	1	6150
		2	546	2	6529
	2	1	556	1	5687
		2	551	2	5790

dynamic modulus for each frequency and corresponding cycle according to the following formula:

$$E = \sigma/\epsilon$$

where: σ is the flexural stress at the location of strain gages at the mid-span of the beam, and is computed by:

$$\sigma = Pl/bd^2$$

P = peak-to-peak load of cyclic load applied

b = width of the beam specimen (b = 6 in.)

d = depth of he beam (d = 6 in.)

In the case of a cylinder, it is given by:

$$\sigma = P/\pi a^2$$

a = radius of a cylinder specimen

For determination of the static elastic modulus of each concrete specimen, the strain gages were connected to and calibrated with Vishay/ Ellis strain indicator. Strain readings from the strain gages were recorded at every 3000 pound and 500 pound load intervals for cylinders and beams, respectively, as the concrete specimen was loaded in the standard compressive strength test. The means of the strain readings were used for determination of the modulus of elasticity. The modulus value is the secant modulus at one-fifth of the compressive strength, f'_c.

6.3 Analysis of Data

6.3.1 Comparison of Dynamic and Static Moduli

The results of this laboratory testing program are summarized in Tables 6.8 through 6.11. It can be noted from these tables that the dynamic modulus is higher than the static modulus by 15 to 50% for most of the beam specimens. For the cylindrical specimens tested in compression, the dynamic modulus appears to be slightly lower than the static modulus.

Table 6.8 Comparison of Dynamic and Static Moduli of Elasticity of Concrete Specimens with Brooksville #67 Aggregate

	Dynamic Modulus (10^6psi)								Stat. Mod. (10^6psi)
Freq.	1 Hz		3 Hz		5 Hz		7 Hz		
Cycles	0	5000	0	5000	0	5000	0	5000	
Beam #1	4.900	4.920	5.071	4.953	5.137	5.385	4.814	5.099	3.925
Beam #2	5.087	6.020	4.800	5.193	4.896	4.920	4.735	5.097	3.883
Cyl. #1	3.689	3.467	4.072	3.572	3.836	3.661	3.883	3.686	3.962
Cyl. #2	3.900	3.631	4.597	3.708	3.900	3.773	3.908	3.697	3.794
Beam #1	3.709	3.760	3.889	3.825	3.912	4.007	3.439	3.339	4.514
Beam #2	5.629	4.790	5.884	5.608	6.422	6.040	6.276	6.691	3.842
Cyl. #1	3.622	3.501	3.567	3.591	3.836	3.525	3.675	4.901	3.735
Cyl. #2	4.370	4.244	4.045	3.923	4.005	3.842	3.946	3.733	3.631

Table 6.9 Comparison of Dynamic and Static Moduli of Elasticity of Concrete Specimens with Brooksville #89 Aggregate

Dynamic Modulus (10^6psi)									Stat. Mod. (10^6psi)
Freq.	1 Hz		3 Hz		5 Hz		7 Hz		
Cycles	0	5000	0	5000	0	5000	0	5000	
Beam #1	4.997	5.143	4.289	4.419	4.004	4.181	5.026	4.927	4.377
Beam #2	--	--	--	--	--	--	--	--	--
Cyl. #1	3.680	3.532	3.637	3.536	3.717	3.519	3.762	3.670	3.740
Cyl. #2	3.995	3.858	4.063	3.833	3.947	3.873	3.831	3.692	4.511
Beam #1	6.316	6.931	6.518	7.000	6.430	6.211	5.712	6.072	4.199
Beam #2	5.543	--	4.887	7.093	5.642	5.819	5.835	4.925	--
Cyl. #1					3.375	3.227	3.762		3.669
Cyl. #2	3.806	3.651	3.642	3.683	3.781	3.716	3.795	3.666	3.851

Table 6.10 Comparison of Dynamic and Static Moduli of Elasticity of Concrete Specimens with Calera #67 Aggregate

Dynamic Modulus (10^6psi)									Stat. Mod. (10^6psi)
Freq.	1 Hz		3 Hz		5 Hz		7 Hz		
Cycles	0	5000	0	5000	0	5000	0	5000	
Beam #1	7.026	9.313	7.841	7.939	7.477	7.883	8.706	7.500	7.683
Beam #2	7.330	8.025	7.133	7.592	7.093	7.754	8.456	8.774	6.335
Cyl. #1	7.572	7.332	7.442	7.196	7.490	7.259	7.400	7.082	6.616
Cyl. #2	5.973	5.900	6.055	5.914	4.903	5.906	5.964	7.243	5.870
Beam #1	7.896	6.418	7.737	7.252	9.600	7.353	8.122	9.518	6.226
Beam #2	6.921	7.018	7.073	7.010	7.309	7.225	7.408	8.027	6.687
Cyl. #1	5.915	5.915	5.880	5.870	5.847	5.749	5.887	5.752	6.241
Cyl. #2	6.402	6.200	6.460	6.294	6.417	6.143	6.135	6.264	6.616

Table 6.11 Comparison of Dynamic and Static Moduli of Elasticity of Concrete Specimens with River Gravel #67 Aggregate

Dynamic Modulus (10^6psi)									Stat. Mod. (10^6psi)
Freq.	1 Hz		3 Hz		5 Hz		7 Hz		
Cycles	0	5000	0	5000	0	5000	0	5000	
Beam #1	5.895	6.287	6.188	6.255	6.288	6.084	6.265	7.087	5.015
Beam #2	7.628	11.069	6.839	6.203	6.746	6.270	7.438	7.424	5.166
Cyl. #1	4.545	4.471	4.556	4.486	4.577	4.479	4.600	4.285	4.666
Cyl. #2	5.891	5.797	5.818	5.800	5.877	5.742	5.980	5.606	5.944
Beam #1	6.228	7.347	6.302	6.392	6.026	6.692	6.389	6.097	5.015
Beam #2	5.601	5.839	5.432	5.573	5.600	5.529	5.106	5.490	4.947
Cyl. #1	3.892	3.772	3.891	3.846	3.892	3.806	3.953	3.772	3.908
Cyl. #2	4.954	4.812	4.984	4.873	5.045	4.884	5.139	4.720	4.621

The change in frequency from 1 to 7 Hz does not seem to have a significant influence on the dynamic modulus. The observed variations in modulus may be due to measurement errors and voltage fluctuation in the main power supply. Another possible cause of error is the shift in the vertical alignment of the load cell at the higher frequencies.

6.3.2 Discussion

The dynamic modulus in flexure seems to be different than that in compression. The dynamic modulus in flexure should be used in pavement analysis since concrete pavement slabs are usually subjected to flexural stresses.

Though the test results represent preliminary data in this area, it can be observed clearly that the dynamic modulus is higher than the static modulus in flexure. It also points to the fact that the measured dynamic modulus in compression could be significantly different from that in flexure. Further testing, however, is needed to substantiate this claim.

CHAPTER 7
IN SITU MEASUREMENT OF LOAD-INDUCED CONCRETE PAVEMENT SLAB RESPONSE FOR VERIFICATION OF ANALYTICAL RESULTS

7.1 Introduction

Stresses in a concrete slab can be generated by one or a combination of these three factors: the slab weight, the thermal gradient (temperature differential) and the applied load.

In the course of this study, maximum stresses in a slab caused by applied load under critical loading conditions for given sets of pavement parameters were computed using FEACONS IV computer program. These maximum stresses could also be used to evaluate the structural adequacy for each given concrete pavement.

However, the computed stresses have not been verified by experimental results. To do this, a series of tests were conducted on the Gainesville Test Road located at the FDOT Materials Office to measure the strains in the slab caused by applying the FWD loads. The total strains in a slab, similar to the stresses, are also produced by the combination of thermal gradient in the slab, the slab weight and the applied load ($\epsilon_{total} = \epsilon_{thermal} + \epsilon_{load} + \epsilon_{weight}$). It should be noted that the strains measured in these field tests were those caused by the applied load only. These measured strains were to be compared with the analytical strains obtained using the FEACONS IV program to check the accuracy and the validity of the model used.

The instrumentation used for this task and the testing methodology have been presented in detail in Chapter 3.

7.2 Estimation of In Situ Concrete Pavement Parameters

Field measurements of slab deflection due to FWD loads were carried out in order to determine realistic pavement parameters to be used in the analytical model. These measured deflection basins are used, in conjunction with the DBCONPAS II program, to back-estimate the in situ pavement parameters required for modeling the concrete pavement. This back-calculation was accomplished through an iterative procedure of matching the measured deflections with those computed using DBCONPAS II program for an assumed set of pavement parameters.

A general description of the DBCONPAS II program as well as the procedures for determination of pavement parameters are presented in the following subsections.

7.2.1 DBCONPAS II Computer Program

A computer program named DBCONPAS II (Data Base for CONcrete PAvement Systems) was developed at the University of Florida as a convenient tool for estimation of pavement parameters from FWD data [51]. Basically, the program uses a database of analytical results generated by the FEACONS IV computer program.

Theoretical deflection basins caused by a 9-kip FWD load applied at three different positions of a concrete pavement slab were computed for a wide range of combinations of pavement parameters (such as the concrete modulus, E_c, subgrade modulus, K_s, edge stiffness, K_e, joint shear stiffness, K_l and joint torsional stiffness, K_t) using a temperature differential in the concrete slab of zero. These calculated deflections and the corresponding regression equations are stored in the database of DBCONPAS II.

The main functions of the DBCONPAS II program can be summarized as follows:

1. The elastic modulus of concrete, subgrade modulus, edge stiffness and joint stiffness can be estimated from FWD deflection data (by using the prediction equations stored in the database).
2. An analytical FWD deflection basin can be obtained for a given set of pavement parameters for various FWD loading positions (from a databank of analytical FWD deflection basins).
3. Both the measured and analytical FWD deflections can be plotted on the computer screen and on paper, for ease of comparison.
4. After the measured and analytical FWD deflections are compared with one another on the screen, the user has an added option to "fine-tune" the estimated pavement parameters manually, and the new analytical FWD deflections will be generated for further comparison and "fine-tuning".
5. Additional analytical FWD deflection basins can be added to the databank.
6. Regression analyses on the analytical FWD deflections in the databank can be performed to generate new prediction equations or to improve existing prediction equations, which are then stored in the database.

7.2.2 Estimation of Subgrade and Concrete Moduli

When both the subgrade modulus and the elastic modulus of concrete of a pavement are to be estimated from FWD data, the DBCONPAS II program will accomplish the task in three main steps. First, an initial estimate of the subgrade modulus is made using the following prediction equation:

$$\log_{10}K_s = 3.59659 - 1.11977 \log_{10}D3$$

or

$$K_s = 3949.9\ D3^{-1.11977} \qquad (7.1)$$

where: K_s = subgrade stiffness (in pci).

D3 = deflection (in micron (10-6m)) at 3 feet away from the center of a 40 kN (9-kip) FWD load applied to the center of the slab.

The above regression equation is applicable for ranges of elastic modulus of concrete E_c between 2000 and 8000 ksi. It was obtained by using 430 data points and had a coefficient of determination (R^2) of 0.9914.

The second step in this estimation procedure is to use the initial estimate of K_s in conjunction with the measured FWD deflection basin to estimate E_c. Prediction equations of the following form were used:

$$\log_{10}E_c = \log_{10}A + B \log_{10}D_0$$

or

$$E_c = A (D_0)^B \qquad (7.2)$$

where E_c = elastic modulus of concrete (ksi)

D_0 = deflection (in micron (10-6m)) at the center of a 9-kip FWD load applied to the center of the slab.

A,B = coefficients of regression equation.

Prediction equations of the above form were obtained through regression analyses for various values of K_s, and stored in the database.

The third step in the estimation procedure is to use the estimate of E_c in conjunction with the measured FWD deflection basin to obtain a final estimate of K_s. Prediction equations of the following form were used:

$$\log_{10}K_s = \log_{10}A + B \log_{10}D_1$$

or

$$K_s = A (D_1)^B \qquad (7.3)$$

where: K_s = subgrade stiffness (pci)

D_1 = deflection (in micron (10-6m)) at one foot away from a 9-kip FWD load applied to the center of the slab

A,B = constants.

These equations are also used by DBCONPAS II program in estimation of K_s when E_c is already known.

7.2.3 Estimation of Edge Stiffness

When both E_c and K_s are fixed or have been estimated, the edge stiffness K_e of a pavement can be estimated by using prediction equations of the following form:

$$\log_{10}(K_e + 1) = A + B\ D_0$$

or

$$K_e = 10^{(A+B\,Do)} - 1 \qquad (7.4)$$

where: K_e = edge stiffness (ksi).

D_0 = deflection (in micron (10-6m)) at the center of a 9-kip FWD load applied to the edge center of the slab.

A,B = constants.

7.2.4 Estimation of Linear Joint Stiffness

When E_c, K_s and the torsional joint stiffness K_t are known, the linear joint stiffness K_l of a pavement can be estimated by using prediction equations of the following form:

$$1/(K_l + 2) = A + B\ D_0$$

or

$$K_l = 1/(A + B\ D_0) - 2 \qquad (7.5)$$

where: K_l = linear joint stiffness (ksi)

D_0 = deflection (in 10-6m) at the center of a 9-kip FWD load applied to the joint center of the slab

A,B = constants.

Since K_t has little effects on the FWD deflections, only two values of K_t were used. Either a value of 0 or 3000 k-in/in has to be specified for K_t.

7.3 Analysis of Data

7.3.1 Estimation of Pavement Parameters

In estimating the pavement parameters, it is assumed that the concrete slab is fully supported by the subbase layer at the loading

position. However, the slab might not be in full contact with the subbase layer due to the presence of temperature differential or moisture in the slab and this would cause the pavement system to have a nonlinear deflection-load characteristic. Thus, to ensure the pavement parameters to be properly estimated, the linearity of the deflection-load characteristics was checked first. The relationship of deflections and FWD loads are shown in Figures 7.1 through 7.4 for the cases of center, edge and joint center loads (loaded and unloaded side for this latter case), respectively. In these figures, D_o represents the deflection measured at the point under the loading plate and D_1 to D_4 represent deflections measured one to four feet away from the loading plate. From these figures, it can be noted that, in general, all the deflections change almost linearly with the change of loads. the small variation in the relationship could be attributed to the measurement errors. Thus, for practical purpose, the deflection-load relationships for these loading conditions are considered to be linear.

The three sets of deflection data were used in conjunction with the DBCONPAS II computer program to estimate the pavement parameters. The deflections measured along the centerline of the slab caused by a center load of 570 kPa were used to determine the elastic modulus of concrete and subgrade stiffness. Figure 7.5 shows the comparison of measured and computed deflections. The estimated concrete modulus and subgrade stiffness are also presented in this figure. Similarly, the estimated edge and joint stiffnesses were determined by matching the measured and computed deflections along the edge and joint, respectively. Figures 7.6 and 7.7 show the estimated edge and joint stiffnesses, respectively.

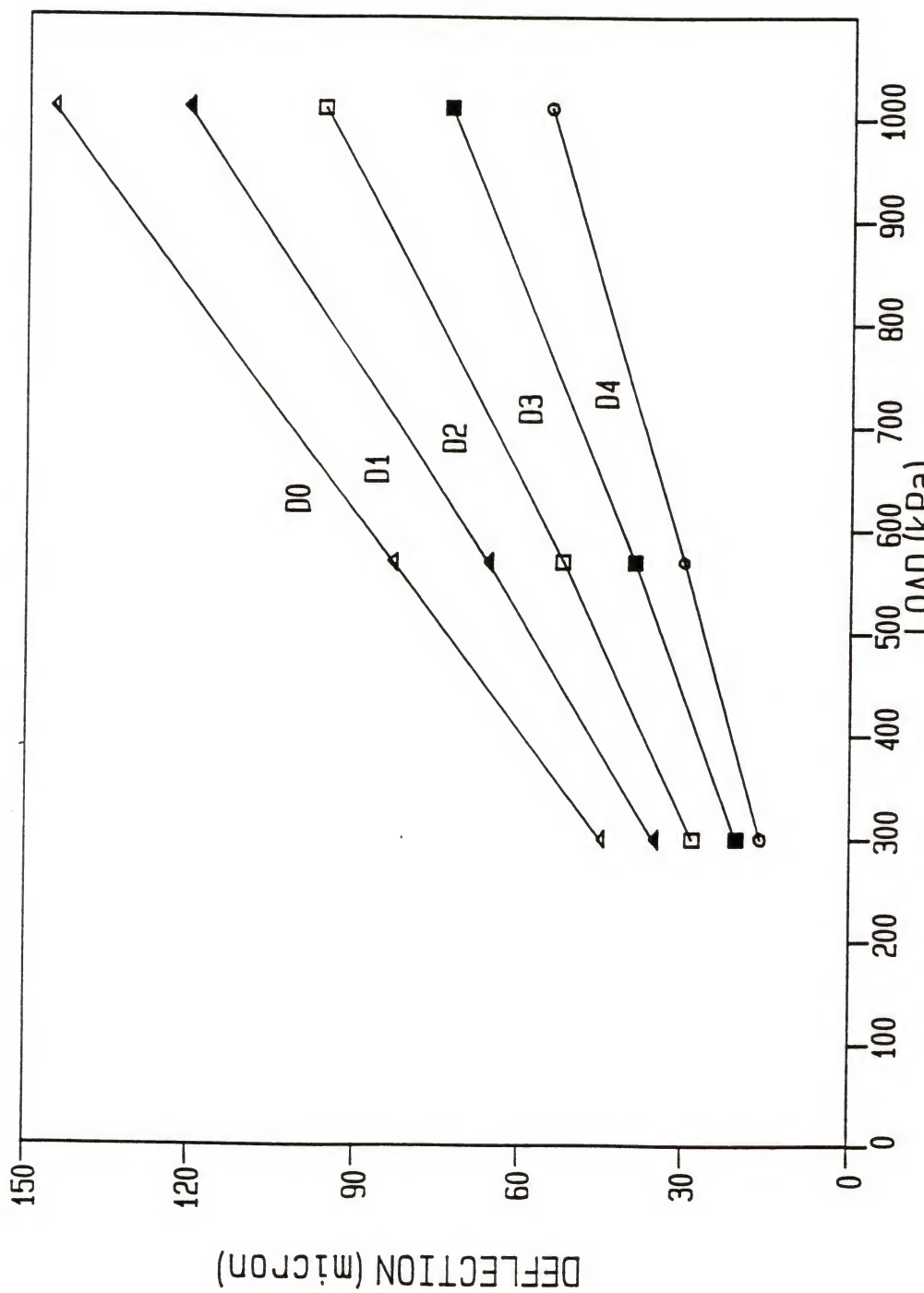

Figure 7.1 Deflection-Load Relationship for the Slab Center Loading Condition at a Temperature differential of 12°F

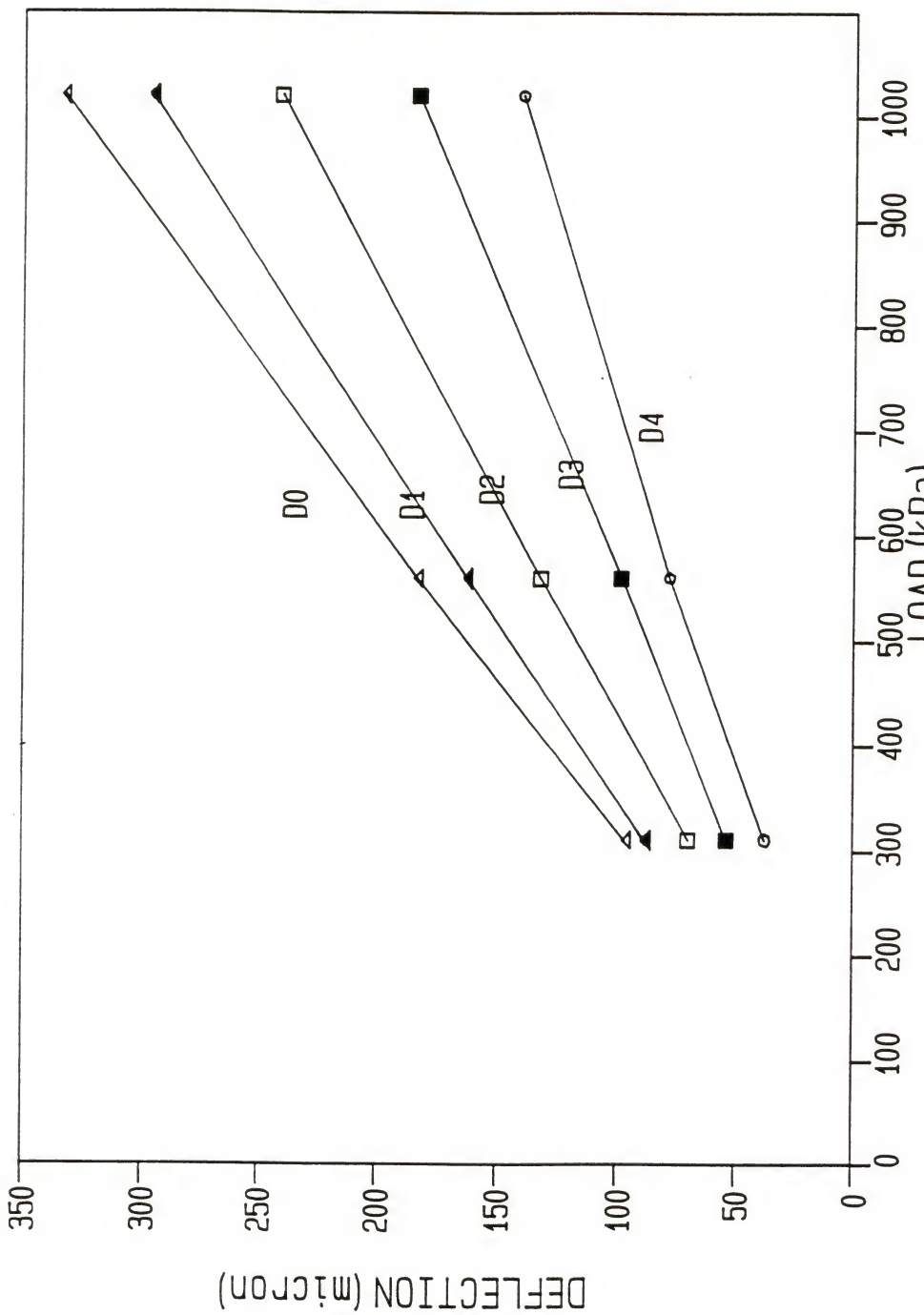

Figure 7.2 Deflection-Load Relationship for the Edge Load Condition at a Temperature Differential of -7°F

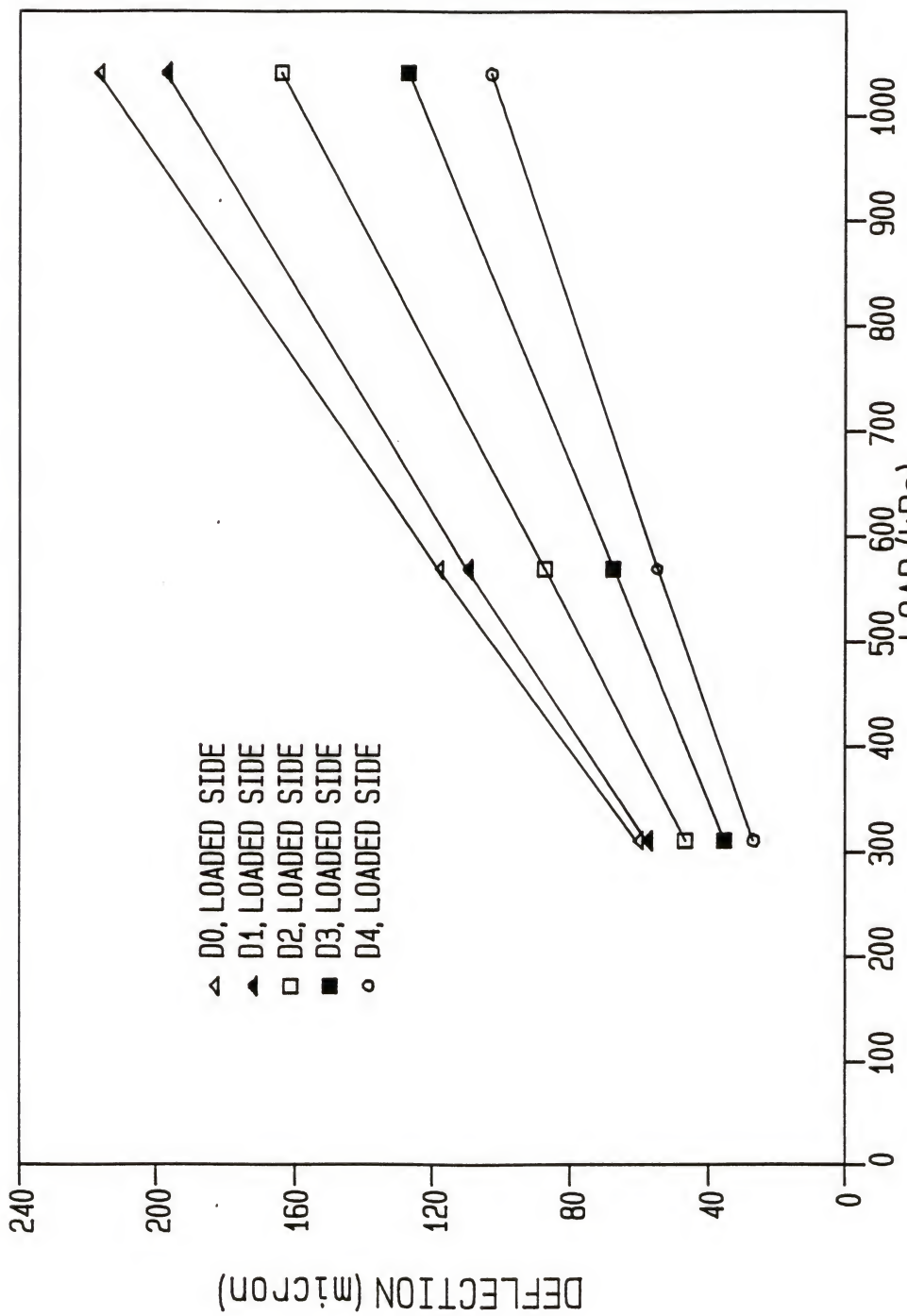

Figure 7.3 Deflection-Load Relationship for the Slab Joint Center Load Condition (loaded Side) at a Temperature Differential of -7°F

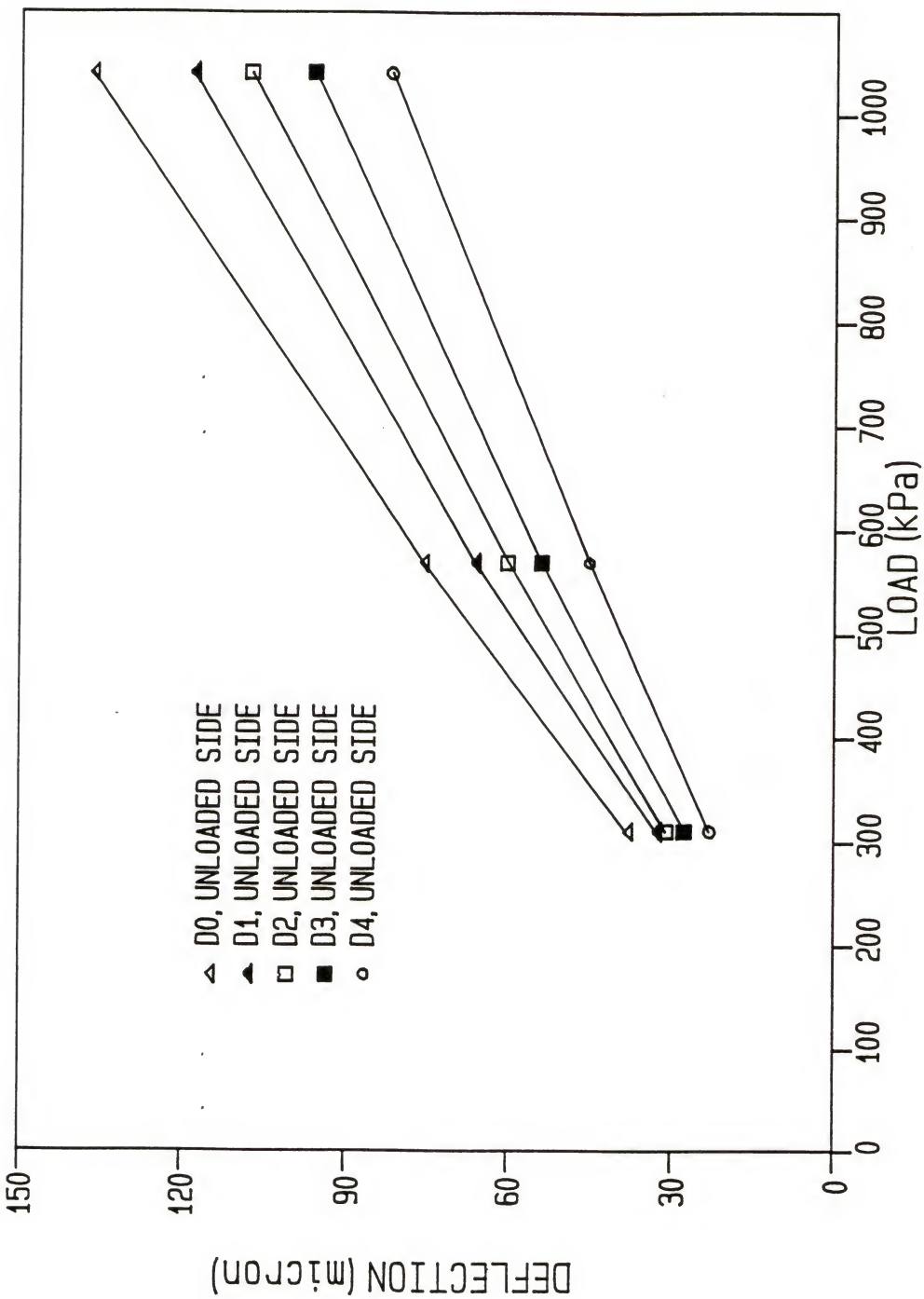

Figure 7.4 Deflection-Load Relationship for the Slab Joint Center Load Condition (Unloaded Side) at a Temperature Differential of -7°F

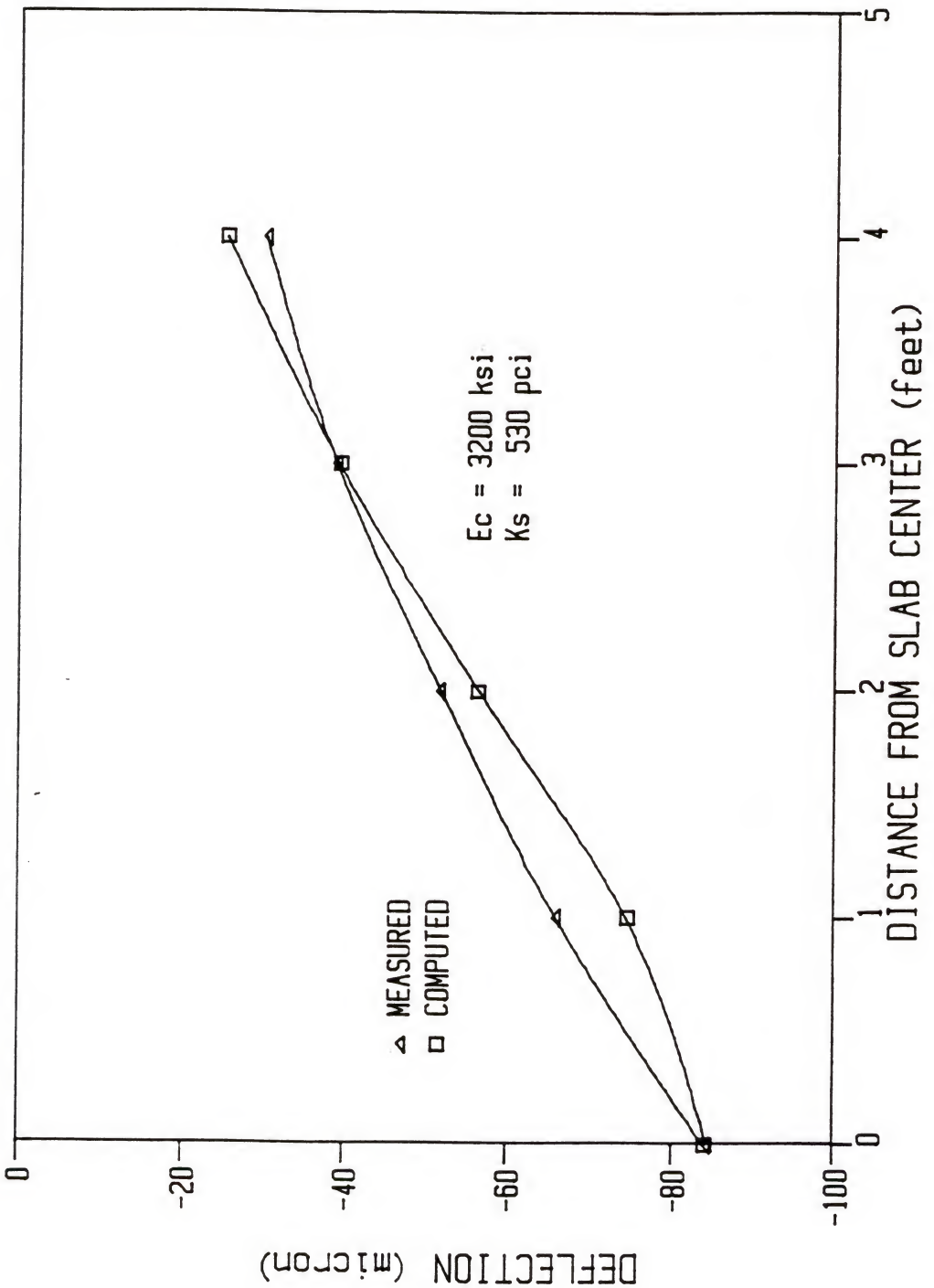

Figure 7.5 Estimation of the Respective Test Pavement Concrete and Subgrade Moduli

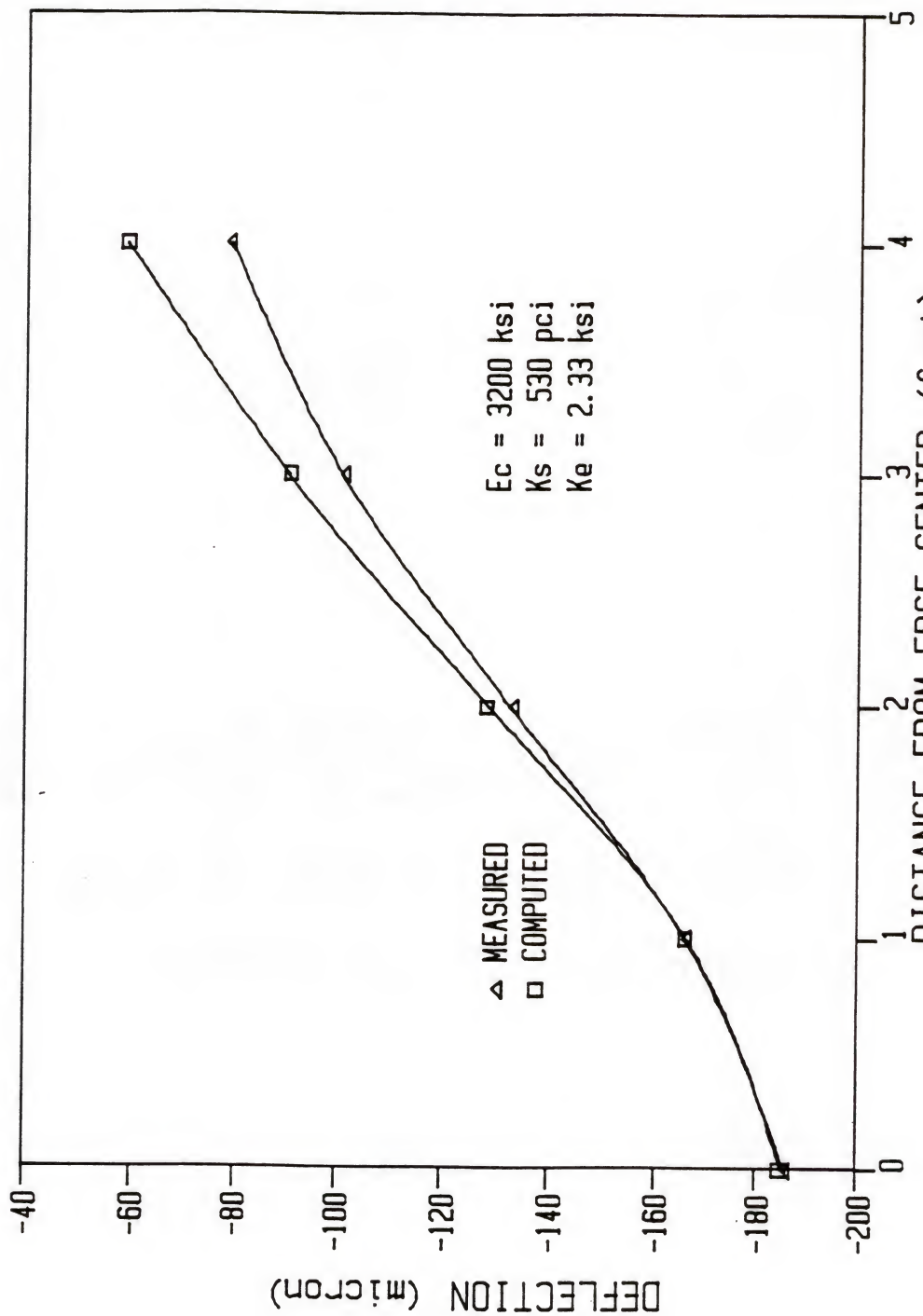

Figure 7.6 Estimation of the Test Pavement Edge Stiffness

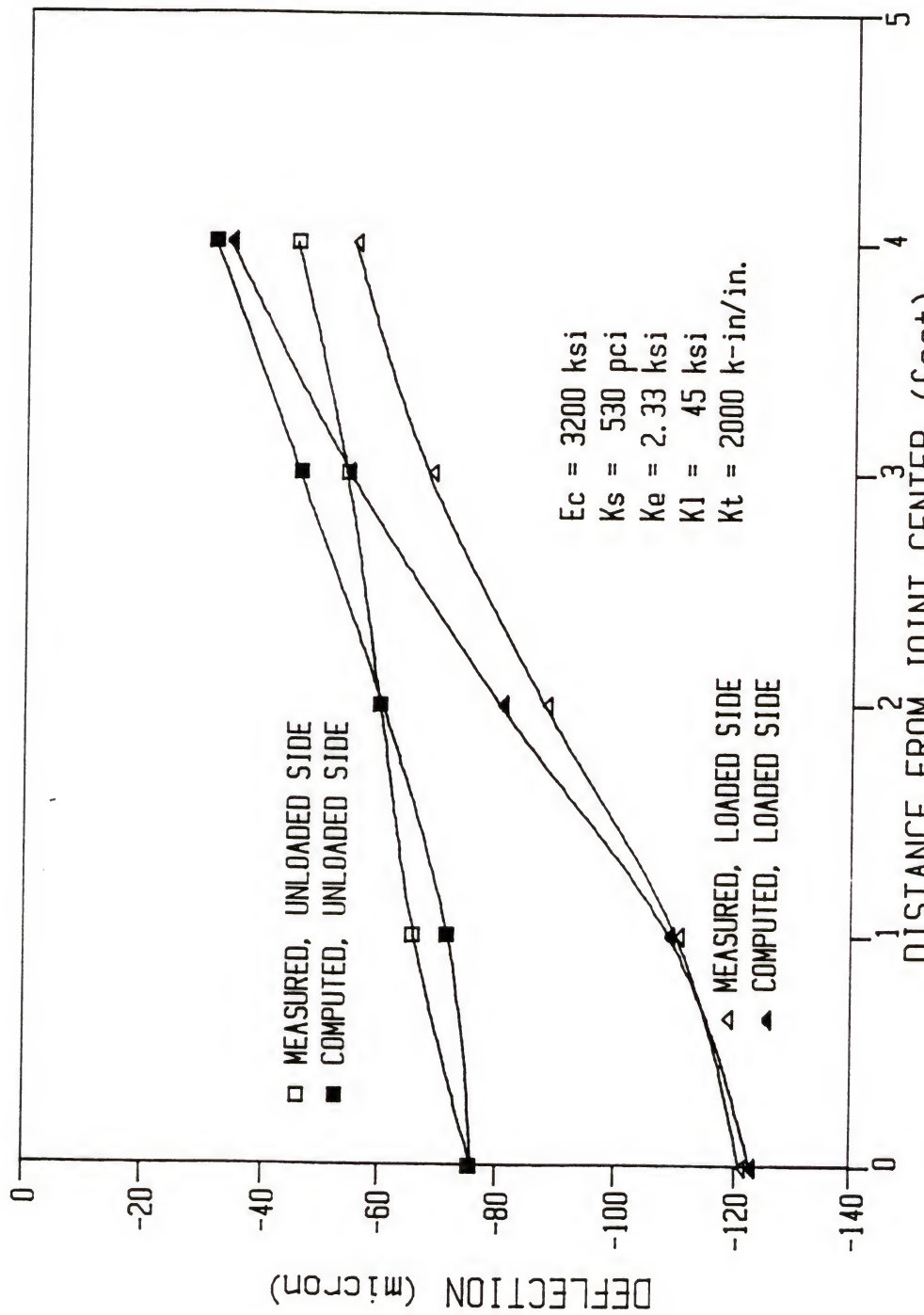

Figure 7.7 Estimation of the Test Pavement Linear and Torsional Joint Stiffnesses

7.3.2 Comparison of Measured and Computed Strains

7.3.2.1 Measurement of FWD load-induced strains. The strains caused by the FWD loads applied at different locations were measured by strain gages attached on the slab. A few typical waves of these load-induced strains are shown in Figure 7.8 through 7.11. The maximum strain was taken from each wave and used in the analysis.

7.3.2.2 Computation of theoretical strains. In computing the load-induced strains in the slab, the total stresses (σ_{total}) caused by the combination of temperature differential, slab weight and the applied load and the initial stresses ($\sigma_{initial}$) due to the slab weight and temperature differential were first computed at each strain gage location in the slab using the FEACONS IV computer program. The change in maximum stress due to the applied load, $\Delta\sigma$, was obtained by subtracting the initial stresses, $\sigma_{initial}$, caused by the thermal gradient in the slab and the slab weight from the total stresses, σ_{final}, caused by all the three factors ($\Delta\sigma = \sigma_{total} - \sigma_{initial}$).

Once the $\Delta\sigma$'s were determined at each gage position for a certain load position, both load-induced longitudinal and transverse analytical strains could be computed according to the following equation:

$$\begin{Bmatrix} \Delta\epsilon_x \\ \Delta\epsilon_y \end{Bmatrix} = \frac{1}{E} \begin{bmatrix} 1 & -\upsilon \\ -\upsilon & 1 \end{bmatrix} \begin{Bmatrix} \Delta\sigma_x \\ \Delta\sigma_y \end{Bmatrix} \tag{7.6}$$

where

$\Delta\sigma_x$ = change in longitudinal stress due to applied load

$\Delta\sigma_y$ = change in transverse stress due to applied load

$\Delta\epsilon_x$ = change in longitudinal strain due to applied load

$\Delta\epsilon_y$ = change in transverse strain due to applied load

υ = Poisson's Ratio

E = modulus of elasticity of concrete

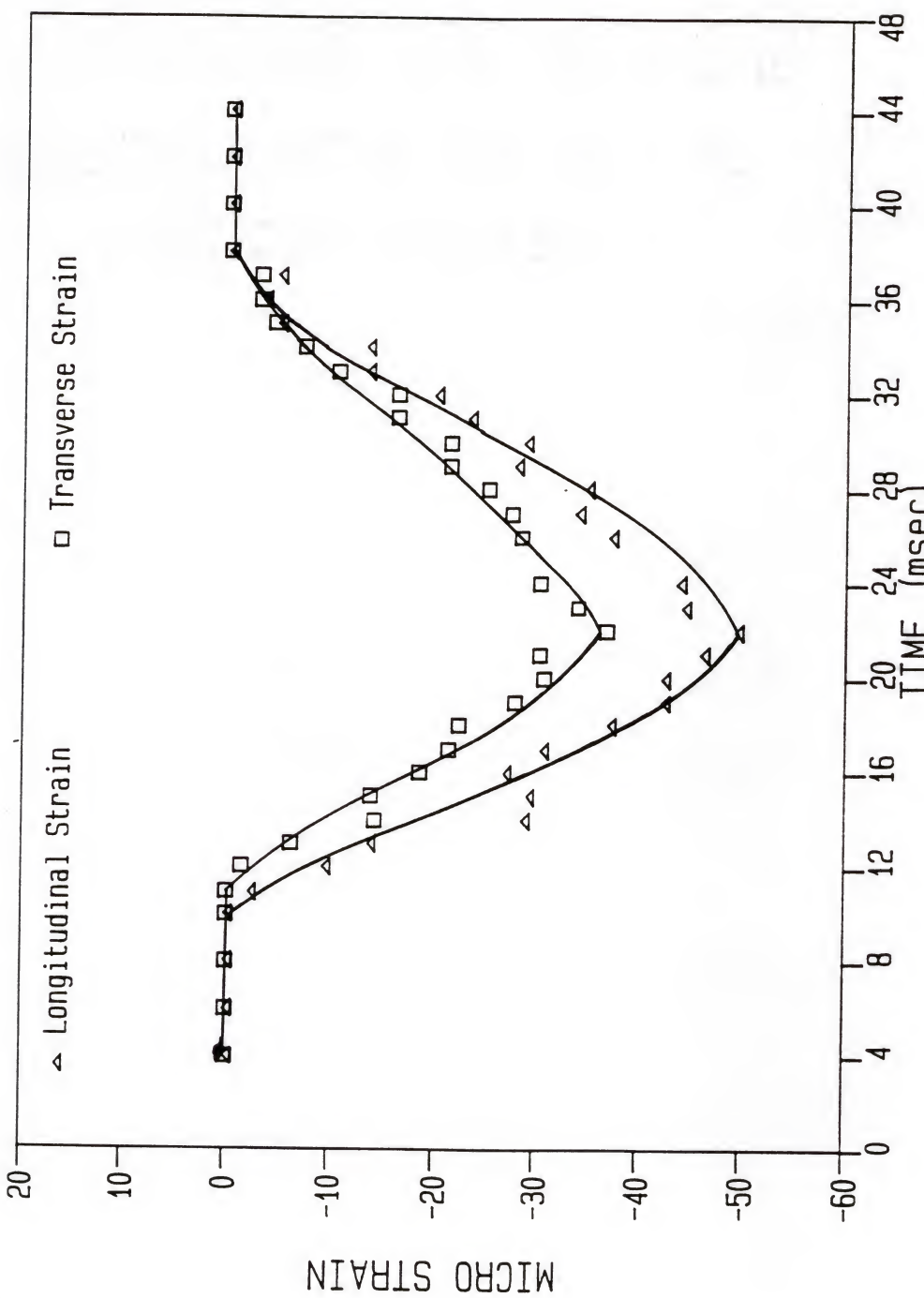

Figure 7.8 Strain Wave Measured at the Slab Center Caused by a FWD Load of 1000 kPa Applied at the Slab Center

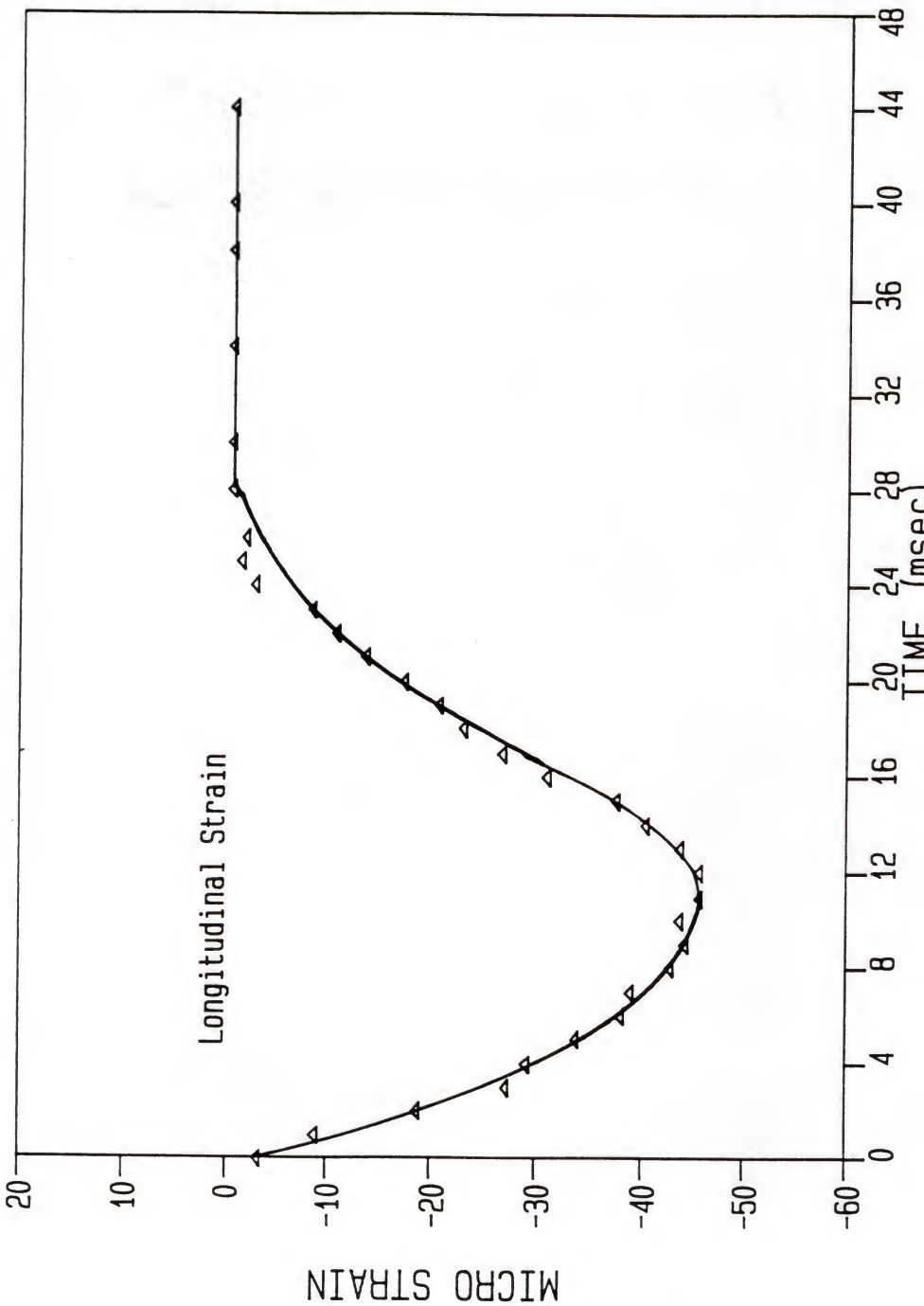

Figure 7.9 Strain Wave Measured at the Slab Edge Center Caused by a FWD Load of 1000 kPa Applied at the Slab Edge Center

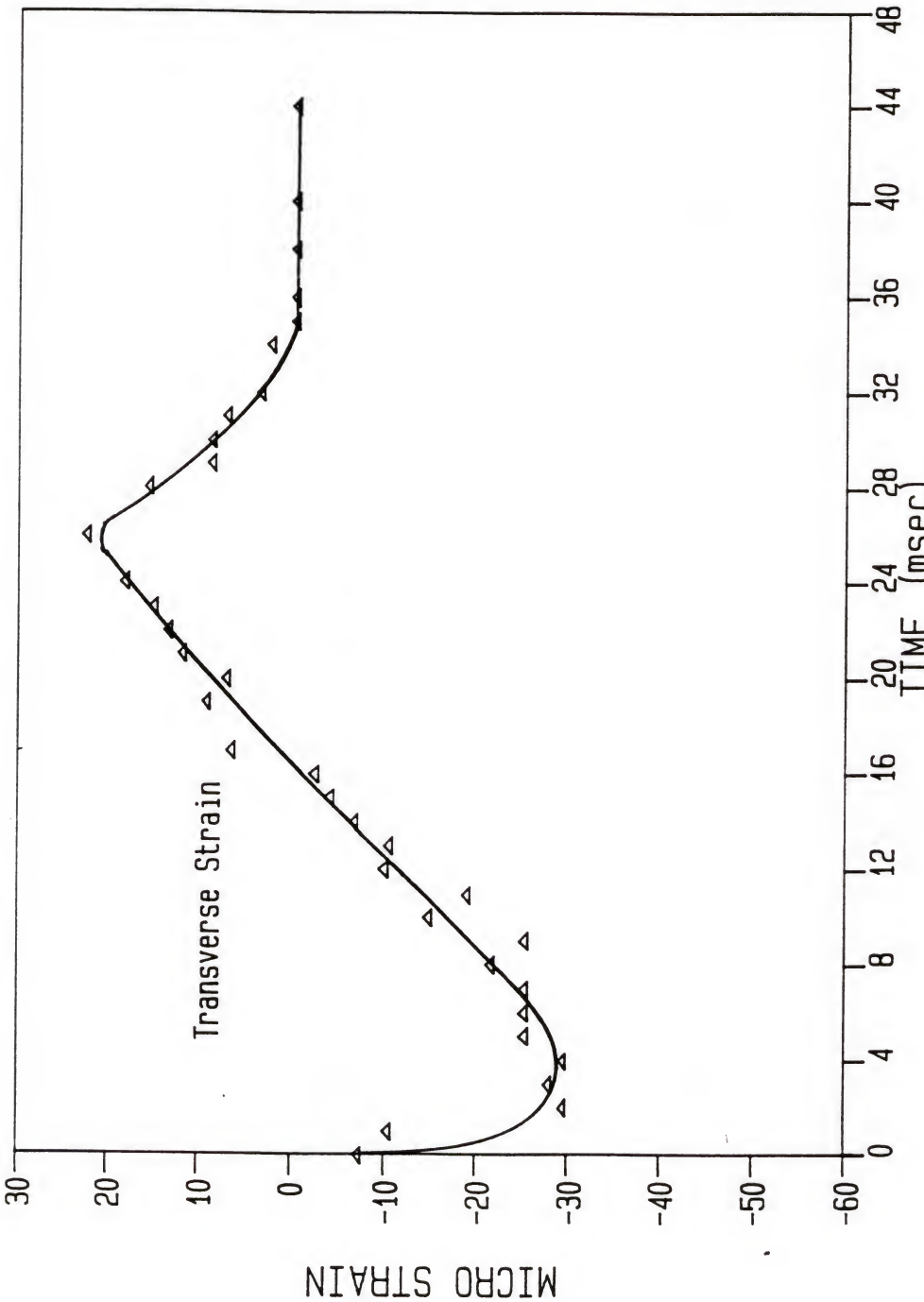

Figure 7.10 Strain Wave Measured at the Slab Joint Center Caused by a FWD Load of 1000 kPa Applied at the Slab Joint Center

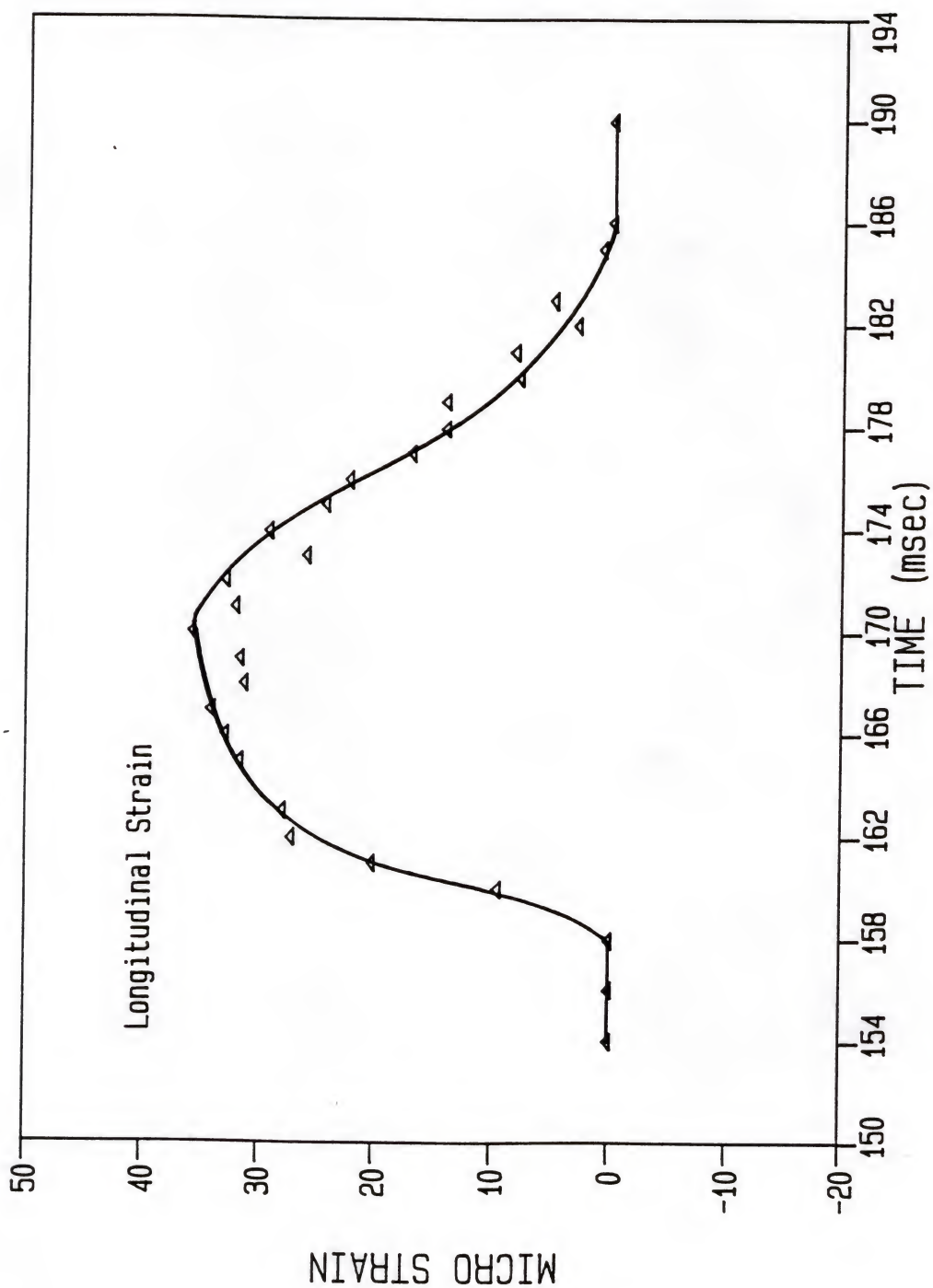

Figure 7.11 Strain Wave Measured at 5 feet from the Slab Corner Along the Slab Edge Caused by a FWD Load of 1000 kPa Applied at the Slab Corner

Moreover, according to J. M. Armaghani [44], the concrete slabs behave as if they were in full contact with the subbase or subgrade underneath it at a temperature differential of -9°F in the slab rather than at a zero temperature differential. Thus, two sets of theoretical strains at each location were computed with one using the actual temperature differentials recorded during the test and the other using the adjusted temperature differentials, which are equal to the actual temperature differentials minus 9°F.

During the preliminary testing phase of this study, on July 1988, the nighttime test temperature differential in the slab remained about constant at -7°F and, therefore, both the temperature differentials of -7°F and -16°F were used in modeling the pavement and computing the load-induced strains. However, for the daytime test, the temperature differential in the slab changed with time throughout the test and, thus, different values of temperature differential were used for different load positions. the computed longitudinal strains at various locations caused by the FWD load producing a plate pressure of 1000 kPa applied at the five positions are presented in Tables 7.1 and 7.2 for the night and day tests, respectively. It can be observed that, at each position in both the day and night tests, the strains computed using the actual temperature differential are very close to those computed using the adjusted temperature differential. Thus, only the strains in the slab caused by a FWD load with the actual temperature differential in the slab were used in all the analyses that followed.

7.3.2.3 Comparison of measured and computed strains. The comparison of measured and computed strains at various locations during the course of this study are illustrated in Figures 7.12 through 7.23.

Table 7.1 Comparison of Computed Longitudinal Strains Using Actual Temperature Differential and Those Using Adjusted Temperature Differential - Night Test

Distance from Load	Load Position									
	Edge Center (1)		Slab Center (2)		Joint Center (3)		Edge Center (4)		Slab Corner (5)	
Transverse Direction	Temperature Differential									
	-7° F	-16° F	-7° F	-16° F	-7° F	-16° F	-7° F	-16° F	-7° F	-16° F
0	-84.05	-85.69	-37.61	-37.77	-12.71	-13.54	-	-	-28.7	-29.99
2	-36.65	-38.01	-18.31	-18.52	-10.04	-10.87	-	-	-25.77	-26.63
4	-11.40	-12.05	-6.53	-6.99	-5.74	-6.25	-	-	-13.30	-14.65
6	-26.2	-2.98	-1.86	-2.64	-2.01	-4.44	-	-	-5.31	-6.24
Longitudinal Direction										
0	-	-	-37.61	-37.77	-12.71	-13.54	-95.93	-96.57	-28.7	-29.99
2.5	-	-	7.68	3.31	12.48	13.16	19.16	17.24	22.34	-21.06
5	-	-	7.43	3.18	10.93	11.74	21.39	19.94	29.31	28.53
7.5	-	-	2.50	1.06	4.34	4.76	7.40	8.36	13.13	14.57
10	-	-	.38	.24	.84	.89	.77	1.20	3.56	5.25

NOTE: Ec = 3200 ksi, Ks = 530 pci, Ke = 2.33 ksi
Kl = 45 ksi, Kt = 2000 k-in/in

Table 7.2 Comparison of Computed Longitudinal Strains Using Actual Temperature Differential and Those Using Adjusted Temperature Differential - Day Test

Distance from Load	Load Position									
	Edge Center (1)		Slab Center (2)		Joint Center (3)		Edge Center (4)		Slab Corner (5)	
Transverse Direction	Temperature Differential									
	10° F	+1° F	+20° F	+11° F	12° F	+3° F	+20° F	+11° F	+19° F	+10° F
0	-81.15	-80.96	-42.27	-41.27	-12.15	-12.40	-	-	-26.08	-26.05
2	-35.35	-35.08	-22.59	-20.86	- 8.71	- 9.49	-	-	-23.33	-23.43
4	-11.29	-10.87	- 9.62	- 7.44	- 5.48	- 5.89	-	-	-11.36	-11.66
6	- 3.30	- 2.70	- 2.92	- 1.71	- 2.14	- 2.41	-	-	- 4.98	- 4.91
Longitudinal Direction										
0	-	-	-42.27	-41.27	-12.15	-12.40	-98.26	-95.27	-26.08	-26.05
2.5	-	-	2.05	5.51	10.31	1.27	19.28	20.17	22.56	23.72
5	-	-	4.37	6.97	8.63	10.65	21.40	21.25	25.59	26.31
7.5	-	-	4.05	3.14	4.04	4.22	7.77	5.52	11.53	11.03
10	-	-	2.64	1.18	1.66	.83	1.18	5.86	3.28	2.50

NOTE: Ec = 3200 ksi, Ks = 530 pci, Ke = 2.33 ksi
Kl = 45 ksi, Kt = 2000 k-in/in

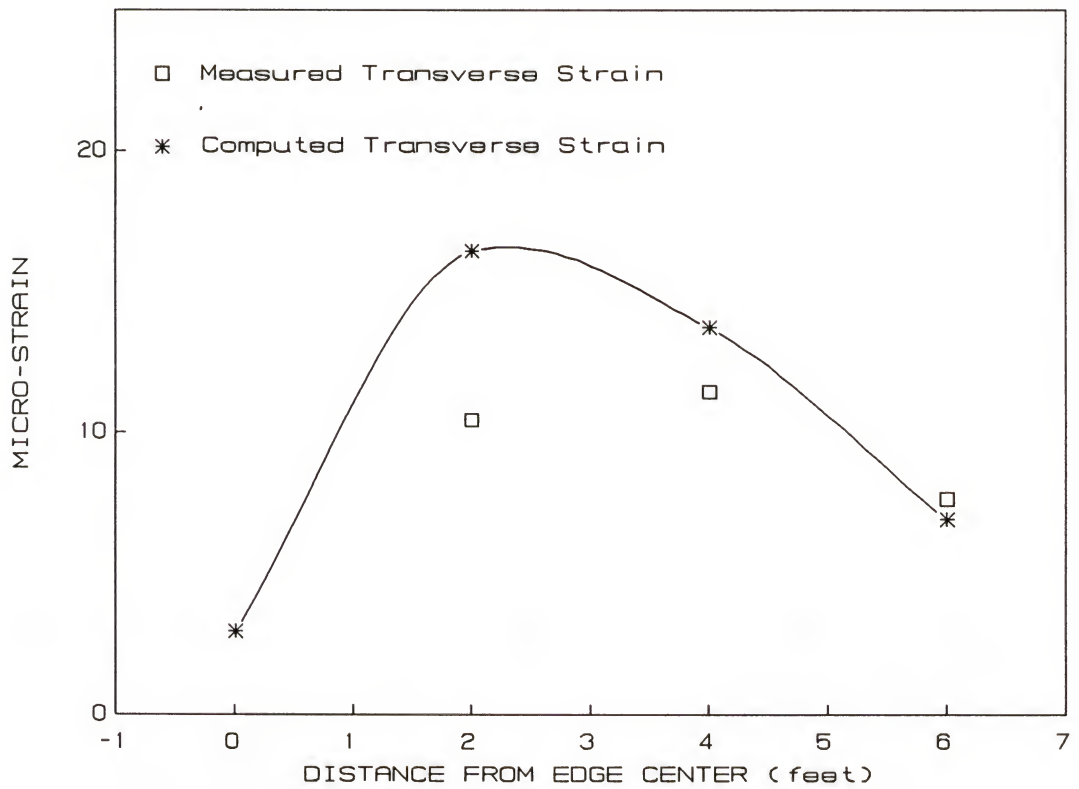

Figure 7.12 Comparison of Computed and Measured Strains Along the Slab Transverse Centerline Caused by a FWD Load of 570 kPa Applied at the Slab Edge Center at a Recorded Temperature Differential of -7°F - Night Test (July 1988)

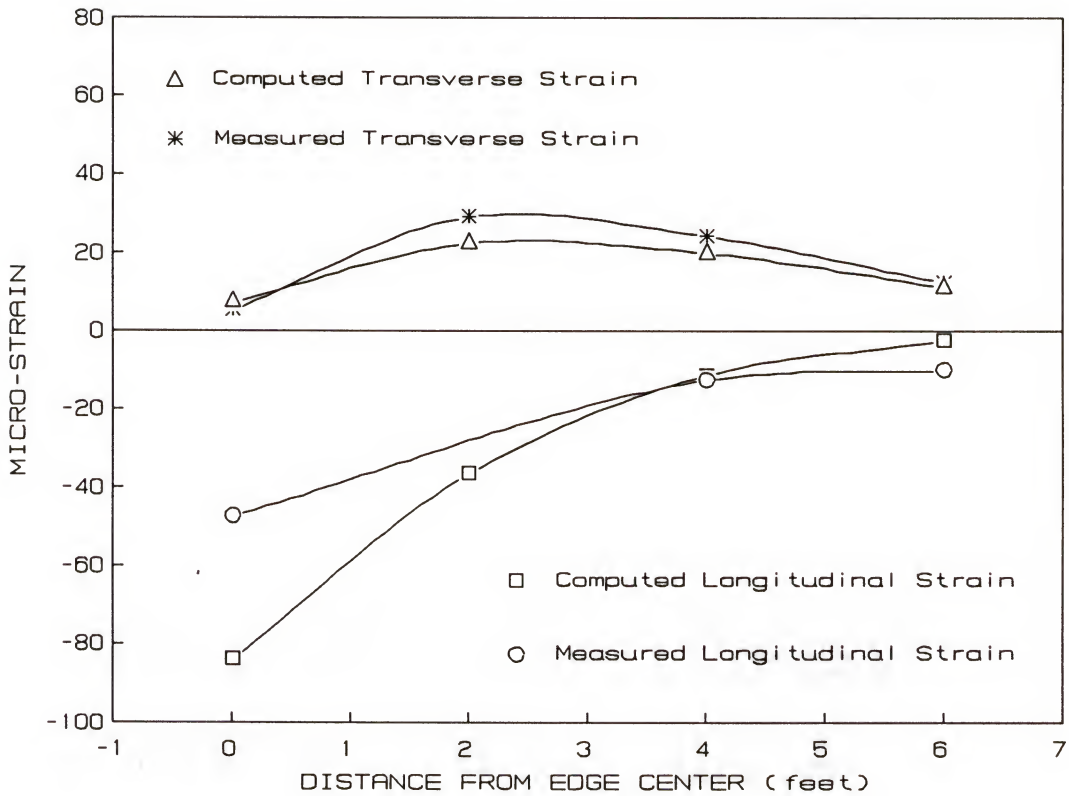

Figure 7.13 Comparison of Computed and Measured Strains Along the Slab Transverse Centerline Caused by a FWD Load of 1000 kPa Applied at the Slab Edge Center at a Recorded Temperature Differential of -7°F - Night Test (July 1988)

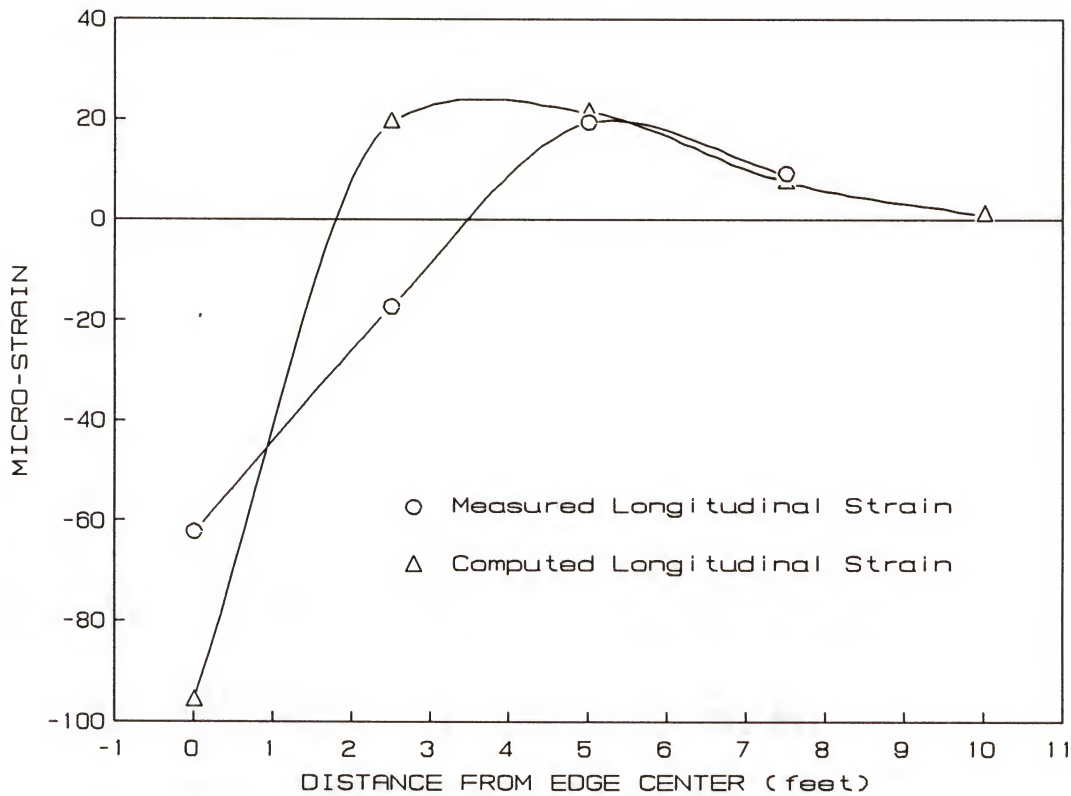

Figure 7.14 Comparison of Computed and Measured Strains Along the Slab Edge Caused by a FWD Load of 1000 kPa Applied at the Slab Edge Center at a Recorded Temperature Differential of -7°F - Night Test (July 1988)

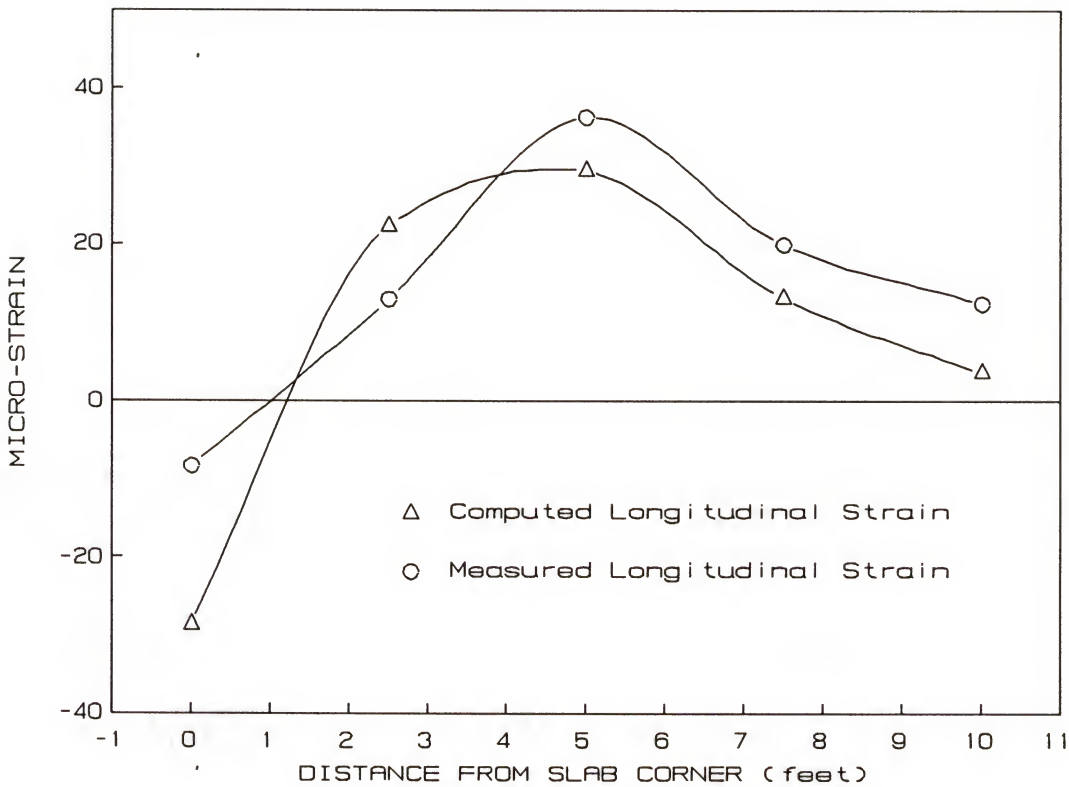

Figure 7.15 Comparison of Computed and Measured Strains Along the Slab Edge Caused by a FWD Load of 1000 kPa Applied at the Slab Corner at a Recorded Temperature Differential of -7°F - Night Test (July 1988)

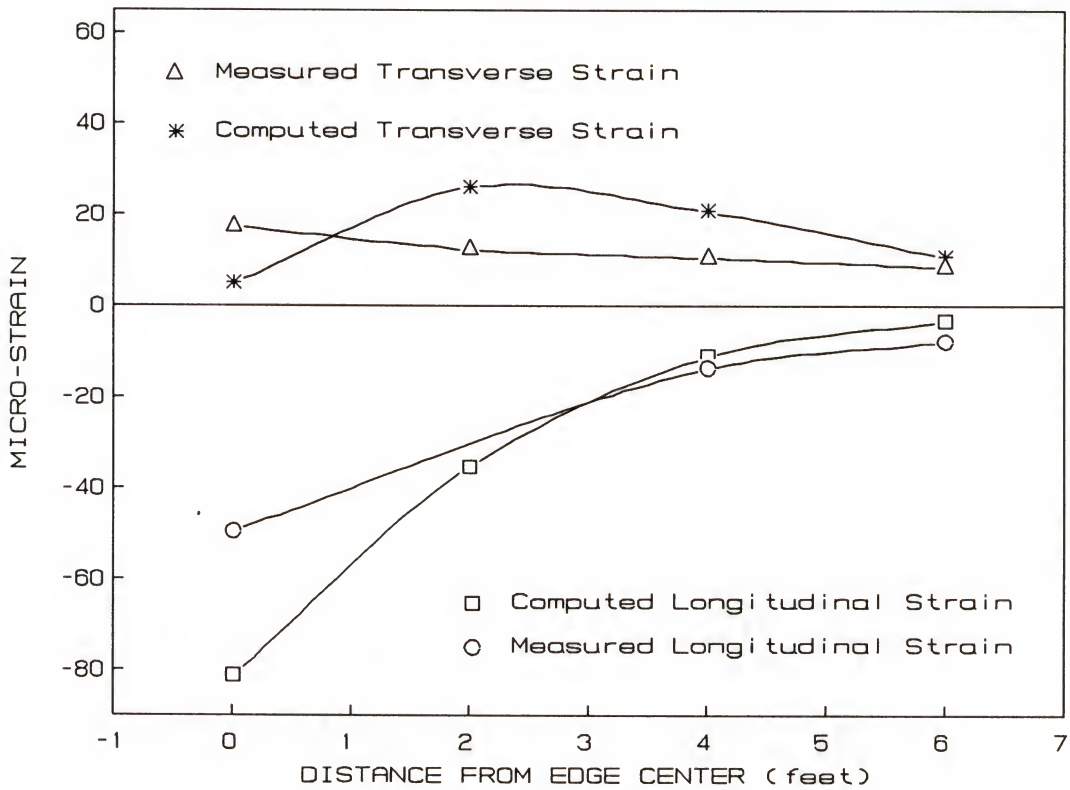

Figure 7.16 Comparison of Computed and Measured Strains Along the Slab Transverse Centerline Caused by a FWD Load of 1000 kPa Applied at the Slab Edge Center at a Recorded Temperature Differential of +10°F - Day Test (July 1988)

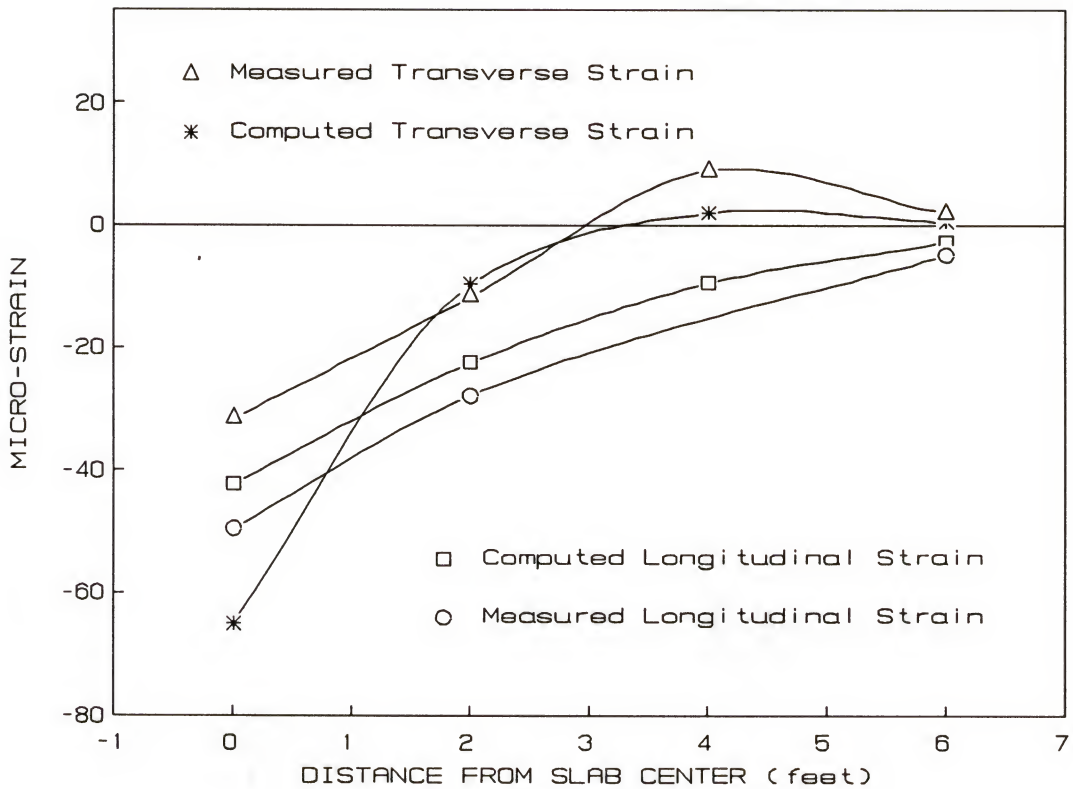

Figure 7.17 Comparison of Computed and Measured Strains Along the Slab Transverse Centerline Caused by a FWD Load of 1000 kPa Applied at the Slab Center at a Recorded Temperature Differential of +20°F - Day Test (July 1988)

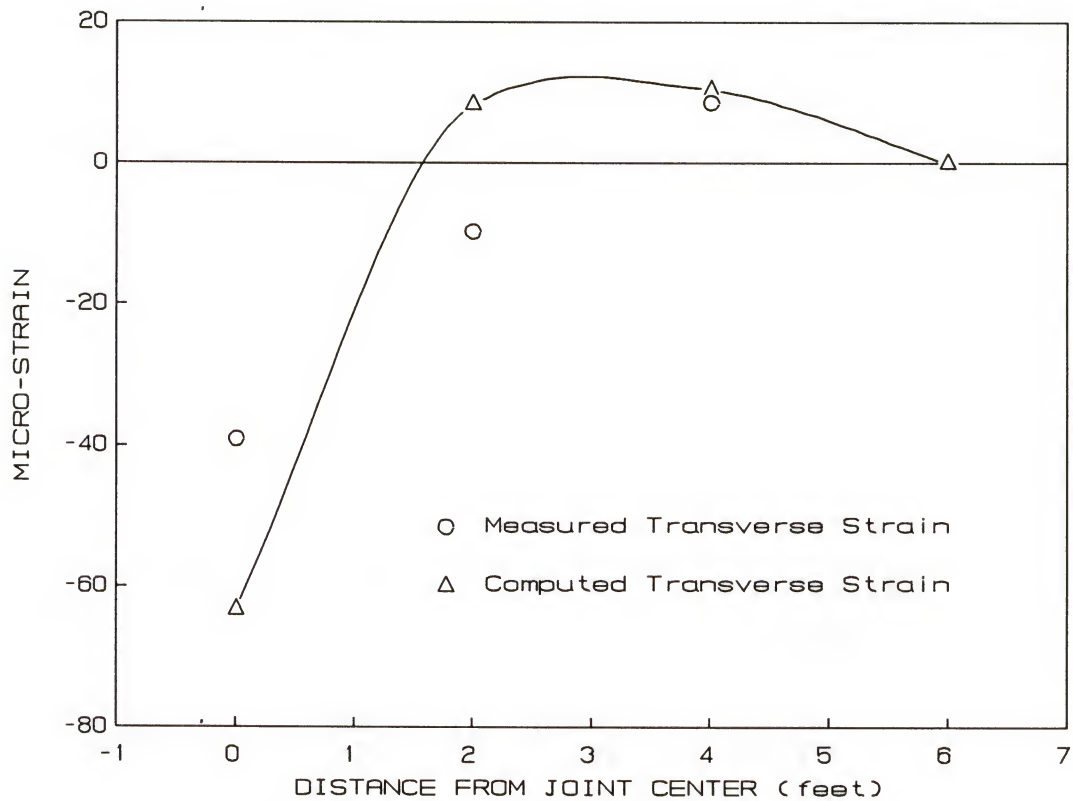

Figure 7.18 Comparison of Computed and Measured Strains Along the Slab Joint Caused by a FWD Load of 1000 kPa Applied at the Slab Joint Center at the Slab Center at a Recorded Temperature Differential of +12°F - Day Test (July 1988)

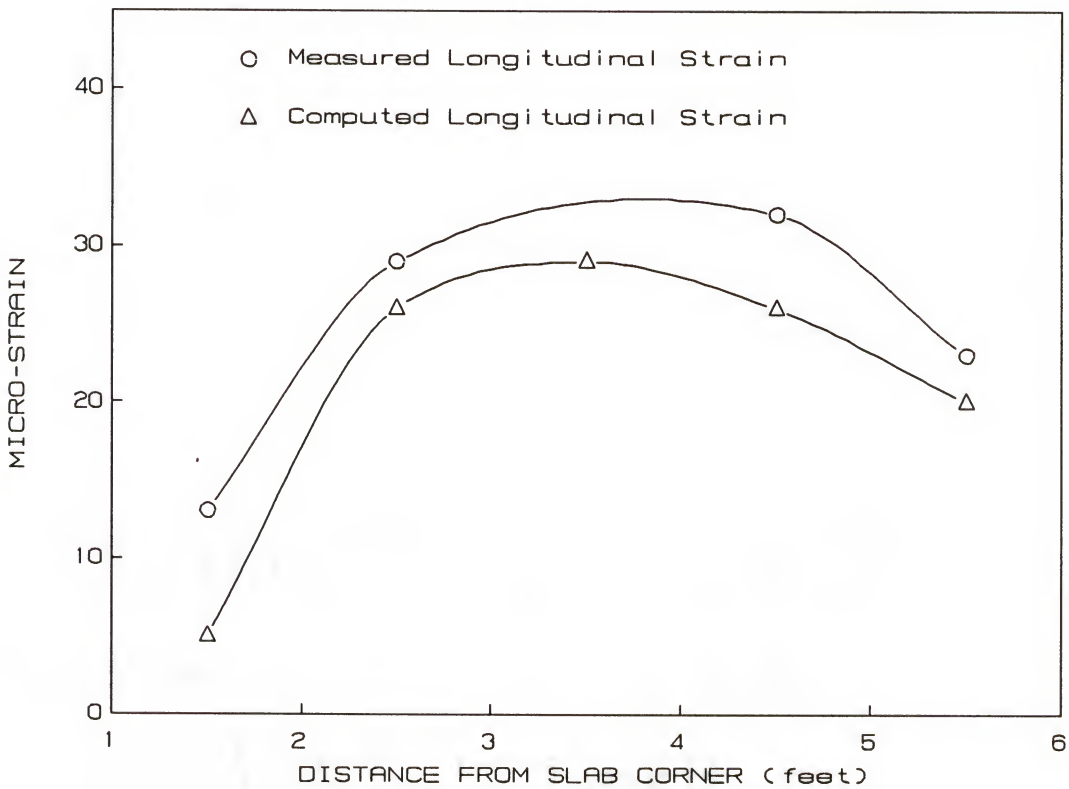

Figure 7.19 Comparison of Computed and Measured Strains Along the Slab Edge Caused by a FWD Load of 1000 kPa Applied at the Slab Corner at a Recorded Temperature Differential of -8°F - Night Test (January 1989)

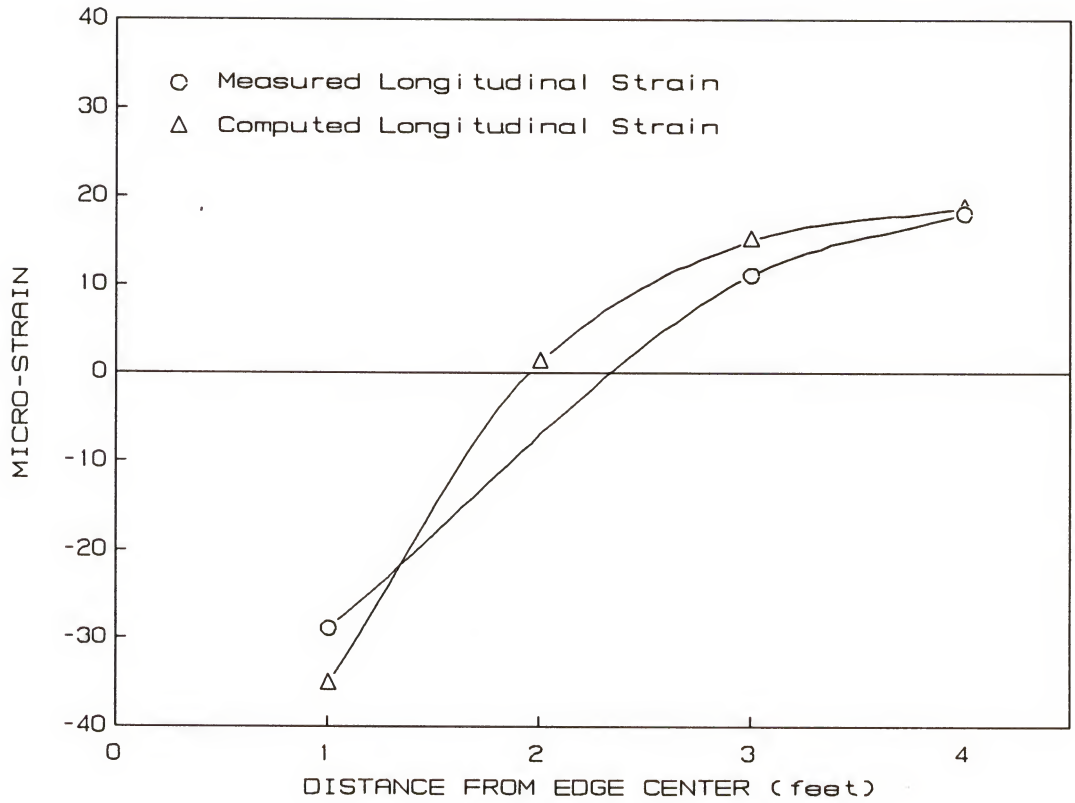

Figure 7.20 Comparison of Computed and Measured Strains Along the Slab Edge Caused by a FWD Load of 1000 kPa Applied at the Slab Edge Center at a Recorded Temperature Differential of -5°F - Night Test (June 1989)

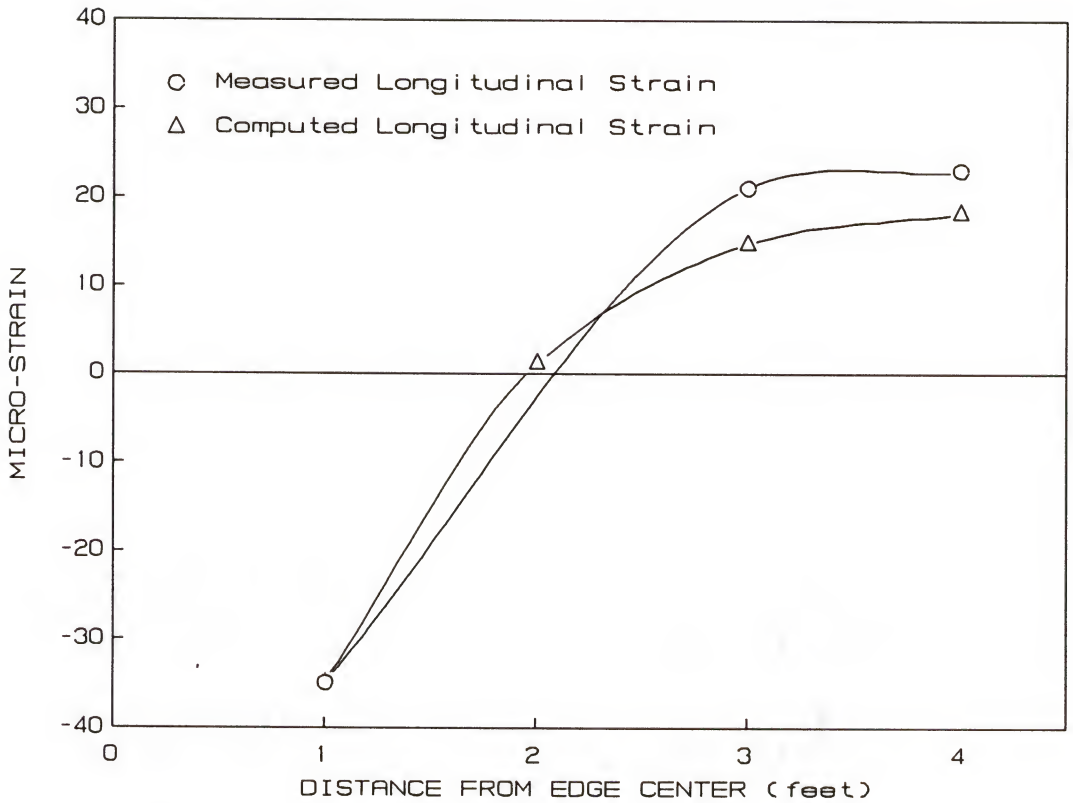

Figure 7.21 Comparison of Computed and Measured Strains Along the Slab Edge Caused by a FWD Load of 1000 kPa Applied at the Slab Edge Center at a Recorded Temperature Differential of +16°F - Day Test (June 1989)

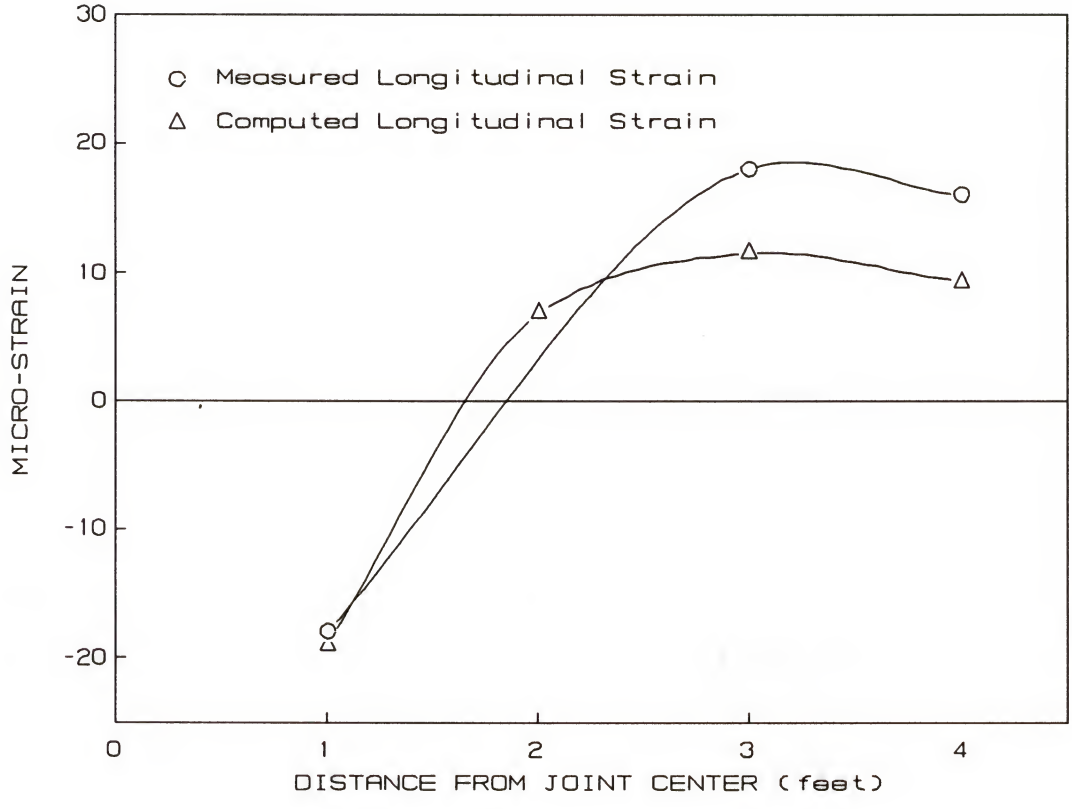

Figure 7.22 Comparison of Computed and Measured Strains Along the Slab Joint Caused by a FWD Load of 1000 kPa Applied at the Slab Joint Center at a Recorded Temperature Differential of -5°F - Night Test (June 1989)

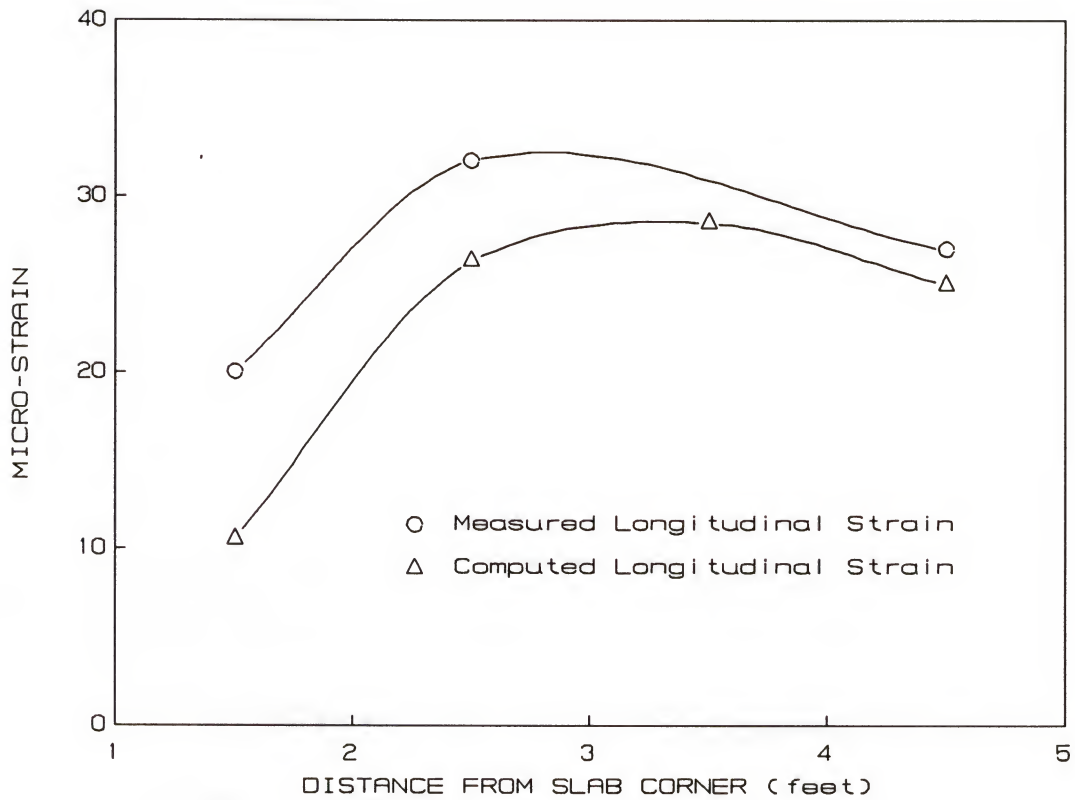

Figure 7.23 Comparison of Computed and Measured Strains Along the Slab Edge Caused by a FWD Load of 1000 kPa Applied at the Slab Corner at a Recorded Temperature Differential of -5°F - Night Test (June 1989)

From Figures 7.12 to 7.18, representing the July 88 field test results, it can be noted that, in almost all the cases, the measured strainsare much less than the computed stains at the positions near the load. The measured and computed strains are closer to each other when the positions are far away from the load. In considering the small amount of strains measured at locations far from the load and the error involved in the field test, these measurements might not be representative of actual strains even though they matched relatively well with the analytical ones. In light of this, another set of field tests was performed during the first week of January 1989 using a different strain gage layout (see Figure 3.3). The length of the gages was increased from 2 to 4 inches. During these tests, some of the gages could not be balanced on the signal conditioner, which provides the bridge completion circuits for the strain gages and also amplifies the output. Consequently, no data were collected from these gages. Figure 7.19 shows the plot of the measured and computed strains caused by the load applied at slab corner during the night tests. It can be noted that the two values are fairly close to each other at all locations. This is also true for the cases where the loads were applied at the edge and slab center, though fewer data were collected at these two positions. However, better results were obtained in the field tests performed on June 1989 using the third gage layout as shown in Figure 3.4. It can be noted from Figures 7.20 to 7.23 that the measured and computed strains, in almost all the cases, are closer, if not matching, to each other at positions near the load. Even at locations far away from the load, the two values are fairly close. However, certain gages could not be read because, most probably, of the small amount of expected strains (less than 10 micro-strains) at these gage locations and noise interference.

7.4 Conclusion

In conclusion, it could be stated that the discrepancy between the measured and computed strains in the slab, as observed in this field testing program, might be attributed to the following causes:

1. In investigating the theoretical strains in the slab computed by the FEACONS IV program, it was observed that the stress and strain changed drastically within a short distance under and near the loading area. Thus, it is critical that the exact gage position and loading position be used in the analysis. This might have resulted in some errors.
2. The calibration of the equipment used in the test might have some errors.
3. It is difficult to observe if the gages were just partially bonded to the slab surface. This might also cause errors in the strains measured.
4. The magnitudes of the strains measured were very small (less than 100 micro-stains) and could easily be affected by the noise interference from the equipment or environment.

7.5 Summary

This chapter has presented in detail the analysis of data in three different sets of field tests to measure load-induced strains in the pavement slab as well as the methodology for estimation of in situ concrete pavement parameters. The experimental set-up and data acquisition system, described in Chapter 3, have generally worked well. The measured strains generally matched fairly well with the computed strains. Needs for improvements and recommended changes in this system have been cited in several specific areas.

CHAPTER 8
CONCLUSIONS AND RECOMMENDATIONS

8.1 Conclusions

This research study was carried out to investigate the effects of the temperature distribution on the induced responses in concrete pavements. An analytical and experimental study was performed to determine and model the actual temperature distribution within typical concrete slabs and to determine the effects of non-linear thermal gradients on the behavior of concrete pavements was performed. In situ thermal-induced vertical displacements, in the absence of load other than gravity, were monitored at various times. A field testing program was conducted to measure strains in concrete pavements. In addition, these in situ measurements were used to investigate the validity and reliability of the mechanistic model used in the analytical phase of this study. A laboratory testing program was also conducted to determine the dynamic elastic modulus of concrete pavement.

The following conclusions were derived from the results obtained in this research:

8.1.1 Temperature Data Analysis

1. The temperature data analysis showed that a close relationship between daily air and pavement temperature variations exist. These variations follow a pattern that could be approximated by a sine wave.
2. Maximum temperatures occur at mid-days between 12 noon and 4 P.M. and minimum temperature occur in early mornings.

3. Temperature differentials between the top and bottom of the concrete slabs also follow a pattern that approximates a sine wave similar to the one of air and pavement temperatures. Generally, the temperature differential is positive during the daytime and negative at nighttime. The maximum positive temperature differential occurs between 1 P.M. to 4 P.M. while the negative temperature differential reaches its peak at about 6 A.M. The zero temperature differential is generally at approximately 9 A.M. and 7 P.M. A maximum temperature differential of 31°F, corresponding to 3.4°F per inch of slab depth, was recorded.
4. The magnitude of temperature variation decreases with the slab depth. At night time, slab temperatures are lower at the surface than at the bottom of the slab. After a short transition, the phenomenon is reversed during the day time. These observations are typical of the temperature attenuation and phase shift characteristics of heat conduction in a body.
5. The temperature data obtained in this study indicated that the temperature variations within the pavement slabs were mostly nonlinear. These temperature distributions throughout the depth of a concrete slab depth can be represented fairly well by a quadratic equation.

8.1.2 Thermal-Induced Pavement Response

1. The relative slab deflection profile measurements indicated that a change in temperature differential induces a change in the concrete slab profile.
2. A relative maximum deflection of approximately 1/4 of an inch was recorded at the center of a 20-ft slab during the month of November when the temperature differential increased from 2 to 15°F.

3. The in situ curling measurements, as compared to the low values computed using FEACONS IV program, suggest that the mechanistic model adopted to determine the deflections induced by the thermal gradient and slab weight might not be adequate.

8.1.3 Analysis of the Thermal-Load Induced Stress In Concrete Slabs

1. The computed warping stresses from Bradbury's equations are slightly higher than those from the FEACONS program for the daytime condition, while they are very close to one another for the nighttime condition.
2. When the temperature distribution is assumed to be linear, the maximum computed tensile stresses in the slab tend to be higher for the daytime condition and lower for the nighttime condition, as compared with the computed stresses with the consideration of the effects of the non-linear temperature distribution.

8.1.4 Measurement of Dynamic Elastic Modulus

1. When measured in flexure, the dynamic elastic modulus of a typical concrete pavement measured at a frequency range of 1 to 7 Hz is approximately 15 to 50% higher than the static elastic modulus.
2. The dynamic modulus of elasticity does not change significantly as the frequency changes within the range of 1 to 7 Hz.
3. The dynamic modulus of elasticity of concrete in flexure is significantly different from that in compression.

8.1.5 In Situ Measurement of Load-Induced Strains in Concrete Slabs

1. The experimental set-up and data acquisition system for measurement of load-induced strains in concrete slabs developed during the course of this study performed well in general.
2. The measured load-induced strains were close to those computed by FEACONS program.

8.2 Recommendations

The following recommendations are made based on the results of this research study:

1. Temperature variations appear to have a significant impact on the behavior of concrete slabs and, therefore, should be considered in concrete pavement design and analysis.
2. For a more accurate analysis of concrete pavement behavior, a nonlinear temperature distribution should be assumed.
3. Since the dynamic modulus of elasticity could be significantly higher than the static modulus and the traffic loads are usually applied dynamically to the pavement slabs, it should be more appropriate to use the dynamic modulus of elasticity in the analysis.
4. The mechanistic model used in FEACONS to determine the deflections due to the thermal gradient and slab weight should be studied for possible refinement.

8.3 Research Needs

The following are suggestions for future research in concrete pavement field:

1. Further data on moisture variations in concrete slabs are needed in order to improve the accuracy of the analysis of the warping phenomenon in concrete slabs.
2. Modeling capabilities of FEACONS IV program should be improved to include the consideration of a non-linear thermal gradient. Further adjustment are also needed to improve the accuracy of its determination of deflections due to the thermal gradient and slab weight.

3. In-situ measurement of static and dynamic strains in concrete slabs should be further investigated.
4. An investigation should be made on how the overall temperature change in the slab would affect the joint openings between adjacent slabs and, consequently, the joint stiffness and the structural performance of the concrete pavement.

APPENDIX A
RELATIVE DEFLECTION MEASUREMENTS

Table A.1 Respective Relative Deflection Profiles, in inches, Along the Slab Longitudinal Centerline as Measured for Various Temperature Conditions

Distance from Slab Center (ft.)	May			July				November	
	11 A.M.	1:30 P.M.	3:30 P.M.	20°F	13°F	-6°F	-2°F	15°F	2°F
1	0.6173	0.6117	0.5908	1.8827	1.8752	1.7937	1.8381	0.7474	0.50465
2	0.6038	0.5982	0.5812	1.736	1.7282	1.6464	1.69	0.71455	0.50795
3	0.5628	0.554	0.5293	1.52995	1.52115	1.44205	1.4811	0.64372	0.46335
4	0.5202	0.5043	0.475	1.3238	1.3141	1.2377	1.2722	0.5729	0.41875
5	0.4574	0.4328	0.4264	1.1097	1.1045	1.0308	1.0626	0.4775	0.3534
6	0.3441	0.3148	0.3096	0.85	0.8458	0.7741	0.805	0.33775	0.2442
7	0.234	0.2019	0.1993	0.6053	0.603	0.567	0.5838	0.21325	0.1467
8	0.107	0.1014	0.1007	0.3763	0.3764	0.3497	0.3611	0.0986	0.0608
9	0.0486	0.043	0.0421	1.1474	0.1558	0.1345	0.14260	0.0281	0.0053
10	0	0	0	0	0	0	0	0	0

Table A.2 Respective Relative Test Slab Deflection Profiles, in inches, Along the Slab Transverse Centerline as Measured for Various Temperature Conditions

Distance from Slab Center (ft.)	July		September			November	
	3°F	21°F	10°F	14°F	16°F	11°F	15°F
1	0.441	0.4719	0.09855	0.1199	0.1237	0.2337	0.2318
2	0.3616	0.3915	0.05695	0.0172	0.0746	0.1683	0.1708
3	0.3127	0.3391	-0.00505	0.0056	0.0102	0.0803	0.0813
4	0.2629	0.284	-0.06665	-0.0601	-0.0581	-0.0155	-0.015
5	0.1775	0.1912	-0.0867	-0.082	-0.0818	-0.0599	-0.0571
6	0	0	0	0	0	0	0

Table A.3 Respective Relative Test Slab Deflection Profiles, in inches, Along the Slab Joint as Measured for Various Temperature Conditions

Distance from Joint Center (ft.)	May			July			November	
	11:15 A.M.	2:00 P.M.	3:40 P.M.	-1°F	13°F	20°F	9°F	15°F
0	0.1863	0.1793	0.2204	0.69905	0.6001	0.6183	0.0602	0.11855
1	0.1559	0.1412	0.1808	0.59435	0.5016	0.5139	0.0422	0.11805
2	0.0857	0.0691	0.1054	0.41375	0.4186	0.4317	-0.0246	0.04585
3	0.0155	0	0.03	0.34315	0.3453	0.3599	-0.0952	-0.02115
4	-0.03	-0.0379	-0.0238	0.24805	0.2501	0.2618	-0.1421	-0.06665
5	-0.0732	-0.076	-0.0649	0.16845	0.1682	0.1771	-0.1125	-0.10155
6	0	0	0	0	0	0	0	0

APPENDIX B
COMPUTED AND MEASURED STRAINS

Table B.1 Comparison of Measured and Computed Strains Caused by FWD Loads Applied at Edge Center (Without Void)--Day Test (July 1988)

Temperature Differential = +10°F

I. Load = 570 kPa				
Distance from Load (feet)	Measured Strain (Micro Strain)		Computed Strain (Micro Strain)	
Transverse Direction	ϵ_{xx}	ϵ_{yy}	ϵ_{xx}	ϵ_{yy}
0	-23.1	-8.4	-46.1	+2.7
2	---	+8.7	-20.0	+14.7
4	-9.7	+7.6	-6.4	+11.6
6	---	---	-1.9	+5.9

II. Load = 1000 kPa				
Distance from Load (feet)	Measured Strain (Micro Strain)		Computed Strain (Micro Strain)	
Transverse Direction	ϵ_{xx}	ϵ_{yy}	ϵ_{xx}	ϵ_{yy}
0	-49.5	+17.3	-81.2	+4.8
2	---	+12.3	-35.4	+25.9
4	-13.9	+10.4	-11.3	+20.6
6	-7.9	+8.4	-3.3	+10.7

Table B.2 Comparison of Measured and Computed Strains Caused by FWD Loads Applied at Edge Center (Without Void)--Night Test (July 1988)

Temperature Differential = -7°F

I. Load = 570 kPa				
Distance from Load (feet)	Measured Strain (Micro Strain)		Computed Strain (Micro Strain)	
Transverse Direction	ϵ_{xx}	ϵ_{yy}	ϵ_{xx}	ϵ_{yy}
0	-20.9	---	-47.6	+2.9
2	---	+10.4	-20.7	+16.4
4	-5.2	+11.4	-6.5	+13.7
6	---	+7.6	-1.4	+6.9

II. Load = 1000 kPa				
Distance from Load (feet)	Measured Strain (Micro Strain)		Computed Strain (Micro Strain)	
Transverse Direction	ϵ_{xx}	ϵ_{yy}	ϵ_{xx}	ϵ_{yy}
0	-47.5	+7.1	-84.0	+5.2
2	---	+22.2	-36.7	+28.9
4	-12.6	+19.7	-11.4	+24.0
6	-10.1	+11.1	-2.6	+12.2

Table B.3 Comparison of Measured and Computed Strains Caused by FWD Loads Applied at Slab Center--Day Test (July 1988)

Temperature Differential = +20°F

I. Load = 570 kPa				
Distance from Load (feet)	Measured Strain (Micro Strain)		Computed Strain (Micro Strain)	
Transverse Direction	ϵ_{xx}	ϵ_{yy}	ϵ_{xx}	ϵ_{yy}
0	-23.9	-9.7	-27.1	-43.1
2	-17.7	-9.3	-15.4	-10.1
4	---	---	-6.8	1.3
5	---	---	-1.9	0.4
Longitudinal Direction	ϵ_{xx}	ϵ_{yy}	ϵ_{xx}	ϵ_{yy}
0	-23.9	-9.7	-27.1	-43.1
2.5	---	---	-6.8	-19.5
5	+7.0	-8.5	+2.6	-12.2
7.5	---	---	+3.0	-5.8
10	---	---	+2.2	-2.8

II. Load = 1000 kPa				
Distance from Load (feet)	Measured Strain (Micro Strain)		Computed Strain (Micro Strain)	
Transverse Direction	ϵ_{xx}	ϵ_{yy}	ϵ_{xx}	ϵ_{yy}
0	-49.5	-31.7	-42.3	-65.1
2	-27.9	-11.8	-22.6	-9.9
4	---	+8.9	-6.8	+2.0
5	-5.0	+2.0	-2.9	+0.5
Longitudinal Direction	ϵ_{xx}	ϵ_{yy}	ϵ_{xx}	ϵ_{yy}
0	-49.5	-31.7	-42.3	-65.1
2.5	---	---	+2.1	-25.7
5	+9.0	-14.5	+4.4	-15.4
7.5	---	---	+4.1	-7.1
10	---	---	+2.6	-3.3

Table B.4 Comparison of Measured and Computed Strains Caused by FWD Loads Applied at Slab Center--Night Test (July 1988)

Temperature Differential = -7°F

I. Load = 570 kPa				
Distance from Load (feet)	Measured Strain (Micro Strain)		Computed Strain (Micro Strain)	
Transverse Direction	ϵ_{yy}	ϵ_{yy}	ϵ_{xx}	ϵ_{yy}
0	-11.3	-7.4	-21.3	-28.3
2	-5.2	---	-10.4	+0.8
4	---	---	-3.7	+3.1
6	---	---	-1.1	+0.2

II. Load = 1000 kPa				
Distance from Load (feet)	Measured Strain (Micro Strain)		Computed Strain (Micro Strain)	
Transverse Direction	ϵ_{xx}	ϵ_{yy}	ϵ_{xx}	ϵ_{yy}
0	-17.5	-17.5	-37.6	-50.0
2	-9.4	---	-18.3	+1.4
4	---	---	-6.5	+5.5
6	---	---	-1.9	+0.3

Table B.5 Comparison of Measured and Computed Strains Caused by FWD Loads Applied at Joint Center--Day Test (July 1988)

Temperature Differential = +12°F

I. Load = 570 kPa				
Distance from Load (feet)	Measured Strain (Micro Strain)		Computed Strain (Micro Strain)	
Transverse Direction	ϵ_{xx}	ϵ_{yy}	ϵ_{xx}	ϵ_{yy}
0	---	-25.0	-6.9	-36.2
2	---	-7.4	-4.7	+4.4
4	---	---	-3.0	+5.8
6	---	---	-1.1	0.0

II. Load = 1000 kPa				
Distance from Load (feet)	Measured Strain (Micro Strain)		Computed Strain (Micro Strain)	
Transverse Direction	ϵ_{xx}	ϵ_{yy}	ϵ_{xx}	ϵ_{yy}
0	---	-39.2	-12.2	-63.3
2	---	-9.7	-8.7	+8.3
4	---	+8.5	-5.5	+10.4
6	---	---	-2.1	0.0

Table B.6 Comparison of Measured and Computed Strains Caused by FWD Loads Applied at Joint Center--Night Test (July 1988)

Temperature Differential = -7°F

I. Load = 570 kPa

Distance from Load (feet)	Measured Strain (Micro Strain)		Computed Strain (Micro Strain)	
Transverse Direction	ϵ_{xx}	ϵ_{yy}	ϵ_{xx}	ϵ_{yy}
0	---	-10.2	+1.0	-35.7
2	---	+1.0	-5.7	+5.1
4	---	---	-3.1	+5.4
6	---	---	-1.2	0.0
Longitudinal Direction	ϵ_{xx}	ϵ_{yy}	ϵ_{xx}	ϵ_{yy}
0	---	-10.2	+1.0	-35.6
2.5	---	---	+7.1	-12.4
5	+13.2	-5.1	+6.2	-3.0
7.5	+4.9	---	+2.5	-0.9
10	---	---	+0.5	-0.3

II. Load = 1000 kPa

Distance from Load (feet)	Measured Strain (Micro Strain)		Computed Strain (Micro Strain)	
Transverse Direction	ϵ_{xx}	ϵ_{yy}	ϵ_{xx}	ϵ_{yy}
0	---	-33.5	-12.7	-60.2
2	---	-11.6	-10.0	+8.8
4	---	---	-5.5	+5.4
6	---	---	-2.0	+0.2
Longitudinal Direction	ϵ_{xx}	ϵ_{yy}	ϵ_{xx}	ϵ_{yy}
0	+7.0	-33.5	-12.7	-60.2
2.5	---	---	+12.5	-22.1
5	+19.9	-7.7	-10.0	-5.4
7.5	+9.8	---	+4.3	-1.6
10	---	---	+0.8	-0.6

Table B.7 Comparison of Measured and Computed Strains Caused by FWD Loads Applied at Slab Corner--Night Test (July 1988)

Temperature Differential = -7°F

I. Load = 570 kPa				
Distance from Load (feet)	Measured Strain (Micro Strain)		Computed Strain (Micro Strain)	
Transverse Direction	ϵ_{yy}	ϵ_{yy}	ϵ_{xx}	ϵ_{yy}
0	---	---	-16.3	+1.1
2	---	+17.1	-14.6	+28.5
4	-7.5	+15.5	-7.5	+21.1
6	-5.2	+13.5	-3.0	+9.8
Longitudinal Direction	ϵ_{xx}	ϵ_{yy}	ϵ_{xx}	ϵ_{yy}
0	---	---	-16.3	+1.1
2.5	---	---	+12.7	-2.5
5	+25.4	---	+16.5	-3.3
7.5	+13.5	---	+7.4	-1.5
10	+9.7	---	+2.1	-0.4

II. Load = 1000 kPa				
Distance from Load (feet)	Measured Strain (Micro Strain)		Computed Strain (Micro Strain)	
Transverse Direction	ϵ_{xx}	ϵ_{yy}	ϵ_{xx}	ϵ_{yy}
0	-8.5	---	-28.7	+1.9
2	---	+22.2	-25.8	+50.2
4	-8.5	+22.2	-13.3	+37.3
6	-7.1	+22.3	-5.3	+17.2
Longitudinal Direction	ϵ_{xx}	ϵ_{yy}	ϵ_{xx}	ϵ_{yy}
0	-8.5	---	-28.7	+1.9
2.5	+12.9	---	+22.3	-4.3
5	+36.2	---	+29.3	-5.8
7.5	+19.9	-5.1	+13.1	-2.6
10	+12.4	-7.7	+3.6	-0.8

Table B.8 Comparison of Measured and Computed Strains Caused by FWD Loads Applied at Edge Center (With Void)--Day Test (July 1988)

Temperature Differential = +20°F

I. Load = 570 kPa				
Distance from Load (feet)	Measured Strain (Micro Strain)		Computed Strain (Micro Strain)	
Longitudinal Direction	ϵ_{xx}	ϵ_{yy}	ϵ_{xx}	ϵ_{yy}
0	-30.0	+5.0	-56.4	+4.0
2.5	---	---	+10.9	-1.2
●	+15.3	---	+12.2	-1.8
2.5	---	---	+4.6	-3.1
10	---	---	+0.8	-0.2

II. Load = 1000 kPa				
Distance from Load (feet)	Measured Strain (Micro Strain)		Computed Strain (Micro Strain)	
Longitudinal Direction	ϵ_{xx}	ϵ_{yy}	ϵ_{xx}	ϵ_{yy}
0	-62.5	+12.0	-98.3	+6.8
2.5	-12.4	---	+19.3	-2.2
●	+20.0	---	+21.4	-3.1
7.5	---	---	+7.8	-1.8
10	---	---	+1.2	-0.2

Table B.9 Comparison of Measured and Computed Strains Caused by FWD Loads Applied at Edge Center (With Void)--Night Test (July 1988)

Temperature Differential = -7°F

I. Load = 570 kPa				
Distance from Load (feet)	Measured Strain (Micro Strain)		Computed Strain (Micro Strain)	
Longitudinal Direction	ϵ_{xx}	ϵ_{yy}	ϵ_{xx}	ϵ_{yy}
0	-29.0	---	-54.3	+3.7
2.5	-10.0	---	+10.9	-1.3
●	+11.5	---	+12.0	-1.6
7.5	+6.1	---	+4.2	-0.5
10	---	---	+0.4	+0.3

II. Load = 1000 kPa				
Distance from Load (feet)	Measured Strain (Micro Strain)		Computed Strain (Micro Strain)	
Longitudinal Direction	ϵ_{xx}	ϵ_{yy}	ϵ_{xx}	ϵ_{yy}
0	-62.5	---	-95.9	+6.7
2.5	-17.5	---	+19.2	-2.2
●	+19.3	---	+21.4	-2.9
7.5	+9.0	---	+7.4	-0.9
10	---	---	+0.8	+0.5

Table B.10 Comparison of Measured and Computed Strains Caused by FWD Load of 1000 kPa Applied at Slab Corner--Day Test (January 1989)

Temperature Differential = 4°F

Gage Code	Distance from Load (feet)	Measured Strain (micro strain)		Computed Strain (micro strain)	
	Transverse Direction	ϵxx	ϵyy	ϵxx	ϵyy
I1&I2	1.5	--	26	-23	42
H3&H4	2.5	--	29	-13	39
H1&H2	3.5	--	--	- 8	30
	Longitudinal Direction	ϵxx	ϵyy	ϵxx	ϵyy
I3&I4	1.5	17	--	12	-0.02
J1&J2	2.5	--	--	26	-0.28
J3&J4	4.5	44	--	27	-1
K1&K2	4.5	--	--	23	-1.2
K3&K4	5.5	--	--	17	-1

Table B.11 Comparison of Measured and Computed Strains Caused by FWD Load of 1000 kPa Applied at Slab Corner--Night Test (January 1989)

Temperature Differential = -8°F

Gage Code	Distance from Load (feet)	Measured Strain (micro strain)		Computed Strain (micro strain)	
	Longitudinal Direction	ϵxx	ϵxx	ϵxx	ϵyy
I3&I4	1.5	13	--	5	-1
J1&J2	2.5	29	--	26	-0.8
J3&J4	3.5	--	--	26	-1.4
K1&K2	4.5	32	--	26	-1.4
K3&K4	5.5	23	--	20	-1.1

Table B.12 Comparison of Measured and Computed Strains Caused by FWD Load of 1000 kPa Applied at Joint Center--Day Test (January 1989)

Temperature Differential = 4°F

Gage Code	Distance from Load (feet)	Measured Strain (micro strain)		Computed Strain (micro strain)	
	Transverse Direction	ϵxx	ϵyy	ϵxx	ϵyy
H1&H2	2.0	--	--	-10	7
H3&H4	3.0	--	--	- 7	12
	Longitudinal Direction	ϵxx	ϵyy	ϵxx	ϵyy
F3&F4	2.0	17	-19	12	-32
F1&F2	3.0	--	--	15	-17

Table B.13 Comparison of Measured and Computed Strains Caused by FWD Load of 1000 kPa Applied at Joint Center--Night Test (January 1989)

Temperature Differential = -7°F

Gage Code	Distance from Load (feet)	Measured Strain (micro strain)		Computed Strain (micro strain)	
	Transverse Direction	ϵxx	ϵyy	ϵxx	ϵyy
H1&H2	2.0	--	--	-10	7
H3&H4	3.0	--	--	- 7	11
	Longitudinal Direction	ϵxx	ϵyy	ϵxx	ϵyy
F3&F4	2.0	24	-20	12	-31
F1&F2	3.0	--	--	15	-17

Table B.14 Comparison of Measured and Computed Strains Caused by FWD Load of 1000 kPa Applied at Edge Center--Day Test (January 1989)

Temperature Differential = 10°F

Gage Code	Distance from Load (feet)	Measured Strain (micro strain)		Computed Strain (micro strain)	
	Transverse Direction	ϵxx	ϵyy	ϵxx	ϵyy
A1&A2	0.5	--	32	-78	5
H3&H4	3.0	-35	33	-40	28

Table B.15 Comparison of Measured and Computed Strains Caused by FWD Load of 1000 kPa Applied at Slab Center--Day Test (January 1989)

Temperature Differential = 12°F

Gage Code	Distance from Load (feet)	Measured Strain (micro strain)		Computed Strain (micro strain)	
	Longitudinal Direction	ϵxx	ϵyy	ϵxx	ϵyy
D1&D2	0.5	--	-56	-43	-60
D3&D4	1.0	--	-52	-17	-47

Table B.16 Comparison of Measured and Computed Strains Caused by FWD Load of 1000 kPa Applied at Edge Center--Day Test (June 1989)

Temperature Differential = 16°F

Gage No.	Distance from Load (feet)	Measured Strain (micro strain)		Computed Strain (micro strain)	
	Longitudinal Direction	ϵ_{xx}	ϵ_{yy}	ϵ_{xx}	ϵ_{yy}
1	1.0	-35	--	-35	--
2	2.0	--	--	1.1	--
3	3.0	21	--	14.7	--
4	4.0	23	--	18.2	--

Table B.17 Comparison of Measured and Computed Strains Caused by FWD Load of 1000 kPa Applied at Edge Center--Night Test (June 1989)

Temperature Differential = -5°F

Gage No.	Distance from Load (feet)	Measured Strain (micro strain)		Computed Strain (micro strain)	
	Longitudinal Direction	ϵ_{xx}	ϵ_{yy}	ϵ_{xx}	ϵ_{yy}
1	1.0	--29	--	-35.4	--
2	2.0	--	--	1.2	--
3	3.0	11	--	15	--
4	4.0	18	--	18.7	--

Table B.18 Comparison of Measured and Computed Strains Caused by FWD Load of 1000 kPa Applied at Slab Center--Day Test (June 1989)

Temperature Differential = 18°F

Gage No.	Distance from Load (feet)	Measured Strain (micro strain)		Computed Strain (micro strain)	
	Longitudinal Direction	ϵ_{xx}	ϵ_{yy}	ϵ_{xx}	ϵ_{yy}
5	1.0	-23	--	-17.8	--
6	2.0	--	--	-1.6	--
7	3.0	--	--	4	--
8	4.0	--	--	5.3	--

Table B.19 Comparison of Measured and Computed Strains Caused by FWD Load of 1000 kPa Applied at Slab Center--Night Test (June 1989)

Temperature Differential = -5°F

Gage No.	Distance from Load (feet)	Measured Strain (micro strain)		Computed Strain (micro strain)	
	Longitudinal Direction	ϵ_{xx}	ϵ_{yy}	ϵ_{xx}	ϵ_{yy}
5	1.0	-23	--	-12	--
6	2.0	--	--	3.1	--
7	3.0	--	--	7.8	--
8	4.0	--	--	8.4	--

Table B.20 Comparison of Measured and Computed Strains Caused by FWD Load of 1000 kPa Applied at Joint Center--Day Test (June 1989)

Temperature Differential = +19°F

Gage No.	Distance from Load (feet)	Measured Strain (micro strain)		Computed Strain (micro strain)	
	Transverse Direction	ϵ_{xx}	ϵ_{yy}	ϵ_{xx}	ϵ_{yy}
9	1.0	--	-30	--	-25.6
10	2.0	--	--	--	2
11	3.0	--	--	--	9.2
12	4.0	--	11	--	8.6

Table B.21 Comparison of Measured and Computed Strains Caused by FWD Load of 1000 kPa Applied at Joint Center--Night Test (June 1989)

Temperature Differential = -5°F

Gage No.	Distance from Load (feet)	Measured Strain (micro strain)		Computed Strain (micro strain)	
	Transverse Direction	ϵ_{xx}	ϵ_{yy}	ϵ_{xx}	ϵ_{yy}
9	1.0	--	-18	--	-19
10	2.0	--	--	--	6.8
11	3.0	--	18	--	11.5
12	4.0	--	16	--	9.3

Table B.22 Comparison of Measured and Computed Strains Caused by FWD Load of 1000 kPa Applied at Slab Corner--Day Test (June 1989)

Temperature Differential = +19°F

Gage No.	Distance from Load (feet)	Measured Strain (micro strain)		Computed Strain (micro strain)	
	Longitudinal Direction	ϵ_{xx}	ϵ_{yy}	ϵ_{xx}	ϵ_{yy}
13	1.5	--	--	11	--
14	2.5	--	--	24.7	--
15	3.5	23	--	26	--
16	4.5	18	--	22.4	--

Table B.23 Comparison of Measured and Computed Strains Caused by FWD Load of 1000 kPa Applied at Slab Corner--Night Test (June 1989)

Temperature Differential = -5°F

Gage No.	Distance from Load (feet)	Measured Strain (micro strain)		Computed Strain (micro strain)	
	Longitudinal Direction	ϵ_{xx}	ϵ_{yy}	ϵ_{xx}	ϵ_{yy}
13	1.5	20	--	10.5	--
14	2.5	32	--	26.3	--
15	3.5	--	--	28.5	--
16	4.5	27	--	25	--

REFERENCES

1. Tia, M., C. L. Wu, B. E. Ruth, D. Bloomquist and Bouzid Choubane, Field Evaluation of Rigid Pavements for the Development of a Rigid Pavement Design System - Phase III," Final Report, Project 245-D54, Department of Civil Engineering, University of Florida, Gainesville, FL, July 1988.

2. Ritter, L.G. and R.J. Paqueete, Highway Engineering, Third Edition, The Ronald Press, New York, 1960, 782 pp.

3. Stock, A.F., Concrete Pavements, Elsevier Applied Science, London, 1988, 433 pp.

4. "An Evaluation of the Development and Current Condition of Interstate 10," Florida Department of Transportation, May, 1983.

5. Yoder, E.J. and M.W. Witczak, Principles of Pavement Design, Second Edition, John Wiley & Sons, New York, 1975, 711 pp.

6. Haas, R. and W.R. Hudson, Pavement Management Systems, McGraw Hill, New York, 1978, 457 pp.

7. Sargious, M., Pavement and Surfacings for Highways and Airports, John Wiley and Sons, New York, 1975, 619 pp.

8. Older, C.,"Highway Research In Illinois," Proceedings ASCE, Vol. 50.1, February 1924, pp. 175-217.

9. Goldbeck, A.T.,"Thickness of Concrete Slabs," Public Roads, April 1919.

10. Kelley, E.F., "Application of the Results of Research to the Structural Design of Concrete Pavements," Public Roads, July 1939, pp. 83-104.

11. Westergaard, H.M.,"Analysis of Stresses in Concrete Roads Caused by Variations of Temperature," Public Roads, May 1927, pp. 54-60.

12. Bradbury, R.D., "Reinforced Concrete Pavements," Wire Reinforcement Institute, Washington, D.C., 1938.

13. Teller, L.W. and E.C. Sutherland, "The Structural Design of Concrete Pavements," Public Roads, Vol. 23, No. 8, June 1943, pp. 167-211.

14. Thomlinsom, J.,"Temperature Variations and Consequent Stresses Produced by Daily and Seasonal Temperature Cycles in Concrete Slabs," Concrete and Construction Engineering, 1940.

15. Lang, F.C., "Temperature and Moisture Variations in Concrete Pavements," Highway Research Board Proceedings, Vol. 21, 1941, pp. 260-271.

16. Pickett, G., "A Study of Stresses in the Corner Region of Concrete Pavement Slabs under Large Corner Loads," Portland Cement Association, Chicago, IL, 1951.

17. Harr, M.E. and Leonards, G.A., "Warping Stresses and Deflections in Concrete Pavements," Highway Research Board Proceedings, Vol. 38, 1959, pp. 286-320.

18. Wiseman, J.F., M.E. Harr and G.A. Leonards, "Warping Stresses and Deflections in Concrete Pavements: Part II," Highway Research Board Proceedings, Vol. 39, 1960, pp. 157-172.

19. Highway Research Board, " The AASHO Road Test. Report 5, Pavement Research," Highway Research Board Special Report 61-E, 1962.

20. Huang, Y.H. and S.T. Wang, "Finite-Element Analysis of Concrete Slabs and its Implications for Rigid Pavement Design," Highway Research Record, No. 466, 1973.

21. Chou, Y. T., "Structural Analysis Computer Programs for Rigid Multicomponent Pavement Structures with Discontinuities - WESLIQID and WESLAYER," Technical Reports 1, 2, and 3, U.S. Army Engineering Waterways Experiment Station, Vicksburg, MS, May 1981.

22. Tayabji, S. P. and B. E. Colley, "Analysis of Jointed Concrete Pavements," Federal Highway Administration, National Technical Information Service, 1981.

23. Ioannides, A. M. and R. A. Salsilli-Murua, "Temperature Curling in Rigid Pavements: An Application of Dimensional Analysis," Transportation Research Record 1227, 1989, pp. 1-11.

24. Timoshenko, S. and J.M. Lessels, Applied Elasticity, Westinghouse, Pittsburgh, PA, 1925.

25. Westergaard, H.M., "Theory of Concrete Pavement Design," Highway Research Board Proceedings, Vol. 7, 1927, pp. 175-181.

26. Hogg, A.H., "Equilibrium of a Thin Plate Symmetrically Loaded, Resting on an Elatic Subgrade of Infinite Depth," Philosophical Magazine, Vol. 25, 1938.

27. Hall, D.L., "Thin Plates on Elastic Foundations," Proceedings of the International Conference of Applied Mechanics, Cambridge, MA, 1938.

28. Pickett, G. and G.K. Ray,"Influence Charts for Rigid Pavements," Transactions, ASCE, 1951.

29. Niu, H.P. and G. Pickett,"The effect of Degree Continuity accross a Void or Crack on Performance of Concrete Pavements," Highway Research Bulletin, No. 291, 1969.

30. Ioannides, A.M., M.R. Thompson and E.J. Barenberg,"Westergaard solutions Reconsidered," Transportation Research Record 1043, 1985.

31. Majidzadeh, K, "A Mechanistic Approach to Rigid Pavement Design," in Concrete Pavements, Edited by A.F. Stock, Elsevier Applied Science, London, 1988, pp. 11-56.

32. Burmister, D.M., "The Theory of Stresses and Displacements in Layered Systems and Applications to the Design of Airport Runway," Highway Research Board Proceedings, Vol.23, 1943.

33. Tabatabaie, A.M. and E.J. Barenberg, "Finite Element Analysis of Jointed or Cracked Concrete Pavements," Transportation Research Record 671, 1978, pp. 11-19.

34. Tia, M., J.M. Armaghani, C.L. Wu, S. Lei, and K.L. Toye, "FEACONS III Computer Program for an Analysis of Jointed Concrete Pavements," Transportation Research Record 1136, 1987, pp. 12-22.

35. Melosh, R. M., "Basis of Derivation of Matrices for the Direct Stiffness Method," AIAA Journal, Vol.1, No. 7, July 1963, pp. 1631-1637.

36. Zienkiewicz, O. C. and Y. K. Cheung, "The Finite Element Method for Analysis of Elastic Isotropic and Orthotropic Slabs,"Proc. Institute of Civil Engineers, Vol. 28, 1964, pp. 471-488.

37. Cable, K.C., Rohde, J.R., Lee, D.Y., and Klaiber, F.W., "Pavement Instrumentation," for the Iowa Department of Transportation and the Iowa Highway Research Board, Ames, Iowa, March 1988.

38. White, D.T., "Guide Instrumentation Plan for Flexible and Rigid Pavements," Federal Highway Administration, Washington, D.C., June 1985.

39. S.F. Brown, "State-of-the-Art Report on Field Instrumentation for Pavement Experiments," Transportation Research Record Number 640, 1977, pp. 13-28.

40. Esch, D. C.,"Temperature and Thaw Depth Monitoring of Pavement Structures," Proceedings of the Symposium on the State-of-the-Art of Pavement Response Monitoring Systems for Roads and Airfields, March 1989.

41. Berg, R. L., "Monitoring Pavement Performance in Seasonal Frost Area," Proceedings of the Symposium on the State-of-the-Art of Pavement Response Monitoring Systems for Roads and Airfields, March 1989.

42. Tabatabaee, N., P. Sebaaly, "State-of-the-Art Pavement Instrumentation," Transportation Research Record 1260, 1990, pp. 246-255.

43. Smith, R.E., M.I. Darter and S.M. Herrin, "Highway Pavement Distress Identification Manual," Federal Highway Administration, Washington, D.C., February 1988.

44. Armaghani, J. M., "Comprehensive Analysis of Concrete Pavement Response to Temperature and Load Effects," Ph.D Dissertation, Department of Civil Engineering, University of Florida, 1987.

45. Bergstom, K.C., "Temperature Stresses in Concrete Pavements," Swedish Cement and Concrete Institute Proceedings, Stockholm, 1950.

46. Faraggi, V., C. Jofres and C. Kraemer, "Combined Effect of Traffic Loads and Thermal Gradients on Concrete Pavement Design," Transportation Research Record Number 1136, 1987, pp. 108-118.

47. Barber, E. S., "Calculation of Maximum Pavement Temperature from Weather Reports," Highway Research Board Bulletin 168, Highway Research Record, Washington, D. C., 1975.

48. Thompson, M.R., B. Dempsey, H. Hill and J. Vogel, "Characterizing Temperature Effects for Pavement Analysis and Design," Paper Presented at 66th Annual Meeting of the Transportation Research Board, 1987.

49. Hsieh, C.K., Q. Chaobin and E.E. Ryder, "Development of Computer Modeling for Prediction of Temperature Distribution Inside Concrete Pavements," Report Prepared for the Florida Department of Transportation, Department of Mechanical Engineering, University of Florida, Gainesville, FL, August 1989.

50. Beam, R.M and R.F. Warming, "An Implicit Factored Scheme for the Compressible Navier-Stokes Equations," AIAA Journal, Vol 16, No. 4, pp. 393-402, 1978.

51. Tia, M., Eom, K.S., Ruth, B.E., "Development of DBCONPAS Computer Program for Estimation of Concrete Pavement Parameters from FWD Data," Nondestructive Testing of Pavements and Backcalculations of Moduli, ASTM STP 1026, American Society for Testing and Materials, Philadelphia, 1989, pp. 291-312.

BIOGRAPHICAL SKETCH

The author was born in Sidi-Aissa, a small town in the high plateau of northern Algeria, on October 27, 1959. After obtaining his high school degree in mathematics, he entered the newly created Institute of Technology at the Centre Universitaire de Tizi-Ouzou where he received the Diplome d'Ingenieur in Civil Engineering in 1984. His class was the first to graduate from the Institute.

In September 1985, he entered the University of Pennsylvania to further his education. In August 1987, he received a Master of Science in civil engineering. The Departments of Civil Engineering and Systems Engineering were, then, combined into a Department of Systems with a deemphasis on classic civil engineering program. As a result, he transferred to the University of Florida in 1988.

While working toward the degree of Doctor of Philosophy in materials, the author served as a research assistant, then a laboratory instructor for the Civil Engineering Materials course.

I certify that I have read this study and that in my opinion it conforms to acceptable standards of scholarly presentation and is fully adequate, in scope and quality, as a dissertation for the degree of Doctor of Philosophy.

Mang Tia, Chairman
Professor of Civil Engineering

I certify that I have read this study and that in my opinion it conforms to acceptable standards of scholarly presentation and is fully adequate, in scope and quality, as a dissertation for the degree of Doctor of Philosophy.

Byron E. Ruth, Cochairman
Professor of Civil Engineering

I certify that I have read this study and that in my opinion it conforms to acceptable standards of scholarly presentation and is fully adequate, in scope and quality, as a dissertation for the degree of Doctor of Philosophy.

David G. Bloomquist
Assistant Professor of Civil Engineering

I certify that I have read this study and that in my opinion it conforms to acceptable standards of scholarly presentation and is fully adequate, in scope and quality, as a dissertation for the degree of Doctor of Philosophy.

Ramesh L. Shrestha
Associate Professor of Civil Engineering

I certify that I have read this study and that in my opinion it conforms to acceptable standards of scholarly presentation and is fully adequate, in scope and quality, as a dissertation for the degree of Doctor of Philosophy.

David C. Wilson
Professor of Mathematics

This dissertation was submitted to the Graduate Faculty of the College of Engineering and to the Graduate School and was accepted as partial fulfillment of the requirements for the degree of Doctor of Philosophy.

August 1993

Winfred M. Phillips
Dean, College of Engineering

Dean, Graduate School